Insights into the effect of substrate crystallinity on the enzymatic degradation of Poly(ethylene terephthalate)

Thomsen, Thore Bach

Publication date:
2023

Document Version
Publisher's PDF, also known as Version of record

DTU Bioengineering
Department of Biotechnology and Biomedicine

Insights into the effect of substrate crystallinity on the enzymatic degradation of Poly(ethylene terephthalate)

Thore Bach Thomsen

PHD Thesis

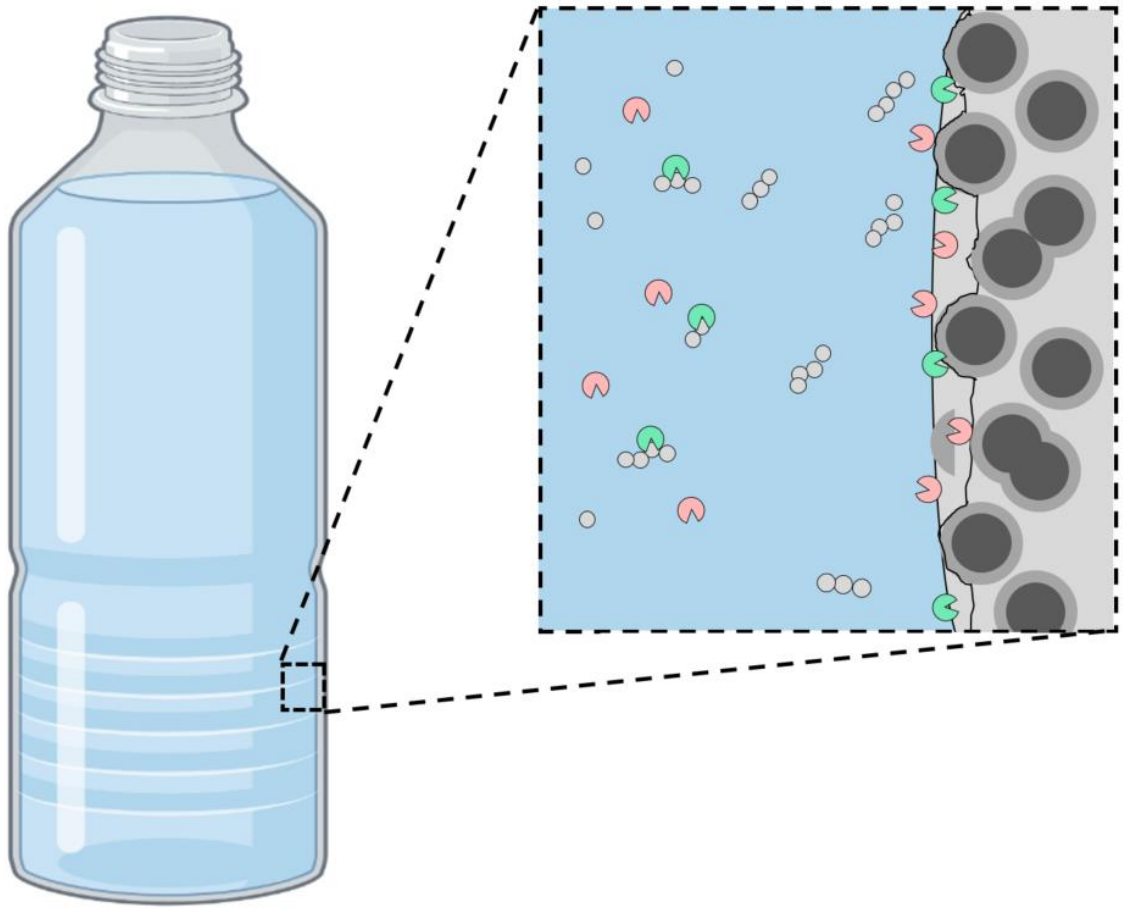

A thesis submitted in partial fulfillment of the requirements of the Technical University of Denmark for the award of Ph.D.

September 2023

Thore Bach Thomsen (Ph.D. Candidate)
15/09/2023

DTU Bioengineering
Department of Biotechnology and Biomedicine

Intentionally left blank

Preface

This Ph.D. Thesis was conducted at the Protein Chemistry and Enzyme Technology Section at the Department of Bioengineering, Technical University of Denmark (DTU), under the guidance of main supervisor Professor Anne S. Meyer and co-supervisors Professor Peter Westh and Cameron James Hunt. The spanned over a three year period starting July 2020. This thesis has been submitted to the Doctoral School of Biotechnology at DTU.

Acknowledgments

This journey has been incredibly rewarding, and I am deeply thankful to the individuals who have played pivotal roles in bringing this Ph.D. thesis to success. First and foremost, my heartfelt gratitude goes to my primary supervisor, Professor Anne S. Meyer, and co-supervisor Cameron James Hunt. Their exceptional guidance, unwavering support, and mentorship have been the bedrock of my Ph.D. voyage, profoundly shaping the outcome of this thesis. Their dedication to both my academic and personal growth has left an indelible mark on this work. I would also like to extend my appreciation to my co-supervisor, Peter Westh, for his valuable guidance and enlightening discussions on the enzymatic degradation of PET.

I owe a debt of gratitude to my colleagues, both past and present, within the PCET section at DTU Bioengineering, particularly the Enzyme Technology group. Their support, stimulating discussions, and the collaborative environment provided fertile ground for my research to thrive. Special acknowledgments are due to Jenny Arnling Bååth, Malene Billeskov Keller, Andrew Rennison, Kristine Stub Rønø Clausen, and Sune Warming Schubert for their invaluable contributions through scientific dialogues on enzymatic degradation of PET. I am particularly grateful to Sune for our highly productive collaboration, which has resulted in several co-authored publications.

My sincere appreciation goes out to my esteemed collaborators. I would like to thank Professor Kristoffer Almdal for generously granting me access to ATR-FTIR and sharing his profound insights into Polymer physics. I am also grateful to Berit Wenzel for her invaluable assistance with SEM imaging.

Lastly, I want to express my heartfelt gratitude to my friends and family, with a special mention of my girlfriend, Mette. Their unwavering support, encouragement, and understanding throughout the highs and lows of my doctoral journey have been my wellspring of strength and inspiration.

Founding

The Ph.D. was funded by the Technical University of Denmark, DTU Bioengineering, as well as partly by a grant from the Villum Foundation (Project no. 40815).

Summary (English Abstract)

Plastic pollution has become a global environmental threat, affecting both aquatic and terrestrial ecosystems. Despite these concerns, the demand for plastics continues to rise, leading to a substantial production of 390 Mt in 2021. A key contributor to plastic pollution is Poly(ethylene terephthalate) (PET), a semi-crystalline plastic polyester material with a global production volume of 83 Mt/year. Currently, less than 10% of all PET is recycled. This recycling, by conventional methods, does furthermore results in lower quality products. Hence, the development of novel recycling technologies is essential for establishing a truly circular economy. Recently, it was demonstrated that certain enzymes may catalyze the degradation of PET. As enzymatic recycling of PET enables the synthesis of new high-quality PET, it has the potential for the establishment of a circular economy of PET. The enzymatic degradation rate is, however, strongly influenced by the properties of PET, notably the degree of crystallinity (X_C). As most post-consumer PET products (Plastic bottles and textiles etc.) have an X_C > 20% a pretreatment step is required for efficient biorecycling of PET. This pretreatment is however very energy-demanding, thus lowering the sustainable potential of biorecycling.

This Ph.D. thesis aimed to study how substrate-related properties affected the enzymatic degradation of PET. For this purpose, we developed a standardized methodology, for controlling the X_C. This method was based on thermal-induced crystallization of commercially available amorphous PET, via annealing at 115 ºC. This substrate was subsequently used to study how several benchmark PET hydrolases were affected by increasing X_C. The initial degradation of PET, denoted as the lag phase, did not result in any formation of soluble products. Once the lag phase was surpassed, the concentration of soluble products, resulting from the enzymatic treatment, was released at a constant rate, denoted as the steady-state rate. The steady-state reaction rate was also heavily affected by the X_C. This negative effect becomes particularly profound once X_C exceeds a certain threshold, ~20%. This threshold was, however, affected by several factors, including reaction temperature, extent of reaction, and the enzyme catalyzing the reaction. We found that LCC, LCC_{ICCG}, and DuraPETase were more prone to increasing levels of X_C compared to HiC, TfC, and PHL7. This increased tolerance was caused by a presumable broader substrate specificity, leading to higher rates and maximal degradation yields at higher X_C. By studying the lag phase during enzymatic treatment we found that the duration of this phenomenon was heavily prolonged at increasing X_C (up to 5 days at X_C > 20%), and lower steady-state rates. We ascribed the lag phase to an initial endo-type degradation pattern, which would not yield any soluble products. This mechanism was consolidated by studying the proton release during this initial stage, which confirmed hydrolysis by the enzyme during the lag phase.

We furthermore studied the effect of the glass transition temperature (T_g) on the enzyme hydrolysis rate. This was done by lowering the T_g of a PET material from 75 ºC to 60ºC by soaking it in water. By assaying these disks at 69ºC (between the T_g of the substrates) we found that the reaction rate was unaffected by the lower T_g.

Summary/Dansk Sammendrag

Plastikforurening er blevet en global trussel for miljøet, der både påvirker økosystemer både i vand og på land. På trods af dette er efterspørgslen efter plastik fortsat stigende, hvilket i 2021 resulterede i en årlig produktion på 390 millioner tons. En betydelig bidragyder til plastforurening er Plasttype Poly(ethylen terephthalat) (PET), der er en semi-krystallin polyester med en global produktionsvolumen på 83 millioner tons om året. Mindre end 10% af PET bliver i øjeblikket genanvendt. Desuden resulterer de konventionelle genanvendelsesmetoder ofte i produkter af lavere kvalitet. Derfor er udviklingen af nye genanvendelsesteknologier afgørende for etableringen af en cirkulær økonomi. For nylig er det blevet vist, at visse enzymer kan nedbryde PET. Enzymatisk genanvendelse af PET muliggør fremstillingen af nyt PET af høj kvalitet, hvilket potentielt muliggøre etableringen af en cirkulær økonomi af PET. Den enzymatiske nedbrydningshastighed er dog kraftig påvirket af PET's egenskaber, især graden af krystallinitet (X_C). Da de fleste PET-produkter (plastflasker og tekstiler, m.v.) har en X_C på over 20%, er et forbehandlingstrin påkravet for at opnå en effektiv PET genanvendelse. Denne forbehandling er dog meget energikrævende, hvilket nedsætter bæredygtigheden af den enzymatiske genanvendelse.

Formålet med denne Ph.D. afhandling var at undersøge, hvordan egenskaberne af PET påvirkede den enzymatiske nedbrydning af PET. Til dette formål udviklede vi en standardiseret metode til at styre X_C af PET. Denne metode var baseret på termisk induceret krystallisering af kommercielt tilgængelige amorfe PET ved at holde PET materialet ved 115 ºC. Substratet blev efterfølgende brugt til at undersøge, hvordan forskellige PET-hydrolaser blev påvirket af stigende X_C. Den indledende nedbrydning af PET, kaldet ”lag-fase”, resulterede ikke i dannelse af opløselige produkter. Efter ”lag-fasen” var overstået, blev koncentrationen af opløselige produkter, fra den enzymatiske behandling, frigivet ved en konstant reaktions-rate, kaldet ”steady-state-raten”. Steady-state-raten blev ydermere kraftigt negativt påvirket af X_C. Denne negative effekt var særlig tydelig, når X_C oversteg ~20%. Denne grænse blev dog påvirket af flere faktorer, herunder reaktionstemperaturen, reaktionens omfang og det enzym, der katalyserede reaktionen. Enzymerne LCC, LCC_{ICCG} og DuraPETase blev mindre påvirket af stigende niveauer af X_C sammenlignet med HiC, TfC og PHL7. Denne øgede tolerance skyldtes sandsynligvis en bredere substratspecificitet, hvilket resulterede i højere reaktionshastigheder og maksimale nedbrydningsudbytter ved højere X_C. Ved at studere ”lag-fasen” under den enzymatisk behandling erfaret vi, at varigheden af dette fænomen blev kraftigt forlænget ved stigende X_C (op til 6 dage ved X_C > 20%), og lavere ”steady-state-rater”. ”Lag-fasen” blev derfor tilskrevet et endo-type nedbrydningsmønster, som ikke ville resultere i opløselige produkter, under den indledende fase. Denne mekanisme blev yderligere bekræftet ved at studere frigivelsen af protoner under ”lag-fasen”, hvilket bekræftede at enzymet hydrolyserede PET under ”lag-fasen”.

Derudover undersøgte vi hvordan effekten af glasovergangstemperaturen (T_g) påvirkede enzymets reaktionshastighed. Dette blev gjort ved at sænke T_g for et PET-materiale fra 75 ºC til 60ºC ved at lade det ligge i vand. Ved at måle den enzymatiske reaktionshastighed for disse substrater ved 69ºC (i mellem T_g for de to substrater) opdagede vi, at reaktionshastigheden ikke blev påvirket af den lavere T_g.

List of Publications

The papers listed below can be found in the appendix

Paper I: **Standardized method for controlled modification of poly (ethylene terephthalate) (PET) crystallinity for assaying PET degrading enzymes.**
Thore B. Thomsen, Cameron J. Hunt, Anne S. Meyer
MethodsX **2022** (9) 101815

Paper II: **Influence of substrate crystallinity and glass transition temperature on enzymatic degradation of polyethylene terephthalate (PET)**
Thore B. Thomsen, Cameron J. Hunt, Anne S. Meyer
New Biotechnology **2022** (25) 28-35

Paper III: **Rate Response of Poly(Ethylene Terephthalate)-Hydrolases to Substrate Crystallinity: Basis for Understanding the Lag Phase**
Thore B. Thomsen*, Sune W. Schubert*, Cameron J. Hunt, Kim Borch, Kenneth Jensen, Jesper Brask, Peter Westh, Anne S. Meyer
ChemSusChem **2023** (16) 1-13

Paper IV: **Relationships of crystallinity and reaction rates for enzymatic breakdown of poly (ethylene terephthalate), PET.**
Sune W. Schubert*, Thore B. Thomsen*, Kristine S. Clausen, Cameron J. Hunt, Kim Borch, Kenneth Jensen, Jesper Brask, Anne S. Meyer, Peter Westh
In preparation

Paper V: **A new continuous assay for quantitative assessment of enzymatic degradation of poly(ethylene terephthalate) (PET)**
Thore B. Thomsen*, Sune W. Schubert*, Cameron J. Hunt, Peter Westh, Anne S. Meyer
Enzyme and Microbial Technology **2023** (167) 1101442

Paper VI: **Current knowledge on the effect of substrate crystallinity of Poly(ethylene terephthalate) (PET) on its enzymatic degradation.**
Thore B. Thomsen, Kristoffer Almdal, Anne S. Meyer
Submitted

Paper VII: **Kinetic assessment of the enzymatic degradation of Poly(ethylene terephthalate) (PET) at various degree of crystallinity**
Thore B. Thomsen, Tobias Radmer, Anne S. Meyer
Early draft manuscript

*Contributed equally

Table of Contents

Abbreviations list

ATR-FTIR	Attenuated total reflection Fourier transform infrared spectroscopy
BHET	Bis(2-hydroxyethyl) terephthalate
BHETeq	BHET equivalents
BOPET	Biaxial oriented PET
DuraPETase	Thermostable variant of IsPETase
HiC	*Humicola idulances* cutiase
^{inv}MM	Inverse Michaelis-Menten kinetics
$^{inv}V_{max}$	Maximal reaction rate
IsPETase	*Ideonella sakaiensis* PETase
k_{cat}	Catalytic constant/turnover number
K_M	Michaelis-Menten constant
k_{mix}	Mixing constant (using in the continious assay)
LCA	Life cycle assessment
LCC	Leaf-branch compost cutinase
LCC_{ICCG}	Variant of LCC
MAF	Mobile amorphous fraction
MD	Molecular dynamics
MHET	Mono(2-hydroxyethyl) terephthalate
PET	Poly(ethylene terephthalate)
PET-C	Amorphous PET film casted from PET-P
PET-F	PET film (h=0.25 mm): Goodfellow Cat. No. ES301445
PET-P	Crystalline PET powder: Goodfellow Cat. No. ES306031
PET-S	PET Sheet (h=1 mm): Goodfellow Cat. No. ES303010
PHL7/PES-H1	Polyester hydrolase Leipzig 7
RAF	Rigid amorphous fraction
RMSF	Root-mean-square-fluctuation
RP-HPLC	Reversed-phase high-performance liquid chromatography
SIC	Stress- or Strain-induced crystallization
TfC	*Thermobifida fusca* cutinase
T_g	Glass transition temperature
t_{lag}	Duration of lag phase
TPA	Terephthalic acid
v_{ss}	Steady-state reaction rate
X_C	Degree of crystallization
$X_{C,50}$	X_C corresponding to the 50% of the v_{ss} at amorphous/low X_C PET
X_{MAF}	Fractional composition of MAF
X_{RAF}	Fractional composition of MAF
Γ_{max}	Maximal density of attack sites

Chapter 1: Motivation and Hypotheses

Plastic pollution has become a global environmental threat affecting aquatic and terrestrial ecosystems [1,2]. Despite these growing concerns, the demand for plastics continues to rise, leading to a substantial production of 390 Mt in 2021 (excluding plastic used in textile fibers) [3]. Post-consumer packaging materials, accounting for 78 Mt/year, substantially contribute to plastic pollution due to their short lifespan and poor collection rate [4]. In fact, 32% of all post-consumer plastics products evade the designated collection systems [4], eventually accumulating as plastic pollution due to their resistance to microbial degradation [5,6]. Poly(ethylene terephthalate) (PET), comprising 10% of the annual plastic production [1], plays a significant role as a major contributor to plastic pollution, as it is extensively used in packaging material, plastic bottles, and textile fibers [2,7].

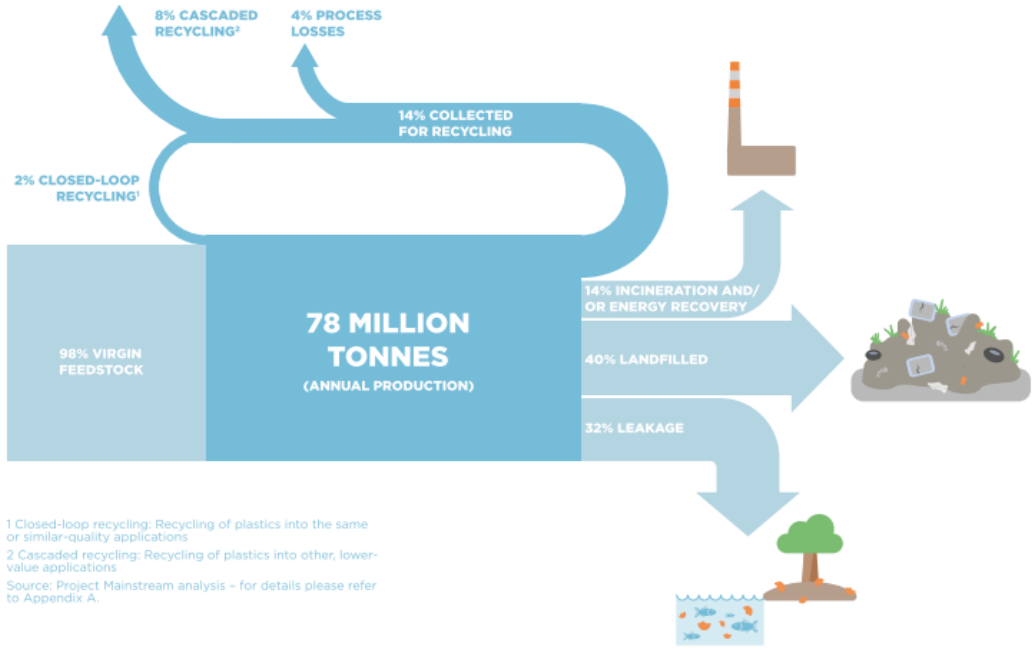

Figure 1.1 – Global flow of plastic packaging material: Sankey diagram illustrating the annual flow of plastics from feedstock to end use (2013 numbers). Notably, 72% of waste products are not effectively utilized, with 40% ending up in landfills and 32% leaking out of the collection system. Of the 14% collected for recycling only 2% attains a quality similar to the virgin feedstock. The remaining 10% is either used in cascade recycling for lower quality products or lost during processing (4%). This figure was originally printed in [4].

Certain enzymes, like cutinases (EC 3.1.1.74), have demonstrated activity against PET in addition to their natural substrates [8–11]. This pivotal discovery has paved the way for enzymatic recycling of plastics. In this process, enzymes break down PET into its constituent monomeric building blocks, which then serve as the feedstock for the synthesis of new PET with properties equivalent to virgin PET [12–14]. Hence, this enzymatic recycling process enables the establishment of a closed-loop circular economy, as the quality of the recycled PET, unlike conventional recycling methods, is maintained. Furthermore, the degradation products obtained from enzymatic degradation can be utilized in other applications[15].

However, the enzymatic degradation of waste PET faces a significant challenge due to its inability of degrade crystalline PET effectivity [12,16–18]. As most PET products possess a high degree of crystallinity (X_C) [18,19], a highly energy-intensive pretreatment step

involving extrusion and micronization becomes necessary for efficient enzymatic degradation of waste PET [12,20]. Overcoming this bottleneck would consequently reduce the energy demand and the production costs of enzymatic recycling of PET [20]. Therefore, the identification of efficient enzymes capable of degrading the crystalline region of PET is crucial to unlocking the full potential of enzymatic recycling of PET.

The overarching goal of this Ph.D. thesis is to enhance our understanding of the enzymatic degradation of semi-crystalline PET by investigating the interplay between enzyme and substrate. This research was guided by the following hypotheses:

H1 *"The X_C of PET material can be systematically controlled through thermal annealing, enabling the creation of a standardized substrate for evaluating the impact of the X_C on the enzymatic hydrolysis of PET"*

H2 *"Enzymatic reaction conducted at temperatures above the T_g of PET will significantly enhance the hydrolysis rate due to increased substrate chain mobility. Lowering the T_g of PET material, using water as a plasticizing agent, will consequently increase the activity of PET degrading enzymes."*

H3 *"The tolerance of enzymes towards increasing X_C of the substrate is different between enzymes. Hence, the tolerance towards X_C may be used as a selection criterion for identifying enzymes with enhanced activity on more crystalline PET"*

H4 *"The tolerance towards substrate X_C* can be attributed to the relative specificity of an enzyme towards X_C, X_{RAF}, or *X_{MAF}"*

H5 *"The initial degradation of crystalline PET is facilitated by an endo-type degradation pattern"*

To ensure that the experimental data collected throughout this thesis would be sufficient to test the five hypotheses, the following objectives were formulated:

Obj. 1 Development of a standardized methodology for altering substrate X_C via thermal annealing. The annealed PET substrate is subsequently used as a model substrate for evaluating the impact the X_C on the enzymatic degradation of PET.

Obj. 2 Investigate how substrate properties (X_C and T_g) are affected during the soaking of PET in water. Assay PET substrate with different T_g, obtained via soaking, to determine the product release rate, and establish correlations with optimal conditions.

Obj. 3 Perform a comparative characterization of the influence of increasing X_C on the enzymatic degradation of PET by several benchmark PET degrading enzymes.

Obj. 4 Propose a degradation mechanism for the enzymatic degradation of semi-crystalline PET by combining the results of various analytical methodologies, including product profiling, surface erosion, and kinetics.

Chapter 2: Introduction

PET is a synthetic polyester composed of repeating units of terephthalic acid (TPA) and ethylene glycol (EG) linked together via ester bonds. PET is a versatile material used in packaging material, plastic bottles, film/coatings, and textile fibers. This is due to its desirable physical and chemical properties, including minimal gas permeability, and low production costs [5,21]. The first patent for the production of PET was filed in 1941 [22]. However, it was not until 1973 that PET began to be used for bottle containers [23], which eventually led to a significant contribution to plastic pollution [2]. Currently, the global production of virgin PET, meaning that it has not previously been recycled, is roughly 75 Mt/year. Of this, 49 Mt/year are used in textile fiber manufacturing, constituting a substantial 45% share of all textile fibers produced [24]. The remaining 26 Mt/y of PET are used in other applications such as plastic bottles, contributing to 6.2% of global plastic production (excluding both textile fibers and recycled plastics) [3].

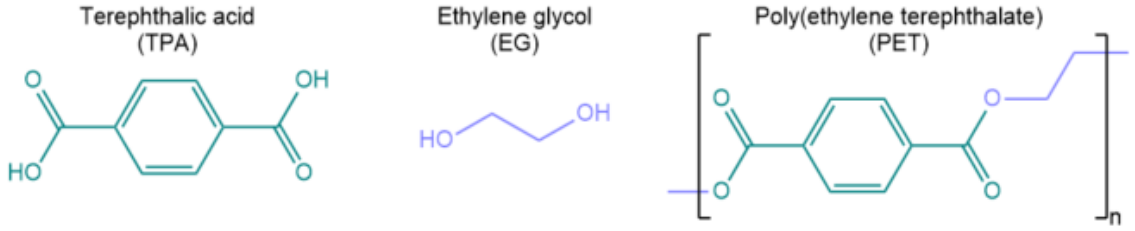

Figure 2.1 – Molecular structure of PET and its constituting monomers

2.1 Structure and morphology of PET

In its molten state, exceeding its melting temperature of 260°C, the polymer chains of PET undergo a transition into an amorphous disordered random coil state. This state is characterized by high flexibility and well-entangled structures. The density of the entanglements may be quantified in terms of the molecular weight of entanglement (MWe). This parameter represents the molecular weight between two entangled chain segments, typically ranging from 1450 to 2120 g/mol for PET[25]. This range corresponds to an entanglement at every 7.5 to 11 repeating units (MHET) of a PET chain.

Upon rapid cooling of the polymer melt below the glass transition temperature (T_g), which is 75°C for amorphous PET [16], the amorphous state of the polymer chains is preserved in the solid state. However, solid PET can also exist in a semi-crystalline state, where it comprises both highly-ordered crystalline regions and amorphous regions [26,27].

2.1.1 Crystalline regions

During the crystallization process, at which the semi-crystalline state is formed, amorphous PET chains undergo a conformational transition from a *trans-gauche-trans* to a linear all-*trans* conformation. Although this linear all-*trans* conformation is energetically less favorable for the free chain, it is stabilized by inter- and/or intramolecular π/π stacking of the aromatic rings of the TPA moieties [28]. Consequently, an increase in X_C leads to a decrease in gauche conformations [29,30].

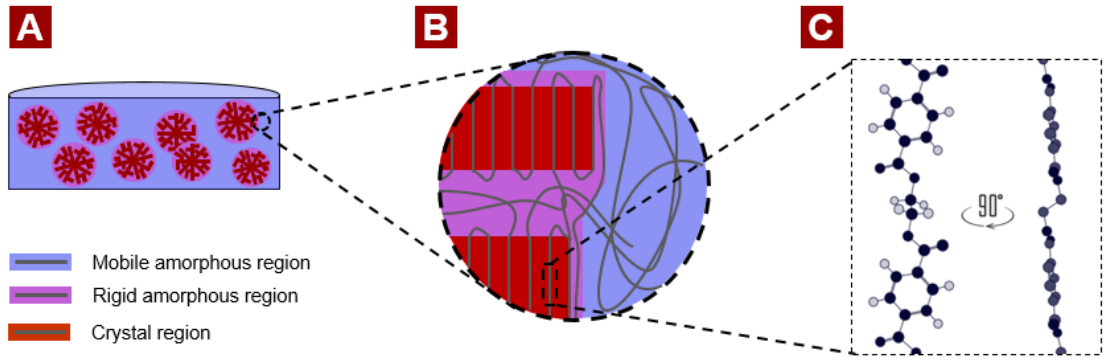

Figure 2.2 – Schematic overview of the microstructures within PET: A) Cross-sectional representation of transection of a semi-crystalline PET, illustrating the distribution of crystalline spherulites. The size and distribution of the spherulites are for an illustrative purpose. B) Schematic representation of the disordered amorphous regions and the highly ordered crystalline lamella. The PET crystals are composed of the crystalline lamella (red) separated by rigid amorphous regions (magenta), while the MAF (blue) surrounds the spherulites. C) Unit cell structure (This *trans* confirmation) of a PET crystal viewed at two different angles. The figure has been adapted from a figure originally presented in Paper VI.

The unit cell structure of PET crystals has been extensively studied, revealing a triclinic shape [31]. However, the specific unit cell parameters of PET crystals are not universal, as they strongly depend on the crystallization and manufacturing process. Factors such as crystallization temperature, draw ratio, and subsequent annealing temperature and duration have been found to influence these unit cell parameters [31]. The unit cell structure of a PET crystal is displayed in Figure 2.2C.

Inside PET crystals, polymer chains are organized in densely packed lamellae structures. These crystalline lamellae are separated by amorphous regions and are interconnected by PET chains known as tie molecules. These tie molecules are bridging the crystal-amorphous interface, as they exist in both phases [26]. Moreover, the crystalline lamellae form higher-level structures that depend on the crystallization process. Thermally-induced crystallization of PET manifests as highly branched spherulites (bulk crystals) or micelles (surface crystals) [27,32,33]. A schematic representation of the spherulite structures is illustrated in Figure 2.2A. The temperature dependence of the crystalline structures was investigated by Shinotsuka et al. [34] using *in situ* Atomic Force Microscopy (AFM) during the annealing of spin-coated PET films (up to 680 nm thickness). The study showed that surface crystals began to form at 70°C, while crystal formation initiated at 85°C. No bulk crystals were observed in films thinner than 10 nm within the temperature range of 50 to 190°C [34]. The size of these crystal structures is moreover influenced by the annealing temperature, with larger crystals formed at higher temperatures [33,35]. As the X_C increases, thermally annealed PET samples become more opaque due to light scattering caused by the crystals [36].

Unlike the spherical shape of the thermally induced crystals, those formed via stress- or strain-induced crystallization (SIC), such as BOPET or blow molted PET bottles, contain elongated rod-like or fibrillary structures [37]. These structures occur as the lamellae in SIC align in the direction of the applied strain, while those in thermally induced crystals are randomly oriented [38]. The crystal size in PET samples subjected to SIC is smaller

compared to thermally induced crystals. As a result, highly crystalline PET that has undergone SIC may appear transparent due to the small crystal size [39].

2.1.2 Amorphous regions

The amorphous phase of PET can be subdivided into two distinct fractions: the mobile amorphous fraction (MAF) and the rigid amorphous fraction (RAF). The MAF encompasses the amorphous regions residing between distinct crystal structures, as depicted in Figure 2.2A, whereas the RAF surrounds the crystalline lamella, such as the interlamellar spacing within PET crystals as illustrated in Figure *2.2*B. Hence, the RAF content in a PET sample generally increases with the X_C, while the MAF content decreases [39–41]. The RAF and MAF content in a PET sample are also affected by the crystal morphology [42]. For instance, the RAF content in biaxially oriented PET (BOPET) film, which is often used as packaging material [43], is higher than in thermally annealed PET, despite both samples having similar X_C [38]. Due to the molecular connection between the RAF and the rigid crystal lamellae, the mobility of the RAF is more restricted compared to the MAF. Consequently, it is only the MAF that transitions into a mobile rubbery state when heated above its T_g value, a process known as devitrification, as the RAF remains in the rigid glassy state [40]. Instead, RAF is believed to fully devitrify at 200°C [44]. The T_g of PET can be influenced by several factors, including the addition of additives to the polymeric material [45] or by the absorption of water or other molecules, which have a plasticizing effect on PET [46,47]. Consequently, the T_g of a PET sample may be lowered to as little as 60°C when exposed to water [16].

2.2 Crystallization of PET

When PET is heated above its T_g the mobility/energy of the polymeric chains in the amorphous state becomes sufficient for crystallization to occur. This process is known as thermal-induced crystallization [35]. PET may therefore crystallize when it is slowly cooled from the molten state or when it is held at temperatures above T_g (known as annealing). This crystallization process is, as previously stated, quenched by rapidly cooling the material to a temperature below its T_g. The rate at which the crystallization occurs increases with temperature until it reaches its maximum at 174°C [48]. Below T_g, the crystallization of PET is limited due to restricted chain mobility, while excessive chain mobility resulting from high temperatures (>174°C) leads to a decrease in the crystallization rate [35]. Other factors, such as moisture content [49] and molecular weight [50], have also been shown to influence the crystallization of PET.

The crystallization of PET material is characterized by two distinct stages: nucleation and crystal growth. During nucleation, amorphous PET chains align to form nuclei, which act as starting points for the development of new crystals. Subsequent to nucleation, crystal growth occurs, which can be further subdivided into primary and secondary crystallization. Primary crystallization involves the growth of heterogeneous crystal structures (i.e. spherulites), resulting in an increase in X_C and the fractional composition of RAF (X_{RAF}). In contrast, secondary crystallization occurs within the boundaries of existing crystal structures and involves the thickening of lamellae structures or the formation of new

lamellae, resulting in an increase in X_C and a decrease in the frational composition of MAF (X_{MAF}) [51].

The crystallization of PET may also be induced mechanically, under SIC where the material typically undergoes stretching at temperatures above T_g [39]. The extent of crystallization induced by SIC increases with higher temperatures and strain rates [52]. This Increased crystallinity resulting from SIC can lead to improvements in the mechanical properties of PET, including higher modulus, toughness, stiffness, tensile strength, and hardness [53]. Consequently, SIC is widely used during the processing of several PET products, such as blow-molded PET bottles, textile fibers, and oriented films, to obtain the aforementioned improvements [54].

As the crystallization of PET may be induced both thermally and mechanically, the X_C of PET material is strongly influenced by its processing history. This may even result in a non-uniform distribution of X_C throughout the material, as exemplified by the case of a PET bottle. Here the finish/neck and base center exhibited lower X_C (1.2% and 11.7%, respectively) compared to the rest of the bottle (>25%) [18].

2.2 Conventional recycling of PET

PET is a thermoplastic, capable of being melted and recast into new material, as no covalent interactions are formed during the processing of the material [55]. This property has enabled the conventional thermo-mechanical recycling process of PET, where waste PET is ground into flakes, and subsequently washed and cleaned using 2-3% NaOH as well as detergents. The cleaned PET flakes can then be re-meted or re-extruded into new PET products [56]. However, there are drawbacks associated with the conventional method. Firstly, not all PET products can be recycled using this process. Textile blends, such as cotton and polyesters, which are found in the majority of fabrics [57], are especially challenging to recycle this way, limiting the effectiveness of conventional recycling in reducing plastic pollution [58]. Secondly, conventional recycling methods often result in lower-quality materials compared to virgin PET. This is primarily due to impurities introduced during the recycling process and thermomechanical degradation [21,59]. Recycled PET from conventional methods may therefore not be suitable for all PET applications [56]. Consequently, the majority of PET is still derived from virgin PET, although the recycling rates are increasing [3].

The predominant method for producing virgin PET involves synthesizing it from petroleum-based precursors [60]. As a result, the largest contributor to the environmental burden caused by PET products is the use of raw materials, as highlighted in a recent life-cycle assessment (LCA) of plastic bottles. This LCA found that as much as 84% of the environmental burden of PET bottles was caused by the production of virgin PET (newly synthesized PET) [61]. Therefore, the development of novel technologies is essential to improve the recycling rates and enhance the displacement potential (quality of the recycled product) of PET, which is crucial for establishing a truly circular economy [62,63].

2.3 Enzymatic recycling of PET

Despite being a synthetic polymer, generally considered to be resistant to microbial degradation, Müller et al. demonstrated in 2005 that the hydrolase TfH (later classified as a cutinase [64]) from *Thermobifida fusca* was capable of degrading PET at a decent rate [14]. Later in 2016, researchers isolated an organism, *Ideonella sakaiensis*, from PET-contaminated soil, which was capable of utilizing PET as its carbon source, under mesophilic conditions, using a dual enzyme system [65]. These discoveries have led to a completely new starting point for the development of an enzyme-mediated recycling process of PET.

Enzymatic recycling of PET involves breaking down PET into its constituent monomers (TPA and EG). The resulting degradation products from enzymatic PET recycling can therefore be used to synthesize new virgin PET, contributing to the establishment of a circular economy for PET [13]. Alternatively, the degradation products may be used as feedstock in other applications, thus offering an alternative route for waste PET (upcycling) [66,67]. PET degrading enzymes may also enable the recycling of polyester fibers in mixed textile blends, as they can specifically target these fibers alone [57,68].

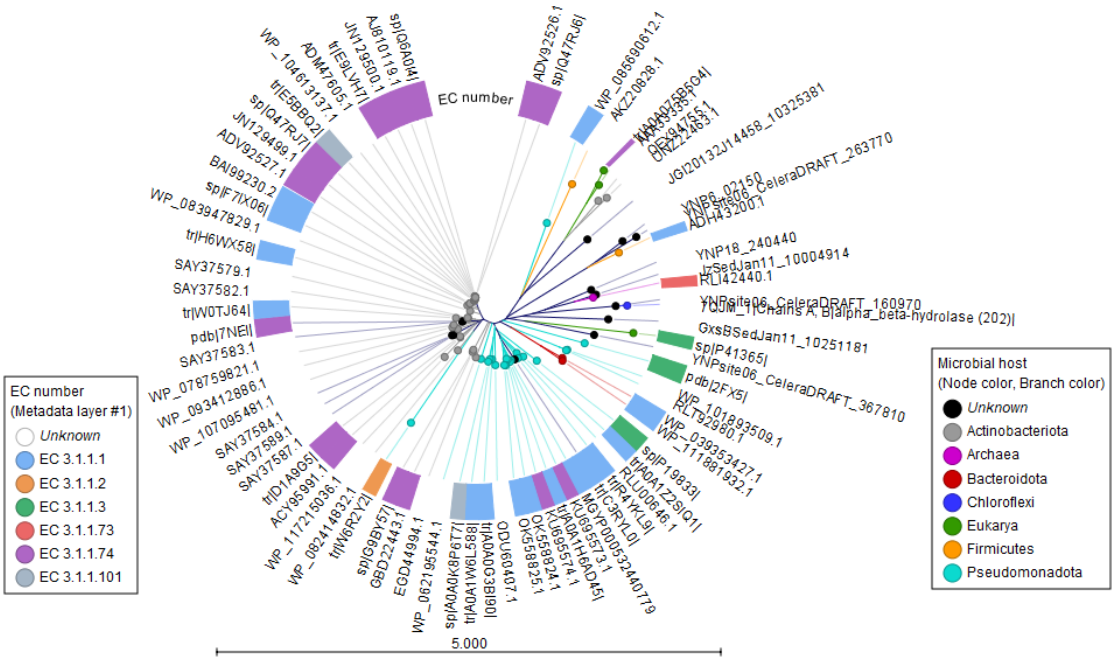

Figure 2.3 – Phylogenetic tree displaying all PET degrading enzymes: The phylogenetic tree was built based on multiple alignment of all entries from the PaZy database. The branch and note color represent the microbial host, while the color of the surrounding layer represents the EC number. This Figure was originally presented in Paper VI.

2.3.1 PET degrading enzymes

Numerous enzymes from various enzyme classes and microbial species have already been identified as PET-degrading enzymes. While the majority fall into the categories of cutinases (EC 3.1.1.47) [69–71] or carboxylesterases (EC 3.1.1.1) [64], specific arylesterases (EC 3.1.1.2) [72] and lipases (EC 3.1.1.3) [73] have also shown activity on PET. Notably, a newly recognized enzyme class termed PETase (EC 3.1.1.101) [74]

emerged from the discovery of Ideonella sakaiensis enzyme, IsPETase. Despite its unique EC number, the IsPETase shares structural similarities with other PET-hydrolyzing bacterial cutinases [75,76]. These enzymes are found across a wide range of microbial organisms, including archaea[77], fungi such as the well-studied *Humicola insolens* cutinase (HiC) [70,78,79], and cutinases derived from Fusarium spp.[80]. An overview of all characterized PET-degrading enzymes is visualized in the phylogenetic tree in Figure 2.3. This tree was constructed based on the entries from the PaZy database [64]. From this phylogenic tree, it is evident that the majority of the currently characterized PET-degrading enzymes originate from Actinobacteriota or Pseudomonadota phyla.

2.3.2 State-of-the-art enzymes

Currently, the most promising candidates for the enzymatic degradation of PET are using the Leaf-branch compost cutinase (LCC) as a scaffold for engineering [12,81]. LCC was initially discovered within the metagenomics of a leaf-branch compost in Japan, having a temperature of 67°C at the time of sampling, making its enzymes prone to withstand elevated temperatures [11]. In 2020 Tournier et al reported a quadruple variant of LCC, namely LCC_{ICCG}, which was engineered towards increased activity (F243I) and stability (D238C/S283C and Y127G). Remarkably, this enzyme was capable of archiving a 90% depolymerization of amorphous PET particles within 10 hours of enzyme treatment[12].

Similarly, another promising enzyme was recently isolated from the metagenomics of a compost site near Leipzig. This enzymes was named PHL-7 (Polyester hydrolase Leipzig 7)[82] or PES-H1 (Polyester hydrolase 1)[83]. A double variant of this enzyme (L92F/Q94Y) showed higher activity than LCC_{ICCG} on low crystalline PET (< 15%), while the activity was substantially lower on a high crystalline PET sample (33%) [83].

The most extensively studied PET hydrolase, the *Is*PETase, was, as previously mentioned, isolated from the PET-utilizing bacterium *Ideonella sakaiensis*. Unlike other benchmark cutinases that have been isolated from metagenomics at temperate environments[11,82] or from thermophilic organisms[71], the IsPETase was discovered in a mesophile organism. Surprisingly, *Is*PETase outperformed cutinases, including LCC, at 30°C, which was attributed to the mesophilic nature of *Ideonella sakaiensis*[65]. As the thermostability of this enzyme was significantly lower than the other cutinases, several attempts have been made to increase the stability and/or activity of this enzyme[18,76,84–88]. This includes, amongst others, the engineered variant named DuraPETase, containing 10 mutations (S214H-I168R-W159H-S188Q-R280A-A180I-G165A-Q119Y-L117F-T140D). This led to a 31°C higher T_M and 300-fold higher activity (at optimal conditions) compared to the wild type [85]. Other noteworthy examples include the FastPETase[18] and HotPETase[87].

2.3.3 Generalized degradation mechanism of PET degrading enzymes

During the enzymatic degradation of PET, the insoluble polymeric chains undergo hydrolysis, resulting in the formation of smaller soluble products. These degradation products primarily include ethylene glycol (EG), terephthalic acid (TPA), mono(2-hydroxyethyl) terephthalate (MHET), and bis(2-hydroxyethyl) terephthalate (BHET) [13,86]. Additionally, larger oligos containing two or more aromatic rings (OETs) have also

been observed [73,89,90]. Interestingly, several PET-degrading enzymes have been found to have activity towards these soluble products, including BHET and MHET [79,91]. This adds complexity to the degradation mechanism, as the presence of degradation products in the reaction media may potentially inhibit the activity of PET-degrading enzymes towards the insoluble substrate [91].

Given the intricate nature of the PET enzymatic degradation process, the precise mechanism by which PET hydrolases degrade the insoluble PET chains remains unclear [92]. However, through an analysis of the chain length distribution using MALDI-TOF and surface chemistry via X-ray photoelectron spectroscopy (XPS) of enzyme-treated PET, Eberl et al. proposed that enzymatic PET degradation involves random endolytic chain scission. This proposition was supported by an increase in smaller insoluble fragments (with fewer than 11 TPA moieties) and an induction of surface polarity upon enzymatic treatment of PET[93]. The increased polarity resulted from the exposure of carboxylic acid groups from partially degraded PET chains.

The work by Eberl et al. also showcased variations in degradation patterns between two PET-degrading enzymes, with one (*T. fusca* cutinase) releasing more soluble products and the other (*T. lanuginosus* lipase) accumulating smaller insoluble fragments [93]. A more comprehensive investigation into the reaction pathway of PET-degrading enzymes was later conducted by Schubert et al., who employed stochastic modeling to track the evolution of product profiles during enzymatic treatment. This study quantified the preference for endo- or exo-type chain scission in four different PET hydrolases, revealing that efficient PET-hydrolases have an increased a tendency for endo-type degredation. [90].

In this particular context, endo-type chain scission was defined as the hydrolysis of an insoluble PET chain, leading to the formation of two smaller insoluble chains. Consequently, this results in a significant decrease in the degree of polymerization (DP) of the PET chains exposed to the surface of the insoluble substrate. Additionally, the surface charge of the substrate becomes more negatively charged, due to the exposure of a carboxylic acid group at the new terminal of the hydrolyzed chain. On the other hand, exo-type chain scission refers to the hydrolysis of an insoluble PET chain leading to the formation of a soluble product, such as MHET. In this case, the surface charge is unchanged, while the DP of the surface chains is only slightly reduced [93].

Wei et al. hypothesized a degradation mechanism that accounts for both the crystalline and amorphous regions of PET [17]. Their hypothesis proposed that the mobile amorphous regions (MAF) could undergo degradation through both endo and exo-type chain scission, whereas the rigid amorphous regions (RAF) and PET crystals would only be susceptible to endo-type scission. This deduction was drawn from an analysis of the molecular weight distribution of PET samples treated with enzymes [17].

2.3.4 Milestones within enzymatic recycling of PET

A historical overview of the key milestones which has led to the industrial viable enzymatic recycling of PET is provided in Figure 2.4. This underscores the swift progress within this field, despite the relatively short duration PET has been a prominent environmental concern. The timeline spans from the patent filling of the production of PET in 1941 [22] until the first operational industrial plant for the enzymatic recycling of PET, which is expected to occur in 2025 [94].

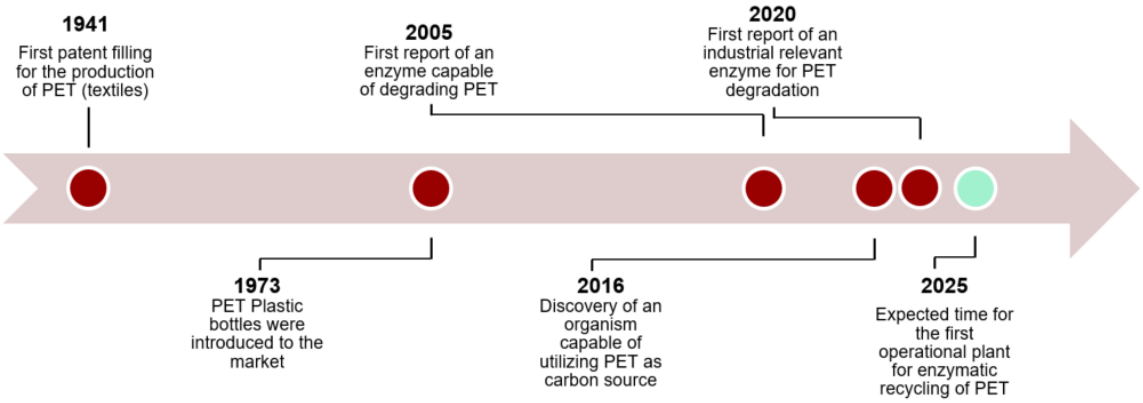

Figure 2.4 – Key milestones for enzymatic recycling of PET: Timeline highlighting selected milestones in the enzymatic recycling of PET [12,14,22,23,65,94]. The spacing between each dot corresponds to the duration of time between the events. Red dots present past events, while the green dot signifies an event expected to occur after the time frame of this thesis.

Chapter 3: Methodology for Evaluating the Effect of X_C

The crystal size and morphology of PET are highly influenced by its crystallization process [33,37]. Consequently, addressing the impact of substrate crystallinity on PET degrading enzymes using PET substrates processed in various ways may introduce bias, as differences in crystal morphology may add an additional dimension to the influence of X_C. At the beginning of this Ph.D. project (July 2020), no standardized method had been published for generating a model substrate suitable for quantifying the effect of X_C on PET-degrading enzymes. The aim of the chapter was therefore to test the first hypothesis, **H1**, of the PHD:

"*The X_C of PET material can be systematically controlled through thermal annealing, enabling the creation of a standardized substrate for evaluating the impact of the X_C on the enzymatic hydrolysis of PET*"

The following sections in this chapter are mainly based on the content of Paper I but also include data from Paper II and III, and describe an experimental platform developed in this thesis for systematically evaluating the effect of X_C on the enzyme degradation of PET. This platform is based on the model substrate obtained via thermal annealing, as specified by **Obj. 1**. An overview of the method is illustrated in Figure 3.

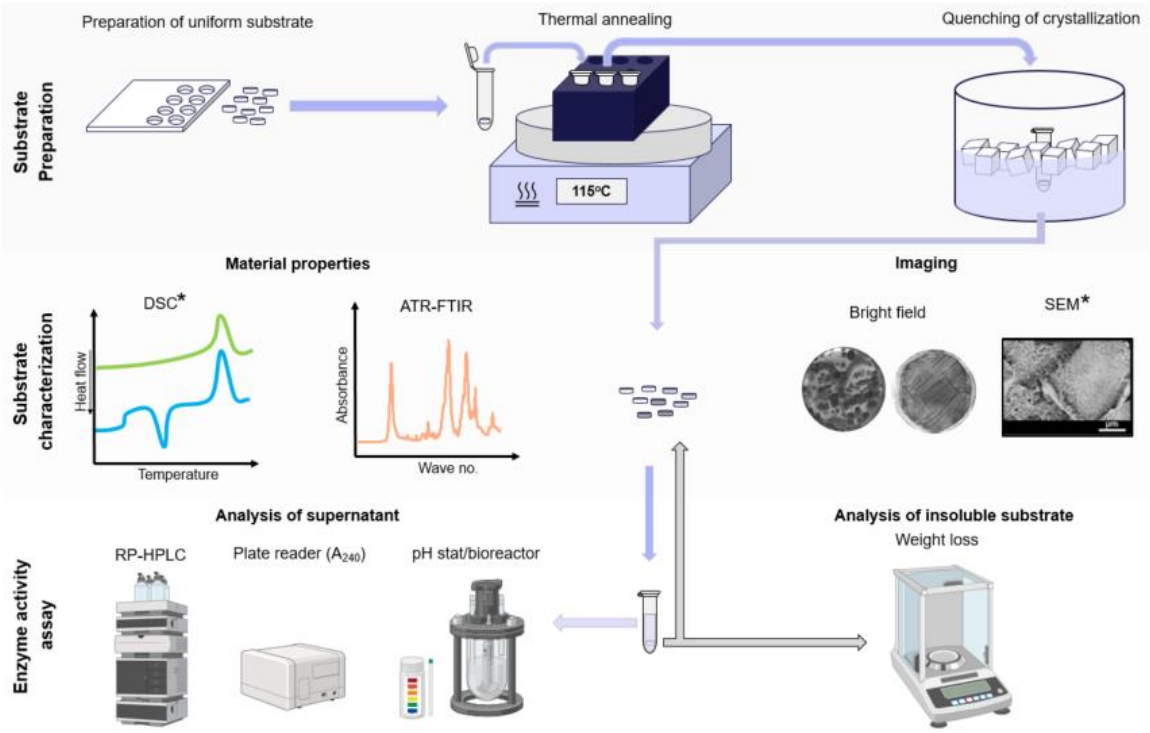

Figure 3.1 Workflow for the modification of substrate crystallinity – Blue arrows represent processes leading to PET substrates at various X_C. * Destructive methods. The PET substrate may therefore be used in a subsequent process. Images from the lower panel are from Biorender. Figure adapted from Paper I.

3.1 Substrate preparation by annealing

The crystallization of PET material occurs, as previously mentioned, when the material is held at temperatures above its T_g value. This property was utilized to generate PET

substrate at various X_C. Commercially available amorphous or low crystalline (<10% X_C) PET film or sheet was used as the starting material. The model substrate with controlled X_C was prepared by the following procedure were followed: The PET material was cut into uniform disks using a generic hole puncher, and placed in a 2 mL Eppendorf tube. The Eppendorf tube(s) containing up to three PET disks were then subjected to annealing at 115 °C for a specified duration (in minutes), by placing the PET-containing Eppendorf tubes in a heating block. The crystallization process was quenched by transferring the Eppendorf tube(s) into an ice water bath.

The amorphous polymeric chains in the “glassy”-state are not at a thermodynamical equilibrium when immediately quenched from melt. Hence, they gradually approach an equilibrium state, resulting in both micro and macroscopic changes in the material. This process is known as enthalpy relaxation or simply physical ageing and is dependent on both time and temperature [95]. This process may however be evoked by heating the material above its T_g [96]. We therefore annealed the “untreated” samples at 85 °C for 5 minutes to eliminate any enthalpy relaxation resulting from polymer aging.

3.2 Substrate characterization

3.2.1 DSC analysis

The most widely used method for quantifying the X_C of PET is by differential scanning calorimetry [97]. During a DSC measurement, a sample and a reference (blank) are heated at a constant rate (typically 10 °C min^{-1} for PET [29]) over a defined temperature range. The sample heat flow required to maintain the constant heating rate, which is proportional to the heat capacity of the sample (C_p), is then monitored over the defined temperature range. DSC can therefore be used to quantify the thermal properties of a material, as these affect the C_p at a given temperature [98]. This includes the change in enthalpy (ΔH) at the cold crystallization (ΔH_{cc}), and melting (ΔH_m). These enthalpies are determined by the crystallinity, and hence the X_C of a PET sample may be calculated according to equation 3.1:

$$X_C = \frac{\Delta H_m - \Delta H_{cc}}{\Delta H_m^0} * 100 \quad (3.1)$$

Here, ΔH_m^0 is the enthalpy of melting of a pure crystalline sample, which according to the literature is 140 J/g [99].

X_{MAF} can also be quantified by DSC. This is done by dividing the increase in specific heat capacity at the T_g ($\Delta c_{p(m)}$), with the expected increase in heat capacity at T_g of a purely amorphous sample ($\Delta c_{p(a)}$) [100], as shown in equation 3.2:

$$X_{MAF} = \frac{\Delta c_{p(m)}}{\Delta c_{p(a)}} * 100 \quad (3,2)$$

X_{RAF} can be calculated according to equation 3.3:

$$X_{RAF} = 100 - X_{MAF} - X_C \quad (3.3)$$

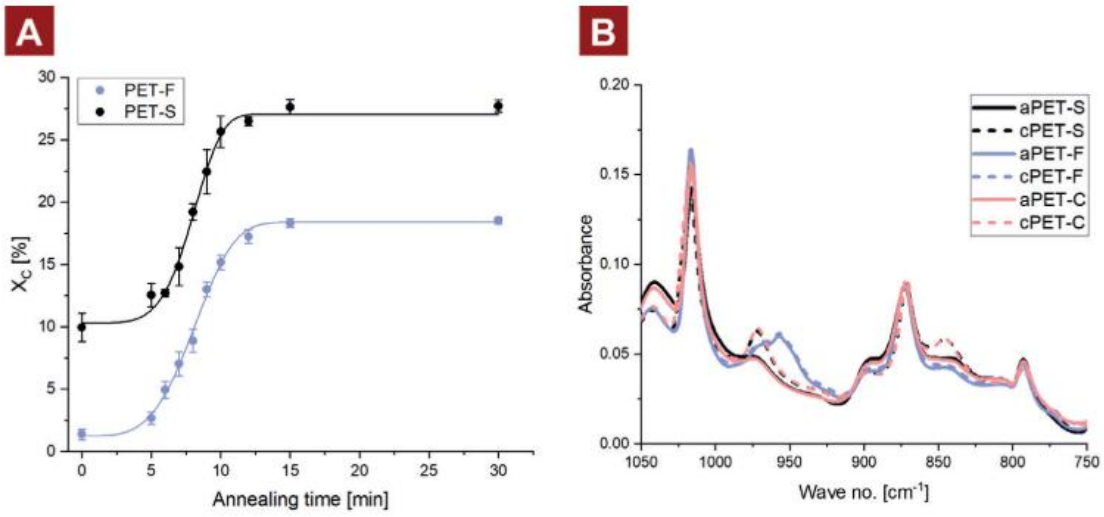

Figure 3.2 – Change in X_C and ATR-FTIR spectrum of PET material after thermal annealing: A) Changes in X_C (measured by DSC) as a function of annealing time for two commercially available PET samples; Goodfellow Cat. No. ES303010 (PET-S) and Cat. No. ES301445 (PET-F). B) ATR-FTIR spectrum of various PET materials, including PET-S, PET-F, and PET powder (Goodfellow Cat. No. ES306031) cast into an amorphous film (PET-C). The materials were either untreated (aPET) or crystallized by 30 annealing at 115°C (cPET). This figure was originally published in Paper I.

The increase in X_C, measured by DSC, as a function of annealing time at 115°C, are shown for two commercially available "amorphous" PET samples is displayed in Figure 3.2A. The starting materials used for the annealing were a 1 mm PET sheet (Goodfellow Cat. No. ES303010), referred to as PET-S, and a 0.25 mm PET film (Goodfellow Cat. No. ES301445), denoted as PET-F. From Figure 3.2A it was evident that the X_C of the untreated materials significantly differed, with PET-S having a X_C of ~10%, while PET-F was ~2%. Notably, the data also revealed that the X_C saturated at different levels ~17% for PET-F and ~27% for PET-S. It has previously been found that the

Although DSC is the most commonly used method for quantifying the X_C of PET material, it has its disadvantages. Especially for characterizing PET used for enzymatic degradation. This is mainly due to the following reason: The calculated values represent an average of the entire sample (bulk), however, as enzymatic degradation of PET is an interfacial process, the bulk values may deviate from the surface. This would be true for PET samples with surface crystals, which are formed at lower temperatures [34].

3.2.2 ATR-FTIR analysis

An alternative method for measuring the X_C of a PET sample is using Fourier Transform Infrared (FTIR) spectroscopy [96,101]. This technique utilizes the absorption of IR radiation caused by molecular vibrations. FTIR can is therefore used to characterize the molecular properties of a sample, as the molecular composition (e.g. functional groups) and their conformation (e.g. *gauche*/*trans*) as the vibrational characteristic of these differs in their IR absorption [102]. As the crystallization process of PET involves a reduction in *gauche* conformers and an increase in *trans* conformers, FTIR has previously been used to quantify the X_C as a ratio between the absorbance of the *gauche* (898 cm^{-1}) and *trans* (973 cm^{-}1) conformers of ethylene glycol [96,101].

Here, Attenuated Total Reflection (ATR)-FTIR is especially useful for analyzing the surface as the reflection of a material is measured at a penetration depth of typically 0.5–5 µm [102]. ATR-FTIR is, unlike DSC, a non-destructive method. Therefore, it can be used before enzyme assays or other analytical measurements, as highlighted in Figure 3.1 The annealed PET disk may therefore be analyzed by ATR-FTIR, as a supplement to DSC, to investigate the presence of surface crystals.

The ATR-FTIR spectra of thermally annealed (heated for 30 min at 115 °C), and untreated PET disks are shown in Figure 3.2B. The starting material of these are PET-S, PET-F, or a casted sheet (PET-C) made from melted PET particles (Goodfellow Cat. No. ES306031). As expected, the absorbance of PET-S and PET-C increased in intensity at 973 cm^{-1}, while they decreased in intensity at 989 cm^{-1}, upon annealing of the samples. In contrast, the spectrum of PET-F exhibited a distinguishing feature not present in the other samples, which was a peak at 955 cm-1. This irregularity was attributed to a possible presence of impurities in the PET film, although such information could not be provided by the supplier. Furthermore, no change in FTIR spectrum was observed between the untreated and annealed PET-F samples, despite the notable increase in X_C measured by the DSC (Figure 3.2A). For this reason, PET-S was recommended as the standardized substrate for the methodology presented in this chapter.

Although it was clear that the ratio of *trans* and *gauche* conformers, quantified as A_{973}/A_{898}, increased during annealing, the value itself is arbitrary in relation to the composition of the microstructures in PET (i.e. X_C). The A_{973}/A_{898} of all PET-S disks annealed at various time points were therefore plotted against the X_C (Figure 3.3A) or X_{MAF} (Figure 3.3B), which subsequently was measured by DSC.

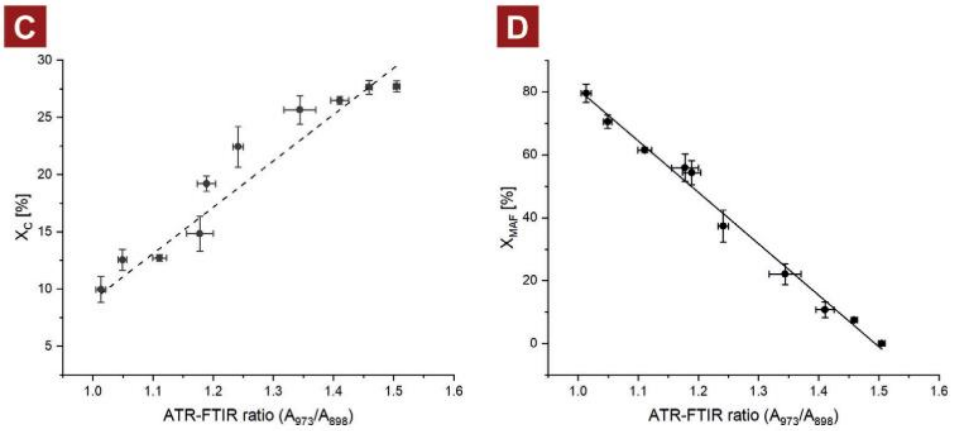

Figure 3.3 – Correlation between A_{973}/A_{898} ratio with X_C and X_{MAF}: Correlation between the A_{973}/A_{898} and A) X_C or B) X_{MAF}. X_C and X_{MAF} were measured by DSC on the same disk used for ATR-FTIR. While a linear correlation exists between A_{973}/A_{898} and X_{MAF} (represented by a solid regression line), a non-linear correlation was observed between A_{973}/A_{898} and X_C (represented by a dashed regression line). This figure was originally published in Paper I.

The relationship between X_C and the A_{973}/A_{898} of PET-S was found to be non-linear (linear model $r^2 = 0.96$) as shown in Figure 3.3A. However, a linear correlation ($r^2 = 0.99$) was observed between X_{MAF} and the A_{973}/A_{898}, as depicted in Figure 3.3B. These findings support the presence of the *gauche* conformation exclusively in amorphous PET (with a majority in X_{MAF}), while *trans* conformers are present in both the amorphous and crystal

regions [100]. Therefore, ATR-FTIR can serve as a non-destructive method for directly quantifying the X_{MAF} of thermally annealed PET-S samples before enzymatic treatment:

$$FTIR\ ratio = \frac{A_{973}}{A_{898}} \propto X_{MAF} \tag{3.4}$$

3.2.3 Surface imaging

The enzymatic degradation of PET is known to occur at the surface of a PET material, thus coursing a change in the surface topography. This effect has been widely studied using amorphous PET substrate [82,103]. By using one large particle (disk) as a substrate, the surface erosion caused by the enzymatic degradation of PET substrates at various X_C could be evaluated throughout a degradation time course, as the substrate can easily be removed from the reaction vessel. Scanning electron microscopy (SEM) imaging of crystalline PET material at 23.3% X_C revealed that the degradation of more crystalline PET resulted in certain areas which were seemingly untouched during the enzymatic degradation. These untouched regions resulted in what appeared a porous surface erosion (see Figure 3.4). A more detailed discussion of the change in topography resulting from the enzymatic treatment of semi-crystalline PET is presented in Chapters 4 and 5.

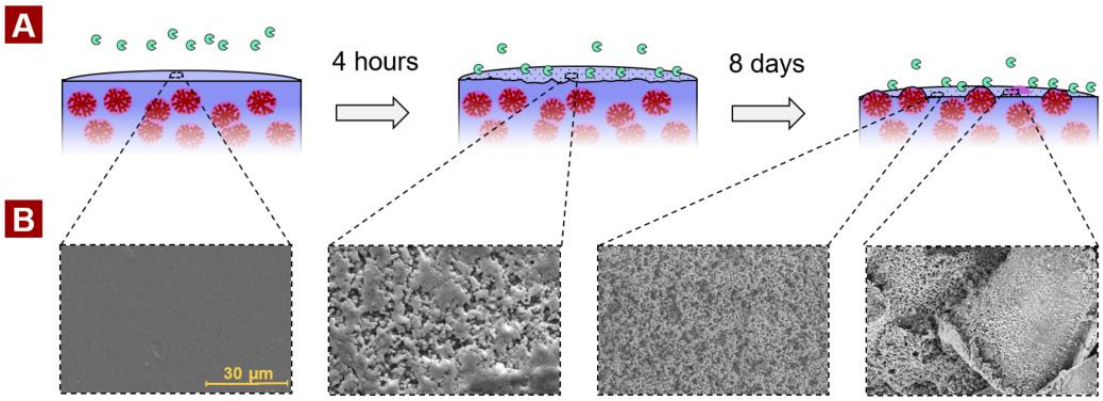

Figure 3.4 – Evolution of surface erosion of semi-crystalline PET disk during enzymatic treatment: A) Schematic representation of the surface erosion on a PET disk during enzymatic treatment B) Scanning electron microscopy (SEM) images of the surface erosion caused by enzymatic treatment of an annealed PET disk (X_C = 23.3%) using LCC_{ICCG}. The first three images are from Paper II, while the last image is from III. The figure was originally published in Paper VI.

3.3 Enzyme activity assaying

Several methods exist for evaluating enzyme activity on PET. This can be archived by either analyzing the insoluble faction [17,104–106] or quantifying the release of soluble products [70,73,90,107], as illustrated in Figure 3.1. The most common methods for quantifying the enzymatic degradation of PET are; reverse phase high-performance liquid chromatography (RP-HPLC) [73,89,90], Quantification of UV absorbance of soluble aromatic rings at 240 nm (BHETeq) [107,108], measuring proton release using a pH-stat system [12,70,90], or simply measuring the weight loss of the remaining PET material [17,109]. Other assays require the use of model substrates [110–112] or nanoparticles [104,113], and are therefore not compatible with the PET disks.

Of the above-mentioned enzyme activity assays, the UV absorbance assay allows the highest throughput, as it can be measured rapidly in a plate reader. However, it has a potential issue as it quantifies the UV absorbance of all aromatic rings in the soluble fraction, and does therefore not distinguish between different degradation products (TPA, MHET, BHET, etc.). Although the extinction coefficients of these products are almost similar [107], we tested the validity of this assay against the total weight loss of the remaining disk, and the total concentration of soluble products measured by RP-HPLC. We conducted these comparisons using four benchmark enzymes: LCC_{ICCG}, LCC, DuraPETase, and PHL7. Notably, we observed variations in relative product profiles among these enzymes (Figure 3.5A). For instance, LCC_{ICCG} released a significantly higher amount of diaromatic compounds compared to the other enzymes, constituting ~25% of the total composition.

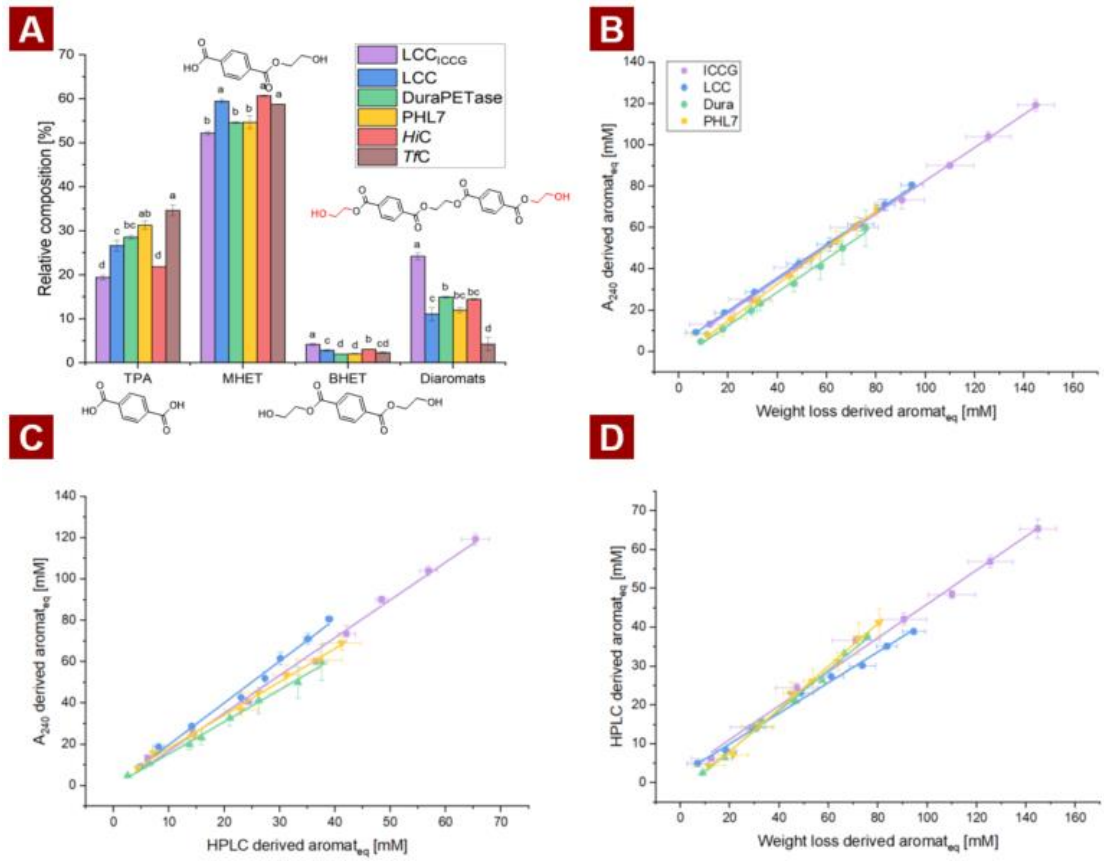

Figure 3.5 – Comparison between the concentration of soluble products quantifyed by different methods: A) Relative composition of TPA, BHET, MHET, or di-aromatic fragments after 1 day of enzyme treatment using low crystalline PET disks (X_C=10.6%) at 55°C pH 9 using 200 nM of either LCC, LCC_{ICCG}, DuraPETase, PHL7, HiC, or TfC. B) to D)The product formation resulting from the enzymatic treatment of low crystalline PET disks (X_C=10.6%) at 55°C pH 9 over an eight-day time course using 200 nM of either LCC, LCC_{ICCG}, DuraPETase, or PHL7. The PET disks were washed and transferred into a new reaction vessel containing fresh enzyme and buffer after each timepoint, to mitigate thermal inactivation. For comparison, the product release measured by the plate reader (A_{240}), Weight loss (WL), or RP-HPLC were converted into $Aromat_{eq}$. The $Aromat_{eq}$'s were quantified as following: $Aromat_{eq,240} = BHET_{eq}$, $Aromat_{eq,HPLC}$ = [TPA] + [MHET] + [BHET] + 2*[diaramats], $Aromat_{eq,WL} = \Delta m_{PET}/MW_{MHET\text{-}H2O}*V$. The figure is an adapted version of figures originally published in in the supplementary information from Paper VI.

Despite differences in the product profiles, the total A_{240} showed a perfect linear correlation with the total concentration of soluble products measured by HPLC for all enzymes (Figure

3.5B). Similarly, the products measured by HPLC or A_{240} (BHETeq) showed a linear correlation with the recorded weight loss (Figure 3.5C and D). Interestingly, the A_{240}/HPLC ratio was consistently higher than 1 (ranging from 1.55 to 2.02) for all enzymes (Table 3.1), indicating that more products were detected by the in the plate reader, compared to the HPLC. This could indicate that a certain fraction of the solubilized compounds escaped RP-HPLC detection. On the other hand, the A_{240}/weight loss ratio was slightly below 1 (ranging from 0.8 to 0.88), implying that certain enzymatically released components were not completely soluble. Nevertheless, the A240 measurement in terms of BHETeq effectively described the progression of product release for all enzymes.

Table 3.1: Slopes of the linear regressions presented in figure 3.5

	Slope [mM/mM]		
Enzyme	**A_{240}/WL**	**A_{240}/HPLC**	**HPLC/WL**
LCC_{ICCG}	0.80 ± 0.008[a]	1.83 ± 0.061[ab]	0.436 ± 0.0145[a]
LCC	0.80 ± 0.01[a]	2.02 ± 0.075[a]	0.395 ± 0.0131[a]
DuraPETase	0.81 ± 0.01[a]	1.55 ± 0.040[b]	0.521 ± 0.0157[b]
PHL7	0.89 ± 0.008[b]	1.61 ± 0.047[b]	0.548 0.0156[b]

3.4 Chapter summary

To summarize the content of Chapter 3, we successfully established an experimental platform for evaluating the X_C on PETase enzymatic degradation. This involved the preparation of a standardized PET with controlled levels of X_C, induced via thermal annealing. Thereby confirming the first hypothesis, **H1**, of the thesis. The chapter did furthermore cover an assessment of the analytical methods for characterizing the substrate before and after enzyme treatment, as well as methods for quantifying the degradation rates of the enzymes. This experimental platform will be used in the following chapters for a more detailed evaluation of the influence of substrate X_C on the enzymatic degradation of PET.

Chapter 4: Enzymatic Degradation of Semi-Crystalline PET

Water is known to have a plasticizing effect on PET [49]. As a result, the T_g is expected to decrease during enzymatic treatment, as enzymatic degradation of PET is generally performed in an aqueous solution. Thus, lowering the temperature at which the polymeric chains devitrifies (transition from the rigid "glassy" state to the more mobile "rubbery" state), resulting in increased chain mobility [70,114–116]. This property of PET led to the second hypothesis, **H2**, of this thesis:

"Enzymatic reaction conducted at temperatures above the T_g of PET will significantly enhance the hydrolysis rate due to increased substrate chain mobility. Lowering the T_g of PET material, using water as a plasticizing agent, will consequently increase the activity of PET degrading enzymes"

The aim of the chapter was to test the abovementioned hypothesis, as specified in **Obj. 2**. The chapter does furthermore introduce the basic concepts of the degradation of semi-crystalline PET which is part of **Obj. 4**. This was done using two thermostable PET degrading enzymes; namely LCC_{ICCG}, and DuraPETase using the standardized substrate introduced in the previous chapter. The results presented in this chapter are primarily based on the content of Paper II but does include data from Paper IV, as well as unpublished data.

4.1 Optimal conditions

Enzyme activity is highly influenced by temperature and pH. Increasing temperatures are known to increase the catalytic constant (k_{cat}), which generally leads to a higher reaction rate. However, as the temperature rises, the enzyme stability decreases, leading to thermal inactivation. Therefore, the optimal temperature of an enzyme is typically considered as the point where the negative impact of thermal inactivation outweighs the positive effect on k_{cat} [117]. Enzymes are also sensitive to the pH of the surrounding environment, as the pH specifies the charge of charged residues at the enzyme's surface, including the active site. This protonation/deprotonation may be essential for ligand binding, driving catalysis, or protein stability [117]. It is therefore essential to determine the combined temperature and pH optimum, as the stability of the enzyme is affected by both temperature and pH. The combined temperature and pH optima for both LCC_{ICCG} and DuraPETase were predicted using response surface methodology (RSM), as shown in Figure 4.1. Both enzymes displayed a pH optimum at pH 9. The temperature optima of DuraPETase was 55°C, consistent with previous findings [18,85]. This was manifested by the significant reduction of the thermostability observed at 60°C, resulting in an ~4-fold decrease in half-time, $t_{½}$, compared to the $t_{½}$ at 55°C (Figure 4.1D). LCC_{ICCG} displayed a temperature optimum of 70°C (Figure 4.1A). This was despite a negligible thermal inactivation at this temperature optima, or even 5°C above (Figure 4.1C). Therefore, the observed decrease in the reaction rate for LCC_{ICCG} at temperatures exceeding its optima was attributed to the crystallization of the substrate rather than thermal inactivation, as pointed out by Tournier et al [12]. In fact, it was shown that surface crystal formation on PET initiates at a temperature of 70°C [34].

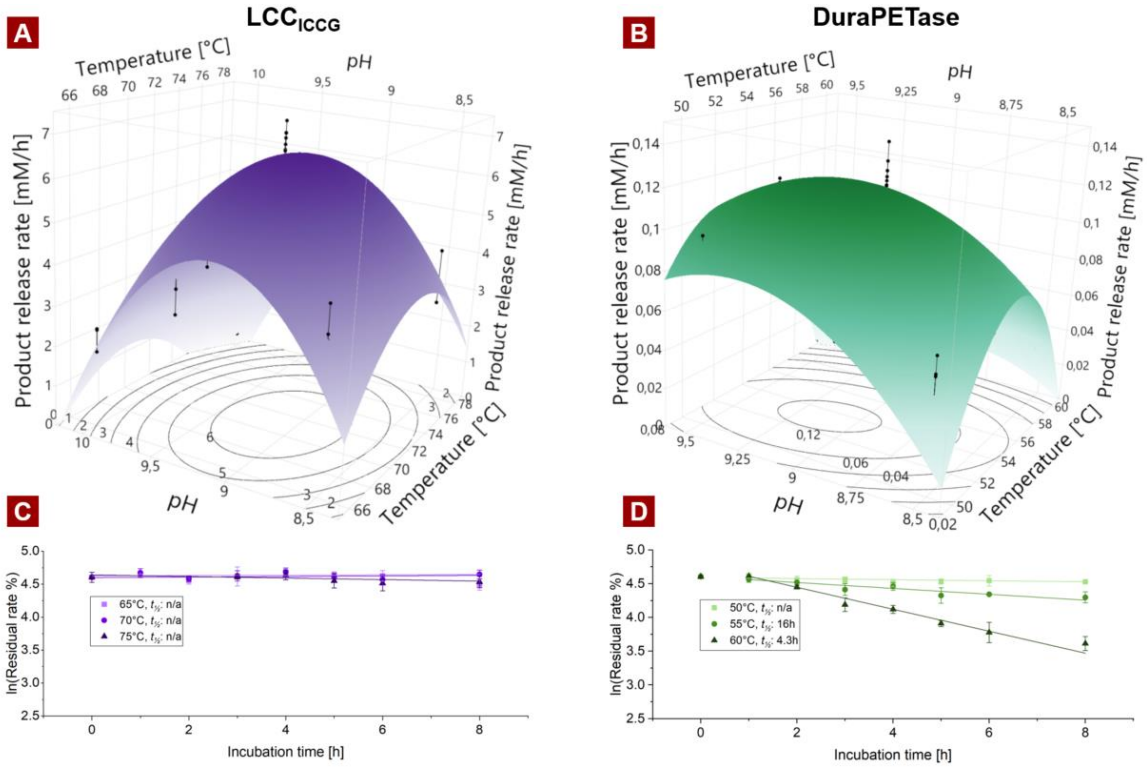

Figure 4.1 RSM and thermal inactivation of LCC$_{ICCG}$ and DuraPETase: Upper panel: Surface plot showing the predicted product release rate as a function of tempera and pH for A) LCC$_{ICCG}$ and B) DuraPETase. The surface plots have been generated by the regression of experimental data (black dots) at which individual conditions were selected based on RSM within the range specified by the limits of the x- and y-axis in both plots. All reactions were performed using 150 nM enzyme. Product formation was recorded after 1 hour (LCC$_{ICCG}$) or 2 hours (DuraPETase) of incubation. Lower panel: Thermal inactivation of C) LCC$_{ICCG}$ and D) DuraPETase. The thermal inactivation was measured at the temperature optima including 5°C and below. The residual activity was measured using 150 nM thermally inactivated enzyme at optimal conditions. This figure was originally published in Paper II.

4.2 Effect of T_g on the hydrolysis rate

The temperature optima of LCC$_{ICCG}$ stands in contrast with the general understanding that enzymatic degradation of PET should be run at temperatures around the T_g [70,118–120]. At T_g, the polymeric chains transition from a rigid “glassy”-state to the more mobile “rubbery”-state, thus leading to an increased chain mobility[121], and thus a potentially enhanced degradation rate. We therefore set out to investigate how this devitrification at temperatures above T_g would affect the enzymatic degradation of PET. To archive this we utilized that water acts as a plasticizer on PET, thus lowering its T_g [46]. By soaking an “amorphous” PET disk (X_C ~11%) for 24 hours in water at 45°C or 65°C, we were capable of reducing the T_g from 75°C to 69°C and 60°C, respectively, without affecting the X_C (Figure 4.2B). These disks were subsequently assayed at a reaction temperature of 68°C. At this temperature, the T_g of the untreated sample would be above the temperature while the T_g of the sample, soaked at 65°C, would be below. Consequently, the polymeric chains within X_{MAF} would be in their mobile “rubbery”-state while the chains of the untreated sample (high T_g) would be in their rigid “glassy”-state, while they would be in their mobile “rubbery”-state for the soaked sample (low T_g).

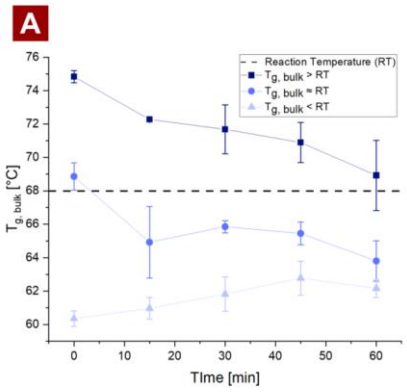

B

	Soaking condition		
	n/a: $T_{g, bulk} > RT$	24h at 45°C: $T_{g, bulk} \approx RT$	24h at 65°C: $T_{g, bulk} < RT$
$T_{g,bulk\ start}$ [°C]	74.8 ± 0.36[a]	68.9 ± 0.81[b]	60.35 ± 0.46[c]
$T_{g,bulk\ final}$ [°C]	68.8 ± 2.10[a]	63.8 ± 1.20[b]	62.2 ± 0.54[b]
$X_{C\ start}$ [%]	11.2 ± 0.97[a]	11.5 ± 1.08[a]	11.7 ± 0.22[a]
$X_{C\ final}$ [%]	10.9 ± 1.47[a]	10.7 ± 0.89[a]	11.2 ± 0.58[a]
Rate [mM/h]	4.81 ± 0.83[a]	4.56 ± 0.64[a]	4.38 ± 0.86[a]

Figure 4.2 – Change on T_g during enzymatic degradation of PET: A) Change in T_g during 1 hour of incubation with LCC_{ICCG} at 68°C. B) Table displaying the change in T_g, X_C during the enzyme reaction in A. The figure in A and table in B are originally from adapted from Paper II.

For this reason, we expected that the reaction rate of the soaked samples would be higher than the untreated sample due to the increased substrate mobility.

Contrary to our expectations, no significant changes were observed between the product release rates between the samples at different T_g (Figure 4.2B). This was despite that the T_g of the untreated sample was kept above the reaction temperate, while the soaked sample was kept below, throughout the reaction (Figure 4.2A). Hence, the increase in the reaction rate of PET degradation enzymes at temperatures just below T_g is likely driven by an increase in k_{cat}, as described by the Arrhenius equation, rather than an increase in chain mobility. It has previously been shown that the T_g of ultra-thin films (<70nm) decreases with the film thickness [34,122,123].

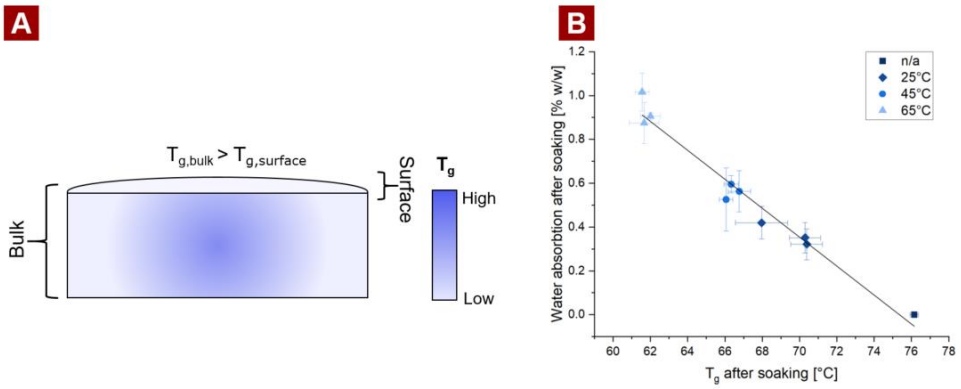

Figure 4.3 – Change in T_g during enzymatic degradation of PET: A) Schematic representation of the presumed gradual decrease in T_g throughout a PET sample. Figure 4.3A was originally published in paper VI. B) Correlation between water absorption and T_g of a PET sample soaked at 25, 45, or 65°C for 1, 2, and 3 days.

This implies that the T_g at the surface of PET is likely lower than the T_g of the bulk PET, as illustrated in Figure 4.3A. This effect may be further enhanced by the diffusion of water into the polymeric material, causing the plasticizing effect, as it was shown that the T_g is directly proportional to the water absorption of the material (Figure 3B). The concentration of absorbed water molecules, and thus the decrease in T_g, would therefore be higher near the surface until an equilibrium is reached, which according to Figure 4.2 did not happen during 60 minutes of incubation. The increased chain mobility, leading to higher rates, would therefore occur at the temperature corresponding to the T_g at the surface, which

may be as low as 40°C [124], rather than the T_g of the bulk. Interestingly, no crystallization was observed during the 24h of soaking at 65°C, although the polymeric chains located at the surface were assumed to be at their devitrified state, during soaking, consistent with the observation by Tournier et al [12]. Thus indicating that the temperature is too low to induce crystallization.

4.3 Product profiling during the initial stage of degradation

The enzymatic degradation of PET is a complex matter as it involves a combination of both heterogeneous catalysis of the insoluble fraction and homogeneous catalysis of solubilized fragments. To gain a deeper understanding of the heterogeneous catalysis of PET by LCC_{ICCG}, we quantified the product profile during the early stage (<4 min) of enzymatic degradation. To ensure that as much of the enzyme catalysis would occur on the insoluble faction we used a very low enzyme-to-substrate ratio; 10 PET-F disks (h=0.25 mm, Ø=6mm, and m=7mg) and 30 nM of LCC_{ICCG}. Hence, we assume that the product profile at the early stage reflects the composition of the products solubilized from the insoluble fraction.

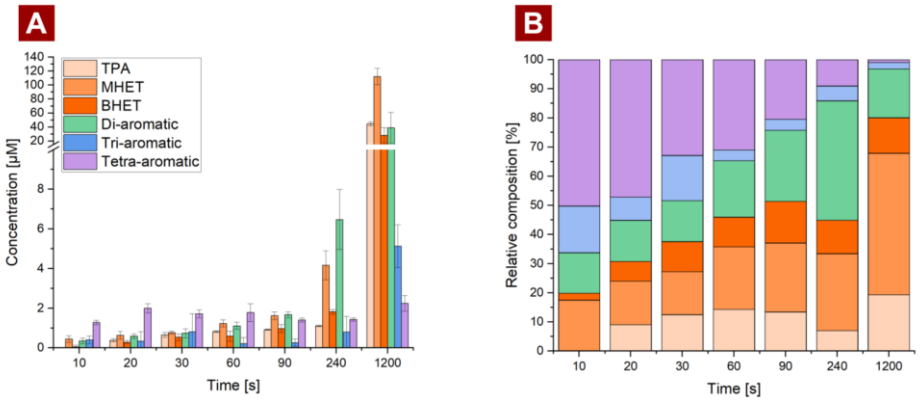

Figure 4.4 – Product profiling during early stage degradation of amorphous PET: A) Change in concentration of the soluble degradation (TPA, MHET, BHET, di-, tri-, and tetra-aromatics) during enzymatic treatment of 10 "amorphous" PET disk using 30 nM of LCC_{ICCG}. *This is an adapted version of a figure from Paper IV.*

During the early stage degradation, we successfully identified six different product species, namely TPA, MHET, BHET, and di-, tri-, and tetrameric OETs. Interestingly, the tetrameric OET accounted for nearly 50% of all products, during the early stage degradation (Figure 4.4.B). This was unexpected as we, to the best of our knowledge, were the first to report this as a soluble degradation product from the enzymatic treatment of PET. Eberl et al did however show that the tetramer was present in relatively large quantities in the insoluble fraction of enzymatic degraded PET [93]. The presence of the tetramer in both the soluble and insoluble fractions was attributed to the low solubility, as highlighted in Paper IV. The concentration of tetramer remained constant during the reaction. This was likely due to its low solubility, or because a steady state had been reached between the tetramer formation from the insoluble fraction and the hydrolysis in the insoluble fraction. The large quantities of the tetramer during early-stage degradation challenge the widely accepted assumption, that monoaromatic products (BHET, MHET, TPA) are the main products from the

enzymatic reaction [70,91,124–127]. Instead, these may be considered as the product of the homogeneous catalysis of OETs as demonstrated by Schubert et al [90].

4.4 Effect of X_C on enzymatic degradation of PET

The impact of X_C on the enzymatic degradation of PET was studied using a standardized PET substrate presented in Chapter 3, with a X_C ranging from 10% to 27%. These samples were then subjugated to an enzymatic treatment by either LCC_{ICCG} or DuraPETase, under their optimal conditions, as specified in section 4.1, over an 8-hour time course. The initial enzymatic treatment of the thermally annealed PET samples with a $X_C > 10\%$, exhibited no product formation (Figure 4.3). This initial stage will henceforth be referred to as the "lag phase". After surpassing the lag phase, the reaction rate remained at a constant level, referred to as the “steady-state rate” (v_{ss}). Notably, both the duration of this lag phase (t_{lag}) and v_{ss} were affected by increasing X_C, as t_{lag} became more profound, while v_{ss} decreased. (Figure 4.3)

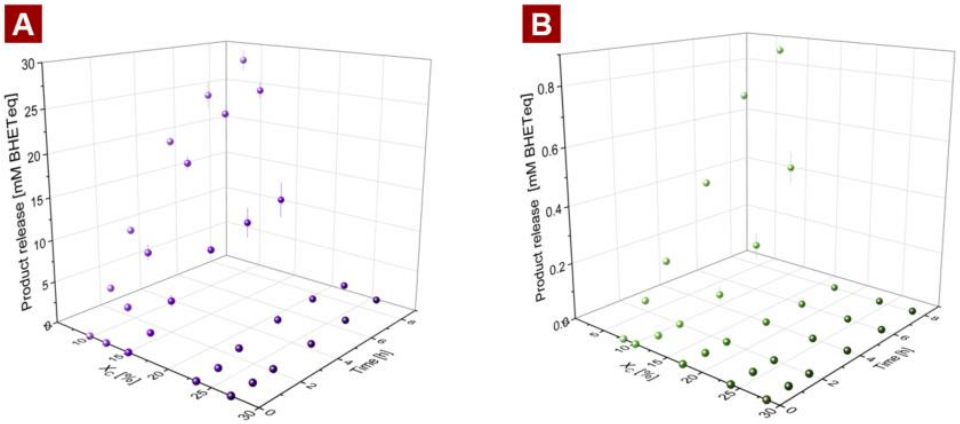

Figure 4.5 – Enzymatic degradation of semi-crystalline PET: Product release during enzymatic degradation of thermally annealed PET samples ranging from 10% to 27% in 50 mM glycine-NaOH buffer using A) 150 nM LCC_{ICCG} at 70°C pH 9, or B) 150 nM DuraPETase at 70°C pH 9. The buffer concentration was increased to 500 mM for the samples at X_C<15% for the samples incubated by LCC_{ICCG} to avoid a decrease in pH. This figure was originally published in Paper II.

4.4.1 Steady-state rate

The progression in the v_{ss} as a function of X_C, occurred in a non-linear manner for both LCC_{ICCG} and DuraPETase, as shown in figure 4.6. Notably, the product release of both enzymes ceased above a certain threshold corresponding to 23% for LCC_{ICCG} and 19% for DuraPETase. Similar observations were observed on the IsPETase and a mutated variant [84]. The absence of product release on the crystalline samples could be attributed to the following factors:

1 **The X_C threshold**: The density/quantity of accessible and degradable ester bonds may have surpassed the minimal level required for efficient degradation of the crystalline substrate. This concept is discussed further in chapter 5.
2 **The lag phase:** t_{lag} on samples with high X_C might extend beyond the total reaction time, leading to insufficient degradation during the course of the enzyme treatment.

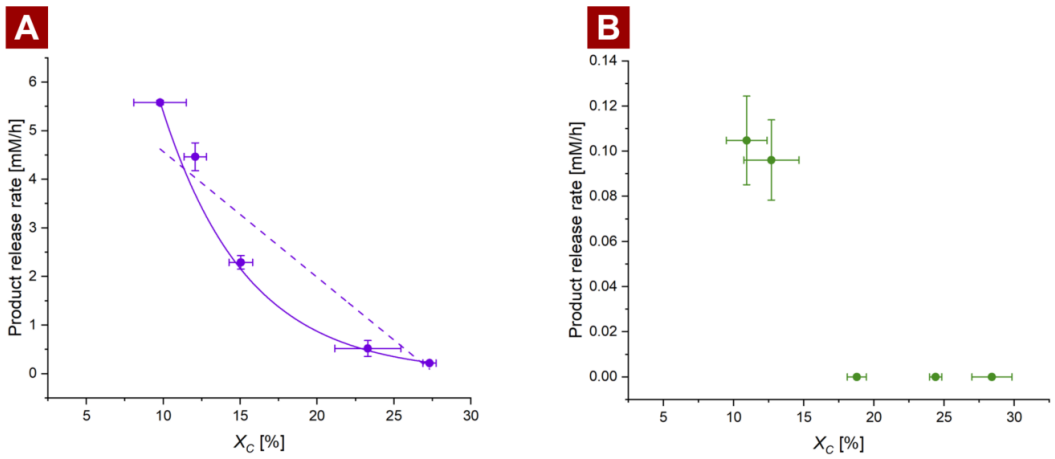

Figure 4.6 – Steady-state rate vs. X_C: A) Steady-state rate for LCC_{ICCG} obtained at different X_C. The rates has been calculated based on the linear region of the progress curves in 4.3A. B) Steady-state rate for DuraPETase obtained at different X_C. The rates has been calculated based on the linear region of the progress curves in 4.3B. This figure was originally published in Paper II.

As the product formation, at a given point in time is dependent on both t_{lag} and v_{ss}, comparative studies should not be performed using a single end-point measure of the total product formation, as this could lead to misconceptions. Instead, multiple sampling or continuous monitoring of the product formation is required to ensure that t_{lag} has been surpassed when quantifying the v_{ss}.

4.4.2 Change in surface topography

In addition to the quantification of the soluble products released during the enzymatic treatment, the change in the topography of the insoluble PET disk after treatment by LCC_{ICCG} was analyzed by SEM (Figure 4.7). All PET samples, independent of X_C, appeared smooth before enzymatic treatment. During the 8-hour enzymatic treatment, the surface topography of the sample at the lowest X_C (9.8%) remained unchanged, within the obtained resolution. In contrast, the annealed samples displayed significant surface erosion. Typically, increased surface areas are associated with higher kinetic rates in interfacial catalytic reactions. However, in this case, the observed surface erosion, resulting in a larger surface area on the crystalline samples, was not indicative of an increased number of catalytic sites accessible to LCC_{ICCG}. Instead, this surface erosion suggested that certain regions were inaccessible to the enzyme. This observation could suggest that the hydrolysis of ester bonds near a previously hydrolyzed bond may be more favorable than randomly located ester bonds, as local cavities are formed on the surface. Similar phenomena have been described in previous studies [17]. While it may be tempting to conclude that the inaccessible areas correspond to the crystal regions, further investigations are necessary to precisely determine the substrate composition in terms of X_C, X_{MAF}, and X_{RAF}.

The extent of erosion seemed to correlate with the enzymatic product release during the initial stage. Hence, the initial enzymatic degradation of the thermally annealed PET samples did neither result in surface erosion (Figure 4.7) nor detectable soluble product formation (Figure 4.5A). These findings could suggest that increased X_C leads to limited formation of productive enzyme-substrate complexes. This limitation arises from the

scarcity of amorphous hydrolyzable sites. Instead, the enzymes may bind unproductively the the crystal regions. Further insights into the mechanism causing the lag phase are provided in Chapter 6 and discussed in Chapter 7.

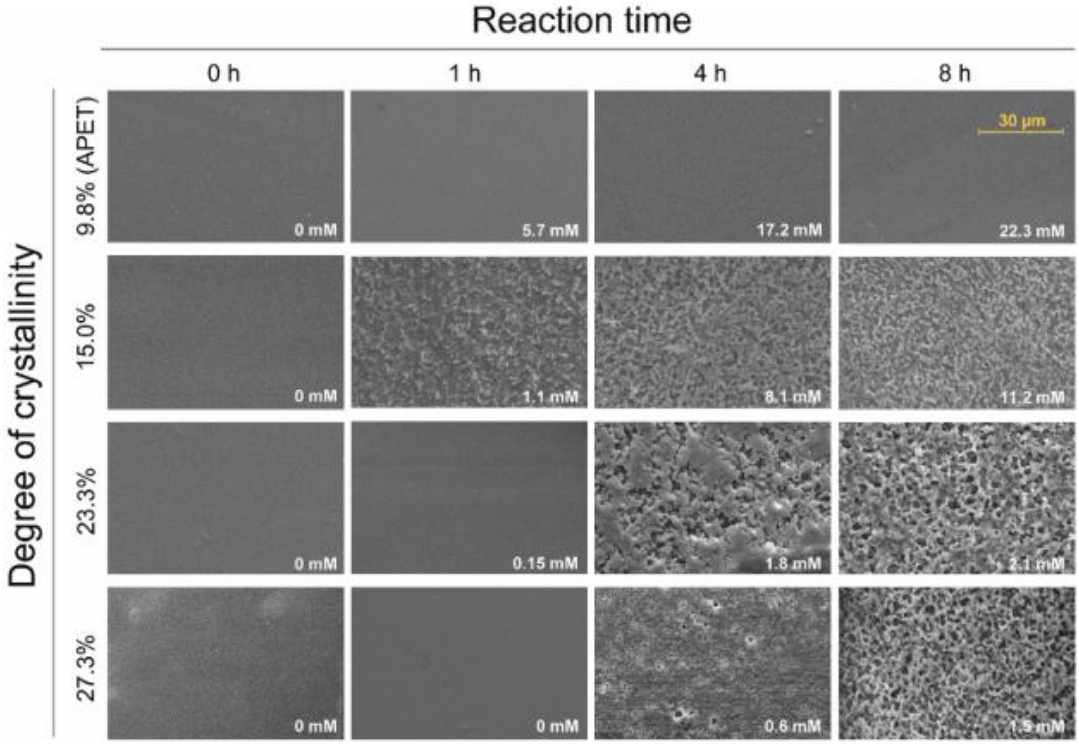

***Figure 4.7* – Change in topography during enzymatic treatment of PET:** SEM images at 1500x magnification of PET at various X_C (9.8 to 27.3%) subjected to enzymatic degradation by 150nM of LCC_{ICCG} at 70°C pH 9 in 50 mM Glycine-NaOH for up to 8 hours. The concentration written in the lower right corner of each image represent the product release during enzymatic treatment. The figure was originally published in Paper II.

4.5 Chapter summary

In conclusion, Chapter 4 delved into the enzymatic degradation of semi-crystalline PET, investigating the interplay between substrate properties and enzymatic activity. It was found that the optimal conditions when degrading amorphous of low crystalline PET enzymatically was ultimately 70°C, as the substrate starts to crystalize above this temperature [12,34]. Although the T_g of the bulk material falls below the reaction temperature after ~1 hour of incubation at 68°C, we did not see any rapid increase in activity within this time scale. We furthermore saw that the v_{ss} two PET samples with different T_g values (75 and 60°C), assayed at 68°C were similar, despite the sample with a lower T_g was expected to be more mobile. On this basis the second hypothesis of this thesis, **H2**, was rejected.

Additionally, we observed the presence of a lag phase at samples with higher X_C during the initial degradation. This lag phase did neither result in the release of soluble products nor surface erosion. After the lag phase had been overcome a steady-state rate was observed. This rate was heavily affected by the X_C and almost depleted at 23% X_C for LCC_{ICCG} and 19% X_C for DuraPETase. These phenomena will be discussed in more detail in the following chapters.

Chapter 5: Tolerance Towards Substrate Crystallinity

From the previous chapter, it was clear that the X_C had a significant effect on the enzyme activity. However, due to the presence of the lag phase, it was not evident whether the lower activity of DuraPETase on X_C PET was caused by its lower activity in general, resulting in longer lag phases, or if it was caused by differences in the tolerance of the enzymes towards increasing substrate X_C. We, therefore, set up a larger comparative characterization of six different benchmark PET-hydrolases: LCC, LCC_{ICCG}, DuraPETase, HiC, TfC, and PHL7, as specified in **Obj. 3**, to test the third hypothesis, **H3**, of this thesis:

"The tolerance of enzymes towards increasing X_C of the substrate is different between enzymes. Hence, the tolerance towards X_C may be used as a selection criterion for identifying enzymes with enhanced activity on more crystalline PET"

The content of the following chapter draws upon the findings presented in Paper III. Here the six thermostable PET degrading enzymes were assayed on PET substrate with X_C spanning from 10.8 to 24.4%. The reactions were conducted during an extensive 8-days of treatment at 55°C, to ensure that the lag phase would be overcome. Although 55°C was not the optimal temperature for all enzymes [11,12,70,82], it was chosen to maintain high catalytic turnover rates while preventing unwanted substrate crystallization during the prolonged incubation.

Enzymatic reactions subjected to prolonged incubation can be negatively influenced by factors such as thermal inactivation [16] or product inhibition of the enzymes [91,128]. To mitigate the impact of these factors, we took specific precautions. At each time point (every 24 hours), we collected, washed, and transferred each enzymatically treated disk to a new reaction container with fresh enzyme and buffer. This approach ensured that the apparent rates, quantified from the linear regions of the progress curves, predominantly reflected the substrate properties (i.e., the X_C) rather than being skewed by potential enzyme-related factors.

5.1 Comparative evaluation of the effect of X_C on the steady-state rate

The cumulative product formation during the 8 days of treatment is displayed in Figure 5.1. These curves reveal notable variations in both v_{ss} and t_{lag} among the six enzymes included in the study. Interestingly, a t_{lag} of up to 6 days was observed at high X_C (Figure 5.1F). This finding corroborates the earlier results from the previous chapter, confirming that the previously observed threshold towards X_C for LCC_{ICCG} and DuraPETase observed in Figure 4.6 was partly due to the lag phase not being overcome. As described previously the v_{ss} could be calculated from the linear regions of the progress curves.

LCC_{ICCG} consistently exhibited the highest degradation rates across all substrate crystallinities (Figure 5.1). The rates of LCC, DuraPETase, and PHL7 were relatively similar on the most amorphous sample (X_C=10.8%). However, at higher X_C values, the rate of PHL7 dropped significantly, resulting in a 4- and 5-fold reduction in v_{ss} compared to LCC or DuraPETase, and as much as 12-fold lower than LCC_{ICCG} at an X_C of 24.4%. PHL7 was therefore more negatively affected by increased substrate crystallinity

compared to LCC, LCC_{ICCG}, and DuraPETase. This observation aligns with a recent study by Plaff et al. who demonstrated that PHL7 (also referred to as PES-H1) exhibited significantly lower activity on highly crystalline PET particle samples (X_C=26%) compared to LCC_{ICCG}, despite performing nearly as well as LCC_{ICCG} on amorphous PET film [83].

HiC and TfC generally exhibited substantially lower rates compared to the other enzymes. At 10.8% X_C, their rates were ~36- and 16-fold lower, respectively, than LCC_{ICCG}. Moreover, HiC and TfC did not show any detectable product formation during the 8-day incubation at X_C values above 19.6% (Figure 5.1).

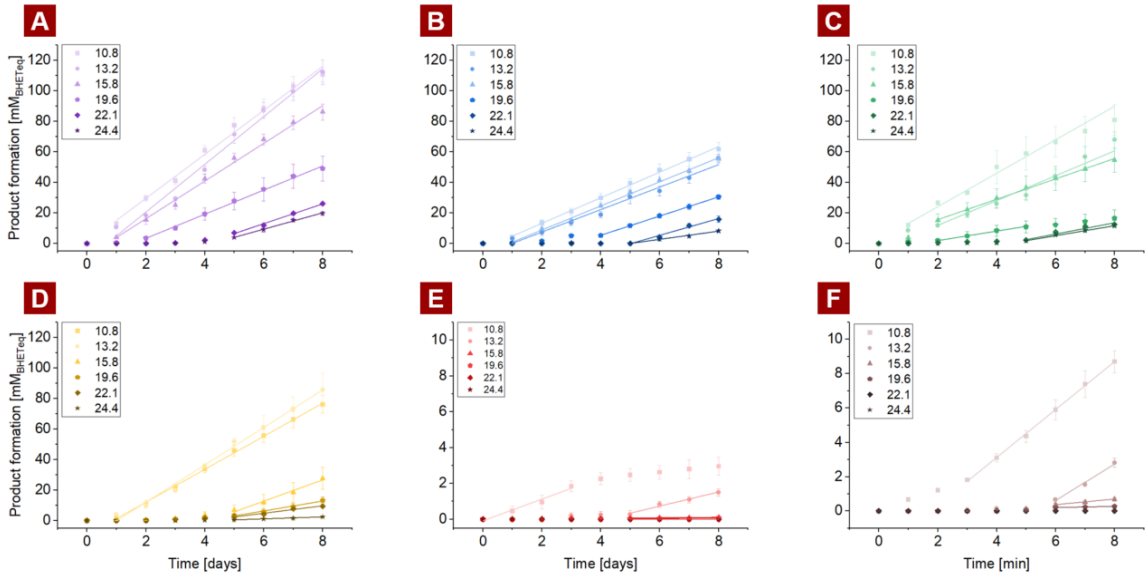

Figure 5.1 – Progress curves during prolonged degradation of semi-crystalline PET at various X_C: Time course showing the formation of soluble products, in terms of BHETeq, during enzymatic treatment of PET disks at various X_C for six thermostable enzymes; A) LCC_{ICCG}, B) LCC, C) DuraPETase, D) PHL7, E) HiC, and F) TfC. Each reaction was performed using 1 PET disk (Ø=6 mm, h=1 mm, m~32 mg) spanning from 10.8 to 24.4%, treated with 200 nM enzyme at 55°C pH 9 in 500 nM glycine-NaOH buffer pH 9. At each time point, (every 24 h) the PET disk was washed in water and 1% SDS, and transferred into a new reaction vessel containing fresh enzyme and buffer. The graph was originally published in Paper III.

5.2 Tolerance towards X_C

To enable a direct comparison of the tolerance towards increasing X_C, we normalized the v_{ss} from Figure 5.2A with respect to the rate obtained on the most amorphous sample (X_C=10.8%). These normalized rates were independent of the overall efficiency of the enzymes at amorphous/low crystalline samples. Consequently, the tolerance curves (Figure 5.2B) focus solely on how the enzyme's performance is impacted by increasing X_C, rather than how well it performs overall. The highest normalized rates at intermediate X_C values (15.5% to 22.1%) were obtained by LCC followed by LCC_{ICCG}. DuraPETase and PHL7 exhibited similar normalized activities up to 19.6% X_C. Beyond this point, DuraPETase reached a plateau, while the rate of PHL7 continued to decrease. LCC, LCC_{ICCG}, and DuraPETase retained similar relative product formation rates at the highest X_C (24.4%), corresponding to 30–40% of the “untreated” sample. In contrast, PHL7 only retained 6% of its activity at the highest X_C (Figure 5.2B).

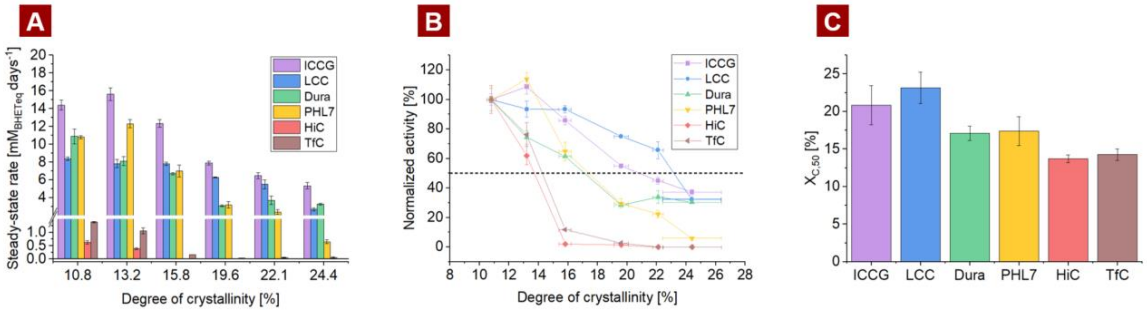

***Figure 5.2* – Comparative comparison of enzyme tolerance to substrate X_C**: A) steady-state rate of LCC_{ICCG}, LCC, DuraPETase, PHL7, Hic, and TfC at X_C ranging from 10.8 to 24.4%. The rates were calculated based on the linear regions of Figure 5.1 B) X_C Tolerance curves for the six enzymes. The normalized activity was calculated by dividing the rates at a given X_C the rate obtained at the most amorphous sample (10.8% X_C) from Figure 5.2A. C) $X_{C,50}$, defined as the X_C at which the activity of an enzyme reaches 50% on the activity on the most amorphous substrate, visualized by the dashed line in Figure 5.2B. This figure is originally from Paper III.

For a single quantitative measure on the influence of the X_C on the hydrolysis rate, we calculated the X_C at which the product formation rate decreased to half of the rate archived on the most amorphous sample. This parameter, denoted as $X_{C,50}$, was calculated by linear interpolation of the tolerance curves (Figure 5.2B). The $X_{C,50}$ values confirmed that LCC and LCC_{ICCG} exhibited the highest tolerance towards X_C, followed by DuraPETase and PHL7. In contrast, the tolerances of TfC and HiC were the lowest, as their activity dropped to very low levels at X_C above 15% (Figure 5.2C).

5.3 Change in surface topography

The change in the topography resulting from the prolonged treatment was further evaluated for LCC, LCC_{ICCG}, DuraPETase, and PHL7 (Figure 5.4). To investigate whether the lower tolerance, and thereby a presumably lower substrate specificity would be manifested as surface erosion (change in surface topography) caused by enzymatic treatment. Due to very low product formation, and thereby extent of reaction, by HiC and TfC, these enzymes were not included in the assessment. The changes in topography resulting from individual enzymatic treatments demonstrated profound variations among the enzymes and with increasing X_C, particularly on more crystalline samples (X_C>10.8%). PHL7-treated samples showed more distinct crater-like surface erosion (Figure 4). The density of these structures decreased with increasing X_C. In contrast, PET disk samples treated with DuraPETase, LCC, or LCC_{ICCG} exhibited less obvious surface erosion, despite their significant PET degrading action. However, PET disks at X_C>15.8% treated with DuraPETase, LCC, or LCC_{ICCG} exposed what are assumed to be crystal structures (Figure 4).

The enzymatic degradation of PET occurs at the plastic-water interface. Here the chains in the MAF regions are presumably at their mobile state, as the $T_{g,surface}$ of PET is substantially lower than the $T_{g,bulk}$ (e.g. around 40°C [124]). These chains (MAF) may therefore change between conformations (*gauche* or *trans*), unlike the more rigid chains (RAF and crystals). As the X_C increases, the overall PET chain mobility gradually decreases due to a lower proportion of MAF [44]. We therefore propose that the higher tolerance to X_C, and the less profound surface erosion, observed for certain PET

hydrolases (specifically LCC and LCC_{ICCG}), is attributed to a broader conformational selectivity towards the *trans* conformation of PET chains. This selectivity is facilitated by the flexibility of their active sites, enabling them to bind to rigid PET chains in either a *gauche* or trans conformation. This interpretation aligns with the recent findings of Guo et al. [129]

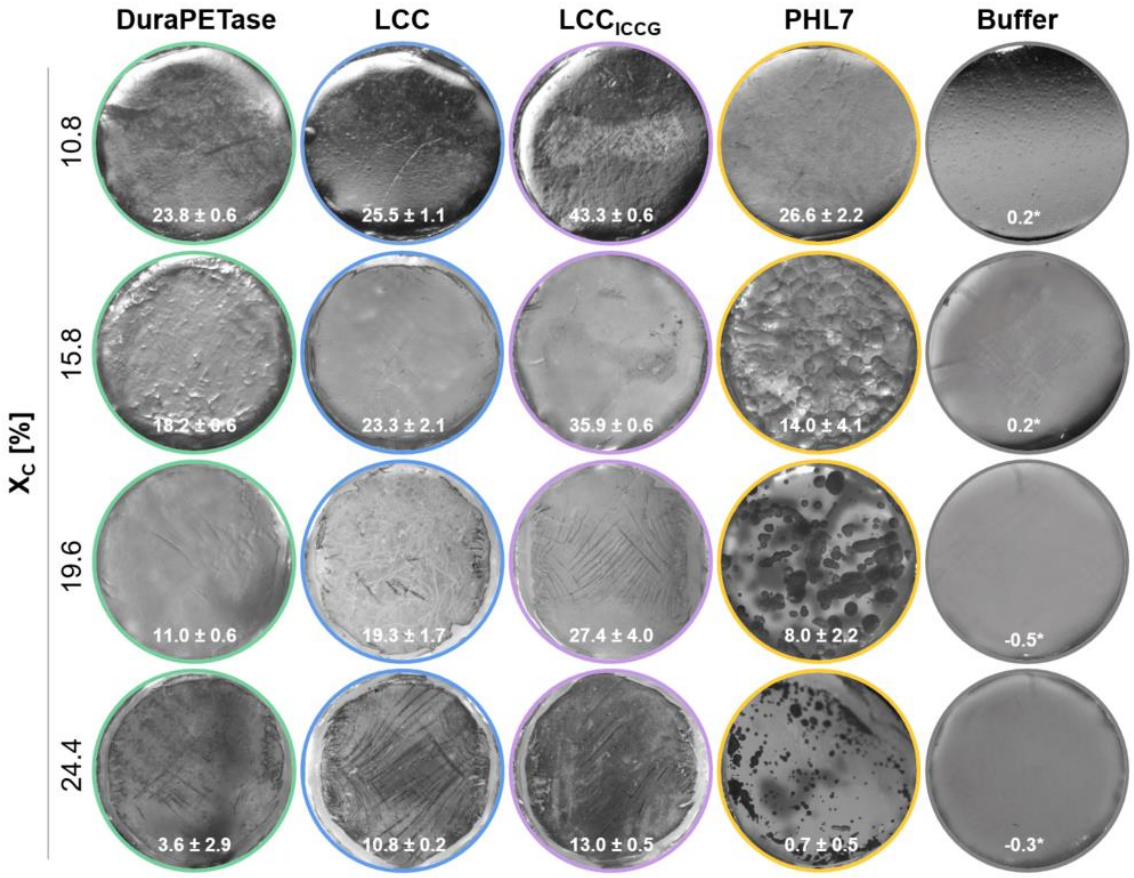

***Figure 5.3* – Change in surface topography of PET samples after enzymatic treatment:** Light microscopy imaging of PET disk at various X_C (10.8 to 24.4%) after eight days of treatment by either DuraPETase, LCC, LCCICCG, PHL7 or without enzyme (Buffer). The disks displayed in this figure were the same disk that was used in Figure 5.1. This figure is originally from Paper III.

5.4 Total hydrolysis yield

To investigate the hypothesis that the lower tolerance to X_C, and more defined surface erosion observed for PHL7 was the result of a lower conformational selectivity, we conducted a prolonged enzymatic treatment on extremely crystalline PET particles (Ø< 300 µm, X_C=38%) using the following enzymes: DuraPETase, LCC, LCC_{ICCG}, and PHL7 (Figure 5.3A). While the enzymatic degradation of the PET disk at the highest X_C resulted in lag phases lasting for days, the same trend was not observed for the highly crystalline PET powder. Instead, the soluble product formation seemed to occur immediately when PET particles were used as substrate, as observed elsewhere [29,79,130]. These differences in the progression of product formation during enzymatic treatment of crystalline PET film and particles are likely due to variations in the substrate's morphology, influenced by the processing of PET particles.

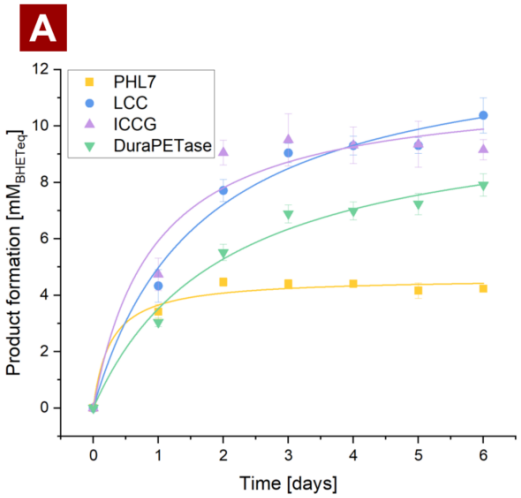

B

Enzyme	Maximal yield [%]
LCC	6.96 ± 0.37[a]
LCC_{ICCG}	5.47 ± 0.21[b]
DuraPETase	4.72 ± 0.24[b]
PHL7	2.53 ± 0.05[c]

Figure 5.4 – Enzymatic degradation of highly crystalline PET powder: A) Soluble product formation during six days of enzymatic treatment of 32 mg/mL highly crystalline PET powder (38% X_C) at 55°C pH 8 using 200 nM of either LCC, LCC_{ICCG}, DuraPETase or PHL7. Table showing the maximal conversion yield calculated based on the product formation after six days of enzyme treatment. Different subscript letters (a, b, or c) indicate a statistical difference in the maximal yield obtained by the enzymes. This figure is originally from the Supplementary information from Paper III.

Resulting in a significantly larger specific surface area which exposes amorphous regions that otherwise would have been retained within the crystal structure. Consequently, the initial density of hydrolyzable sites for enzymatic attack would be higher on the particles, leading to immediate hydrolysis, as shown by Chang et al. [131].

Looking at the maximum hydrolysis yield achieved by the four enzymes on the crystalline PET particles, it becomes evident that the total hydrolysis of PHL7 was significantly lower than the other enzymes, corresponding to half of what LCC_{ICCG} and DuraPETase accomplished, and nearly a third of LCC (Figure 5.4). Notably, the maximal yields obtained for LCC_{ICCG} were significantly lower than previously reported (23.5% [130]). This discrepancy may be attributed to the much lower enzyme-to-substrate ratio used in our study (0.2 µM enzyme per 32 g/L substrate) compared to the previous study (1 µM enzyme per 10 g/L). Nonetheless, the tolerance to X_C (Figure 5.2B) correlated with the maximal conversion yield achieved for the different enzymes. The inefficiency of PHL7 on crystalline PET samples exemplifies this correlation, supporting the proposed hypothesis that PHL7 exhibits lower selectivity towards the more crystalline regions exposed on the surface of the annealed samples.

5.5 Structural comparison

A structural comparison of PHL7, LCC, LCC_{ICCG}, and DuraPETase was performed to investigate if the lower tolerance to X_C of certain enzymes could be attributed to the structure. It has previously been observed that the active site of IsPETase (The wild type of DuraPETase) displays a greater flexibility compared to other PET degrading enzymes, including LCC [132]. This increased flexibility of IsPETase was assumed to contribute to its higher activity at ambient temperatures, where the amorphous polymer chains are at their rigid “glassy” state [65,132]. Based on this insight, we hypothesized that increased flexibility of the active site would accommodate the more rigid chains in the RAF region

which, as previously mentioned, increases with X_C. Thus, increasing the tolerance towards X_C.

The structural flexibility of LCC, LCC_{ICCG}, DuraPETase, and PHL7 was studied by molecular dynamic (MD) simulation. A notable backbone root-mean-square-fluctuation (RMSF), at approximately the same locations, namely residues 30–40 and 89–92, was observed for all enzymes as displayed in Figure 5.5A. However, these flexible regions were less was less profound for PHL7, compared with the other enzymes.

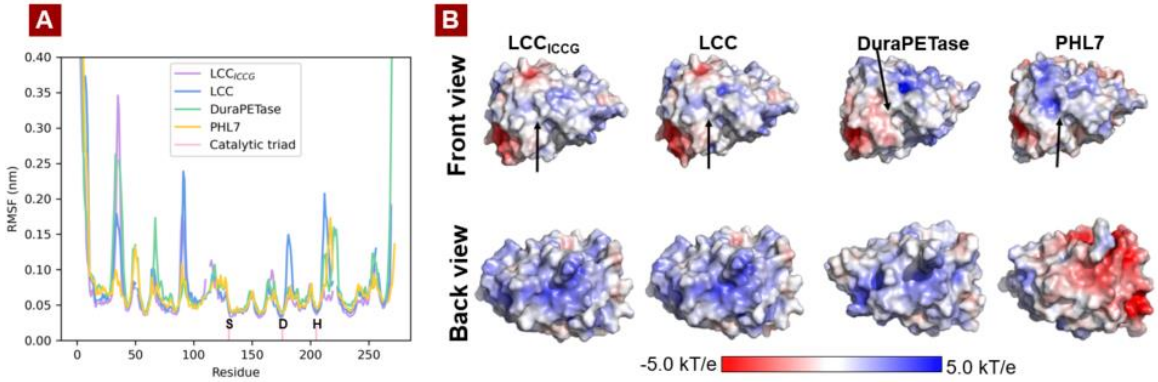

Figure 5.5 – Structural comparison of LCC, LCC_{ICCG}, DuraPETase, and PHL7: A) Aligned and gaped RMSF of LCC_{ICCG}, LCC, DuraPETase and PHL7 during the 100 ns MD simulation. B) Comparison of the surface electrostatic potential of LCC_{ICCG}, LCC, DuraPETase, and PHL7, calculated using the APBS plugin in PyMOL. The front and back view is defined by the location of the active site, which are highlighted by an arrow. This figure has been adapted from figures originally published in Paper III.

A possible explanation may lie in the hydrogen bonding interactions involving the bulkier glutamine and aspartic acid residing at positions 33 and 35 in PHL7 compared to the two serine residues at the same positions for LCC, LCC_{ICCG}, and DuraPETase (Figure S3 Paper III). While none of these positions are directly linked to the active site of the enzymes, residues 89-92 were near the binding subsite II, which accommodates the binding of the polymer to with the enzyme [127,133]. This increased flexibility of the active site of IsPETase is centered around the loop bearing the catalytic residue D179 of IsPETase [132]. However, this flexibility has been reduced for the engineered variants DuraPETase and LCC_{ICCG}, as demonstrated by the RMSF (Figure 5.5A), to increase the overall activity at elevated temperatures [12,85]. Similarly, PHL7 exhibited lower RMSF, and thus flexibility, than LCC at this region. The selection criteria for increased activity for both DuraPETase and LCC_{ICCG} was based on their specific activity towards low crystalline PET material (<10.5% X_C) [12,85]. Hence, the tolerance towards X_C was not considered when selecting the improved variant. It is therefore noteworthy that the present tolerance assessment outlined in this chapter revealed that the four mutations differentiating LCC_{ICCG} from LCC did not substantially affect the response of LCC_{ICCG} towards increased crystallinity, despite its decreased flexibility. It is therefore unlikely that the increased flexibility around the loop bearing the catalytic residue D179 is the main contributor to the lower tolerance towards X_C of PHL7, as both DuraPETase and LCC_{ICCG} had a similar RMSF at this region.

A notable difference among these four thermostable PET-hydrolases is their variation in surface charge (Figure 5.5B). Generally, DuraPETase, LCC_{ICCG}, and LCC exhibited a

positive electrostatic potential across their solvent-excluded surface. An exception to this was the presence of a negative pocket situated near their active site, as illustrated in Figure 5.5. In contrast, PHL7 displays a significant area of negative electrostatic potential. This was located almost directly opposite to the active site, as shown in Figure 5.5B.

The hydrolysis of polyester materials, such as PET, leads to a net increase in negative charges on the surface. This occurs as carboxylic acids-groups, located at ends of polymeric chains, are exposed during bond cleavage, which does not result in the release of a soluble product [93]. Hence, the negative pocket located at the opposite side of the active site of PHL7 (Figure 5.5) might generate a repulsive force between the enzyme and substrate interface. This electrostatic repulsion could hinder PHL7 from swirling at the surface of PET, instead maintaining the enzyme in a position that enables an apparent pseudo-processive behavior following the initial bond cleavage. This observation could potentially explain the observed crater structures for PHL7 in Figure 5.3. It is also plausible that the profound surface erosion observed at higher X_C would yield a higher negative surface charge, due to the increased specific surface area. This could potentially contribute to the lower tolerance observed for PHL7.

5.6 Chapter summary

In summary, the main objective of this chapter was to test the third hypothesis, **H3**, stating that the activity towards the crystalline regions differs amongst PET degrading enzymes, and may therefore serve as a selection criteria for the identification of effective enzymes. For this purpose, we defined the concept of "tolerance" towards X_C was introduced as a quantifiable parameter to assess enzyme responsiveness towards X_C. Notably, LCC_{ICCG}, emerged as the most efficient enzyme in terms of both activity and tolerance to X_C, while PHL7 demonstrated decreased tolerance to X_C, despite its high rates on low crystalline PET (X_C <15%). The lower tolerance towards X_C PHL7 was further manifested by a lower total hydrolysis yield and the presence of untouched regions following enzymatic degradation. Thus confirming **H3**, as we showed that both LCC and DuraPETase were more robust towards increasing X_C than PHL7, while their activity on the low crystalline samples was comparable. These enzymes would therefore serve as better candidates for the enzymatic degradation of waste PET with higher X_C. Through MD simulation, we observed that the increased tolerance towards X_C was not directly linked to the flexibility of the active site, but is instead to regions associated with regions that accommodate binding of substrate moieties, which are not directly linked to the point of hydrolysis.

Chapter 6: Enzymatic Degradation Mechanism on Semi-crystalline PET

The initial stage of enzymatic PET degradation, referred to as the lag phase, is characterized by the absence of product release. This phenomenon is influenced by various factors, including the enzyme catalyzing the reaction, as highlighted in Paper III, the specific surface area of the substrate [131], and the X_C as shown in Paper I, II, and III. Consequently, studying the kinetics of thermally annealed PET substrates with increasing X_C has proven challenging due to the need for extensive sampling. To address this issue we developed a continuous assay for monitoring the product formation, which enabled quantitation of the kinetic constants of LCC_{ICCG} on substrate with different X_C, X_{RAF}, and X_{MAF}. By studying the relative decrease in the maximal reaction rate ($^{inv}V_{max}$) as a function of the change in substrate composition, we were able to test the fourth hypothesis, **H4,** of the thesis:

"The tolerance towards substrate X_C can be attributed to the specificity of an enzyme towards X_C, X_{RAF}, or X_{MAF}*"*

We further studied the initial stage of PET degradation by combining two complementary assays, namely RP-HPLC and proton release. This allowed us to test the fifth and final hypothesis, **H5**, of the thesis:

"The initial degradation of crystalline PET is facilitated by an endo-type degradation pattern"

The following chapter is built upon **Obj. 4**, and is based on the results from Paper IV, V and, VII. To enable continuous monitoring of the product release, we developed a simple compartmentalized spectrophotometric assay, based on modified microtiter plates. The underlying principle of this method is illustrated in Figure 6.1.

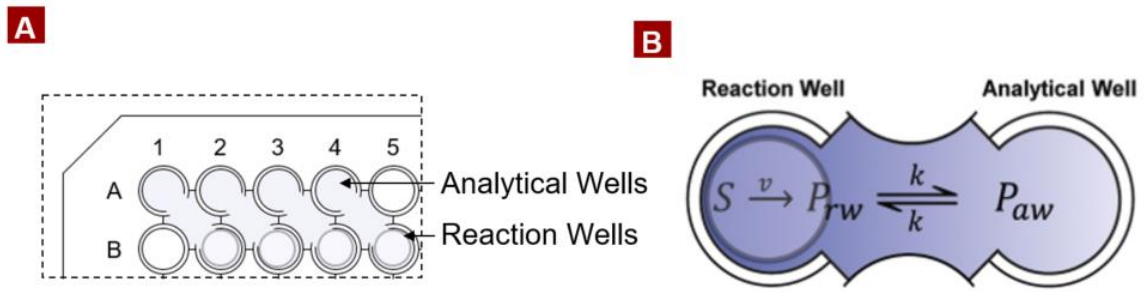

Figure 6.1 – Overview of the modification of a 96-well plate for the compartmentalized assay: A) Schematic representation of the compartmentalized microtiter plates used for the continuous assay. The insoluble substrate was retained in the reaction well, while the product formation was measured in the analytical well B) Kinetic reaction scheme describing the flow of soluble products between the reaction- and analytical well. This figure is adapted from figures originally published in Paper V.

6.1 Validation of UV-based continuous assay

6.1.1 Evaporation

The continuous assay was performed at 50°C in an open system and was therefore subjected to water evaporation during the reaction. The evaporation occurred at a constant rate of 2.15 µL/min, causing a ~40% reduction in reaction volume after 120 min (as shown in Paper V). Despite the significant reduction in volume, the absorbance of soluble products remained constant over a two-hour time course, consistent with Lambert-Beer's law. The absorbance monitored by the continuous assay does therefore accurately reflect the product release (in moles). The evaporation did however lead to an upconcentration of the enzyme during the reaction. Hence, an adjustment for the evaporation was necessary, to determine the actual enzyme concentration at a given time (i.e. at the time of regression of v_{ss}).

6.1.2 Mixing

Due to the compartmentalized design, a slight time delay occurs before the product has diffused from the reaction well into the analytical well, as shown by the reaction scheme in Figure 6.1B. Assuming the system is well mixed, the concentration in the analytical well, n_{aw}, at a given time, t, can be quantified according to equation 6.1

$$n_{aw}(t) = n_{eq} + \exp(-2 * k_{mix} * t) * c \qquad (6.1)$$

Here n_{eq} is the equilibrium concentration between both wells, k is the mixing rate constant, and c is the constant of integration. A detailed deviation of equation 6.1 is shown in Paper V.

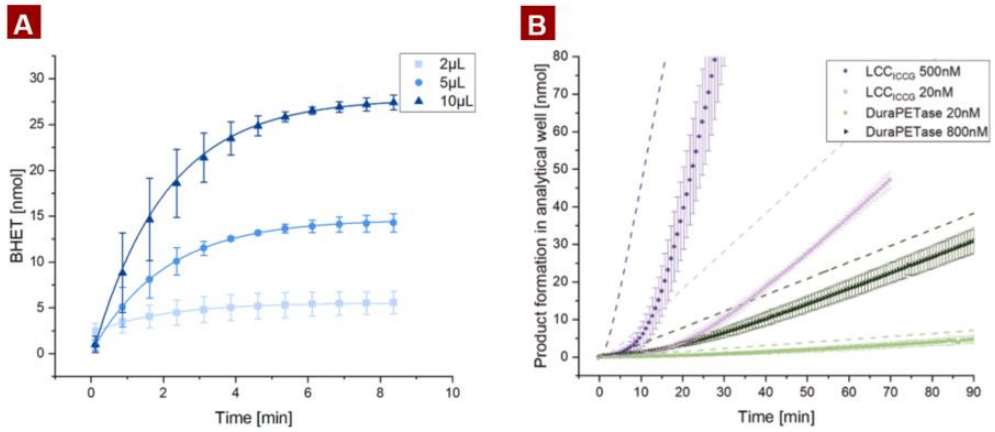

Figure 6.2 – Evaluation of the responsiveness of the diffusion of soluble products into the analysis well: A) Progression in the diffusion of various volumes of a 2.5 mM BHET suspension from the reaction well into the analysis well. The solid line represents the global fit of the experimental data to equation 6.1. B) Comparison of the product formation obtained experimentally with the simulated data, estimated by numerically solving the ODEs presented in equation 6.2 using the experimentally obtained v_{ss} and k_{mix}. This figure is adapted from figures originally published in Paper V

To quantify the mixing constant, a known quantity of a concentrated BHET suspension was added to the reaction well, and the absorbance was subsequently monitored in the analytical well. The progression in n_{aw} was fitted to equation 6.1 using global fitting (Figure 6.2A), resulting in a mixing constant of 0.247± 0.002 min^{-1}. Importantly, this constant was found to be independent of the presence of a PET disk or the type hydrolysis product type (MHET, BHET, or TPA), as shown in paper V. Instead, the well dimensions, especially the intersection, had a significant effect on the mixing constant. Therefore, ensuring uniformity in the modified plates is essential for achieving reproducibility.

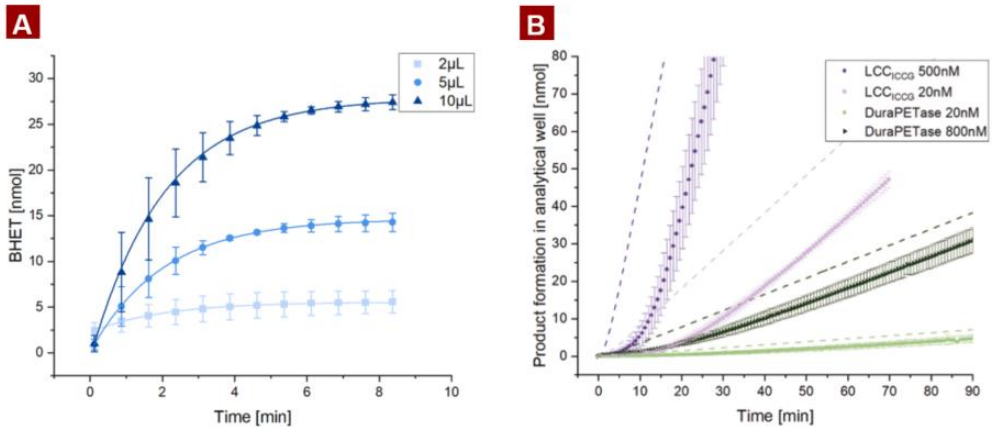

Figure 6.2 – Evaluation of the responsiveness of the diffusion of soluble products into the analysis well: A) Progression in the diffusion of various volumes of a 2.5 mM BHET suspension from the reaction well into the analysis well. The solid line represents the global fit of the experimental data to equation 6.1. B) Comparison of the product formation obtained experimentally with the simulated data, estimated by numerically solving the ODEs presented in equation 6.2 using the experimentally obtained v_{ss} and k_{mix}. This figure is adapted from figures originally published in Paper V

6.1.3 Responsiveness of the system

The responsiveness, defined as the time it took to reach 95% of the steady-state rate, was quantified by simulating $n_{aw}(t)$ by solving the following ODEs numerically:

$$\frac{\Delta n_{aw}}{\Delta t} = v_{ss} * V + k_{mix} * n_{rw} - k_{mix} * n_{aw}$$
$$\frac{\Delta n_{rw}}{\Delta t} = v_{ss} * V + k_{mix} * n_{aw} - k * n_{rw} \quad (6.2)$$

The v_{ss} used in the simulations were based on experimental data from the following enzymatic reactions; namely using 500 or 20 nM of LCC_{ICCG} or DuraPETase. V was set to 325 µL, corresponding to half of the total reaction volume (i.e. the volume of one well), while the k was 0.247 min^{-1} as previously described.

The simulations estimated the on-set time, $t_{onset,sim}$, to 8 min (Figure 6.2B and Table 6.1). This means that it would take the system 8 min before the v_{ss} in the analytical well would correspond to the actual v_{ss}. Interestingly, the experimentally determined onset time, $t_{onset,exp}$, was 3.5–10 times shorter than $t_{onset,sim}$. This shows that the observed lag phases from the experimental data could not be solely explained by the system responsiveness alone, even though a low crystalline PET was used as substrate (8.6% X_C).

Table 6.1 – Experimental and simulated on-set times for the continuous assay: The $t_{onset,\ exp}$ and v_{ss} were calculated based on the experimental data presented in Figure 6.2B. the $t_{onset,\ sim}$ was calculated according to equation 6.2 using the experimentally obtained v_{ss} and k_{mix}.

Enzyme	E_0 [nM]	v_{ss} [nmol min^{-1}]	$t_{onset,\ sim}$ [min]	$t_{onset,\ exp}$ [min]
LCC_{ICCG}	500	5.75	8	28
	20	1.01	8	56
DuraPETase	500	0.87	8	58
	20	0.16	8	83

6.2 Steady-state kinetics during enzymatic degradation of X_C PET

The influence of substrate composition on steady-state kinetics for LCC_{ICCG} was evaluated by inverse Michealis-Menten kinetics (^{inv}MM) [134]. The extent of the reactions was limited to 120 min, due to evaporation of the reaction media, as mentioned in section 6.1.1. The X_C used in the continuous assay, was therefore limited to X_C<13% as the duration of the lag phase would extend beyond the maximal incubation time, at a X_C above this level (Figure 6.3A).

Despite the narrow range of X_C used in the ^{Inv}MM analysis, an increase in X_C from 8.6% to 12.2% led to a significant 3-fold reduction in the maximal reaction rate from 0.22 to 0.07 µMs^{-1}, as specified in Table 6.2. As previously established in [134] the $^{inv}V_{max}$ is a product of the k_{cat}, initial substrate loading in g/L ($S_{0,mass}$), and the density of attack sites (Γ_{max}) :

$$^{inv}V_{max} = S_{0,mass} * \Gamma_{max} * k_{cat} \tag{6.3}$$

Since $S_{0,mass}$ is the same in all reactions, the observed decrease in $^{inv}V_{max}$ can be attributed to a reduction in Γ_{max}, a decrease in the apparent k_{cat}, or both factors concurrently. As emphasized in the previous chapters, PET-degrading enzymes are incapable of degrading the crystalline regions of PET. Hence, it is evident that the increase in X_C of a PET substrate would decrease the Γ_{max}.

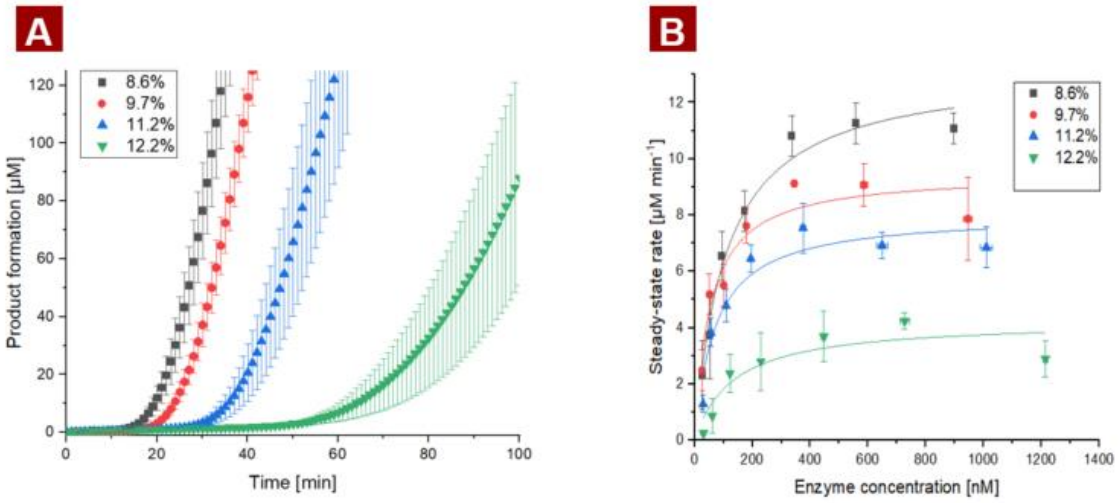

Figure 6.3 – ^{Inv}MM kinetics at different substrate crystallinities: A) Soluble product formation was monitored by the continuous assay during enzymatic degradation of PET disks at various X_C (8.6 to 12.2%) using 300nM LCC_{ICCG} at 50°C pH 9. B) ^{Inv}MM curves of LCC_{ICCG} substrate at various X_C (ranging from 8.6% to 12.2%). The steady-state rate was calculated from the linear region of the progress curves from the continuous assay.

Table 6.2 - Kinetic parameters of LCC_{ICCG} on PET disks at various X_C: The substrate composition (X_C, X_{MAF}, and X_{RAF}) was calculated by DSC. The kinetic constants ($^{inv}V_{max}$ and $^{inv}K_m$) were quantified from the ^{inv}MM curves in Figure 6.3A. Different subscript letters (a, b, or c) indicate a statistically.

Annealing condition	X_C [%]	X_{MAF} [%]	X_{RAF} [%]	$^{inv}V_{max}$ [μM s^{-1}]	$^{inv}K_m$ [μM]	$^{inv}V_{max}/^{inv}K_m$ [min^{-1}]
5 min at 85°C	8.6 ± 0.78^{a}	77.4 ± 1.9^{a}	13.8 ±1.2^{a}	0.22 ± 0.011^{a}	0.11 ± 0.018^{a}	2.0 ± 0.44^{a}
3 min at 115°C	9.7 ± 0.45^{ab}	70.9 ± 5.9^{ab}	19.4 ± 6.4^{a}	0.16 ± 0.011^{b}	0.054 ± 0.016^{a}	2.9 ± 1.1^{a}
4 min at 115°C	11.2 ± 0.31^{ab}	64.4 ± 2.6^{ab}	24.5 ± 2.8^{a}	0.13 ± 0.010^{b}	0.072 ± 0.0220^{a}	1.9 ± 1.8^{a}
5 min at 115°C	12.2 ± 0.89^{b}	62.3 ± 1.9^{ab}	25.8 ± 0.78^{a}	0.07 ± 0.011^{c}	0.13 ± 0.074^{a}	0.5 ± 0.865^{a}

To test if Γ_{max} would solely be linked to the fractional composition of the PET in terms of the rigid all-*trans* X_C, the rigid *trans*-rich X_{RAF}, or the mobile *gauche*-rich X_{MAF}, we proposed two scenarios to describe the relationship between Γ_{max} and the fractional composition:

- **Scenario 1:** LCC_{ICCG} may degrade all of the amorphous PET (MAF and RAF) equally, while the crystalline regions are resistant to enzymatic hydrolysis. Hence, $\Gamma_{max} = X_{MAF} + X_{RAF} = 100 - X_C$
- **Scenario 2:** LCC_{ICCG} may only degrade the MAF, hence both RAF and crystalline regions are resistant to the enzymatic hydrolysis. Hence, $\Gamma_{max} = X_{MAF}$

In both scenarios, we assumed that the enzyme is only acting on the specified amorphous regions. Furthermore, it is assumed that the k_{cat} is unaffected by substrate type (i.e. MAF or RAF) or changes in factional composition. To test if either of the substrate preferences specified by the scenarios could be directly correlated to the Γ_{max}, we plotted the normalized $^{inv}V_{max}$, against the normalized substrate composition, as specified by scenario 1 or 2. The slope of this plot would then correspond to the relative change in $^{inv}V_{max}$ as a function of the relative change in substrate composition. Should either of these scenarios be true, then the slope of the plots should be equal to 1. This was however not the case for either of the scenarios, as both slopes were greater than 1 (3.0 ± 0.7 for scenario 1 and 15± 2.8 for scenario 2). Both scenarios were therefore rejected.

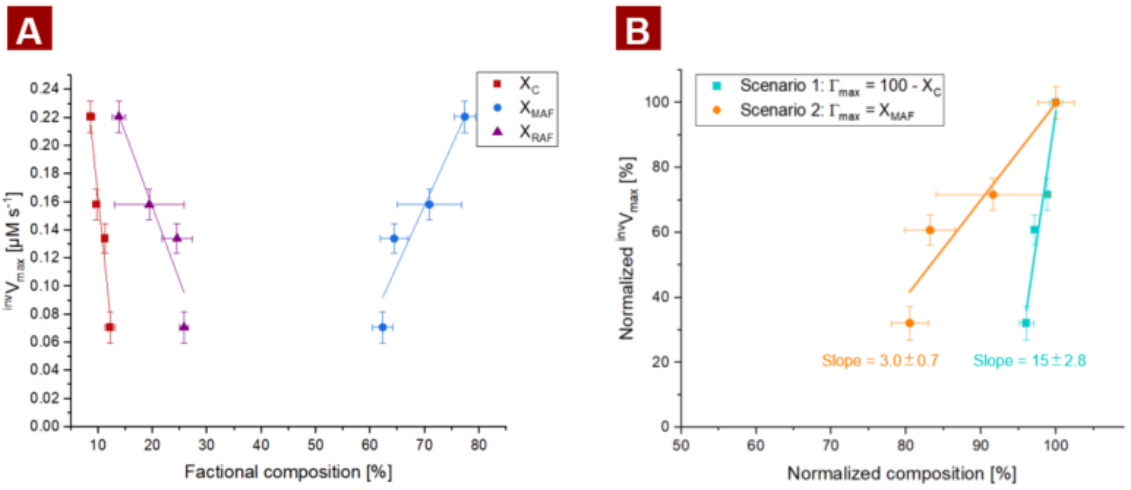

Figure 6.4 – Correlation between $^{inv}V_{max}$ and substrate composition: A) Correlation $^{inv}V_{max}$ between the fractional composition of either X_C, X_{RAF}, or X_{MAF}. B) Correlation between the normalized $^{inv}V_{max}$, estimated from the ^{inv}MM curves, normalized amorphous fraction (scenario 1), or the normalized X_{MAF} (scenario 2). The linear regression of the fits is represented by solid lines. It was hypothesized that the Γ_{max} would be equal to either $X_{MAF} + X_{RAF}$ (scenario 1) or X_{MAF} alone (scenario 2). In such a case, the slope of the regression would equal 1.

Thus, it becomes evident that neither the X_C nor X_{MAF} alone can adequately account for the reduction in $^{inv}V_{max}$. Nevertheless, X_{MAF} appears to serve as a better indicator of Γ_{max}, as the slope was 5 times lower. It is worth noticing that the relative decrease in the $^{inv}V_{max}$ by LCC_{ICCG} caused by increasing X_C was more profound than the influence of X_C on the v_{ss} of LCC_{ICCG} as shown in the previous chapters (Figure 4.7A and 5.1A). These inconsistencies are likely caused by differences in the experimental conditions. As previously mentioned the operating conditions of the continuous assay were limited to two hours at 50°C. Hence, factors such as the increase in chain mobility (induced by temperature) or increase in surface erosion, leading to a higher specific surface area (induced by prolonged degradation) may contribute to enhanced tolerance towards X_C.

6.3 Duration of lag phase

The continuous monitoring of the product formation allowed for an in-depth analysis of the lag phase. t_{lag} was quantified for all of the enzymatic reactions, used in the ^{inv}MM curves from Figure 6.3. While the v_{ss} was defined as the linear region of the progress curves the t_{lag} was defined empirically, as the intersection between the regression line of the v_{ss} and the baseline as shown in Figure 6.5A.

A clear correlation was observed between the t_{lag} and the v_{ss}, indicated by the linear regressions shown in Figure 6.5B. This negative correlation became more profound at increasing in X_C. These observations led to the following hypothesis that the lag phase was caused by a random/endo-type degradation pattern of the insoluble PET chains. Hence the average DP of the PET chains, exposed at the surface, would decrease during the initial stage. Thereby increasing the probability of chain scissoring at the terminal, resulting in the formation of a soluble product. The product formation rate would consequently be inversely proportional to the average degree DP of the surface-exposed PET chains.

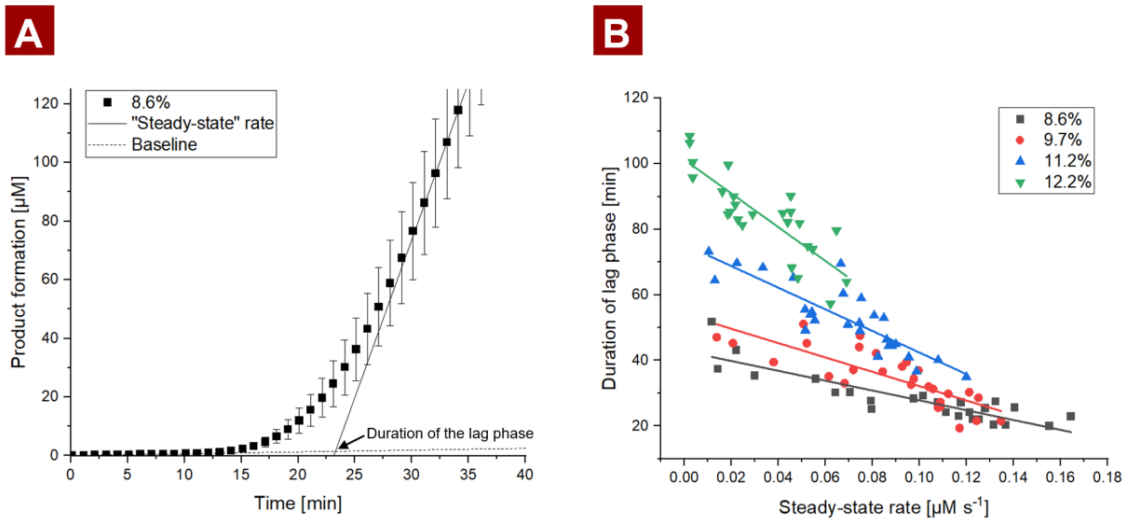

***Figure 6.5* – Correlation between the duration of lag phase steady-state rate:** A) Progress curve showing the quantification of both v_{ss} and t_{lag}. B). Correlation between the v_{ss} and t_{lag} for each data point included in the inverse MM plot in 6.3A.

Hence, t_{lag} can be attributed to the time it takes to hydrolyze the necessary number of ester bonds required to reach a steady state where the average degree of polymerization (DP) of the exposed polymeric chains remains constant. The increase in t_{lag} resulting from the increase in X_C would therefore imply that the necessary number of ester bonds required to reach a steady-state increases with X_C. A possible explanation for this phenomenon could be attributed to the density of entanglements in the amorphous regions, as it has been shown that crystal formation during annealing at temperatures < 120°C (which is the case in this study) does not unfold entanglements in the amorphous regions [135]. Hence the relative density of entanglements in the amorphous regions would increase as the X_C increases. These entanglements could potentially shield the free ends of the polymeric chains, which are required, to yield a soluble product.

6.4 Proton release during enzymatic degradation of PET

While endo-type chain scissoring does not result in any product formation, the hydrolysis still results in the release of a positively charged proton. Hence the preference of an enzyme towards endo- or exo-type chain scissoring can be determined by comparing the total production of a soluble product with the total release of protons, as demonstrated by Schubert et. al [90]. We, therefore, assayed LCC_{ICCG} in a pH-stat system, while periodically sampling for HPLC measurements, to test the aforementioned hypothesis, that enzymatic degradation of more crystalline PET substrate would be facilitated by more endo-type cleavage compared to amorphous PET.

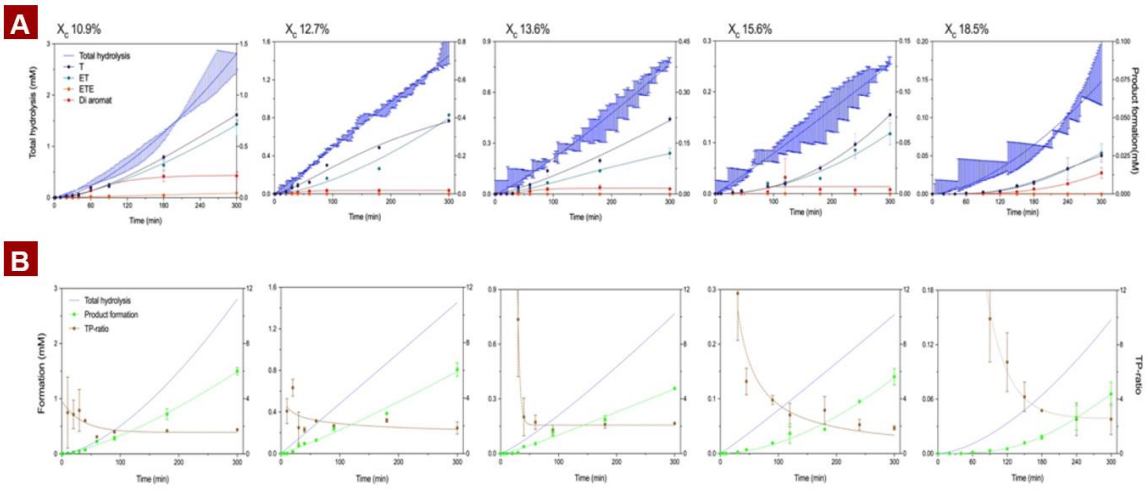

Figure 6.6 – Progress curves of soluble product formation and proton release during enzymatic degradation of PET at various X_C: A) Total hydrolysis measured in terms of C_{H+} (left ordinate) or concentration of soluble products measured by HPLC (right ordinate) in terms of TPA (T), MHET (TE), BHET (ETE), and diaromatic OET during 300 min of enzymatic treatment of PET disks at various X_C. B) Comparison of the cumulative product formation with the total hydrolysis. The TP ratio indicates the total hydrolysis divided by the product formation. All reactions were performed using 150 nM $LCCI_{CCG}$ at 65°C in a pH-stat system with a set point of pH 9, using 9 PET disks in 9.5 mL water.

The progress curves depicted in Figure 6.6 reveal a noticeable difference in the behavior of lag phases when assessed in terms of the cumulative release of soluble products, C_P, (quantified by RP-HPLC), or the release of protons, C_{H+}, (quantified by NaOH consumption). As expected, a lag phase was observed for the progress curves measured

in terms of C_P, which became more distinct as the X_C increased. This was however not the case for the progress curves measured in terms of C_{H+}, as it was only substrate at a X_C of 18.5% that a significant lag phase was observed. This lag phase was even less profound compared to the one measured in terms of C_P at 18.5% X_C. The shorter t_{lag} observed from the progress curves based on C_{H+} compared to C_P substantiated the aforementioned mechanism stating that the lag phase was caused by random/endo-type chain scissoring. Interestingly, no proton release was observed during the initial stage of the degradation of the sample at 18.5% X_C. Thus indicating that no hydrolysis was occurring during the initial stage of the enzyme treatment. It could be speculated if this observation is caused by unproductive binding, which has previously been shown to be the major interaction between PET and PET degrading enzymes [136].

6.5 Chapter summary

In summary, Chapter 6 introduced a novel compartmentalized setup for continuous monitoring of the product formation during enzymatic hydrolysis of PET. This assay was used to quantify the kinetic constants, for LCC_{ICCG} at various substrate X_C, using ^{inv}MM kinetics. These results indicated that neither the amorphous fraction (X_{MAF} and X_{RAF}) nor the X_{MAF} alone corresponded to the Γ_{max}, thereby rejecting **H4**.

By analyzing the progress curves from individual data points in the ^{inv}MM, it was observed that the t_{lag} correlated with the v_{ss}. Here, the t_{lag} became more district with increasing X_C. This observation was suggested to be caused by an initial random-type degradation pattern that would not yield any product formation during the initial stage due to the shortening of the PET chains rather than solubilization. This proposed degradation pattern was supported by the detection of proton release during the lag phase. Indicating that the insoluble PET chains underwent hydrolysis through endo-type chain scissoring, during the initial stage. Thus confirming **H5**.

Chapter 7: Discussion

7.1 Considerations for enzymatic degradation of PET

The enzymatic degradation of PET is a complex matter as the reaction conditions itself may affect the substrate properties of PET. This includes thermal-induced crystallization of PET, which occurs at reaction temperatures of 70°C or higher [12,34]. Consequently, enzyme degradation above this temperature is not feasible as increasing X_C, as highlighted in this thesis, significantly lowers the efficiency of enzyme hydrolysis. The thermostability of PET degrading enzymes does therefore not need to exceed 70°C, as evident from LCC_{ICCG}, which had a temperature optimum at 70°C despite being thermally stable at 75°C (Figure 4.1).

Another property that is affected by reaction conditions is the T_g, which is lowered due to the plasticizing effect of water. It has previously been suggested that enzymatic reactions should be performed at temperatures above T_g, as the increased chain mobility resulting from the devitrification (transition from the rigid "glassy" state to the more mobile "rubbery" state)[70,114–116]. However, we observed that this devitrification of the bulk material (specified by the bulk T_g) of a PET sample did not affect the enzyme hydrolysis rate. Instead, we proposed that the increase in reaction rate with increasing temperatures near T_g results from thermal activation of the enzyme (i.e., the Arrhenius effect) rather than increased mobility of the polymeric chains resulting from the devitrification.

In fact, it has previously been shown that the T_g at the surface of PET is substantially lower than the T_g of the bulk [34,122,123]. This may be as low as 40°C[124], which explains the drastic increase in reaction rate around this temperature [70,124]. This effect is however less profound for a more crystalline sample as it presumable has a limited content of MAF, while a greater content of RAF and crystals, thus retaining the overall mobility at the surface [137]. This could explain why enzymatic degradation of PET is lower on PET substrate at higher X_C. A schematic representation of the factors affecting the temperature optima of PET degrading enzymes is shown in Figure 7.1.

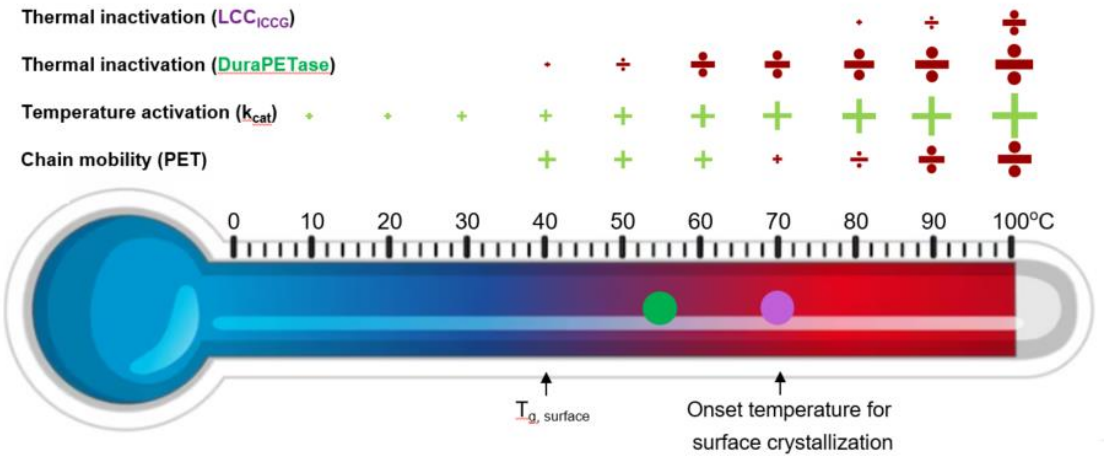

Figure 7.1 – Temperature dependence of selected factors affecting the temperature optima of PET degrading enzymes: The green "+" indicates a positive effect to the v_{ss}, while the red "÷" indicate a negative effect. The size of the symbol scales with the contribution to the v_{ss}. The temperature optima of DuraPETase and LCC_{ICCG} are indicated by circles.

In a recent study by Ding et al., it was shown that the temperature optima of a six-point mutant of LCC_{ICCG}, namely LCC_{ICCG_I6M}, had higher 1.26-fold activity on highly crystalline PET powder, compared to LCC_{ICCG} when assayed at their temperature optima. The enhanced activity of LCC_{ICCG_I6M} was attributed to its higher thermostability [81]. However, as the increased thermostability of LCC_{ICCG_I6M} only resulted in a 1.26-fold increase in activity between 65 to 80°C, we believe that increased thermostability of PET degrading enzymes alone is not sufficient to archive efficient degradation of high X_C PET. Instead, the substrate selectivity of the enzymes should be improved to facilitate a higher activity on the more crystalline regions

7.2 Standardized method for evaluation of the influence of substrate X_C on PET degrading enzymes

As described in Chapter 3, there is no standardized methodology for evaluating the effect of substrate crystallinity on the enzymatic degradation of PET. Previous investigations on the effect of crystallinity have therefore been conducted using PET substrates processed in various manners (e.g. amorphous film and crystalline PET powder) or using PET material processes in the same manner but with a limited number of different levels of X_C [70,73,81,83,84,106,129,138,139]. Due to the complex nature of PET (conformational heterogeneity, chain mobility, crystal morphology, etc.), as highlighted in Chapter 2, it is not ideal to use PET, which has been processed differently (e.g. film and particles) for evaluating the effect of X_C. This is because these substrates may differ in other properties (SSA, crystal morphology, etc.), which may also affect the hydrolysis rate [17,130,131]. Hence, a bias is introduced as observed changes in the rate may be caused by other factors than X_C. A standardized, well characterized, model substrate is consequently a prerequisite to ensure reproducibility and a direct comparison between studies performed in different labs [140].

This led to the development of a standardized method for the evaluation of X_C on the enzymatic degradation of PET. As described in Chapter 3, our method involved thermally induced crystallization via annealing of a commercially available amorphous PET sheet (Goodfellow, Cat. No. ES303010). These sheets were cut into uniform disks using a hole puncher (Ø=6 mm) before the annealing. This procedure was able to obtain a range of PET substrates with X_C ranging from ~10% X_C (untreated sample) to ~30% X_C. This range was ideal for the evaluation of the influence of PET-degrading enzymes, as it previously has been shown that the rate of a PET-degrading enzyme (namely the IsPETase) is most drastically affected between 16 and 25% X_C [84]. Thermal-induced crystallization has previously been used to modify the X_C of PET. This was however done by either annealing of spin-coated PET film [106], or via isothermal crystallization from melt [84]. However, these methods are more labor intensive and require special equipment, which is not common in all biochemistry laboratories, which is unlike the method proposed in this thesis.

7.2.1 Tolerance towards substrate crystallinity

Once the standardized methodology for modifying the substrate crystallinity of PET had been developed, a deeper insight into the influence of the X_C on the enzymatic degradation

of PET could be obtained. From the progress curves, it was evident that the initial degradation, referred to as the lag phase did not yield any product formation or surface erosion. Once this this lag phase had been overcome a v_{ss} was reached. This rate was significantly reduced by increasing X_C as previously established [17,84,106]. This effect becomes particularly profound once X_C exceeds a certain threshold, ~20%. A similar observation was observed by Erickson et al. who found that the activity of the IsPETase and a double mutant depleted around 20% X_C [84]. By studying the v_{ss} of LCC_{ICCG} and other PET hydrolases at various reaction conditions, we found that the threshold dependent on both enzyme and reaction conditions, as the threshold seemingly increased at elevated temperatures and longer reaction times.

As previously described, the increase in X_C results in a reduction in chain mobility and a change in the conformational state (increased *trans* conformers). The negative effect of the X_C is therefore expected to be more profound at temperatures above the surface T_g (40°C[124]), as the MAF chains are at their mobile state, thus allowing them to change between conformations (*gauche* or *trans*). In contrast, when the X_C increases the overall chain mobility of PET is gradually hindered as the proportion MAF decreases with X_C as highlighted in Paper I, while RAF generally increases [96,135]. We, therefore, propose that a high tolerance towards the X_C observed for LCC_{ICCG}, compared to PHL7, is due to a broader conformational selectivity towards the *trans* conformation of the PET chains. As shown by the RSMF, the enhanced selectivity is presumably governed by the flexibility in proximity to the active site. This flexibility would be required to facilitate the binding of PET chains existing in both *gauche* or *trans* conformations.

The conformational selectivity the IsPETase was recently studied by Guo et al. By studying the substrate-enzyme binding via molecular docking OETs combined with the enzyme activity on *trans*-rich microwave pretreated substrate, they showed that an A238S variant obtained a presumably higher specificity towards *trans* conformers. In contrast, the WT IsPETase had a preference for *gauche* conformations. This preference towards either gauche or trans conformers was attributed to the orientation of W185 [129]. Although this Tryptophan is conserved in LCC, LCC_{ICCG}, DuraPETase, and PHL7, no differences were observed in the RSMD this residue, which corresponds to position 159 in the RSMF in figure 5.5A. Hence, no direct link could be observed between our observations and the ones made by Guo et al. There were however certain drawbacks associated with the methodology useed by Guo et al. Firstly, the molecular docking of PET oligomers may not reflect the binding of larger PET chains as specified by Wei et al [141]. Secondly, the microwave-assisted pretreatment resulted in the partial degradation of the PET, thus lowering the average DP substantially to a DP of 12 [129,142]. The higher activity on the pretreated substrate might as well reflect an increased preference towards shorter chains rather than *trans* conformers. Consequently, it would be interesting to determine the tolerance towards X_C for the $IsPETase_{S238A}$ using the standardized substrate presented in this thesis. As this would enable a more direct comparison of the activity on PET samples with different ratios of *gauche-trans* ratios.

7.3 Proposed degradation mechanism

7.3.1 Chain scissoring of PET degrading enzymes

The enzymatic degradation of PET has previously been reported to occur via a combination of endo and exo-type chain scissoring [17,90,93]. A recent study by Schubert et al [90], demonstrated that the main degradation products from the heterogeneous catalysis of PET, using IsPETase, LCC, HiC, and TfC, are larger OETs containing two or three TPA moieties (denoted dimer and trimer, respectively). In fact, more than 70% of the monoaromatic degradation products (TPA, MHET, and BHET), were generated through the homogeneous catalysis of OETs. The observed accumulation of MHET is therefore a consequence of a substantially lower specificity constant with MHET as substrate compared to the other larger fragments [90].

A similar observation during the initial degradation of amorphous PET film using LCC_{ICCG} was demonstrated in Chapter 4. However, the main degradation product was an oligomer with four TPA moieties (tetramer). The tetramer did In fact contribute to ~50% of soluble products during the initial 20 s of enzyme treatment. This observation suggests that the degradation mechanism of LCC_{ICCG} is not governed by completely random endo-type chain scissoring, as that, from a stoichiometric point of view would result in a product profile with a uniform distribution of mono- di- tri- and tetra-aromatics during the initial stage of degradation (before the homogeneous catalysis). We therefore postulate that LCC_{ICCG} has a preference for releasing larger fragments (i.e. tetramers), which are subsequently hydrolyzed further into smaller fragments via homogeneous catalysis in the soluble fraction.

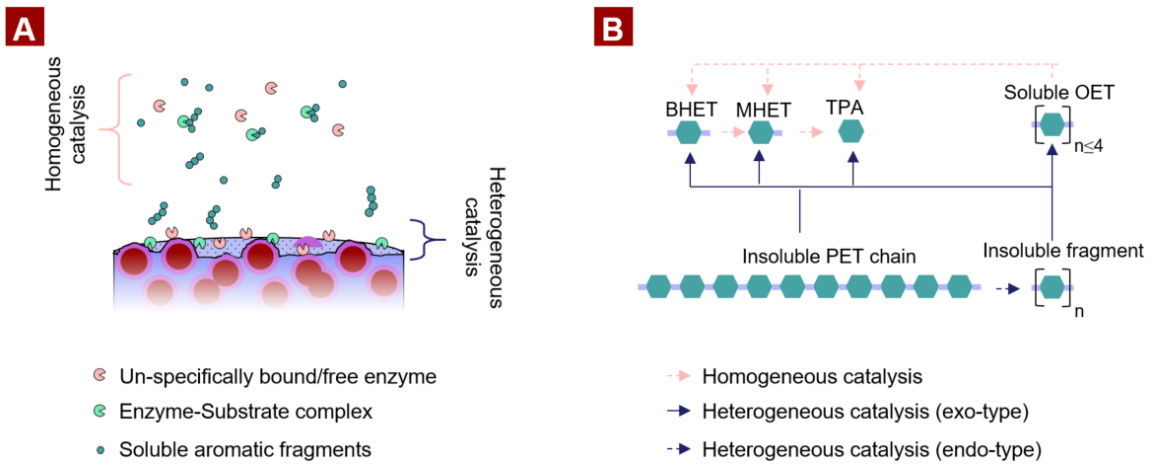

Figure 7.2 – Schematic representation of the enzymatic degradation of PET: A) Enzymatic degradation of PET is governed by heterologous catalysis (at the interface between the insoluble polymer and the aqueous solution) and homogeneous catalysis (in the aqueous solution). At the surface of PET, the enzymes may either bind specifically to the substrate, thus yielding a productive ES complex, which may result in the release of a soluble Oligomer (preferably tetramers). The enzyme may also bind nonproductively, which does not result in any hydrolysis. The effect is more profound on the ungradable crystalline regions illustrated by red spheres with purple edges. The degradation products from the heterologous catalysis are subsequently hydrolyzed further via homogeneous catalysis. B) Simplified reaction scheme of the enzymatic degradation of PET. The dashed lines represent reactions at which new soluble products are formed.

A schematic illustration of this proposed degradation mechanism is shown in Figure 7.2A. This preference for releasing larger OETs rather than monoaromatics is likely caused by a reduced preference towards hydrolyzing the ester bonds nearest the terminal of the PET chain, as shown for cutinases originating from *T. cellulosilytica* and *T. fusca* [143]. These tetramers are, however, rapidly hydrolyzed into smaller fragments (primarily TPA and MHET) via homogeneous catalysis by the enzyme, once released into the soluble fraction as shown in Figure 7.2B. This proposed mechanism stands in contrast to other proposed degradation mechanism where MHET has been proposed as the main degradation product of the heterogeneous catalysis [73,128,144,145]. These mechanisms have, however, been postulated based on a structural analysis of the enzyme-substrate binding. However, as these have been made using PET fragments, such as $MHET_4$ (tetramer) or other smaller fragments, they may not reflect the actual enzyme-substrate interaction with larger and more rigid PET chains as specified in [141].

Another explanation could be that the tetramer is an intermediate product which, as previously mentioned, is rapidly hydrolyzed into smaller fragments, and are may therefore be difficult to detect. In fact, we observed that the tetramer accounted for <10% of the total composition of soluble products after 4 min, and <1% after 20 min. This was despite a very high substrate to enzyme loading, which would facilitate heterogeneous catalysis. This effect may even be more profound on enzymes that are less efficient on PET, as it has been shown the specificity constant of different PET degrading enzymes may be quite similar on di- or trimers, despite their difference on PET [90]. The bottleneck for PET degrading enzymes is therefore related to the heterogeneous catalysis yielding oligomers, rather than the homogeneous catalysis of solubilized products into the monomers. This bottleneck becomes even more evident when it comes to more crystalline PET samples, due to the limited activity of PET degrading enzymes on X_C PET, as highlighted in this thesis.

7.3.2 Degradation mechanism on X_C PET

The initial stage of the enzymatic degradation of PET, denoted as the lag phase, did not yield any product formation. The duration of these lag phases was further shown to increase with increasing X_C, as highlighted in Chapter 6. This phenomenon was attributed to an initial random/endo-type degradation, which as highlighted in Figure 7.2B does not result in any immediate product formation. Instead, the average chain length of the PET chains exposed to the surface becomes shorter. As the chain length decreases due to endo-type degradation, the probability of a cleavage near the terminal (exo-type degradation) increases, resulting in the release of a soluble product (primarily tetramers). Thus resulting in a gradual increase in the product formation rate (lag phase), until a steady-state rate has been reached. Based on the large quantities of the tetramer, during the initial stage of degradation, we hypothesized that a steady state rate occurs as a consequence of the formation of new free chain ends, resulting from endo-type degradation. At some point, the concentration of free ends reaches a level at which the concentration of ES complexes resulting in exo-type degradation would reach a steady-state, resulting in a constant product release. This is either obtained via saturation of the enzymes by the number of free hydrolyzable ends (low X_C) or saturation of these hydrolyzable ends by the enzymes (high X_C). The rate at low X_C is therefore limited by the

enzyme concentration, while the rate at higher X_C is limited by the density of attackable sites suitable for endo-lytic degradation. This mechanism does furthermore explain the observed correlation between the v_{ss} and t_{lag} observed in Chapter 6.

Combinatorial degradation mechanisms have previously been reported in the literature for TfCut2, IsPETase, and Cut190 [17,145,146]. Thus, suggesting that this degradation mechanism is conserved among PET degrading enzymes (Cutinases). While the degradation mechanism may be conserved, the preference towards endo- and exo-type degradation is shown to differ between different PET degrading enzymes [90,93]. In fact, we observed that the t_{lag} as a function of substrate X_C differs for different enzymes. PHL7, HiC, and TfC had profoundly longer lag phases at higher X_C than LCC, LCC_{ICCG}, and DuraPETase. This observation concurs with a recent study by Schubert et al. [90] who via stochastic modeling showed that HiC was less likely to perform endo-type degradation compared to LCC.

It has previously been shown that PET-degrading enzymes primarily bind nonproductively to PET [136]. We, therefore, propose that longer lag phases observed for PHL7 compared to LCC are caused by nonproductive binding. As the accessible site, quantified by Γ_{max} would be more scares for PHL7 it would be less likely to form a productive ES complex, compared to LCC. Based on the observation of local cavities in the SEM imaging we speculate that once a productive ES complex has been formed, the enzymes are more capable of forming a new productive ES complex, as the enzyme is in proximity to another hydrolyzable regions in what would appear as “exo”-type degradation. The preference towards endo or exo-type could therefore also be explained by the substrate specificity, as an enzyme with a lower Γ_{max} (i.e. HiC or PHL7) would be capable of degrading fewer chain segments at the surface. Hence the average reduction in DP (which has previously been used to determine and distinguish between endo or exp-type degradation) at the surface would be less profound, as fewer chain segments are degraded.

Lastly, we observed that PHL7, unlike LCC, LCC_{ICCG}, or DuraPETase had a negative surface charge located at the opposite site of the active site. We propose that PHL7 may only degrade in one direction, as the enzyme is aligned by repulsion forces between the negative charge on the backside of PHL7 and the negative charges of the carboxylic end-groups of the hydrolyzed PET, which could explain the observed crater formations.

.

Chapter 8: Conclusion and Perspectives

The work of this thesis focused on elaborating the current knowledge of how substrate-related properties affected the enzymatic degradation of PET. We hypothesized that The X_C of PET material can be systematically controlled through thermal annealing, enabling the creation of a standardized substrate for evaluating the impact of X_C on the enzymatic hydrolysis of PET, **H1**, which we confirmed by successfully implementing an experimental platform for evaluating the effect of X_C using thermally annealed PET disks as a model substrate.

We further hypothesized that enzyme reactions at high temperatures near T_g would increase the hydrolysis rate due to increased mobility, **H2**. This hypothesis was, however, rejected; instead, we ascribe the increase in reaction rates at elevated temperatures to thermal activation. However, there is a possibility that the increase in mobility caused by the devitrification occurs at a much lower temperature, as the T_g at the surface may be drastically lower than in the bulk.

The third hypothesis of the thesis, **H3**, was centered around the effect of X_C on enzyme activity. Using the thermally annealed PET substrate we quantitatively evaluated the influence of X_C on the action of PET degrading enzymes. This was done by characterizing six benchmark PET-hydrolases in terms of their robustness towards increasing levels of X_C. For this purpose, we introduced the term "tolerance to X_C" as a quantitative measure to evaluate the decrease in reaction rate caused by increasing X_C. Interestingly, we observed that LCC, LCC_{ICCG}, and DuraPETase were more robust towards increasing X_C than PHL7, TfC, and HiC, thus confirming the third hypothesis of the thesis.

To investigate whether enhanced tolerance towards X_C exhibited by LCC_{ICCG} could be directly attributed to the selectivity of the enzyme in terms of substrate composition (X_C, X_{RAF}, or X_{MAF}), as specified in **H4**, we further studied the kinetics of LCC_{ICCG} on PET with different substrate compositions. Although the ${}^{inv}V_{max}$ was heavily affected by changes in the substrate composition, Γ_{max}, which is a quantitative measure for the substrate selectivity, was not directly linked to either X_{MAF} or the entire amorphous fraction (100- X_C). Although X_{MAF} was found to be the better descriptor for Γ_{max} it was still a too broad term as the relative decrees in ${}^{inv}V_{max}$ decrease by 3% for each 1% decrease in X_{MAF}. Thus declining the fourth hypothesis.

Lastly, the degradation mechanism of PET-degrading enzymes was studied as specified by the fifth and final hypothesis (**H5**). We observed that the initial stage of degradation did not yield any product formation. This phenomenon was attributed to an endo-type degradation mechanism, in which the initial hydrolysis of PET would result in a lowering of the average chain DP without releasing products. Eventually, the chain becomes so small that hydrolysis results in the release of products. This mechanism was consolidated by monitoring the proton release during degradation of PET substrate at various X_C levels, as the lag phase obtained here was less distinct compared to that obtained through soluble products. This confirms the fifth hypothesis of this thesis, as we could gain a deeper understanding of the degradation mechanism of PET-degrading enzymes by studying the degradation of crystalline PET samples.

In conclusion, this Ph.D. thesis has advanced our understanding of enzymatic degradation of PET by studying the relationships between substrate-related properties and enzyme behavior. The knowledge gained not only contributes to the academic understanding of enzymatic degradation of PET, but also holds promise for practical applications in waste management and environmental sustainability.

8.1 Future perspectives

Recently, The European Union enacted a legislation mandating a levy of EUR 0.80 per kilo on newly produced plastics, excluding those made from recycled plastics [147]. This levy corresponds to 100% to 160% of the costs of the clean PET flakes, which are the precursors for the molding of new PET products [20]. This legislation is expected to have a positive impact on the recycling of plastic and further drive the adaptation of enzymatic recycling as a sustainable technology choice.

Several engineering strategies have already successfully enhanced the activity and stability of PET-degrading enzymes [12,18,83,85]. In fact, the benchmark enzyme LCC_{ICCG} has proven effective for industrial applications when applied on amorphous or low X_C PET substrates [12,20,94]. However, an enzyme that may efficiently degrade PET substrate at higher X_C (>20%) has not yet been discovered. This is however essential to fully unlock the potential of this technology by eliminating the need for a substrate pretreatment step. This would result in increased cost efficiency and a reduced environmental footprint [20].

Archiving this requires a better understanding of the enzymatic degradation mechanism of the crystalline regions and RAF regions of PET. We anticipate that the methodology presented in Chapter 3 could be used as the standardized model substrate for the characterization of the isolated effect of the X_C on the enzymatic degradation of PET. This insight could help drive research towards a better understanding of the structural features of an enzyme, required for efficient degradation of high X_C waste PET. This knowledge would allow a rational approach for selecting and engineering enzymes that may efficiently degrade the crystalline regions of PET.

.

List of References

[1] Geyer R, Jambeck JR, Law KL. Production, use, and fate of all plastics ever made. Sci Adv 2017;3:e1700782. https://doi.org/10.1126/sciadv.1700782.

[2] European Commission. A circular economy for plastics – Insights from research and innovation to inform policy and funding decisions. 2019. https://doi.org/10.2777/269031.

[3] Plastics Europe. Plastics – the Facts 2022. Available at: Https://Plasticseurope.Org/Knowledge-Hub/Plastics-the-Facts-2022/: 2022.

[4] World Economic Forum Ellen MacArthur Foundation McKinsey & Company. The New Plastics Economy: Rethinking the future of plastics. Available at: Https://Ellenmacarthurfoundation.Org/the-New-Plastics-Economy-Rethinking-the-Future-of-Plastics: 2016.

[5] Marathe KV, Chavan KR, Nakhate P. Life Cycle Assessment (LCA) of PET Bottles. Elsevier Inc.; 2019. https://doi.org/10.1016/b978-0-12-811361-5.00008-0.

[6] Barnes DKA, Galgani F, Thompson RC, Barlaz M. Accumulation and fragmentation of plastic debris in global environments. Philos Trans R Soc B Biol Sci 2009;364:1985–98. https://doi.org/10.1098/rstb.2008.0205.

[7] Rosevelt C, Los Huertos M, Garza C, Nevins HM. Marine debris in central California: Quantifying type and abundance of beach litter in Monterey Bay, CA. Mar Pollut Bull 2013;71:299–306. https://doi.org/10.1016/j.marpolbul.2013.01.015.

[8] Zumstein MT, Rechsteiner D, Roduner N, Perz V, Ribitsch D, Guebitz GM, et al. Enzymatic Hydrolysis of Polyester Thin Films at the Nanoscale: Effects of Polyester Structure and Enzyme Active-Site Accessibility. Environ Sci Technol 2017;51:7476–85. https://doi.org/10.1021/ACS.EST.7B01330.

[9] Tokiwa Y, Suzuki T. Hydrolysis of polyesters by lipases. Nature 1977;270:76–8. https://doi.org/10.1038/270076a0.

[10] Wei R, Zimmermann W. Microbial enzymes for the recycling of recalcitrant petroleum-based plastics: how far are we? Microb Biotechnol 2017;10:1308–22. https://doi.org/10.1111/1751-7915.12710.

[11] Sulaiman S, Yamato S, Kanaya E, Kim JJ, Koga Y, Takano K, et al. Isolation of a novel cutinase homolog with polyethylene terephthalate-degrading activity from leaf-branch compost by using a metagenomic approach. Appl Environ Microbiol 2012;78:1556–62. https://doi.org/10.1128/AEM.06725-11.

[12] Tournier V, Topham CM, Gilles A, David B, Folgoas C, Moya-Leclair E, et al. An engineered PET depolymerase to break down and recycle plastic bottles. Nature 2020;580:216–9. https://doi.org/10.1038/s41586-020-2149-4.

[13] Zimmermann W. Biocatalytic recycling of polyethylene terephthalate plastic. Philos Trans R Soc A 2020;378. https://doi.org/10.1098/RSTA.2019.0273.

[14] Müller RJ, Schrader H, Profe J, Dresler K, Deckwer WD. Enzymatic degradation of poly(ethylene terephthalate): Rapid hydrolyse using a hydrolase from T. fusca. Macromol Rapid Commun 2005;26:1400–5. https://doi.org/10.1002/marc.200500410.

[15] Tiso T, Narancic T, Wei R, Pollet E, Beagan N, Schröder K, et al. Bio-upcycling of polyethylene terephthalate. BioRxiv 2020:2020.03.16.993592. https://doi.org/10.1101/2020.03.16.993592.

[16] Thomsen TB, Hunt CJ, Meyer AS. Influence of substrate crystallinity and glass transition temperature on enzymatic degradation of polyethylene terephthalate (PET). N Biotechnol 2022;69:28–35. https://doi.org/10.1016/j.nbt.2022.02.006.

[17] Wei R, Breite D, Song C, Gräsing D, Ploss T, Hille P, et al. Biocatalytic Degradation Efficiency of Postconsumer Polyethylene Terephthalate Packaging Determined by Their

Polymer Microstructures. Adv Sci 2019;6. https://doi.org/10.1002/advs.201900491.

[18] Lu H, Diaz DJ, Czarnecki NJ, Zhu C, Kim W, Shroff R, et al. Machine learning-aided engineering of hydrolases for PET depolymerization. Nat 2022 6047907 2022;604:662–7. https://doi.org/10.1038/s41586-022-04599-z.

[19] Karacan I. An in Depth Study of Crystallinity, Crystallite Size and Orientation Measurements of a Selection of Poly(Ethylene Terephthalate) Fibers. Fibers Polym 2005;6:186–99.

[20] Singh A, Rorrer NA, Nicholson SR, Erickson E, DesVeaux JS, Avelino AFT, et al. Techno-economic, life-cycle, and socioeconomic impact analysis of enzymatic recycling of poly(ethylene terephthalate). Joule 2021. https://doi.org/10.1016/j.joule.2021.06.015.

[21] Torres N, Robin JJ, Boutevin B. Study of thermal and mechanical properties of virgin and recycled poly(ethylene terephthalate) before and after injection molding. Eur Polym J 2000;36:2075–80. https://doi.org/10.1016/S0014-3057(99)00301-8.

[22] Rex Whinfield J, Tennant Dickson J. Polymeric Linear Terephthalic Esters. US2465319, 1949.

[23] Wyeth NC, Mendenhall P, Roseveare RN. Biaxially oriented poly(ethylene terephthalate) bottle. US3733309, 1973.

[24] Textile Exchange. Preferred Fiber & Materials Market Report 2021. Available at: Https://Textileexchange.Org/Knowledge-Center/Reports/Preferred-Fiber-Materials-Market-Report-2021//: 2021.

[25] Cusano I, Campagnolo L, Aurilia M, Costanzo S, Grizzuti N. Rheology of Recycled PET. Materials (Basel) 2023;16:1–23. https://doi.org/10.3390/ma16093358.

[26] Hu W, Zha L. Theoretical aspects of polymer crystallization. Control. Morphol. Polym. Mult. Scales Struct. Process., Springer International Publishing; 2016, p. 101–43. https://doi.org/10.1007/978-3-319-39322-3_4.

[27] Bartczak Z. Deformation of semicrystalline polymers – the contribution of crystalline and amorphous phases. Polimery 2017;62:787–99. https://doi.org/10.14314/POLIMERY.2017.787.

[28] Kurita T, Fukuda Y, Takahashi M, Sasanuma Y. Crystalline Moduli of Polymers, Evaluated from Density Functional Theory Calculations under Periodic Boundary Conditions. ACS Omega 2018;3:4824–35. https://doi.org/10.1021/acsomega.8b00506.

[29] Thomsen TB, Hunt CJ, Meyer AS. Standardized method for controlled modification of poly (ethylene terephthalate) (PET) crystallinity for assaying PET degrading enzymes. MethodsX 2022;9:101815. https://doi.org/10.1016/J.MEX.2022.101815.

[30] Karagiannidis PG, Stergiou AC, Karayannidis GP. Study of crystallinity and thermomechanical analysis of annealed poly(ethylene terephthalate) films. Eur Polym J 2008;44:1475–86. https://doi.org/10.1016/j.eurpolymj.2008.02.024.

[31] Liu J, Geil PH. Crystal structure and morphology of poly(ethylene terephthalate) single crystals prepared by melt polymerization. J Macromol Sci - Phys 1997;36:61–85. https://doi.org/10.1080/00222349708220415.

[32] Mitchell GR, Tojeira A. Controlling the morphology of polymers: Multiple scales of structure and processing. 2016. https://doi.org/10.1007/978-3-319-39322-3.

[33] Al Raheil IAM. Morphology and crystallization of poly(ethylene terephthalate). Polym Int 1994;35:189–95. https://doi.org/10.1002/pi.1994.210350209.

[34] Shinotsuka K, Assender H. In situ AFM study of near-surface crystallization in PET and PEN. J Appl Polym Sci 2016;133. https://doi.org/10.1002/app.44269.

[35] Mandal S, Dey A. PET Chemistry. Recycl Polyethyl Terephthalate Bottles 2019:1–22. https://doi.org/10.1016/b978-0-12-811361-5.00001-8.

[36] Tsai RS, Lee DK, Fang HY, Tsai HB. Crystalline study of amorphous poly(ethylene terephthalate) sheets through annealing. Asia-Pacific J Chem Eng 2009;4:140–6. https://doi.org/10.1002/apj.189.

[37] Jabarin SA. Strain-induced crystallization of poly(ethylene terephthalate). Polym Eng Sci 1992;32:1341–9. https://doi.org/10.1002/pen.760321802.

[38] Li Y, Makita Y, Zhang G, Rui G, Li ZM, Zhong GJ, et al. Effects of Rigid Amorphous Fraction and Lamellar Crystal Orientation on Electrical Insulation of Poly(ethylene terephthalate) Films. Macromolecules 2020;53:3967–77. https://doi.org/10.1021/acs.macromol.0c00646.

[39] Zekriardehani S, Jabarin SA, Gidley DR, Coleman MR. Effect of Chain Dynamics, Crystallinity, and Free Volume on the Barrier Properties of Poly(ethylene terephthalate) Biaxially Oriented Films. Macromolecules 2017;50:2845–55. https://doi.org/10.1021/acs.macromol.7b00198.

[40] Androsch R, Wunderlich B. The link between rigid amorphous fraction and crystal perfection in cold-crystallized poly(ethylene terephthalate). Polymer (Guildf) 2005;46:12556–66. https://doi.org/10.1016/J.POLYMER.2005.10.099.

[41] Di Lorenzo ML, Righetti MC, Cocca M, Wunderlich B. Coupling between Crystal Melting and Rigid Amorphous Fraction Mobilization in Poly(ethylene terephthalate). Macromolecules 2010;43:7689–94. https://doi.org/10.1021/MA101035H.

[42] Slobodian P. Rigid amorphous fraction in poly(ethylene terephthalate) determined by dilatometry. J Therm Anal Calorim 2008;94:545–51. https://doi.org/10.1007/s10973-007-8566-x.

[43] Zhang Q, Zhang R, Meng L, Lin Y, Chen X, Li X, et al. Biaxial stretch-induced crystallization of poly(ethylene terephthalate) above glass transition temperature: The necessary of chain mobility. Polymer (Guildf) 2016;101:15–23. https://doi.org/10.1016/J.POLYMER.2016.08.054.

[44] Chen H, Cebe P. Vitrification and devitrification of rigid amorphous fraction of PET during quasi-isothermal cooling and heating. Macromolecules 2009;42:288–92. https://doi.org/10.1021/ma802104a.

[45] Choi J, Cakmak M. Morphological evolution during thermal and strain induced crystallization in poly(ethylene terephthalate)/poly(ether imide) blend films. Polymer (Guildf) 2016;84:10–20. https://doi.org/10.1016/J.POLYMER.2015.12.038.

[46] Levine H, Grenet J, Slade L. Water as a plasticizer: physico-chemical aspects of low-moisture polymeric systems. Eur Polym J 1993;30:339–45. https://doi.org/10.1017/cbo9780511552083.002.

[47] Chen Y, Lin Z, Yang S. Plasticization and Crystallization of Poly(ethylene Terephthalate) Induced by Water. J Therm Anal Calorim 1998 522 1998;52:565–8. https://doi.org/10.1023/A:1010123723719.

[48] Jog JP. Crystallization of Polyethyleneterephthalate. J Macromol Sci Part C 1995;35:531–53. https://doi.org/10.1080/15321799508014598.

[49] Jabarin SA. Crystallization kinetics of poly(ethylene terephthalate). III. Effect of moisture on the crystallization behavior of PET from the glassy state. J Appl Polym Sci 1987;34:103–8. https://doi.org/10.1002/APP.1987.070340109.

[50] Baldenegro-Perez LA, Navarro-Rodriguez D, Medellin-Rodriguez FJ, Hsiao B, Avila-Orta CA, Sics I. Molecular weight and crystallization temperature effects on poly(ethylene terephthalate) (PET) homopolymers, an isothermal crystallization analysis. Polymers (Basel) 2014;6:583–600. https://doi.org/10.3390/polym6020583.

[51] Lu XF, Hay JN. Isothermal crystallization kinetics and melting behaviour of poly(ethylene terephthalate). Polymer (Guildf) 2001;42:9423–31. https://doi.org/10.1016/S0032-3861(01)00502-X.

[52] Llana PG, Boyce MC. Finite strain behavior of poly(ethylene terephthalate) above the glass transition temperature. Polymer (Guildf) 1999;40:6729–51. https://doi.org/10.1016/S0032-3861(98)00867-2.

[53] Demirel B, Yaraş A, Elçiçek H. Crystallization Behavior of PET Materials. BAÜ Fen Bil Enst Derg Cilt 2011;13:26–35.

[54] Gorlier E, Haudin JM, Billon N. Strain-induced crystallisation in bulk amorphous PET under uni-axial loading. Polymer (Guildf) 2001;42:9541–9. https://doi.org/10.1016/S0032-3861(01)00497-9.

[55] Tournier V, Duquesne S, Guillamot F, Cramail H, Taton D, Marty A, et al. Enzymes' Power for Plastics Degradation. Chem Rev 2023;123:5612–701. https://doi.org/10.1021/acs.chemrev.2c00644.

[56] Welle F. Twenty years of PET bottle to bottle recycling - An overview. Resour Conserv Recycl 2011;55:865–75. https://doi.org/10.1016/j.resconrec.2011.04.009.

[57] Jönsson C, Wei R, Biundo A, Landberg J, Schwarz Bour L, Pezzotti F, et al. Biocatalysis in the Recycling Landscape for Synthetic Polymers and Plastics towards Circular Textiles. ChemSusChem 2021;14:4028–40. https://doi.org/10.1002/cssc.202002666.

[58] Thiounn T, Smith RC. Advances and approaches for chemical recycling of plastic waste. J Polym Sci 2020;58:1347–64. https://doi.org/10.1002/pol.20190261.

[59] Ragaert K, Delva L, Van Geem K. Mechanical and chemical recycling of solid plastic waste. Waste Manag 2017;69:24–58. https://doi.org/10.1016/j.wasman.2017.07.044.

[60] Luo ZW, Lee SY. Biotransformation of p-xylene into terephthalic acid by engineered Escherichia coli. Nat Commun 2017;8:1–8. https://doi.org/10.1038/ncomms15689.

[61] Ingrao C, Wojnarowska M. Findings from a streamlined life cycle assessment of PET-bottles for beverage-packaging applications, in the context of circular economy. Sci Total Environ 2023;892:164805. https://doi.org/10.1016/j.scitotenv.2023.164805.

[62] Geyer R, Kuczenski B, Zink T, Henderson A. Common Misconceptions about Recycling. J Ind Ecol 2016;20:1010–7. https://doi.org/10.1111/jiec.12355.

[63] Lau WWY, Shiran Y, Bailey RM, Cook E, Stuchtey MR, Koskella J, et al. Evaluating scenarios toward zero plastic pollution. Science (80-) 2020;369. https://doi.org/10.1126/SCIENCE.ABA9475.

[64] Buchholz PCF, Feuerriegel G, Zhang H, Perez-Garcia P, Nover L-L, Chow J, et al. Plastics degradation by hydrolytic enzymes: The plastics-active enzymes database—PAZy. Proteins 2022;90:1443–56. https://doi.org/10.1002/PROT.26325.

[65] Yoshida S, Hiraga K, Takehana T, Taniguchi I, Yamaji H, Maeda Y, et al. A bacterium that degrades and assimilates poly(ethylene terephthalate). Science (80-) 2016;351:1196–9. https://doi.org/10.1126/science.aad6359.

[66] Tiso T, Narancic T, Wei R, Pollet E, Beagan N, Schröder K, et al. Towards bio-upcycling of polyethylene terephthalate. Metab Eng 2021;66:167–78. https://doi.org/10.1016/j.ymben.2021.03.011.

[67] Sadler JC, Wallace S. Microbial synthesis of vanillin from waste poly(ethylene terephthalate). Green Chem 2021;23:4623–904. https://doi.org/10.1039/d1gc00931a.

[68] Quartinello F, Vajnhandl S, Volmajer Valh J, Farmer TJ, Vončina B, Lobnik A, et al. Synergistic chemo-enzymatic hydrolysis of poly(ethylene terephthalate) from textile waste. Microb Biotechnol 2017;10:1376–83. https://doi.org/10.1111/1751-7915.12734.

[69] Sulaiman S, You DJ, Kanaya E, Koga Y, Kanaya S. Crystal structure and thermodynamic and kinetic stability of metagenome-derived LC-cutinase. Biochemistry 2014;53:1858–69. https://doi.org/10.1021/bi401561p.

[70] Ronkvist ÅM, Xie W, Lu W, Gross RA. Cutinase-Catalyzed hydrolysis of poly(ethylene

terephthalate). Macromolecules 2009;42:5128–38. https://doi.org/10.1021/ma9005318.

[71] Kawai F. The current state of research on PET hydrolyzing enzymes available for biorecycling. Catalysts 2021;11:1–10. https://doi.org/10.3390/catal11020206.

[72] Haernvall K, Zitzenbacher S, Yamamoto M, Schick MB, Ribitsch D, Guebitz GM. A new arylesterase from Pseudomonas pseudoalcaligenes can hydrolyze ionic phthalic polyesters. J Biotechnol 2017;257:70–7. https://doi.org/10.1016/j.jbiotec.2017.01.012.

[73] Vertommen MAME, Nierstrasz VA, Veer M Van Der, Warmoeskerken MMCG. Enzymatic surface modification of poly(ethylene terephthalate). J Biotechnol 2005;120:376–86. https://doi.org/10.1016/j.jbiotec.2005.06.015.

[74] IUBMB. IUBMB Nomenclature Home Page 2016. https://iubmb.qmul.ac.uk/enzyme/EC3/0101b.html#101 (accessed August 10, 2023).

[75] Kawai F, Kawabata T, Oda M. Current State and Perspectives Related to the Polyethylene Terephthalate Hydrolases Available for Biorecycling. ACS Sustain Chem Eng 2020;8:8894–908. https://doi.org/10.1021/ACSSUSCHEMENG.0C01638/ASSET/IMAGES/LARGE/SC0C01638_0002.JPEG.

[76] Wei R, Von Haugwitz G, Pfaff L, Mican J, Badenhorst CPS, Liu W, et al. Mechanism-Based Design of Efficient PET Hydrolases. ACS Catal 2022;12:3382–96. https://doi.org/10.1021/ACSCATAL.1C05856/ASSET/IMAGES/LARGE/CS1C05856_0004.JPEG.

[77] Perez-Garcia P, Chow J, Costanzi E, Gurschke M, Dittrich J, Dierkes RF, et al. An archaeal lid-containing feruloyl esterase degrades polyethylene terephthalate. Commun Chem 2023;6:1–13. https://doi.org/10.1038/s42004-023-00998-z.

[78] Eugenio E de Q, Campisano ISP, de Castro AM, Coelho MAZ, Langone MAP. Kinetic Modeling of the Post-consumer Poly(Ethylene Terephthalate) Hydrolysis Catalyzed by Cutinase from Humicola insolens. J Polym Environ 2022;30:1627–37. https://doi.org/10.1007/S10924-021-02301-4/TABLES/3.

[79] Arnling Bååth J, Borch K, Jensen K, Brask J, Westh P. Comparative Biochemistry of Four Polyester (PET) Hydrolases. ChemBioChem 2021;22:1627–37. https://doi.org/10.1002/cbic.202000793.

[80] Silva CM, Carneiro F, Neill AO, Fonseca SP. Cutinase — A New Tool for Biomodification of Synthetic Fibers. J Polym Sci PART A-POLYMER Chem 2005;43:2448–50. https://doi.org/10.1002/pola.20684.

[81] Ding Z, Xu G, Miao R, Wu N, Zhang W, Yao B, et al. Rational redesign of thermophilic PET hydrolase LCCICCG to enhance hydrolysis of high crystallinity polyethylene terephthalates. J Hazard Mater 2023;453:131386. https://doi.org/10.1016/j.jhazmat.2023.131386.

[82] Sonnendecker C, Oeser J, Richter PK, Hille P, Zhao Z, Fischer C, et al. Low Carbon Footprint Recycling of Post-Consumer PET Plastic with a Metagenomic Polyester Hydrolase. ChemSusChem 2022;15:e202101062. https://doi.org/10.1002/CSSC.202101062.

[83] Pfaff L, Gao J, Li Z, Jäckering A, Weber G, Mican J, et al. Multiple Substrate Binding Mode-Guided Engineering of a Thermophilic PET Hydrolase. ACS Catal 2022;12:9790–800. https://doi.org/10.1021/ACSCATAL.2C02275/SUPPL_FILE/CS2C02275_SI_002.TXT.

[84] Erickson E, Shakespeare TJ, Bratti F, Buss BL, Graham R, Hawkins MA, et al. Comparative Performance of PETase as a Function of Reaction Conditions, Substrate Properties, and Product Accumulation. ChemSusChem 2022;15. https://doi.org/10.1002/CSSC.202101932.

[85] Cui Y, Chen Y, Liu X, Dong S, Tian Y, Qiao Y, et al. Computational Redesign of a PETase

for Plastic Biodegradation under Ambient Condition by the GRAPE Strategy. ACS Catal 2021;11:1340–50. https://doi.org/10.1021/acscatal.0c05126.

[86] Austin HP, Allen MD, Donohoe BS, Rorrer NA, Kearns FL, Silveira RL, et al. Characterization and engineering of a plastic-degrading aromatic polyesterase. Proc Natl Acad Sci U S A 2018;115:E4350–7. https://doi.org/10.1073/pnas.1718804115.

[87] Bell EL, Smithson R, Kilbride S, Foster J, Hardy FJ, Ramachandran S, et al. Directed evolution of an efficient and thermostable PET depolymerase. Nat Catal 2022;5:673–81. https://doi.org/10.1038/s41929-022-00821-3.

[88] Son HF, Cho IJ, Joo S, Seo H, Sagong HY, Choi SY, et al. Rational Protein Engineering of Thermo-Stable PETase from Ideonella sakaiensis for Highly Efficient PET Degradation. ACS Catal 2019;9:3519–26. https://doi.org/10.1021/acscatal.9b00568.

[89] Arnling Bååth J, Novy V, Carneiro L V., Guebitz GM, Olsson L, Westh P, et al. Structure-function analysis of two closely related cutinases from Thermobifida cellulosilytica. Biotechnol Bioeng 2022;119:470–81. https://doi.org/10.1002/BIT.27984.

[90] Schubert SW, Schaller K, Bååth JA, Hunt C, Borch K, Jensen K, et al. Reaction pathways for the enzymatic degradation of poly(ethylene terephthalate): What characterizes an efficient PET-hydrolase? ChemBioChem 2022;24:e202200516. https://doi.org/10.1002/CBIC.202200516.

[91] Barth M, Oeser T, Wei R, Then J, Schmidt J, Zimmermann W. Effect of hydrolysis products on the enzymatic degradation of polyethylene terephthalate nanoparticles by a polyester hydrolase from Thermobifida fusca. Biochem Eng J 2015;93:222–8. https://doi.org/10.1016/J.BEJ.2014.10.012.

[92] Ellis LD, Rorrer NA, Sullivan KP, Otto M, McGeehan JE, Román-Leshkov Y, et al. Chemical and biological catalysis for plastics recycling and upcycling. Nat Catal 2021;4:539–56. https://doi.org/10.1038/s41929-021-00648-4.

[93] Eberl A, Heumann S, Brückner T, Araujo R, Cavaco-Paulo A, Kaufmann F, et al. Enzymatic surface hydrolysis of poly(ethylene terephthalate) and bis(benzoyloxyethyl) terephthalate by lipase and cutinase in the presence of surface active molecules. J Biotechnol 2009;143:207–12. https://doi.org/10.1016/J.JBIOTEC.2009.07.008.

[94] Carbios, Indorama Ventures. Carbios to build in France its first-of-a-kind manufacturing plant for fully bio-recycled PET in partnership with Indorama Ventures. Press Relese 2022. https://www.carbios.com/en/carbios-to-build-in-france-its-plant/#_ftn2 (accessed August 2, 2023).

[95] Weyhe AT, Andersen E, Mikkelsen R, Yu D. Accelerated physical aging of four PET copolyesters: Enthalpy relaxation and yield behaviour. Polymer (Guildf) 2023;278. https://doi.org/10.1016/j.polymer.2023.125987.

[96] Karagiannidis PG, Stergiou AC, Karayannidis GP. Study of crystallinity and thermomechanical analysis of annealed poly(ethylene terephthalate) films. Eur Polym J 2008;44:1475–86. https://doi.org/10.1016/j.eurpolymj.2008.02.024.

[97] Kong Y, Hay JN. The measurement of the crystallinity of polymers by DSC. Polymer (Guildf) 2002;43:3873–8. https://doi.org/10.1016/S0032-3861(02)00235-5.

[98] Schick C. Differential scanning calorimetry (DSC) of semicrystalline polymers. Anal Bioanal Chem 2009;395:1589–611. https://doi.org/10.1007/s00216-009-3169-y.

[99] Mehta A, Gaur U, Wunderlich B. EQUILIBRIUM MELTING PARAMETERS OF POLY(ETHYLENE TEREPHTHALATE). J Polym Sci Polym Phys Ed 1978;16:289–96. https://doi.org/10.1002/pol.1978.180160209.

[100] Chen H, Liu Z, Cebe P. Chain confinement in electrospun nanofibers of PET with carbon nanotubes. Polymer (Guildf) 2009;50:872–80. https://doi.org/10.1016/j.polymer.2008.12.030.

[101] Chen Z, Hay JN, Jenkins MJ. FTIR spectroscopic analysis of poly(ethylene terephthalate) on crystallization. Eur Polym J 2012;48:1586–610. https://doi.org/10.1016/j.eurpolymj.2012.06.006.

[102] Blum MM, John H. Historical perspective and modern applications of Attenuated Total Reflectance - Fourier Transform Infrared Spectroscopy (ATR-FTIR). Drug Test Anal 2012;4:298–302. https://doi.org/10.1002/dta.374.

[103] Lippold H, Kahle L, Sonnendecker C, Matysik J, Fischer C. Temporal and spatial evolution of enzymatic degradation of amorphous PET plastics. Npj Mater Degrad 2022;6:1–6. https://doi.org/10.1038/s41529-022-00305-6.

[104] Wei R, Oeser T, Barth M, Weigl N, Lübs A, Schulz-Siegmund M, et al. Turbidimetric analysis of the enzymatic hydrolysis of polyethylene terephthalate nanoparticles. J Mol Catal B Enzym 2014;103:72–8. https://doi.org/10.1016/j.molcatb.2013.08.010.

[105] Frank R, Krinke D, Sonnendecker C, Zimmermann W, Jahnke HG. Real-Time Noninvasive Analysis of Biocatalytic PET Degradation. ACS Catal 2022;12:25–35. https://doi.org/10.1021/acscatal.1c03963.

[106] Weinberger S, Haernvall K, Scaini D, Ghazaryan G, Zumstein MT, Sander M, et al. Enzymatic surface hydrolysis of poly(ethylene furanoate) thin films of various crystallinities. Green Chem 2017;19:5381–4. https://doi.org/10.1039/c7gc02905e.

[107] Arnling Bååth J, Borch K, Westh P. A suspension-based assay and comparative detection methods for characterization of polyethylene terephthalate hydrolases. Anal Biochem 2020;607. https://doi.org/10.1016/j.ab.2020.113873.

[108] Zhong-Johnson EZL, Voigt CA, Sinskey AJ. An absorbance method for analysis of enzymatic degradation kinetics of poly(ethylene terephthalate) films. Sci Reports 2021 111 2021;11:1–9. https://doi.org/10.1038/s41598-020-79031-5.

[109] Falkenstein P, Gräsing D, Bielytskyi P, Zimmermann W, Matysik J, Wei R, et al. UV Pretreatment Impairs the Enzymatic Degradation of Polyethylene Terephthalate. Front Microbiol 2020;11:689. https://doi.org/10.3389/fmicb.2020.00689.

[110] Belisário-Ferrari MR, Wei R, Schneider T, Honak A, Zimmermann W. Fast Turbidimetric Assay for Analyzing the Enzymatic Hydrolysis of Polyethylene Terephthalate Model Substrates. Biotechnol J 2019;14:10–4. https://doi.org/10.1002/biot.201800272.

[111] Sulaiman S, You D-J, Kanaya E, Koga Y, Kanaya S. Crystal Structure and Thermodynamic and Kinetic Stability of Metagenome-Derived LC-Cutinase. Biochemistry 2014;53:1858–69. https://doi.org/10.1021/BI401561P.

[112] Pirillo V, Pollegioni L, Molla G. Analytical methods for the investigation of enzyme-catalyzed degradation of polyethylene terephthalate. FEBS J 2021;288:4730–45. https://doi.org/10.1111/febs.15850.

[113] Vogel K, Wei R, Pfaff L, Breite D, Al-Fathi H, Ortmann C, et al. Enzymatic degradation of polyethylene terephthalate nanoplastics analyzed in real time by isothermal titration calorimetry. Sci Total Environ 2021;773:145111. https://doi.org/10.1016/j.scitotenv.2021.145111.

[114] Oda M, Yamagami Y, Inaba S, Oida T, Yamamoto M, Kitajima S, et al. Enzymatic hydrolysis of PET: functional roles of three Ca2+ ions bound to a cutinase-like enzyme, Cut190*, and its engineering for improved activity. Appl Microbiol Biotechnol 2018;102:10067–77. https://doi.org/10.1007/s00253-018-9374-x.

[115] Maurya A, Bhattacharya A, Khare SK. Enzymatic Remediation of Polyethylene Terephthalate (PET)–Based Polymers for Effective Management of Plastic Wastes: An Overview. Front Bioeng Biotechnol 2020;8:1–13. https://doi.org/10.3389/fbioe.2020.602325.

[116] Marty A. WO2020094646A1. WO2020094646A1, 2020.

[117] Bisswanger H. Enzyme assays. Perspect Sci 2014;1:41–55. https://doi.org/10.1016/j.pisc.2014.02.005.

[118] Kawai F. Emerging Strategies in Polyethylene Terephthalate Hydrolase Research for Biorecycling. ChemSusChem 2021;14:4115–22. https://doi.org/10.1002/cssc.202100740.

[119] Wei R, Zimmermann W. Biocatalysis as a green route for recycling the recalcitrant plastic polyethylene terephthalate. Microb Biotechnol 2017;10:1302–7. https://doi.org/10.1111/1751-7915.12714.

[120] Biundo A, Ribitsch D, Guebitz GM. Surface engineering of polyester-degrading enzymes to improve efficiency and tune specificity. Appl Microbiol Biotechnol 2018;102:3551–9. https://doi.org/10.1007/s00253-018-8850-7.

[121] Roudaut G, Simatos D, Champion D, Contreras-Lopez E, Le Meste M. Molecular mobility around the glass transition temperature: a mini review. Innov Food Sci Emerg Technol 2004;5:127–34. https://doi.org/10.1016/J.IFSET.2003.12.003.

[122] Zhang Y, Zhang J, Lu Y, Duan Y, Yan S, Shen D. Glass Transition Temperature Determination of Poly(ethylene terephthalate) Thin Films Using Reflection−Absorption FTIR. Macromolecules 2004;37:2532–7. https://doi.org/10.1021/MA035709F.

[123] Zuo B, Liu Y, Liang Y, Kawaguchi D, Tanaka K, Wang X. Glass Transition Behavior in Thin Polymer Films Covered with a Surface Crystalline Layer. Macromolecules 2017;50:2061–8. https://doi.org/10.1021/acs.macromol.6b02740.

[124] Tarazona NA, Wei R, Brott S, Pfaff L, Bornscheuer UT, Lendlein A, et al. Rapid depolymerization of poly(ethylene terephthalate) thin films by a dual-enzyme system and its impact on material properties. Chem Catal 2022;2:3573–89. https://doi.org/10.1016/j.checat.2022.11.004.

[125] Furukawa M, Kawakami N, Tomizawa A, Miyamoto K. Efficient Degradation of Poly(ethylene terephthalate) with Thermobifida fusca Cutinase Exhibiting Improved Catalytic Activity Generated using Mutagenesis and Additive-based Approaches. Sci Rep 2019;9:1–9. https://doi.org/10.1038/s41598-019-52379-z.

[126] Avilan L, Lichtenstein BR, Koenig G, Zahn M, Allen MD, Oliveira L, et al. Concentration-dependent inhibition of mesophilic PETases on poly(ethylene terephthalate) can be eliminated by enzyme engineering. ChemSusChem 2023;202202277:1–13. https://doi.org/10.1002/cssc.202202277.

[127] Richter PK, Blázquez-sánchez P, Zhao Z, Engelberger F, Wiebeler C, Künze G, et al. Structure and function of the metagenomic plastic-degrading polyester hydrolase PHL7 bound to its product. Nat Commun 2023;14:1–11. https://doi.org/10.1038/s41467-023-37415-x.

[128] Liu Y, Liu C, Liu H, Zeng Q, Tian X, Long L, et al. Catalytic Features and Thermal Adaptation Mechanisms of a Deep Sea Bacterial Cutinase-Type Poly(Ethylene Terephthalate) Hydrolase. Front Bioeng Biotechnol 2022;10:1–11. https://doi.org/10.3389/fbioe.2022.865787.

[129] Guo B, Vanga SR, Lopez-Lorenzo X, Saenz-Mendez P, Ericsson SR, Fang Y, et al. Conformational Selection in Biocatalytic Plastic Degradation by PETase. ACS Catal 2022;12:3397–409. https://doi.org/10.1021/acscatal.1c05548.

[130] Brizendine RK, Erickson E, Haugen SJ, Ramirez KJ, Miscall J, Pickford AR, et al. Particle Size Reduction of Poly(ethylene terephthalate) Increases the Rate of Enzymatic Depolymerization But Does Not Increase the Overall Conversion Extent. ACS Sustain Chem Eng 2022;10:9131–49. https://doi.org/10.1021/acssuschemeng.2c01961.

[131] Chang AC, Patel A, Perry S, Soong Y V., Ayafor C, Wong HW, et al. Understanding Consequences and Tradeoffs of Melt Processing as a Pretreatment for Enzymatic Depolymerization of Poly(ethylene terephthalate). Macromol Rapid Commun 2022:2100929. https://doi.org/10.1002/marc.202100929.

[132] Fecker T, Galaz-Davison P, Engelberger F, Narui Y, Sotomayor M, Parra LP, et al. Active Site Flexibility as a Hallmark for Efficient PET Degradation by I. sakaiensis PETase. Biophys J 2018;114:1302–12. https://doi.org/10.1016/j.bpj.2018.02.005.

[133] Benoit I, Culleton H, Zhou M, DiFalco M, Aguilar-Osorio G, Battaglia E, et al. Closely related fungi employ diverse enzymatic strategies to degrade plant biomass. Biotechnol Biofuels 2015;8:107. https://doi.org/10.1186/s13068-015-0285-0.

[134] Kari J, Andersen M, Borch K, Westh P. An Inverse Michaelis-Menten Approach for Interfacial Enzyme Kinetics. ACS Catal 2017;7:4904–14. https://doi.org/10.1021/acscatal.7b00838.

[135] Rastogi R, Vellinca WP, Rastogi S, Schick C, Meijer HEH. The three-phase structure and mechanical properties of poly(ethylene terephthalate). J Polym Sci Part B Polym Phys 2004;42:2092–106. https://doi.org/10.1002/POLB.20096.

[136] Badino SF, Bååth JA, Borch K, Jensen K, Westh P. Adsorption of enzymes with hydrolytic activity on polyethylene terephthalate. Enzyme Microb Technol 2021;152:109937. https://doi.org/10.1016/J.ENZMICTEC.2021.109937.

[137] Shinotsuka K, Bliznyuk VN, Assender HE. Near-surface crystallization of PET. Polymer (Guildf) 2012;53:5554–9. https://doi.org/10.1016/J.POLYMER.2012.09.048.

[138] Sagong HY, Son HF, Seo H, Hong H, Lee D, Kim KJ. Implications for the PET decomposition mechanism through similarity and dissimilarity between PETases from Rhizobacter gummiphilus and Ideonella sakaiensis. J Hazard Mater 2021;416:126075. https://doi.org/10.1016/j.jhazmat.2021.126075.

[139] Makryniotis K, Nikolaivits E, Gkountela C, Vouyiouka S, Topakas E. Discovery of a polyesterase from Deinococcus maricopensis and comparison to the benchmark LCCICCG suggests high potential for semi-crystalline post-consumer PET degradation. J Hazard Mater 2023;455:131574. https://doi.org/10.1016/j.jhazmat.2023.131574.

[140] Ellis LD, Rorrer NA, Sullivan KP, Otto M, McGeehan JE, Román-Leshkov Y, et al. Chemical and biological catalysis for plastics recycling and upcycling. Nat Catal 2021;4:539–56. https://doi.org/10.1038/s41929-021-00648-4.

[141] Wei R, Song C, Gräsing D, Schneider T, Bielytskyi P, Böttcher D, et al. Conformational fitting of a flexible oligomeric substrate does not explain the enzymatic PET degradation. Nat Commun 2019;10:3–6. https://doi.org/10.1038/s41467-019-13492-9.

[142] Guo B, Lopez-Lorenzo X, Fang Y, Bäckström E, Capezza AJ, Vanga SR, et al. Fast Depolymerization of PET Bottle Mediated by Microwave Pre-treatment and an Engineered PETase. ChemSusChem 2023:e202300742. https://doi.org/10.1002/cssc.202300742.

[143] Herrero Acero E, Ribitsch D, Steinkellner G, Gruber K, Greimel K, Eiteljoerg I, et al. Enzymatic surface hydrolysis of PET: Effect of structural diversity on kinetic properties of cutinases from Thermobifida. Macromolecules 2011;44:4632–40. https://doi.org/10.1021/ma200949p.

[144] Falkenstein P, Zhao Z, Di Pede-Mattatelli A, Künze G, Sommer M, Sonnendecker C, et al. On the Binding Mode and Molecular Mechanism of Enzymatic Polyethylene Terephthalate Degradation. ACS Catal 2023;13:6919–33. https://doi.org/10.1021/acscatal.3c00259.

[145] Joo S, Cho IJ, Seo H, Son HF, Sagong HY, Shin TJ, et al. Structural insight into molecular mechanism of poly(ethylene terephthalate) degradation. Nat Commun 2018;9. https://doi.org/10.1038/s41467-018-02881-1.

[146] Kawai F, Furushima Y, Mochizuki N, Muraki N, Yamashita M. Efficient depolymerization of polyethylene terephthalate (PET) and polyethylene furanoate by engineered PET hydrolase Cut190. AMB Express 2022. https://doi.org/10.1186/s13568-022-01474-y.

[147] WTS Global. Plastic Taxation in Europe: Update 2023. Available at: Https://Wts.Com/Global/Publishing-Article/20230522-Plastic-Taxation-Europe-Update-2023~publishing-Article: 2023.

Paper I

Standardized method for controlled modification of poly (ethylene terephthalate) (PET) crystallinity for assaying PET degrading enzymes.

Thore B. Thomsen, Cameron J. Hunt, Anne S. Meyer

MethodsX **2022** (9) 101815

I

Intentionally left blank

MethodsX 9 (2022) 101815

Contents lists available at ScienceDirect

MethodsX

journal homepage: www.elsevier.com/locate/mex

Method Article

Standardized method for controlled modification of poly (ethylene terephthalate) (PET) crystallinity for assaying PET degrading enzymes

Thore Bach Thomsen, Cameron J. Hunt, Anne S. Meyer*

Department of Biotechnology and Biomedicine, Protein Chemistry and Enzyme Technology Section, DTU Bioengineering, Technical University of Denmark, Kgs., Lyngby 2800, Denmark

A B S T R A C T

Poly(ethylene terephthalate) (PET) is a polyester plastic, which is widely used, notably as a material for single-use plastic bottles. Its accumulation in the environment now poses a global pollution threat. A number of enzymes are active on PET providing new options for industrial biorecycling of PET materials. The enzyme activity is strongly affected by the degree of PET crystallinity (X_C), and the X_C is therefore a relevant factor to consider in enzyme catalyzed PET recycling. Here, we present a new experimental methodology, based on systematic thermal annealing for controlled preparation of PET disks having different X_C, to allow systematic quantitative evaluation of the efficiency of PET degrading enzymes at different degrees of PET substrate crystallinity. We discuss the theory of PET crystallinity and compare PET crystallinity data measured by differential scanning calorimetry and attenuated Fourier transform infrared spectroscopy.

- This study introduces a simple method for controlling the crystallinity of PET samples via annealing in a heat block.
- The present methodology is not limited to the analytical methods included in the methods details.

A R T I C L E I N F O

Method name: Standardized method for controlled modification of poly(ethylene terephthalate) (PET) crystallinity for assaying PET degrading enzymes

Keywords: PET hydrolase, PET crystallinity, Enzyme assay

Article history: Received 12 April 2022; Accepted 4 August 2022; Available online xxx

DOI of original article: 10.1016/j.nbt.2022.02.006

* Corresponding author.
E-mail address: asme@dtu.dk (A.S. Meyer).

https://doi.org/10.1016/j.mex.2022.101815

Specifications table

Subject Area:	Chemical Engineering
More specific subject area:	*Enzyme Technology*
Method name:	*Standardized method for controlled modification of poly(ethylene terephthalate) (PET) crystallinity for assaying PET degrading enzymes*
Name and reference of original method:	*N/A*
Resource availability:	*N/A*

Method details

Background: Polyethylene terephthalate as an enzyme substrate

Poly(ethylene terephthalate) (PET) is a synthetic polyester used in packaging materials and plastic bottles. PET accounts for ~7% of global plastic usage [1], and is a key contributor to the increasing plastic pollution [2]. The polymeric chains of PET consist of repeating units of ethylene glycol and terephthalic acid linked together by ester bonds. These polymer chains are either in an amorphous state (absence of long-range molecular order) or in a crystal structure (highly ordered) [3].

The degree of crystallinity (X_C) of a PET sample refers to the fraction of the total polymer chains being in the crystal structure state. The X_C is a result of the PET process history, as crystallization is induced either thermally, at temperatures above the glass transition temperature T_g (T_g is 76°C for amorphous PET), or during certain mechanical operations [4,5]. The amorphous fraction of PET is in fact comprised of two fractions, namely a rigid amorphous fraction (RAF) and a mobile amorphous fraction (MAF); the ratio of each is written as X_{RAF} and X_{MAF}, respectively. The RAF is present at the interface between the crystal and the amorphous regions as an immobilized phase caused by the crystallization, and the mobility of RAF is more restrained than the completely amorphous region MAF. The X_{RAF} of a PET sample increases with the X_C, while X_{MAF} decreases [6,7].

Although PET is a synthetic polymer, recent data have shown that certain esterolytic enzymes (EC 3.1.1,x), including the PET hydrolase from the bacterium Ideonella sakaineses 201-F6, originally specified as a PETase (or IsPETase) [8], now classified as EC 3.1.1.101, are capable of catalyzing hydrolysis of the ester bonds within PET. The activity of these enzymes are, however, limited on PET samples with a high X_C [9–12]. X_C of PET in water bottles ranges from 21–31% [13] making the significance of X_C on PET degrading enzyme activity of critical importance in biobased industrial PET recycling.

Here we present the practical details and the theory behind an experimental methodology that we have developed for preparing PET samples of different degrees of crystallinity, X_C, to allow systematic evaluation of the efficiency of PET degrading enzymes in response to the X_C of PET [11]. We introduce annealing involving controlled heating and isothermal cold crystallization to control the X_C of standardized PET sheets (Fig. 1).

Substrate preparation

Preparation of PET material

Amorphous or low crystalline PET films or sheets (e.g. 1 mm thick amorphous PET cat. No. ES30301 from Goodfellow Cambridge Ltd, Huntingdon, UK) are used as starting material to obtain PET materials having different X_C via annealing and isothermal cold crystallization. The PET material is cut into uniform disks using a generic hole punch (Ø 6mm), prior to annealing. Although the starting materials are categorized as amorphous PET materials, it is important to note that the crystallinity of the PET films and sheets differ, and observe that they are not completely amorphous (see Method Validation, below).

Annealing and isothermal cold crystallization of PET

The X_C of the PET discs is systematically altered via annealing followed by cold crystallization as follows: A PET disk is transferred into a 2 mL Eppendorf tube and annealed in a heating block at

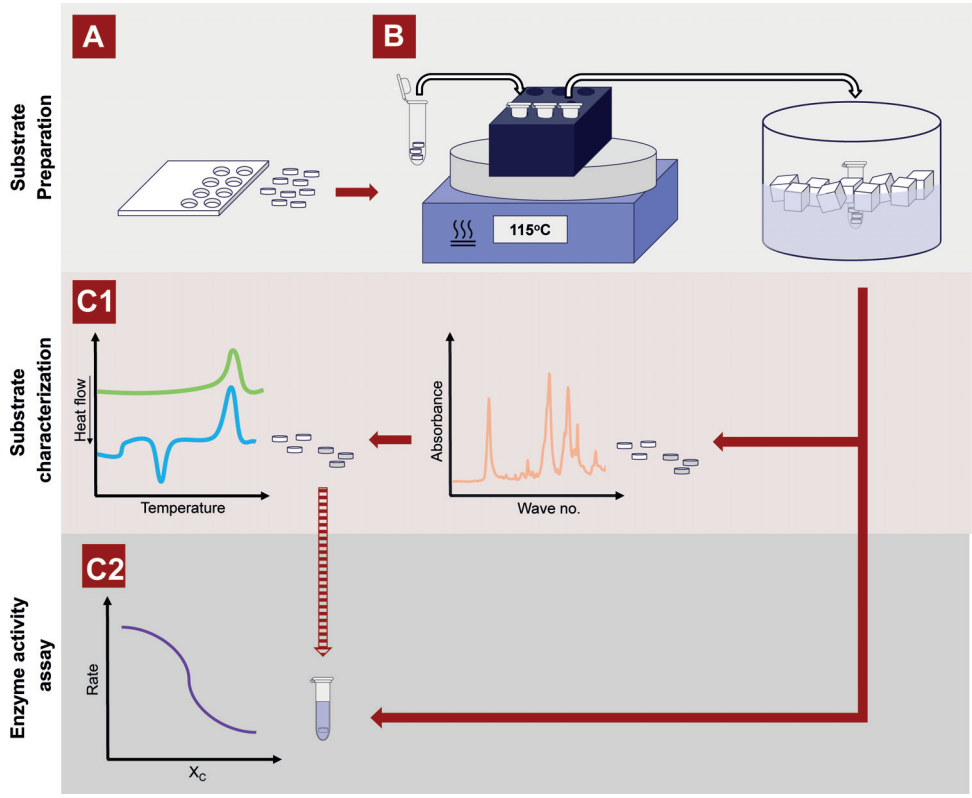

Fig. 1. Schematic representation of the method presented in this paper. (A) Amorphous PET material is cut into disks (Ø 6mm) using a hole punch. (B) The disks are transferred into a 2 mL Eppendorf tube, and annealed at 115°C for a specified period of time to induce crystal formation via cold crystallization. The crystallization is quenched by cooling the annealed sample in ice water. The annealed PET samples are then analyzed by ATR-FTIR to quantify X_{MAF}, and/or identify contaminants. The samples used for ATR-FTIR may be used directly for reaction or other analyses, including: (C1) DSC analysis for further characterization of substrate properties such as X_C or (C2) enzymatic reactions for quantifying the effect of substrate X_C for a specific PET degrading enzyme.

115°C for a defined amount of time (minutes); up to three disks can be added per Eppendorf tube, still achieving the same crystallization result as is if only one disk is added at a time. The crystallization of the annealed PET sample is quenched by immediately transferring the Eppendorf tube into an ice water bath. It is kept on ice for at least 30 sec to ensure that the crystallized sample has been sufficiently cooled. "Untreated" samples to be used for comparison should be annealed at 85°C for 5 min to remove the enthalpy relaxation caused by the aging of the polymer [14].

Substrate characterization

Quantification of X_{MAF} by ATR-FTIR

Attenuated total reflection Fourier-transform infrared spectroscopy (ATR-FTIR) does not required any substrate preparation and can thus be performed directly on the PET disks after annealing. As it is a non-destructive method, the samples analyzed by ATR-FTIR can be used for further analysis, such as differential scanning calorimetry (DSC) or enzymatic treatment.

The peaks of interests described in this paper are at 973 cm^{-1} and 898 cm^{-1}.These two peaks are associated with the *trans* (973 cm^{-1}) and *gauche* (898 cm^{-1}) conformer of ethylene glycol [14,15]. While the *gauche* conformer is only associated with amorphous PET the *trans* conformer is present

in both the crystalline and amorphous regions [14]. The ratio of the absorbances at these two peaks (A_{973}/A_{898}) is proportional with the X_{MAF} of the sample.

Quantification of the X_C and X_{MAF} by DSC

DSC can be used to quantify the X_C of a sample annealed for a specific period of time, by analyzing a few samples (n=3) from the batch. A temperature range from 20°C to 270°C is sufficient to determine the thermal features required to estimate X_C and X_{MAF} of PET samples. A constant heating rate of 10°C min^{-1} is recommended, as some thermal features are dependent on the heating rate [9,11,16]. The X_C of a PET sample, measured by DSC, is then calculated according to Eq. (1):

$$X_C = \frac{\Delta H_m - \Delta H_{cc}}{\Delta H_m^0} \cdot 100\% \tag{1}$$

Here, ΔH_{cc} is the cold crystallization enthalpy (numerical value) of the sample, ΔH_m is the heat of melting of the sample, and ΔH_m^0 is the heat of melting of a pure crystalline sample. According to literature ΔH_m^0 is 140 J g^{-1} [17].

The X_{MAF} is calculated according to Eq. (2):

$$X_{MAF} = \frac{\Delta C_{P(m)}}{\Delta C_{P(a)}} \tag{2}$$

Where $\Delta C_{P(m)}$ is the change in heat capacity of the sample at T_g and $\Delta C_{P(a)}$ is the change in heat capacity at T_g of a completely amorphous sample. By extrapolation from a linear regression curve of measured $\Delta C_{P(m)}$ values and X_C of PET disk samples we have previously estimated $\Delta C_{P(a)}$ of an amorphous PET disk sample to be approximately 0.47 J g^{-1} K^{-1} [11].

Enzyme assay

The effect of the increased substrate crystallinity on the particular enzyme activity is evaluated on PET disks of different X_C by measuring the concentration of soluble products formed during enzymatic reaction. Products are measured in terms of bis(2-hydroxyethyl)-terephthalic acid (BHET) equivalents via absorbance measurements of the reaction at 240 nm [18]. The rate of the product formation is then plotted against X_C of the PET disks used.

The enzyme reactions are performed in Eppendorf tubes using 1 disk and a reaction volume of 1 mL in buffer. During the enzymatic treatment, 10µL of the reaction is sampled at various time points. The concentration of soluble product should be normalized with respect to the starting volume V_0 according to Eq. (3).

$$C_i = \frac{C_{s,i} * V_i + \sum_{i-1}^{n} (C_{s,n} * V_{s,n})}{V_0} \tag{3}$$

Where C_i and V_i is the normalized concentration of soluble products and the reaction volume at time point *i*. $C_{s,i}$, $C_{s,n}$, and $V_{s,n}$ is the measured concentration of soluble products in the sample measured at time point *i* or *n* and the sampling volume at time point *n*.

The product release rate on each PET sample is then calculated from the linear regions of the progress curves. The rate data are then plotted against the X_C or X_{MAF} quantified by either DSC or ATR-FTIR.

Method validation (Case study)

Materials and instrumentation

PET material

1 mm thick amorphous PET sheets (Cat. No. ES303010) denoted as PET-S. 250 µm thick amorphous PET film (Cat. No. ES301445) denoted as PET-F, and semi-crystalline PET particles, Ø<300µm (Cat. No. ES306031), denoted as PET-P were all from Goodfellow (Cambridge Ltd, Huntingdon, UK). The PET-P particles were cast into an amorphous PET sheet by melting 0.5 g of particles in an aluminum dish

(Ø 2.6 cm) for 1 min at 270°C and subsequent quenching in ice water. These latter samples will be denoted as PET-C. Starting crystallinity was measured to be: PET-S: 9.1 ± 1.3%, PET-F: 1.3 ± 0.4%, PET-P: 37.5 ± 0.7%.

Isothermal crystallization

PET-S, PET-F, and PET-C were all cut into disks using a generic hole punch (Ø 6mm). Samples were annealed at 115°C for 5, 6, 7, 8, 9, 10, 12, 15 min (PET-S, PET-F), and for 30 min (PET-S, PET-F, and PET-C) in a heating block. At the specific time points the samples were quenched (cold crystallized), by transferring the annealed samples into ice water for 30 sec. "Untreated" PET samples were annealed at 85°C for 5 min, and subsequently quenched in ice water for 30 sec.

ATR- FTIR analysis

ATR-FTIR was performed directly on the PET disks (n=3) using a Spectrum 100 FTIR spectrometer (PerkinElmer, MA, USA). Samples were monitored from 4000 to 650 cm^{-1} with a resolution of 4 cm^{-1}. Each spectrum consisted of an average of 4 scans.

DSC analysis

The X_C of the PET samples was quantified using DSC measurements (n=3) on a Pyris 1 Calorimeter (Perkin Elmer, Waltham, Massachusetts, USA). A constant heating rate of 10°C min^{-1} was applied on samples weighing 8.5 ± 0.5 mg for PET-P and PET-S or 6.5 ± 0.5 mg for PET-F between temperatures of 20°C and 270°C. X_C and X_{MAF} was calculated according to Eqs. (1) and (2), respectively.

Enzymes

LCC_{ICCG} was expressed recombinantly in *E. coli* Shuffle T7 and purified as described in [11] (Expression also works in *E. coli* BL21 (DE3) cells).

Enzyme activity assay

1 disk of PET was treated with 150 nM LCC_{ICCG} in 1 mL 0.5M glycine-NaOH buffer pH 9 at 70°C during shaking in a thermomixer (Eppendorf, Hamburg, Germany) for up to 8 h. 10 µL were sampled at specific time points during the reaction. The product formation, at the time points, was quantified by measuring the absorbance at 240 nm using a Synergy HT™ plate reader (BioTek, Winooski, Vermont, United States) as described in [18]. A sample containing 32.6 mg/mL PET-P, corresponding to the average weight of a PET-S disk, was included as a benchmark and assayed under the same conditions as PET-S. All reactions were performed in triplicate.

Results validation

The increase in X_C caused by the annealing followed the characteristic Avrami equation (Fig. 2A), which is associated with crystal growth during annealing [19,20] and the X_C data obtained per annealing time were higher for the PET-S (sheet) that the PET-F (film) samples (Fig. 2A).

As a supplement to the DSC measurements the ATR-FTIR spectra of the untreated PET samples and extensively annealed PET samples (heated for 30 min at 115°C), respectively, were obtained for the PET-C, PET-F, and PET-S. From the ATR-FTIR spectra, it was observed that the peak at 973 cm^{-1} increased upon annealing while the absorbance at 898 cm^{-1} decreased for both the PET-S and the PET-C samples. A non-linear relationship was observed between the X_C and the A_{973}/A_{898} ratio of PET-S (linear model $r^2 = 0.96$) (Fig. 2C), but a linear correlation, $r^2 = 0.99$, was observed between the X_{MAF} and A_{973}/A_{898} ratio (Fig. 2D). These observations are in agreement with the *gauche* conformation only being present in X_{MAF}. For PET-S, ATR-FTIR can thereby be used as a non-destructive method to directly quantify the X_{MAF} of thermally annealed samples before enzymatic treatment.

It is important to note that no changes were observed on the ATR-FTIR spectrum of the PET-F samples. Moreover, both the untreated and annealed PET-F samples produced a broad peak with absorbance maximum at 955 cm^{-1}. We attribute these data to the possible presence of impurities in the original PET film. For this reason, PET-S is recommended as a substrate for the method presented here for quantification of the effect of X_C on the product release rate of PET degrading enzymes.

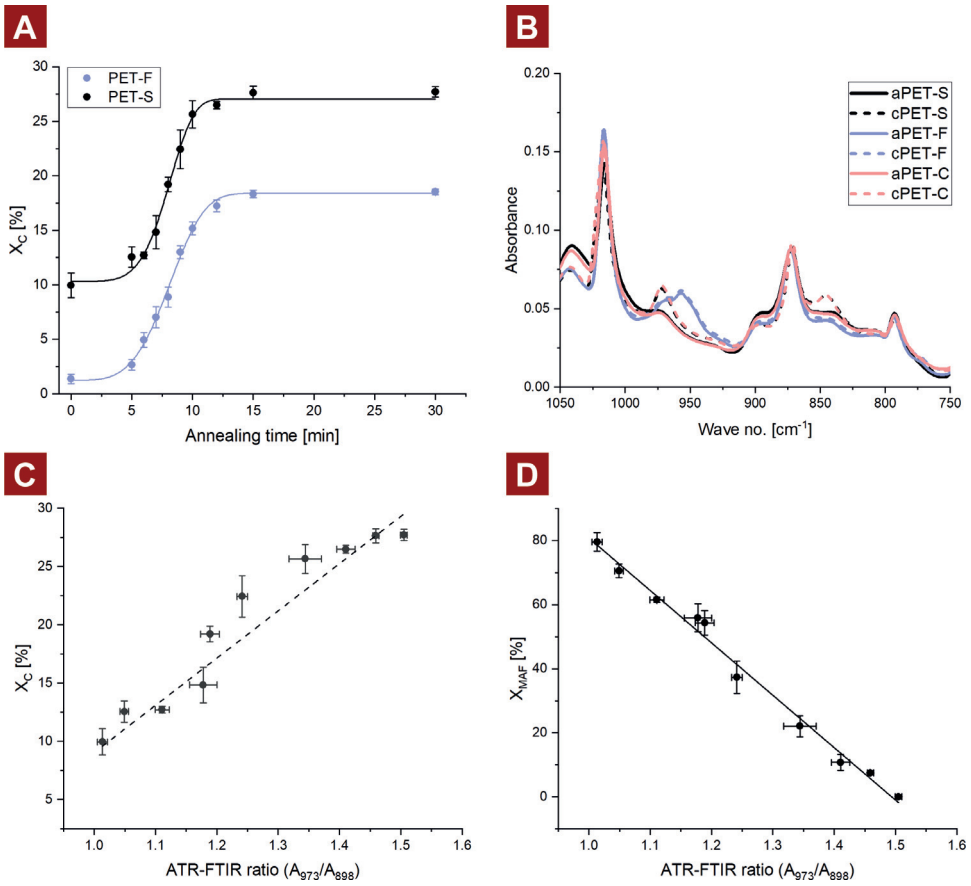

Fig. 2. Characterization of PET samples (n=3) annealed at 115°C. (A) Change in the degree of crystallinity (X_C), measured by DSC of amorphous PET-P (light blue dots) and PET-S (black dots) as a function of annealing time at 115°C. The bold lines represent a nonlinear curve fit to a modified version of the Avrami equation. (B) ATR-FTIR spectrum of PET-C (light red), PET-F (light blue), and PET-S (black lines) which are either untreated (solid lines) or cold crystallized (dashed lines) at 115° for 30 min. (C) Correlation (non-linear) between the X_C measured by DSC and the ATR-FTIR ratio A_{973}/A_{898}; the dotted line is included only as an aid for the eye. (D) Linear correlation between the X_{MAF} measured by DSC and the ATR-FTIR ratio A_{973}/A_{898}.

From the enzymatic reaction progress curves it was evident that the product release rate catalyzed by LCC_{ICCG} on the untreated sample (X_C=8.2%) was constant throughout the 8 h of the enzymatic treatment (Fig. 3A). A lag phase was evident for the samples with higher X_C [11]. The substrate X_C, induced by annealing affected the length of the observed lag phases, which increased with an increasing substrate crystallinity. The samples with a low X_C (9.3 and 13.8%) thus also displayed lag phases, although the product release rate did not differ once a steady-state reaction rate had been reached. Once a steady-state was reached for the samples with 9.3 or 13.8% X_C (determined by the linear region of the progress curves displayed in Fig. 3A), it was observed that the product release rate of these samples had reached the same level as the untreated sample. In contrast, the samples with a X_C of 18.8 % or higher displayed significantly lower product release rates.

The correlation between the product release rate and the X_C followed a sigmoidal trend (Fig. 3B). This indicates that the negative effect on the LCC_{ICCG} catalyzed product release rate caused by increasing substrate crystallinity, reached a critical point at a X_C between 13.8 and 18.8%, as the reaction rate decreased ~10 fold within this range. A similar observation was made for the *Ideonella sakaiensis* PETase, IsPETase, using PET-F samples crystallized via non-isothermal crystallization from melt [10].

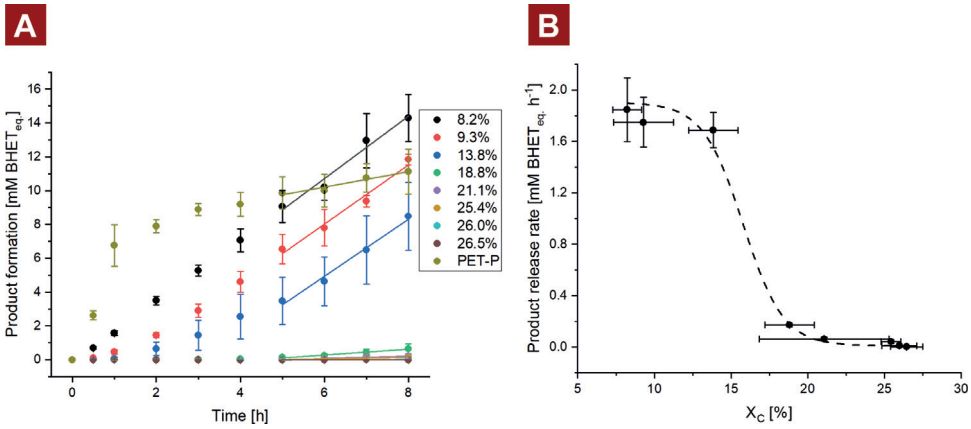

Fig. 3. Enzymatic degradation of PET-S samples with various degrees of crystallinity. (A) Progress curves made by continuous sampling of PET samples (n=3) using 150 nM LCC_{ICCG} in 50 mM Glycine-NaOH pH 9 at 70°C. A sample containing 32.6 mg/mL of highly crystalline PET-P (X_C =37.5 ± 0.7 %) was included as a reference. (B) Product release rate of LCC_{ICCG} against the substrate crystallinity. The rates were calculated based on the linear regions from Fig. 3A).

Important considerations

The annealing temperature affects the crystallization rates, X_C at saturation/metastable state, and the crystal thickness [7]. The annealing temperature of 115°C was chosen as X_C saturation was reached within a reasonable amount of time [11]. The enzyme response data (Fig. 3B) underline that it is particularly important to evaluate the reaction rates based on progress curves rather than on end-point measurements. Although PET hydrolase activity as EC 3.1.1.101 has now been defined as producing mono(2-hydroxyethy) terephthalate (MHET) and $(\text{ethylene terephthalate})_{n-1}$ from $(\text{ethylene terephthalate})_n$ (www.BRENDA-enzymes.org), it is known that many PET degrading (poly)esterases, including the *I. sakaiensis* PETase, produce some BHET in addition to MHET [18,21] measureable by HPLC. In the present method, we employed direct spectrophotometry of supernatant samples at 240 nm, principally as described in [18]. This quantification of the products as $BHET_{eq}$ is thus mainly a method for enzyme screening or for assessing e.g. the significance of systematic substrate alterations.

A sample containing 32.6 mg of PET-P, corresponding to the average mass of a PET-S disk, was included as a benchmark. The X_C of PET-P was very high (37.5 ± 0.7 %), while the total surface area of the PET-P sample was several fold larger than that of a PET-S disc (according to our calculations minimum 6 times larger considering a particle diameter of 300 µm of each PET-P particle). During the initial 1.5 h of incubation, the initial product release rate on the PET-P was significantly higher than the low crystalline PET-S sample. After this point (after an extent of reaction of approximately 4%) the product release rate decreased 14 fold, from 7 ± 0.9 mM $BHET_{eq.}$ h^{-1} to 0.5 ± 0.03 mM $BHET_{eq.}$ h^{-1}. This observed leveling off with time agrees with other studies and appears to be a common trait of enzymatic PET degradation [9,11,12]. Based on recording a large variation in the enzymatic degradability of PET chips from different parts of postconsumer packaging material, it has been suggested [9], that differences in degradability may be due to differences in the distribution of the crystalline microstructures within heterogeneous PET samples. Our data on PET-P versus PET-S (Fig. 3) agree with this interpretation. Taken together, the results underline the importance of annealing the PET disks in a controlled manner to examine the significance of crystallinity on PET hydrolase degradation rates.

Conclusion

In this study, we present a new methodology used to quantitatively evaluate the influence of PET substrate crystallinity, X_C, on the action of PET degrading enzymes. The method involves the

preparation of PET samples having different levels X_C, by annealing PET samples above their T_g using commercially available PET sheets as starting material.

As a validation of the methodology the effect of the X_C, on the product release rate of the gold standard thermostable PET-hydrolyzing enzyme LCC_{ICCG} was investigated. The findings showed that the enzymatic rate was heavily dependent on the X_C. Especially between a X_C of 13.8 and 18.8%, at which the reaction rate decreased ~10 fold. Furthermore, it was observed that the product release rates were not constant during the reaction using PET at a $X_C > 8.2\%$. The data thus emphasize the importance of using progress curves rather than end-point measures when evaluating the catalytic efficiency of PET degrading enzymes on PET, and notably on PET substrate samples of different X_C.

It is suggested that the methodology presented in this paper is used as a standardized methodology for addressing the influence of X_C on PET degrading enzymes to allow a direct comparison between different studies.

Perspectives

As a final remark, it is important to state that this methodology is not limited to the characterization of the influence of X_C on the enzyme activity. An alternate annealing temperature (above T_g) may be used. This will, however, result in different crystallization rates, X_C at saturation/metastable state, and crystal thickness. The thermally annealed PET samples may also be used in other enzyme assays, which are addressing different properties than the product release rate.

Declaration of Competing Interest

The authors declare that they have no known competing financial interests or personal relationships that could have appeared to influence the work reported in this paper.

Data availability

Data will be made available on request.

Acknowledgements

Funding from The H.C. Ørsted Cofund Postdoc Program, Technical University of Denmark, and DTU Bioengineering, Technical University of Denmark,

References

[1] European Commission. A circular economy for plastics – Insights from research and innovation to inform policy and funding decisions. 2019. doi:10.2777/269031.
[2] World Economic Forum Ellen MacArthur Foundation McKinsey & Company. The New Plastics Economy: Rethinking the future of plastics. 2016.
[3] Mitchell G.R., Tojeira A. Controlling the morphology of polymers: multiple scales of structure and processing. 2016. doi:10.1007/978-3-319-39322-3.
[4] N. Sun, J. Yang, D. Shen, The effect of water absorption on the physical ageing of amorphous poly(ethylene terephthalate) film, Polymer 40 (1999) 6619–6622 (Guildf), doi:10.1016/S0032-3861(99)00246-3.
[5] S. Mandal, A. Dey, PET chemistry, in: Recycling Polyethylene Terephthalate Bottles, Elsevier, 2019, pp. 1–22, doi:10.1016/b978-0-12-811361-5.00001-8.
[6] R Androsch, B. Wunderlich, The link between rigid amorphous fraction and crystal perfection in cold-crystallized poly(ethylene terephthalate), Polymer 46 (2005) 12556–12566, doi:10.1016/J.POLYMER.2005.10.099.
[7] R. Rastogi, W.P. Vellinca, S. Rastogi, C. Schick, H.E.H. Meijer, The three-phase structure and mechanical properties of poly(ethylene terephthalate), J. Polym. Sci. Part B Polym. Phys. 42 (2004) 2092–2106, doi:10.1002/POLB.20096.
[8] S. Yoshida, K. Hiraga, T. Takehana, I. Taniguchi, H. Yamaji, Y. Maeda, et al., A bacterium that degrades and assimilates poly(ethylene terephthalate), Science 351 (2016) 1196–1199, doi:10.1126/science.aad6359.
[9] R. Wei, D. Breite, C. Song, D. Gräsing, T. Ploss, P. Hille, et al., Biocatalytic degradation efficiency of postconsumer polyethylene terephthalate packaging determined by their polymer microstructures, Adv. Sci. 6 (2019), doi:10.1002/advs.201900491.
[10] E. Erickson, T.J. Shakespeare, F. Bratti, B.L. Buss, R. Graham, M.A. Hawkins, et al., Comparative performance of PETase as a function of reaction conditions, substrate properties, and product accumulation, ChemSusChem 15 (2022), doi:10.1002/CSSC.202101932.

[11] T.B. Thomsen, C.J. Hunt, A.S. Meyer, Influence of substrate crystallinity and glass transition temperature on enzymatic degradation of polyethylene terephthalate (PET), New Biotechnol. 69 (2022) 28–35, doi:10.1016/j.nbt.2022.02.006.
[12] V. Tournier, C.M. Topham, A. Gilles, B. David, C. Folgoas, E. Moya-Leclair, et al., An engineered PET depolymerase to break down and recycle plastic bottles, Nature 580 (2020) 216–219, doi:10.1038/s41586-020-2149-4.
[13] C. Bach, X. Dauchy, S. Etienne, Characterization of poly(ethylene terephthalate) used in commercial bottled water, IOP Conf. Ser. Mater. Sci. Eng. 5 (2009) 012005, doi:10.1088/1757-899X/5/1/012005.
[14] P.G. Karagiannidis, A.C. Stergiou, G.P. Karayannidis, Study of crystallinity and thermomechanical analysis of annealed poly(ethylene terephthalate) films, Eur. Polym. J. 44 (2008) 1475–1486, doi:10.1016/j.eurpolymj.2008.02.024.
[15] Z. Chen, J.N. Hay, M.J. Jenkins, FTIR spectroscopic analysis of poly(ethylene terephthalate) on crystallization, Eur. Polym. J. 48 (2012) 1586–1610, doi:10.1016/j.eurpolymj.2012.06.006.
[16] R.M.R. Wellen, E. Canedo, M.S. Rabello, Nonisothermal cold crystallization of poly(ethylene terephthalate), J. Mater. Res. 26 (2011) 1107–1115, doi:10.1557/jmr.2011.44.
[17] A. Mehta, U. Gaur, B. Wunderlich, Equilibrium melting parameters of poly(ethylene terephthalate), J. Polym. Sci. Polym. Phys. Ed. 16 (1978) 289–296, doi:10.1002/pol.1978.180160209.
[18] J. Arnling Bååth, K. Borch, P. Westh, A suspension-based assay and comparative detection methods for characterization of polyethylene terephthalate hydrolases, Anal. Biochem. 607 (2020), doi:10.1016/j.ab.2020.113873.
[19] Z. Chen, J.N. Hay, M.J. Jenkins, The kinetics of crystallization of poly(ethylene terephthalate) measured by FTIR spectroscopy, Eur. Polym. J. 49 (2013) 1722–1730, doi:10.1016/j.eurpolymj.2013.03.020.
[20] T.W. Chan, A.I. Isayev, Quiescent polymer crystallization: modelling and measurements, Polym. Eng. Sci. 34 (1994) 461–471, doi:10.1002/pen.760340602.
[21] E.Z.L. Zhong-Johnson, C.A. Voight, A.J. Sinskey, An absorbance method for analysis of enzymatic degradation kineticsof poly(ethylene terephthalate) films, Sci. Rep. 11 (2021) 928, doi:10.1038/s41598-020-79031.

Intentionally left blank

Paper II

Influence of substrate crystallinity and glass transition temperature on enzymatic degradation of polyethylene terephthalate (PET)

Thore B. Thomsen, Cameron J. Hunt, Anne S. Meyer

New Biotechnology **2022** (25) 28-35

II

Intentionally left blank

New BIOTECHNOLOGY 69 (2022) 28–35

Contents lists available at ScienceDirect

New BIOTECHNOLOGY

journal homepage: www.elsevier.com/locate/nbt

Influence of substrate crystallinity and glass transition temperature on enzymatic degradation of polyethylene terephthalate (PET)

Thore Bach Thomsen, Cameron J. Hunt, Anne S. Meyer *

Protein Chemistry and Enzyme Technology Section, DTU Bioengineering, Department of Biotechnology and Biomedicine, Technical University of Denmark, 2800 Kgs. Lyngby, Denmark

ARTICLE INFO

Keywords:
Polyethylene terephthalate
Enzymatic degradation
Crystallinity
Glass transition temperature
Scanning electron microscopy

ABSTRACT

This work examines the significance of the degree of crystallinity (X_C) of polyethylene terephthalate (PET) and the PET glass transition temperature (T_g) on enzymatic degradation of PET at elevated temperatures using two engineered, thermostable PET degrading enzymes: LCC_{ICCG}, a variant of the leaf-branch compost cutinase, and DuraPETase, evolved from the *Ideonella sakaiensis* PETase. The X_C was systematically varied by thermal annealing of PET disks (Ø 6 mm, thickness 1 mm). The X_C affected the enzymatic product release rate that essentially ceased at X_C 22–27% for the LCC_{ICCG} and at X_C ~17% for the DuraPETase. Scanning Electron Microscopy revealed that enzymatic treatment produced cavities on the PET surface when the X_C was > 10% but resulted in a smooth surface on amorphous PET (X_C ~10%). The T_g of amorphous PET disks decreased from 75 °C to 60 °C during 24 h pre-soaking in water at 65 °C, while the X_C remained unchanged. Enzymatic reaction on pre-soaked disks at 68 °C, i.e. above the T_g, did not affect the enzymatic product release rate catalyzed by LCC_{ICCG}. These findings improve the understanding of enzymatic PET degradation and have implications for development of efficient enzymatic PET upcycling processes.

Introduction

Plastic pollution is a major environmental concern at a global scale [1]. A key contributor to this is post-consumer packaging material including single use plastic bottles and various food containers and wrappings that currently have a poor collection rate. The annual production of plastic packaging material is at least 78 Mt of which 32% leak outside the collection system [2]. One of the major types of plastics used for bottles and as packaging material is polyethylene terephthalate (PET). However, new discoveries that show that certain microbial enzymes can catalyze degradation of plastics [3–5] provide a completely new starting point for addressing a global ecosystem threat and develop enzyme-driven plastic recycling processes.

PET is a semi-crystalline polyester polymer composed of repeating units of ethylene glycol and terephthalic acid. The amorphous regions of PET consist of a mobile amorphous fraction (X_{MAF}) and a rigid amorphous fraction (X_{RAF}). The X_{RAF} forms the interface between the crystalline regions and the X_{MAF} [6]. The formation of crystalline regions of PET are induced either mechanically or thermally. Mechanically induced crystallization occurs when PET is exposed to stress or strain (during grinding, stretching etc.) [7], while thermally induced crystallization occurs when PET is held at temperatures above its glass transition temperature (T_g). Thermally induced crystallization can occur either non-isothermally, e.g. during cooling from melt, or isothermally, i.e. via annealing. Thermally induced crystallization does not occur, or is very limited, below the T_g of the PET material due to the inadequate chain mobility of the amorphous regions [8]. The T_g of a PET sample increases with its degree of crystallinity (X_C), and the T_g is highly affected by exposure of PET to water. PET is thus capable of absorbing water molecules into the amorphous regions, exerting a plasticizing effect on the polymer. This absorption of water also results in a decrease in both T_g and the cold crystallization temperature (T_{cc}) [9,10] (T_{cc} being the temperature peak of the region where crystallization takes place). At temperatures below the T_g, the amorphous chains within the PET molecules are rigid, and behave as a solid glass. When heated above the T_g the amorphous chains within the X_{MAF} transition into a more mobile

Abbreviations: APET, Amorphous PET; ATR-FTIR, Attenuated total reflection Fourier-transform infrared spectroscopy; BHET, bis(2-Hydroxyethyl) terephthalate; DSC, Differential scanning calorimetry; MAF, Mobile amorphous fraction (X_{MAF}); PET, Polyethylene terephthalate; PVAc, Polyvinyl acetate; RAF, Rigid amorphous fraction (X_{RAF}); RSM, Response surface methodology; SEM, Scanning Electron Microscopy; T_g, Glass transition temperature; X_C, Degree of crystallinity.

* Corresponding author.
E-mail address: asme@dtu.dk (A.S. Meyer).

https://doi.org/10.1016/j.nbt.2022.02.006
Received 27 September 2021; Received in revised form 23 January 2022; Accepted 27 February 2022
Available online 2 March 2022

rubber-like state [6]. It has therefore been suggested that enzymatic hydrolysis of PET should be performed at temperatures above the T_g due to the increased mobility of the amorphous chains providing better substrate accessibility [11,12].

This study was undertaken to examine the significance of the crystallinity of PET on its enzymatic degradation. The effect of X_C on the enzymatic product release rate during enzymatic degradation of PET at elevated temperatures is reported using two engineered, highly thermostable PET degrading enzymes [3,13]: LCC_{ICCG}, a variant of the leaf-branch compost cutinase (LCC), and DuraPETase, a variant of the *Ideonella sakaiensis* PETase. In addition, Scanning Electron Microscopy was used to explore surface changes of PET samples during enzymatic degradation, and the effect on the enzymatic product release of phase transition from the solid glass to the rubber-like state of X_{MAF} above the T_g of the PET sample was analyzed.

Materials and methods

Isothermal crystallization of PET

1 mm thick amorphous PET sheets (Goodfellow Cambridge Ltd, Huntingdon, UK) (Cat. No. ES303010) were used as the starting material for the PET substrates having different X_C used in this study. The PET sheet of 1 mm thickness was selected rather than the thinner (250 μm) PET film (Goodfellow Cambridge Ltd, Huntingdon, UK) (Cat. No. ES301445) based on its DSC and ATR-FTIR characteristics (Supplementary Information, Fig. S1). To prepare the PET substrate disks, the PET sheet was cut into disks using a generic Ø 6 mm hole punch. The crystallinity of the PET disks was systematically altered by annealing via dry heat treatment as follows. A PET disk in a 2 mL Eppendorf tube was placed in a heating block at 115 °C for a controlled time period, and subsequently quenched in ice water. The samples denoted as amorphous PET (APET) samples (X_C ~10%) were heat treated at 85 °C for 5 min, to remove the enthalpy relaxation, caused by ageing of the polymer [14].

Differential scanning calorimetry analysis of samples

The X_C, X_{MAF}, T_g, and the change in heat capacity at T_g ($\Delta C_{P(m)}$) were all derived from differential scanning calorimetry (DSC) measurements. DSC measurements were performed on a Pyris 1 Calorimeter (Perkin Elmer, Waltham, MA, USA). A constant heating rate of 10 °C min^{-1} was applied on samples weighing 8.5 ± 0.5 mg between temperatures of 20 °C and 270 °C. The X_C was calculated according to Eq. (1):

$$X_C = \frac{\Delta H_m - \Delta H_{cc}}{\Delta H_m^0} \bullet 100\% \quad (1)$$

ΔH_{cc} is the cold crystallization enthalpy (numerical value) of the sample. ΔH_m is the heat of melting of the sample, while ΔH_m^0 is the heat of melting of a pure crystalline sample which, according to [15], is 140 J g^{-1}. The X_{MAF} was calculated according to Eq. (2) as follows:

$$X_{MAF} = \frac{\Delta C_{P(m)}}{\Delta C_{P(a)}} \bullet 100\% \quad (2)$$

where $\Delta C_{P(a)}$ is the change in heat capacity at the T_g of a completely amorphous sample. The $\Delta C_{P(a)}$ (0.47 ± 0.02 J g^{-1} K^{-1}) was estimated by extrapolation of linear regression data of the $\Delta C_{P(m)}$ versus X_C (Supplementary Information, Fig. S2).

Soaking of PET

The T_g of PET was lowered by soaking an APET disk in 1 mL deionized water in a 2 mL Eppendorf tube placed in a thermomixer (Eppendorf, Hamburg, Germany). Incubation was performed at 25, 45 or 65 °C for 24 h. The soaking was halted by removing the water and subsequently drying the soaked samples using paper tissue. APET disks incubated in the atmosphere (in Eppendorf tubes without water) at 45 or 65 °C were included to quantify the potential negative effect caused by ageing of the samples at elevated temperatures. Samples pre-incubated in water are referred to as soaked samples while those aged directly in air (atmosphere) are referred to as aged samples.

Enzymes

The genes encoding the enzyme LCC_{ICCG} (Genbank: AEV21261.1 F243I/D238C/S283C/Y127G) and DuraPETase (Genbank: GAP38373.1 S214H/I168R/W159H/S188Q/R280A/A180I/G165A/Q119Y/L117F/T140D) were commercially synthesized with codon optimization for expression in *Escherichia coli* cells (GenScript, Piscataway, NJ, USA) without the predicted signal peptide (as determined by SignalP [16]). The genes were cloned into the *NcoI* (5′ end) and *XhoI* (3′ end) restriction sites of a pET-28a vector including a C-terminal hexa-histidine tag--coding sequence. Both LCC_{ICCG} and DuraPETase were expressed in *E. coli* BL21 (DE3) competent cells (New England Biolabs, Ipswich, MA, USA) via auto induction with 0.2% lactose in Terrific Broth at 30 °C for 24 h.

Cells were harvested by centrifugation (4,400g, 30 min, 4 °C) and suspended in lysis buffer (20 mM Tris-HCl, pH 8, 300 mM NaCl, 40 mM imidazole). Cells were disrupted using a Stansted pressure cell homogenizer (Homogenising Systems Ltd, Harlow, UK) over 2 passes and the soluble fraction clarified by centrifugation (16,000g, 30 min, 4 °C). The soluble fraction was loaded onto a 5 mL HisTrap FF crude column (GE Healthcare, Chicago, IL, USA) using an Äkta purifier (GE Healthcare), and eluted using a gradient up to 500 mM imidazole over 20 min at a rate of 5 mL/min. 4 mL volumes were collected over the elution period with target protein monitored by absorbance at 280 nm. Those factions containing protein were pooled and concentrated using a Vivaspin 20 centrifugal concentrator with a 10 kDa MWCO (Sartorius, Göttingen, Germany). During concentration the buffer was exchanged for storage buffer (20 mM Tris-HCl, pH 8, 300 mM NaCl, 0.02% w/v NaN_3).

Optimal conditions

The combined temperature and pH optima was estimated by response surface methodology (RSM) using an on-face central composite design (CCD) with three repeated center points and three replicas at each condition. The design, multivariate analyses, and graphical representation were aided by SAS JMP Pro 15 software (SAS Institute, Cary, NC, USA). The temperature and pH ranges were 66–78 °C and 8.5–10 for LCC_{ICCG}, and 50–60 °C and 8.5–9.5 for DuraPETase. The enzymatic product release rates were measured at standard conditions using the temperature and pH values specified by the CCD. The pH levels of the 50 mM glycine-NaOH buffers were in each case adjusted at the specific enzymatic reaction temperature.

Thermal inactivation

150 nM enzyme was incubated in 50 mM glycine-NaOH buffer pH 9 at 65, 70 or 75 °C for LCC_{ICCG} and at 50, 55 or 60 °C for DuraPETase for up to 8 h and sampling at set time points. The thermal inactivation was measured in terms of residual product release rate at the standard optimal reaction condition determined for each enzyme.

Standard enzymatic conditions

150 nM enzyme in 50 mM glycine-NaOH buffer was preheated to the reaction temperature. The reaction was initiated by the addition of one amorphous PET (APET) disk to the reaction. Reactions were then run by 1 h incubation of the samples in a thermomixer (Eppendorf, Hamburg, Germany) at 70 °C for LCC_{ICCG} and at 55 °C for DuraPETase. Each reaction was terminated by the addition of 6 M HCl to a final concentration of 0.118 M.

Enzymatic product release

The soluble product release from each enzyme reaction was quantified as bis(2-Hydroxyethyl) terephthalate (BHET) equivalents by measuring the absorbance at 240 nm using a Synergy HT™ plate reader (BioTek, Winooski, VT, USA), principally as described by [17]. Enzymatic product release rates were calculated in mM BHETeq/h from a BHET standard curve.

Progress curves

The enzymatic degradation of PET by LCC_{ICCG} and DuraPETase was assessed as soluble product release on PET substrates with varying X_C. The enzymes were incubated for specific times between 1 and 8 h at the standard conditions specified above.

Scanning Electron Microscopy (SEM)

The enzyme treated PET samples were washed in deionized water to remove impurities from the insoluble PET sample, and the samples were dried at room temperature overnight, prior to the SEM imaging. The dry samples were mounted on Carbon tape and coated with ~4 nm gold using a Quorum Q150T ES coater (Quorum Technologies, Lewes, UK). Samples were magnified 1500 × using a Quanta FEG 250 Analytical Environmental SEM (FEI, Hillsboro, Oregon, USA), and the signal was detected using an Everhart-Thornley detector.

Results and discussion

Optimal conditions for LCC_{ICCG} and DuraPETase

The combined temperature and pH optima of the two enzymes was estimated using RSM and found to be 70 °C, pH 9 for LCC_{ICCG} (Fig. 1A), and 55 °C pH 9 for DuraPETase B). The temperature and pH optima estimated in this study were in agreement with previously reported optima of the two enzymes [3,13]. The pH optimum of LCC_{ICCG} was slightly higher than the pH values previously used for this variant. These differences could be caused by the buffers used, as sodium phosphate buffers are not stable at pH values above 8. Furthermore, it has been shown that the activity of LCC depends on the buffer type, and that it is inhibited by Tris or MOPS [18]. However, the glycine-NaOH buffer does not seem to affect LCC activity, as the activity was not affected by increasing the buffer concentration to 500 mM (Supplementary Information, Fig. S3).

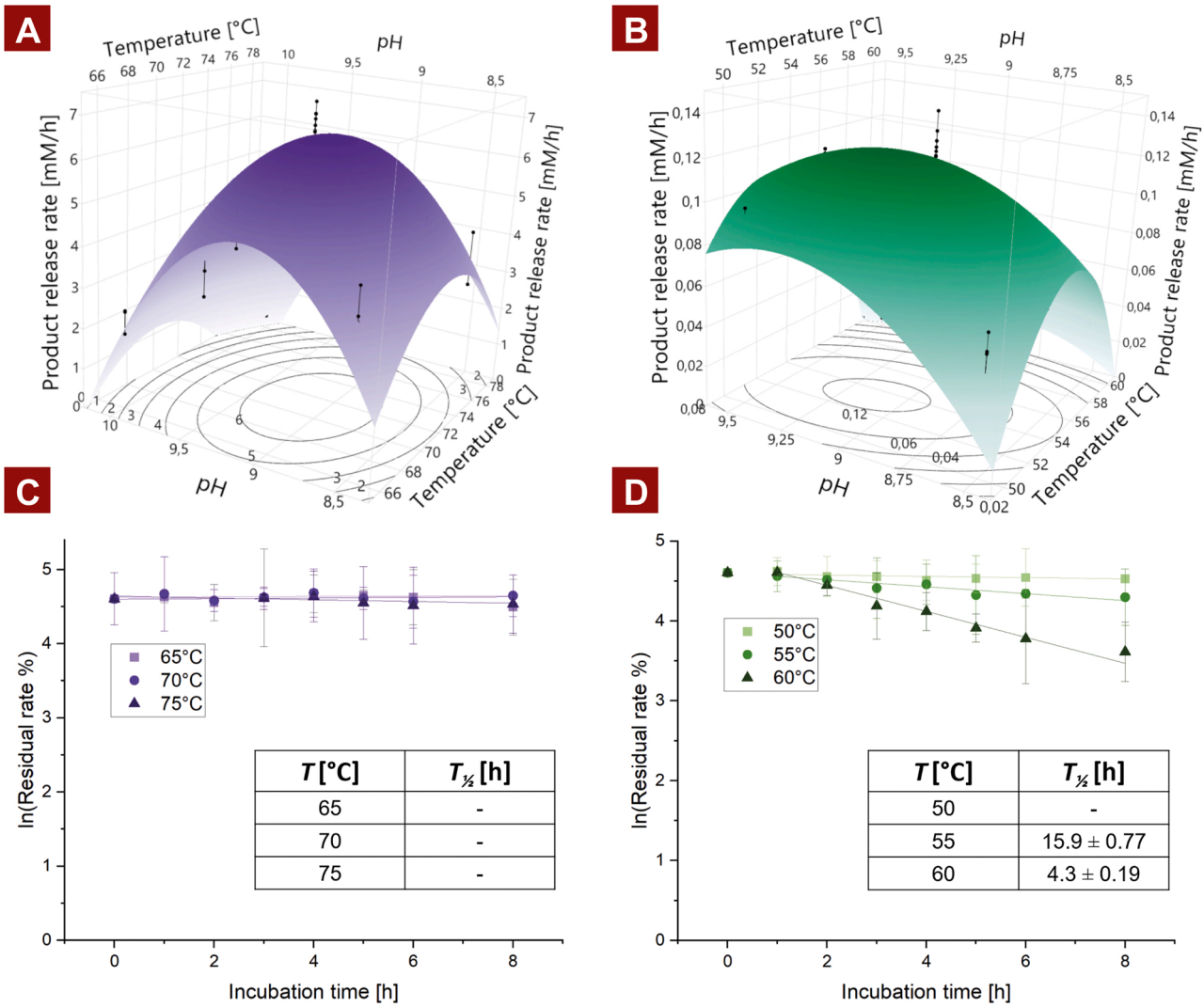

T [°C]	$T_{½}$ [h]
65	-
70	-
75	-

T [°C]	$T_{½}$ [h]
50	-
55	15.9 ± 0.77
60	4.3 ± 0.19

Fig. 1. Combined temperature and pH optima estimated by RSM methodology for A) LCC_{ICCG} and B) DuraPETase. 150 nM enzyme and one APET disk was used in each reaction. Thermal inactivation of C) LCC_{ICCG} and D) DuraPETase. The half-life, $T_{½}$ [h], at each inactivation is tabulated. The "- "sign indicates no detectable thermal inactivation during 8 h of incubation.

At the enzyme and substrate dosages applied, 150 nM enzyme and 1 APET disk, the predicted maximum reaction rates achieved (Fig. 1A, B), measured as product release rates, were 6.7 ± 0.32 mM_{BHETeq}/h for the LCC_{ICCG} and much lower at 0.124 ± 0.007 mM_{BHETeq}/h for the DuraPETase. These rates are equivalent to 750 ± 36 mM_{BHETeq} min^{-1} mM_{Enzyme}^{-1} for the LCC_{ICCG} and 14 ± 0.8 mM_{BHETeq} min^{-1} mM_{Enzyme}^{-1} for the DuraPETase.

Thermal stability

The thermal stability of the two enzymes was evaluated in terms of thermal inactivation during an 8-hour time course, at temperatures around their respective temperature optima. The residual product release rate of DuraPETase gradually decreased with increasing temperatures (Fig. 1D), thus indicating a temperature optimum balanced by thermal inactivation. LCC_{ICCG}, on the other hand, was not inactivated at its optima or at 5 °C above (Fig. 1C). The decline in the reaction rate of LCC_{ICCG}, at temperatures above the observed temperature optimum, was therefore not a result of significant thermal inactivation of the enzyme, but most likely a result of changes in the physical properties of the substrate, e.g isothermal crystallization during the reaction, which has previously been demonstrated at temperatures above 65 °C [3].

Impact of X_C on enzymatic product release rate

Several studies have reported that the enzymatic degradation of PET is hindered on substrates with a high X_C [3,4,19–22]. The decrease in enzymatic product release rate by LCC_{ICCG} and DuraPETase, caused by an increased X_C, was investigated on commercially available amorphous PET. The PET disks were annealed at 115 °C to obtain a range of PET substrates having different X_C.

To validate the annealing method, it was verified that the increase in X_C as a function of the annealing time (Fig. 2) followed the characteristic sigmoidal function associated with the Avrami equation [14]. The crystallinity reached saturation after 15 min at a X_C of ~27% (Fig. 2), similar to the observations reported in [14].

To explore the evolution of the enzymatic PET degradation reactions in response to crystallinity, LCC_{ICCG} and DuraPETase were incubated over an 8 h time period on thermally annealed PET substrates, with varying X_C. The product release rate on these substrates (Fig. 3C, D) were evaluated based on the linear region of the progression curves (Fig. 3A, B). The correlation between the product release rate, measured over the linear range, of LCC_{ICCG} and X_C followed an exponential rather than a linear trend (Fig. 3C). This trend could not be observed with DuraPETase, as no product release was measured during enzymatic treatment on the three samples with the highest X_C (Fig. 3B). The product release rate and the X_C were not significantly different on the samples that had a detectable product release for DuraPETase (Fig. 3D). However, a lag phase was observed on the sample which had been annealed at 115 °C (X_C of 12.7%). Similar lag phases were observed for LCC_{ICCG} on the annealed samples having elevated X_C, but LCC_{ICCG} was more active at higher X_C than DuraPETase (Fig. 3A,B). The length of the lag phases for both enzymes correlated with the X_C.

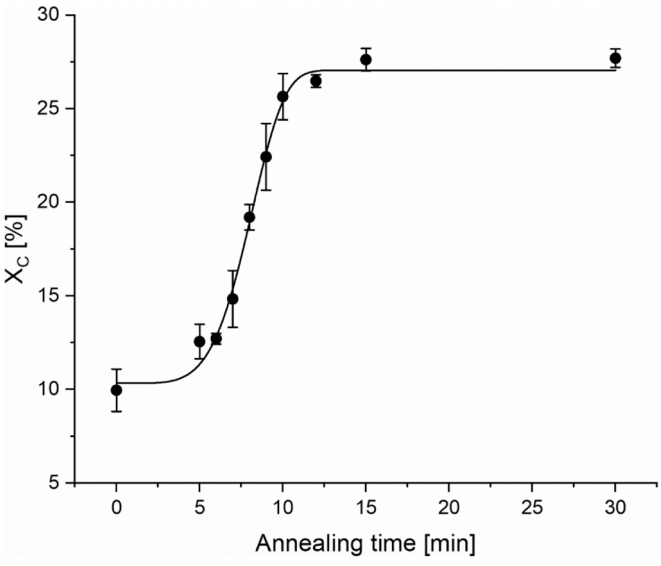

Fig. 2. Change in X_C as function of annealing time at 115 °C. The solid fitting is a modified version of the Avrami equation.

The lag phases observed with increased X_C are most likely a result of the initial random, endo-scission action of the enzymes, which at elevated X_C may initially provide cleaved ester bonds that are spread at the polymer surface, with preferred attack points at the few amorphous sites, but not immediately releasing detectable soluble products. The lag-phase may be further extended due to the slow rate resulting from limited formation of productive enzyme-substrate collisions as the access to amorphous sites decreases with increased X_c. Once a sufficient number of cleavage points has been achieved, the continued enzymatic action results in release of detectable hydrolysis products by further chain scission on the polymer surface by degradation of solubilized bulky polymers. This order of events agrees with the degradation mechanism proposed by Wei et al. for another PET hydrolase, namely *Tf*Cut2 [19]. This mechanistic explanation further considers that the initial endo-scission action of the PET hydrolase may change to what in effect is an exo-type scission of the neighboring ester bonds in the MAF region of the PET substrate as the reaction progresses [19,23]. A firmer confirmation of this series of events, and a detailed mechanistic interpretation of the different responses of enzymes to changes in PET substrate crystallinity, obviously require detailed mathematical modeling. However, the present data clearly infer that the increases in X_C affected the pre-steady-state kinetics of the product release rate for both LCC_{ICCG} and DuraPETase to a degree where essentially no product release occurred above X_C of 23–27% for LCC_{ICCG} and above X_C of 19% for DuraPETase.

The lack of product release on the crystalline samples could be caused by: (1) the lag phase on the samples with high X_C being longer than the total reaction time; (2) the X_C threshold at which the enzymes can degrade the substrate had been exceeded; (3) a combination of (1) and (2).

A deceleration in the reaction rate of LCC_{ICCG} was observed after 4 h of reaction. During the hydrolysis of PET, protons are released. The pH of the samples with the lowest X_C, and thereby highest product release, had decreased to pH 5.6 after the reaction (data not shown). As the buffer concentration did not affect the product release rate (Supplementary Information, Fig. S3), a 500 mM glycine-NaOH pH 9 buffer was used for the samples with 9.8% and 12.1% incubated with LCC_{ICCG}. However, even though the pH was stable using a higher buffer concentration, a decline in the reaction rate was still observed after 6 h. Less than 10% of the substrate was solubilized (Supplementary Information, Fig. S3) during the 8 h. The data suggest that the decrease in reaction rate is likely caused by changes in the physical properties, such as crystallinity, at the substrate surface, rather than thermal inactivation of the enzyme, since LCC_{ICCG} was not significantly inactivated at these reaction conditions (Fig. 1C). As no changes in surface topology could be observed on the APET samples (X_C ~10%), it is assumed that if any changes have occurred they would be smaller than what is visible at the resolution of the SEM images (Fig. 4).

A linear relationship between the degradation rate of *Tf*Cut2 and the initial X_C of PET has previously been reported [19]. The effect of the X_C on the activity of *Tf*Cut2 was investigated using PET samples in which the X_C was altered enzymatically (by removal of the amorphous regions) by measuring the weight loss after 24 h [19]. It is uncertain whether *Tf*Cut2 and LCC_{ICCG} are affected differently by substrate crystallinity or if the contradictions are due to differences in the substrate or

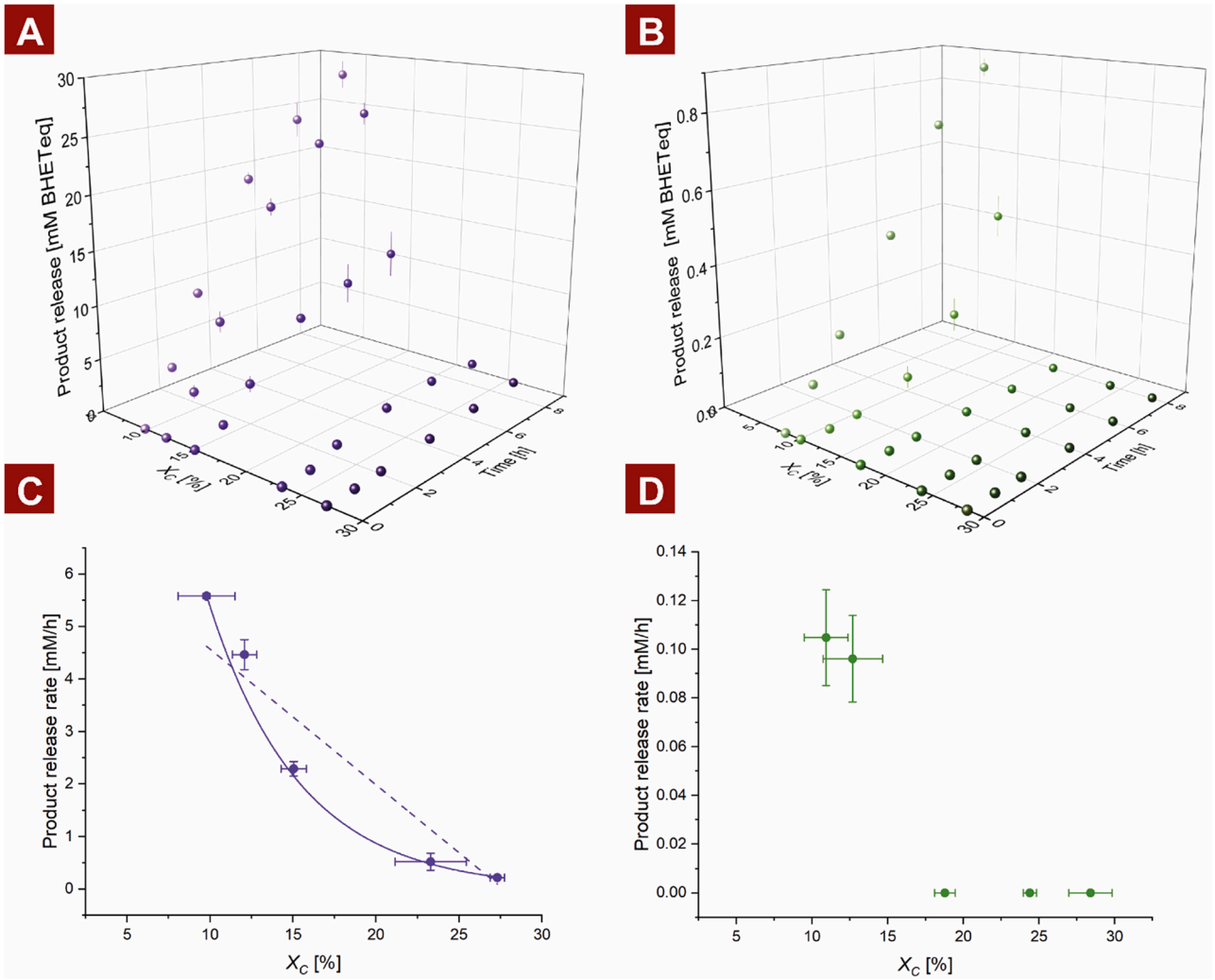

Fig. 3. Enzymatic hydrolysis of PET samples of different X_C, obtained via annealing at 115 °C PET samples using 150 nM enzyme in 50 mM glycine-NaOH buffer at pH 9. A) LCC_{ICCG} assayed at 70 °C and B) DuraPETase assayed at 55 °C. C) Product release rate of LCC_{ICCG} calculated from the linear region from A). The bold line represents a linear fit of the data, while the dashed line represents an exponential decay. D) Product release rate of DuraPETase calculated from the linear region of C). (The buffer concentration of the samples in A) and C) with X_C = 9.8% or 12.1% was 500 mM).

methodology used for the assessment. It is important to note that the X_C measured by DSC is an average of the entire sample. The local X_C at the surface may therefore vary and a systematic deviation is therefore expected to be present between the kinetics of the activity of PET degrading enzymes against crystalline PET, measured in terms of bulk or surface X_C, as these enzymes are interfacial enzymes.

Changes in the surface topology evaluated by Scanning Electron Microscopy (SEM)

The surface topology observed on the APET samples (X_C ~10%) and thermally annealed samples appeared smooth prior to the enzymatic treatment (at t = 0 min), based on SEM imaging (Fig. 4). During the 8 h of enzymatic treatment, the observed surface topology of the APET sample did not change. In contrast, the surface of the annealed samples showed significant surface erosion, with the degree of erosion appearing to correlate with the enzymatic product release over time (Fig. 4). In interfacial catalytic reactions, increased surface areas are often associated with increase kinetic rates. This was, however, not the case here, as the observed surface erosion, resulting in a larger surface area on the crystalline samples, must be caused by regions which are inaccessible to LCC_{ICCG}. The increasing surface area during enzymatic treatment is therefore not equivalent to an increasing number of catalytic sites and the observed surface erosion is therefore an indication of the preference of LCC_{ICCG} towards the amorphous regions, as the PET samples were degraded uniformly when the crystallinity of the substrate was low. This preference of PET degrading enzymes, including LCC_{ICCG}, towards amorphous regions has been proposed previously in several articles [3, 23–25].

The initial enzymatic degradation of the thermally annealed PET samples did not result in surface erosion or in detectable soluble product formation. The data thus agree with the observed lag phases on the progress curves (Fig. 3A,B) and are in accord with the understanding that increased X_C of the PET substrate results in both limited formation of productive enzyme-substrate complexes, due to a limited number of amorphous attack points, that essentially impedes a sufficient number of successful enzymatic attacks from being achieved. The SEM images of the samples with a 23.3% and 27.3% X_C imaged after 4 h enzymatic treatment shows the presence of local cavities rather than a uniform distribution of the surface erosion. This observation could indicate that the hydrolysis of ester bonds near a previously hydrolyzed bond is more favorable than a randomly located ester bond. As discussed above, a similar phenomenon has been described previously [19]. Although it is tempting to conclude that the inaccessible area corresponds to the crystal regions, further studies are required to determine the exact composition of the substrate in terms of X_C, X_{MAF}, and X_{RAF}.

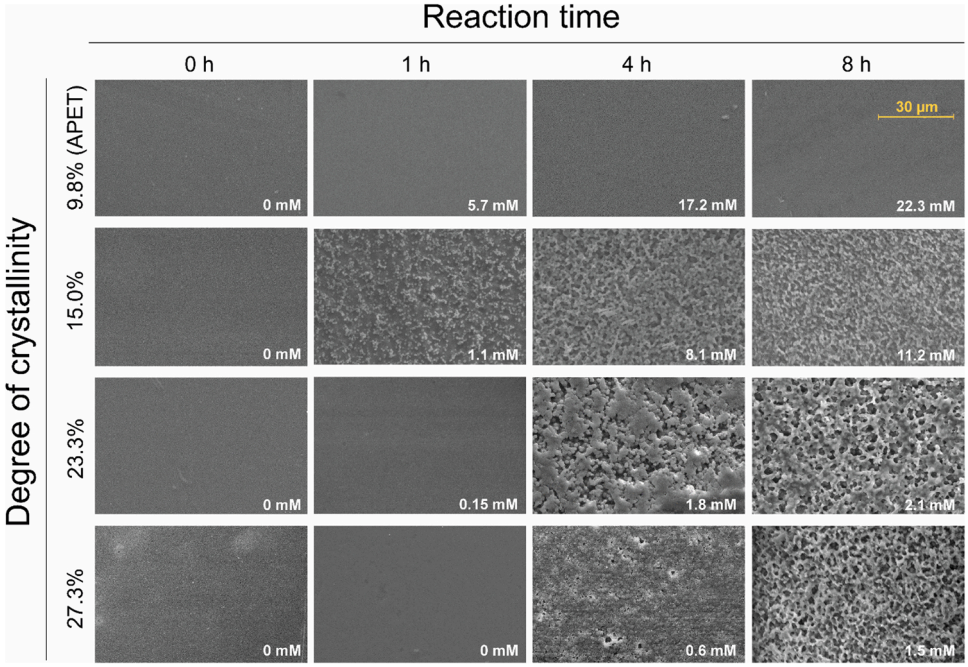

Fig. 4. SEM imaging (1500 × magnification) of PET disks of various X_C treated with 150 nM LCC in 50 mM glycine-NaOH pH 9 at 70 °C (Fig. 2A). The bold white text in the lower right corner of each SEM image indicates the product release measured by A_{240} after the enzymatic hydrolysis.

Effect of T_g on product release rate

The T_g of PET was lowered by soaking APET disks in water for 24 h at 45 or 65 °C. This soaking resulted in a decrease in the T_g from 75 ± 0.4 °C to 69 ± 0.8 °C or 60 ± 0.5 °C, respectively (Fig. 5A, t = 0 min), without affecting the X_C (Fig. 5C, t = 0 min). The mobility of the polymer chains within the mobile amorphous fraction (X_{MAF}) will increase when PET is heated to temperatures above its T_g (while the X_{MAF} % remains constant). The effect of this increased mobility in the amorphous fraction, resulting from the thermal transition at T_g, was evaluated by comparing product release rates on presoaked PET samples (low T_g) versus un-soaked PET samples (high T_g) at a temperature between their T_g-values, i.e. 68 °C (Fig. 5B). Throughout the enzymatic treatment, the T_g-value of the un-soaked PET sample remained above the reaction temperature, while the T_g-value of the pre-soaked sample remained below. Consequently, the amorphous regions of the un-soaked PET sample would be in a less mobile glass-state, while the amorphous regions of the pre-soaked PET sample would be in the more mobile rubber-like state. The X_C of the samples was not affected during the reaction (Fig. 5C). It was previously shown that the activity of the PET-hydrolysing cutinase (HiC) from *Humicola insolens*, measured on PET films with a low X_C, increases dramatically at temperatures above 65 °C [21]. The same trend was, however, not observed when the enzyme was assayed on polyvinyl acetate (PVAc) [26]. These observed differences were suggested to be attributed to the T_g values of the two substrates being 75 °C for PET and 32 °C for PVAc. PET would therefore, unlike PVAc, undergo a phase transition, increasing the substrate mobility at temperatures around the T_g [21]. Based on these observations, the soaked PET sample might be expected to produce the highest product release rate during enzymatic treatment (with LCC_{ICCG}), due to increased substrate mobility. However, no difference in enzymatic product release rate between the soaked and untreated samples was observed (Fig. 5B). Likewise, no changes in product release rate were observed on the aged samples incubated in atmosphere at 45 °C or at 65 °C. These observations imply that the increased mobility caused by the transition at the T_g does not affect the enzymatic product release rate, as the latter was neither positively affected by the plasticizing effect of water nor negatively affected by the ageing resulting from the elevated soaking temperatures during one day of pretreatment.

This is an important result, as pre-soaking of PET at elevated temperatures may invariably take place during large scale high-temperature enzyme-assisted recycling of PET.

The data obtained comply with the estimated temperature optimum being 70 °C for LCC_{ICCG} as predicted from the RSM data, and the thermal stability data verified that the enzyme was robust at this temperature (Fig. 1A). For 1 h soaking at 70 °C it was observed that the T_g value of PET decreased from 75 °C to just below 70 °C (Supplementary Information, Fig. S4). During enzymatic reaction at 70 °C in an aqueous solution, the T_g of the PET substrate would thus gradually decrease. As this T_g lowering effect of soaking is both time and temperature dependent, the substrate mobility would be expected to be higher on the samples assayed at temperatures above 70 °C. If the substrate mobility had a positive effect on the product release rate, a temperature optimum above 70 °C would be expected, as LCC_{ICCG} is stable even at 75 °C (Fig. 1C). These data thus corroborate that the substrate mobility does not affect the rate of product release during enzymatic degradation of PET with the thermostable enzyme LCC_{ICCG}. The increased mobility of the amorphous chains also affects the crystallization rate. When T_g falls to or below the reaction temperature, isothermal crystallization can be expected to occur. This phenomenon is facilitated by an increase in the kinetic energy of the amorphous chains, which become sufficient for crystal growth when the temperature exceeds the T_g [27]. Hence, a positive effect on enzyme activity-caused increased substrate mobility could potentially be overshadowed by an increase in X_C or X_{RAF}.

However, the rate is expected to be slow at temperatures just above T_g, as the overall crystallinity of the samples soaked at 65 °C was unaffected, although the T_g dropped below the soaking temperature during the pretreatment (Fig. 5A, C).

Conclusions

This work presents an experimental methodology for evaluation of the effect of PET crystallinity on the enzymatic product release rate of PET degrading enzymes, by altering crystallinity of PET via isothermal crystallization at 115 °C. It was demonstrated that an increase in crystallinity affected the pre-steady-state kinetics of both LCC_{ICCG} and

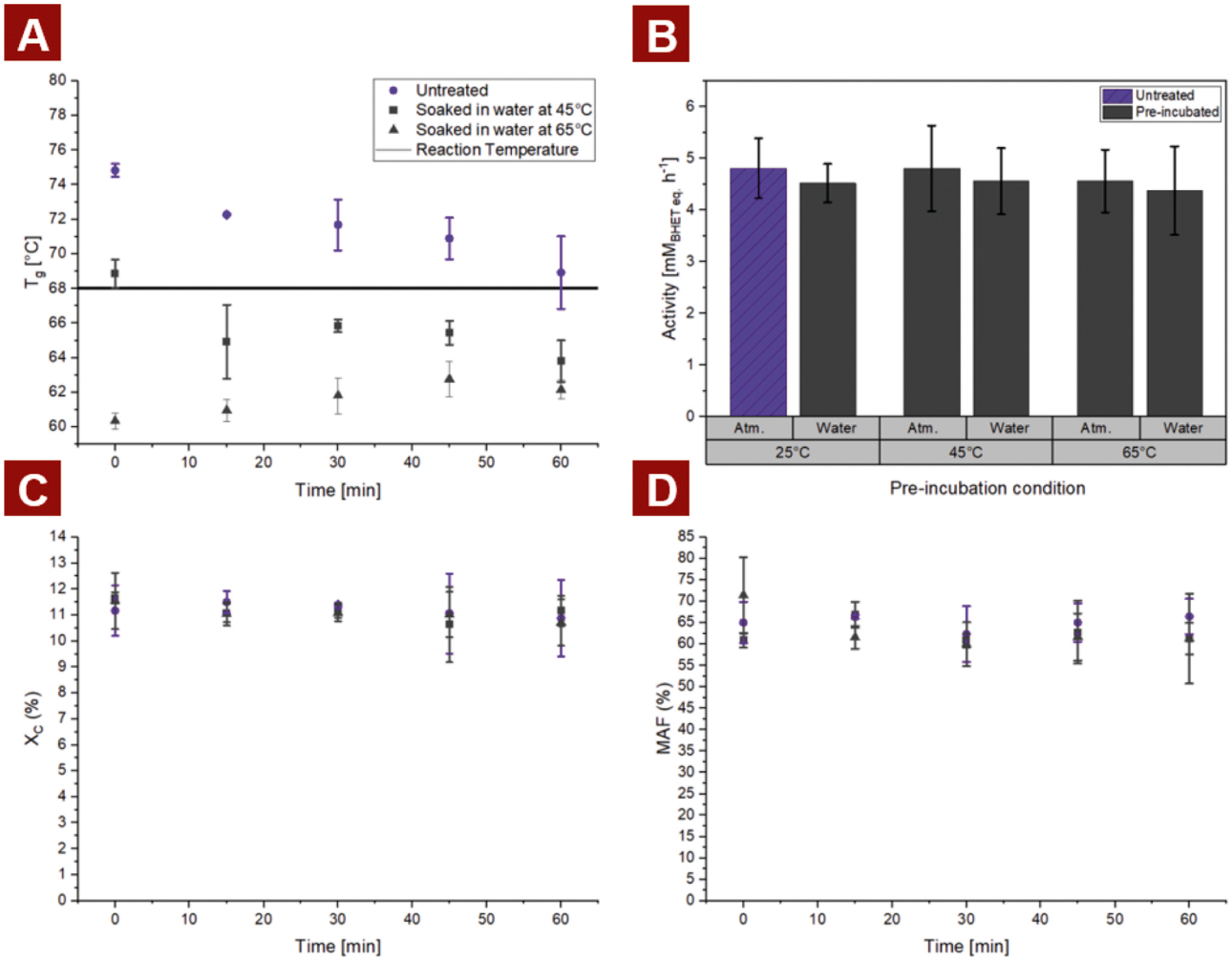

Fig. 5. Enzymatic treatment of PET samples at different T_g-values: The APET samples with decreased T_g-values were obtained by soaking the samples in water at 45 or 65 °C for 24 h. A) Change in T_g during enzymatic treatment. The bold line represents the reaction temperature. B) Product release rate of PET samples pretreated at various conditions during enzymatic treatment. C) Change in X_C during enzymatic treatment. D) Change in X_{MAF} during enzymatic treatment. All enzyme reactions were performed using 150 nM LCC_{ICCG} in 50 mM Glycine-NaOH buffer pH 9, reacting at 68 °C for 15 min.

DuraPETase, while the steady-state kinetics of LCC_{ICCG} was affected negatively in a non-linear manner. The effect of the X_C on the steady-state kinetics of DuraPETase could not be determined, as no product release was detected on samples with high X_C. SEM imaging of PET samples revealed that LCC_{ICCG} was modifying the surface homogeneously on low X_C PET (X_C 10%), and heterogeneously, by creating cavities, on higher X_C PET.

The decrease in reaction rate of LCC_{ICCG} at temperatures above its optimum of 70 °C was most likely caused by physical changes of the substrate rather than by thermal inactivation of the enzyme. The product release rate of LCC_{ICCG} was unaffected by an increase in substrate mobility caused by the transition of the amorphous regions from a glassy to a rubbery state above the T_g - thus emphasizing that research on evolving thermostable PET degrading enzymes should focus on improving their catalytic efficiency on crystalline PET in addition to thermal stability.

CRediT authorship contribution statement

Thore Bach Thomsen: Conceptualization, Investigation, Methodology, Visualization, Formal analysis, Writing. **Cameron J. Hunt:** Conceptualization, Investigation, Methodology, Formal analysis, Funding acquisition, Resources, Writing. **Anne S. Meyer:** Conceptualization, Project administration, Supervision, Funding acquisition, Resources, Writing.

Acknowledgements

Funding from The H.C. Ørsted Cofund Postdoc Program, Technical University of Denmark. We also wish to thank the National Centre for Nano Fabrication and Characterization at DTU for assistance with Scanning Electron Microscopy.

Conflicts of interest

There are no conflicts to declare.
All authors declare no conflict of interests.

Appendix A. Supporting information

Supplementary data associated with this article can be found in the online version at doi:10.1016/j.nbt.2022.02.006.

References

[1] European Commission A circular economy for plastics – Insights from research and innovation to inform policy and funding decisions 2019 doi: 10.2777/269031.
[2] World Economic Forum Ellen MacArthur Foundation McKinsey & Company The New Plastics Economy: Rethinking the future of plastics 2016.

[3] Tournier V, Topham CM, Gilles A, David B, Folgoas C, Moya-Leclair E, et al. An engineered PET depolymerase to break down and recycle plastic bottles. Nature 2020;580:216–9. https://doi.org/10.1038/s41586-020-2149-4.
[4] Yoshida S, Hiraga K, Takehana T, Taniguchi I, Yamaji H, Maeda Y, et al. A bacterium that degrades and assimilates poly(ethylene terephthalate). Science 2016;351:1196–9. https://doi.org/10.1126/science.aad6359.
[5] Wei R, Tiso T, Bertling J, O'Connor K, Blank LM, Bornscheuer UT. Possibilities and limitations of biotechnological plastic degradation and recycling. Nat Catal 2020;3:867–71. https://doi.org/10.1038/s41929-020-00521-w.
[6] Chen H, Cebe P. Vitrification and devitrification of rigid amorphous fraction of PET during quasi-isothermal cooling and heating. Macromolecules 2009;42:288–92. https://doi.org/10.1021/ma802104a.
[7] Forestier E, Combeaud C, Guigo N, Sbirrazzuoli N, Billon N. Understanding of strain-induced crystallization developments scenarios for polyesters: comparison of poly(ethylene furanoate), PEF, and poly(ethylene terephthalate), PET. Polymer 2020;203:122755. https://doi.org/10.1016/j.polymer.2020.122755.
[8] Shieh YT, Lin YS, Twu YK, Tsai HB, Lin RH. Effect of crystallinity on enthalpy recovery peaks and cold-crystallization peaks in PET via TMDSC and DMA studies. J Appl Polym Sci 2010;116:1334–41. https://doi.org/10.1002/app.31570.
[9] Levine H, Grenet J, Slade L. Water as a plasticizer: physico-chemical aspects of low-moisture polymeric systems. Eur Polym J 1993;30:339–45. https://doi.org/10.1017/cbo9780511552083.002.
[10] Zhang W, Yan Q, Ye K, Zhang Q, Chen W, Meng L, et al. The effect of water absorption on stretch-induced crystallization of poly(ethylene terephthalate): an in-situ synchrotron radiation wide angle X-ray scattering study. Polymer 2019;162:91–9. https://doi.org/10.1016/j.polymer.2018.12.029.
[11] Austin HP, Allen MD, Donohoe BS, Rorrer NA, Kearns FL, Silveira RL, et al. Characterization and engineering of a plastic-degrading aromatic polyesterase. Proc Natl Acad Sci USA 2018;115:E4350–7. https://doi.org/10.1073/pnas.1718804115.
[12] Kawai F. The current state of research on PET hydrolyzing enzymes available for biorecycling. Catalysts 2021;11:1–10. https://doi.org/10.3390/catal11020206.
[13] Cui Y, Chen Y, Liu X, Dong S, Tian Y, Qiao Y, et al. Computational redesign of a PETase for plastic biodegradation under ambient condition by the GRAPE Strategy. ACS Catal 2021;11:1340–50. https://doi.org/10.1021/acscatal.0c05126.
[14] Karagiannidis PG, Stergiou AC, Karayannidis GP. Study of crystallinity and thermomechanical analysis of annealed poly(ethylene terephthalate) films. Eur Polym J 2008;44:1475–86. https://doi.org/10.1016/j.eurpolymj.2008.02.024.
[15] Mehta A, Gaur U, Wunderlich B. Equilibrium melting parameters of poly(ethylene terphthalate). J Polym Sci Polym Phys Ed 1978;16:289–96. https://doi.org/10.1002/pol.1978.180160209.
[16] Almagro Armenteros JJ, Tsirigos KD, Sønderby CK, Petersen TN, Winther O, Brunak S, et al. SignalP 5.0 improves signal peptide predictions using deep neural networks. Nat Biotechnol 2019;37:420–3. https://doi.org/10.1038/s41587-019-0036-z.
[17] Arnling Bååth J, Borch K, Westh P. A suspension-based assay and comparative detection methods for characterization of polyethylene terephthalate hydrolases. Anal Biochem 2020;607:113973. https://doi.org/10.1016/j.ab.2020.113873.
[18] Schmidt J, Wei R, Oeser T, Belisário-Ferrari MR, Barth M, Then J, et al. Effect of Tris, MOPS, and phosphate buffers on the hydrolysis of polyethylene terephthalate films by polyester hydrolases. FEBS Open Bio 2016;6:919–27. https://doi.org/10.1002/2211-5463.12097.
[19] Wei R, Breite D, Song C, Gräsing D, Ploss T, Hille P, et al. Biocatalytic degradation efficiency of postconsumer polyethylene terephthalate packaging determined by their polymer microstructures. Adv Sci 2019;6:1900491. https://doi.org/10.1002/advs.201900491.
[20] Weinberger S, Haernvall K, Scaini D, Ghazaryan G, Zumstein MT, Sander M, et al. Enzymatic surface hydrolysis of poly(ethylene furanoate) thin films of various crystallinities. Green Chem 2017;19:5381–4. https://doi.org/10.1039/c7gc02905e.
[21] Ronkvist ÅM, Xie W, Lu W, Gross RA. Cutinase-catalyzed hydrolysis of poly(ethylene terephthalate). Macromolecules 2009;42:5128–38. https://doi.org/10.1021/ma9005318.
[22] Vertommen MAME, Nierstrasz VA, Van Der Veer M, Warmoeskerken MMCG. Enzymatic surface modification of poly(ethylene terephthalate). J Biotechnol 2005;120:376–86. https://doi.org/10.1016/j.jbiotec.2005.06.015.
[23] Ellis LD, Rorrer NA, Sullivan KP, Otto M, McGeehan JE, Román-Leshkov Y, et al. Chemical and biological catalysis for plastics recycling and upcycling. Nat Catal 2021;4:539–56. https://doi.org/10.1038/s41929-021-00648-4.
[24] Webb HK, Arnott J, Crawford RJ, Ivanova EP. Plastic degradation and its environmental implications with special reference to poly(ethylene terephthalate). Polymers 2013;5:1–18. https://doi.org/10.3390/polym5010001.
[25] Kawai F, Kawabata T, Oda M. Current knowledge on enzymatic PET degradation and its possible application to waste stream management and other fields. Appl Microbiol Biotechnol 2019;103:4253–68. https://doi.org/10.1007/s00253-019-09717-y.
[26] Ronkvist ÅM, Lu W, Feder D, Gross RA. Cutinase-catalyzed deacetylation of poly(vinyl acetate). Macromolecules 2009;42:6086–97. https://doi.org/10.1021/ma900530j.
[27] Wellen RMR, Rabello MS. The kinetics of isothermal cold crystallization and tensile properties of poly(ethylene terephthalate). J Mater Sci 2005;40:6099–104. https://doi.org/10.1007/s10853-005-3173-3.

Paper III

Rate Response of Poly(Ethylene Terephthalate)-Hydrolases to Substrate Crystallinity: Basis for Understanding the Lag Phase

Thore B. Thomsen*, Sune W. Schubert*, Cameron J. Hunt, Kim Borch, Kenneth Jensen, Jesper Brask, Peter Westh, Anne S. Meyer

ChemSusChem **2023** (16) 1-13

*Contributed equally

III

Intentionally left blank

ChemSusChem

Research Article
doi.org/10.1002/cssc.202300291

Chemistry Europe
European Chemical Societies Publishing

www.chemsuschem.org

Rate Response of Poly(Ethylene Terephthalate)-Hydrolases to Substrate Crystallinity: Basis for Understanding the Lag Phase

Thore B. Thomsen[+],[a] Sune Schubert[+],[a] Cameron J. Hunt,[a] Kim Borch,[b] Kenneth Jensen,[b] Jesper Brask,[b] Peter Westh,[a] and Anne S. Meyer*[a]

The rate response of poly(ethylene terephthalate) (PET)-hydrolases to increased substrate crystallinity (X_C) of PET manifests as a rate-lowering effect that varies significantly for different enzymes. Herein, we report the influence of X_C on the product release rate of six thermostable PET-hydrolases. All enzyme reactions displayed a distinctive lag phase until measurable product formation occurred. The duration of the lag phase increased with X_C. The recently discovered PET-hydrolase PHL7 worked efficiently on "amorphous" PET disks ($X_C \approx 10\%$), but this enzyme was extremely sensitive to increased X_C, whereas the enzymes LCC_{ICCG}, LCC, and DuraPETase had higher tolerance to increases in X_C and had activity on PET disks having X_C of 24.4%. Microscopy revealed that the X_C-tolerant hydrolases generated smooth and more uniform substrate surface erosion than PHL7 during reaction. Structural and molecular dynamics analysis of the PET-hydrolyzing enzymes disclosed that surface electrostatics and enzyme flexibility may account for the observed differences.

Introduction

Materials made of plastic have become an integral part of our modern society. In 2021 the annual production of plastics exceeded 390 Mt, of which the vast majority (90.2%) were made from fossil-based raw materials.[1] Among these synthetic plastics, poly(ethylene terephthalate) PET is one of the major types, accounting for 10.2% of the total global plastic production.[2] PET products are primarily used in single-use products with short life span such as plastic bottles, packaging material, and textile fibers.[1,3] The plastic waste generated from PET products currently represents an increasing ecological challenge, as only a fraction of PET is recycled.[3] Several enzymes have been reported to show PET-hydrolyzing activity. These enzymes include cutinases (EC 3.1.1.74), lipases (EC 3.1.1.3), and esterases (EC 3.1.1.1 and EC 3.1.1.2).[4] Furthermore, following the discovery of the PET consuming *Ideonella sakaiensis* (*I. sakaiensis*) bacterium together with its PETase-MHETase enzyme system in 2016,[5] the International Union of Biochemistry and Molecular Biology Enzyme Commission classified these enzymes as EC 3.1.1.101 (PETase) and EC 3.1.1.102 (MHETase), respectively.[6] Despite its unique EC number the *I. sakaiensis* PETase is structurally similar to other PET-hydrolyzing bacterial cutinases.[7,8] The environmental plastic burden combined with the discovery of PET degrading enzymes has created an enormous incentive for developing biocatalysis based recycling of PET.[9,10]

In order to overcome the relatively slow catalytic rates of the enzymes, the structural and biophysical properties of PET-hydrolases are taking center stage.[11–15] Enzyme engineering efforts on promising candidates[13,16–20] have been intense, and several groups have succeeded in discovering and developing novel PET degrading enzymes that work at elevated rates[17,18,21] and/or have improved thermostability.[17,19] In contrast, fewer studies have focused on how the physical properties of the PET substrate influence the enzymatic degradation process.[22–25]

An understanding of the significance of the PET substrate crystallinity (X_C) on the enzymatic action is nevertheless of critical importance, especially when considering that many PET products (plastic bottles, textile fibers etc.) and polyester materials in micro plastic tend to have high crystallinity. For example, although the neck of a PET bottle may have low crystallinity, the X_C of the bulk of a PET bottle is easily above 25%.[17,26] The weathering/aging processes that PET waste (including micro plastics) are subjected to may furthermore increase the X_C.[27]

Although some PET hydrolases may degrade highly crystalline PET particles (~40% X_C) at high initial rates, the enzymatic conversion yields reported on such highly crystalline PET particles have been low.[28,29] The high initial rates on such particles are presumably a result of the extremely high surface area of the PET micro particles that excessively exposes the attackable sites of the heterogeneous PET substrate. In addition, the physicochemical features of the exposed surface layer of

[a] T. B. Thomsen,[+] S. Schubert,[+] Dr. C. J. Hunt, Prof. P. Westh, Prof. A. S. Meyer
Department of Biotechnology and Biomedicine
Technical University of Denmark
Søltofts Plads, DK-2800 Kgs. Lyngby (Denmark)
E-mail: asme@dtu.dk
[b] Dr. K. Borch, Dr. K. Jensen, Dr. J. Brask
Novozymes A/S
Biologiens Vej 2, 2800 Kgs. Lyngby (Denmark)
[+] These authors contributed equally to this work.

Supporting information for this article is available on the WWW under https://doi.org/10.1002/cssc.202300291

the PET particles, such as increased mobility,[30] may exacerbate the initial enzymatic degradation rate of such particles. On more industrially relevant PET substrates, increases in X_C markedly decrease the catalytic performance of PET-hydrolases, and for most currently known PET-hydrolases, most of the activity is completely lost at X_C above 20%.[22–24]

In the present study, we investigate the influence of X_C on the enzymatic hydrolysis by six different PET degrading enzymes of PET disks (Ø = 6 mm) having different X_C values. The enzymes include the leaf compost cutinase LCC[31] and its engineered thermostable variant, LCC_{ICCG},[18] the bacterial PET degrading cutinase from *Thermofibida fusca* (*Tf*C),[32] a fungal cutinase from *Humicula insolens* (*Hi*C),[33] a recently discovered cutinase, PHL7, derived from metagenomic DNA isolated from mixed plant waste compost,[34] and the so called DuraPETase, a thermostable variant of the original *I. sakaiensis* PETase.[35]

We specifically examine differences in the enzymatic product release rates of the six enzymes in response to increasing X_C and propose possible explanations for the initial lag phase in the kinetics progress curves of enzymatic PET degradation. We also elucidate differences in the enzymatic surface erosion patterns of the PET substrate in relation to electrostatic and molecular dynamics properties of the enzymes.

Results and Discussion

The influence of the X_C on the enzymatic degradation of semi-crystalline PET was evaluated during prolonged treatment for eight days at 55 °C with the six different benchmark PET-hydrolases; LCC, LCC_{ICCG}, DuraPETase, *Hi*C, *Tf*C, and the newly discovered PHL7 enzyme. For this purpose, assays were conducted on thermally annealed PET disks with X_C values ranging from 10.8 to 24.4% as well as on commercially available PET powder (Ø < 300 μm) having a degree of crystallinity X_C of 37.5%.[28]

The bulk glass transition temperature (T_g) of PET material is about 75 °C, but is known to decrease during prolonged submersion of PET in water,[36] with a typical decrease to 60–65 °C.[22,37] Furthermore, even lower values of T_g, as low as 40 °C in aqueous solution,[30] have been reported for very thin PET films (< 50 nm). This latter phenomenon has been interpreted to mean that the T_g of the surface layer of PET materials may be lower than the bulk T_g.[30,38] Exposure of PET to temperatures above the bulk T_g is generally known to induce crystallization.[39] Yet, the onset temperature of surface crystallization of PET is known to be at 70 °C while bulk crystals are formed at 85 °C.[38] This thermally induced crystallization (above 70 °C) represents a tradeoff for enzymatic hydrolysis process design, as higher operating temperatures can offer higher enzymatic reaction rates provided the enzymes are thermostable, but may at the same time decrease the hydrolysis yields due to a gradual increase in X_C in turn causing increased recalcitrance to enzymatic hydrolysis.[18,22] All reactions were therefore performed at 55 °C to obtain high catalytic turnover rates even though this temperature was not the optimal temperature for all enzymes,[18,31,33,34] but it was chosen to avoid any unwanted crystallization of the substrate during the prolonged incubation.

Product formation during prolonged incubation of PET disks at various degrees of crystallinity

The product formation rate of enzyme catalyzed reactions, subjected to prolonged incubations may be negatively affected by factors such as thermal inactivation[22] or product inhibition of the enzymes.[40] To avoid any influence from these factors, we collected, washed, and transferred each enzymatically treated disk to a new reaction container with fresh enzyme and buffer at each time point, i.e., every 24 h. Hence, the apparent rates, quantified from the linear regions of the progress curves, were considered to predominantly reflect the substrate properties (i.e., the X_C). Three-dimensional progress curves displaying the accumulated product formation as a function of X_C and time for each of the six enzymes are displayed in Figure 1. These curves clearly show that a comparison of end-point measurements might be misleading when evaluating the effect of X_C on the product formation of PET hydrolases. This is because the product formation at a given time, as previously shown,[22] mainly depends on the following factors:

- The duration of the lag phase, i.e. the time it takes before soluble products are detected
- The steady-state rate of the product formation, once the lag phase has been overcome

The influence of the X_C on the six PET hydrolases was therefore quantified with respect to these two phenomena.

As discussed further below, the data obtained revealed profound differences in the catalytic abilities of the six enzymes. A first glance clearly showed that on the low-crystallinity PET disks, the LCC_{ICCG} liberated the highest level of soluble products (measured as BHETeq), followed by PHL7 and DuraPETase, whereas *Hi*C and *Tf*C liberated the lowest amounts of products (Figure 1).

Duration of the lag phase

During the initial enzymatic treatment of thermally induced crystalline PET disks, no detectable product formation was observed. This phenomenon has previously been referred to as a "lag phase".[22,29,42] The enzymatic degradation of PET evidently takes place at a solid-liquid interface, and thus depends on both the enzyme, for example, activity, stability, active site structure, overall molecular flexibility,[18,43] and the physical state of the substrate. Recent work from various research groups has emphasized the significance of the substrate surface area[43] and "plasticization" of the polymer surface layer, respectively, to foster high enzymatic PET-hydrolyzing activity.[30] Yet, the reasons for the increased lag phase in response to increased PET crystallinity remain elusive.

To quantitatively compare the duration of the lag phases for each enzyme, we defined the duration of a lag phase as "The time it took to reach a product formation level

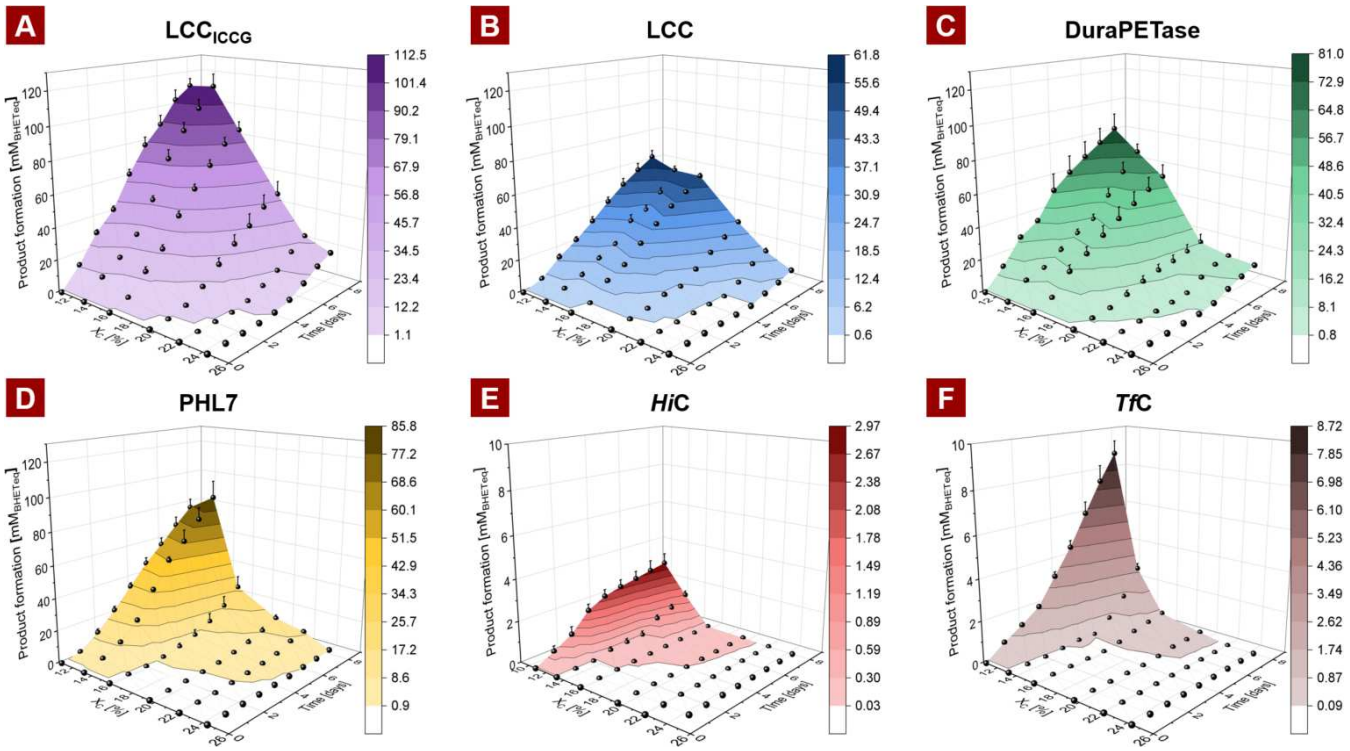

Figure 1. Time course showing the release of soluble hydrolysis products measured in mM levels of BHETeq[41] over eight days, for PET disks (Ø = 6 mm, thickness 1 mm, ~32 mg) with crystallinities ranging from 10.8–24.4%. All reactions were performed at 55 °C with enzyme loads of 200 nM. Every 24 h the activity was measured, where after the PET disk was washed, and transferred into a new reaction mixture in which the enzyme load was replenished with a fresh stock. Error bars represent the standard deviation of experimental runs performed in triplicates.

corresponding to 1% of the maximal product formation obtained during the eight days of enzyme treatment". This threshold value is represented as the border of the white contour in the surface plots displayed in Figure 1 (the standard error on the mean values was generally < 5%, except in a few cases for the low product release data at high crystallinity, where it was ~15%).

The validity of the absorbance measurements, A_{240}, calculated to BHET equivalents, BHETeq, was confirmed by HPLC profiling of the enzymatic product release during extended reaction for each of the six enzymes acting on PET disks of X_C 10.8% (Figure S1 in the Supporting Information). Weight loss of individual PET disks was also monitored for the reactions of the four most active enzymes, LCC$_{ICCG}$, LCC, DuraPETase, and PHL7. Although some differences in the relative product profiles for the different enzymes were evident by HPLC analysis, such as a substantially higher content of di-aromatic products for LCC$_{ICCG}$ (~25% of the total composition), the total A_{240} correlated perfectly linearly with the total level of released products measured by HPLC for all enzymes (Figure S2). Likewise, the products measured by HPLC or A_{240} (BHETeq) correlated linearly with the recorded weight loss (Figure S2).

Interestingly, the data ratio A_{240}/HPLC was higher than 1 (1.55–2.02) (Figure S2) for all enzymes implying that more products were detected by the absorbance measurement A_{240} than by HPLC, indicating that a certain fraction of solubilized compounds escaped the HPLC analysis. On the other hand, the A_{240}/weight loss ratio was slightly below 1 (0.8–0.88) suggesting that certain enzymatically released components were not completely soluble. Nevertheless, the A_{240} measurement in terms of BHETeq satisfactorily described the progression of the product release for all enzymes.

The evolution in the duration of the lag phase as a function of the X_C was similar for LCC, LCC$_{ICCG}$ and DuraPETase (Figure 2). These three enzymes displayed a rapid increase in the duration of the lag phase when X_C increased to 19.6%. In comparison, a profound increase in the lag phase occurred at a much lower value for PHL7, namely at 15.8% X_C, and already at X_C 13.2% for *Hi*C and *Tf*C (Figure 2). These observations clearly confirm that the duration of the lag phase varied profoundly for the different enzymes. The data concur with a recent study from our lab[42] where it was found that *Hi*C and *Tf*C were inferior to LCC by yielding a longer lag phase on nano PET particles.[42]

Steady-state rate of the product formation

Once the lag phase had occurred, the product formation for all reactions maintained a constant rate (Figure 3A–F). These rates are listed in Table 1. The highest rates were obtained for LCC$_{ICCG}$ at all degrees of PET crystallinity (Figure 3G). The rates of LCC, DuraPETase, and PHL7 were lower and almost similar on the most amorphous sample (X_C = 10.8%). This similarity was, however, not observed at higher X_C, as the rate of the PHL7

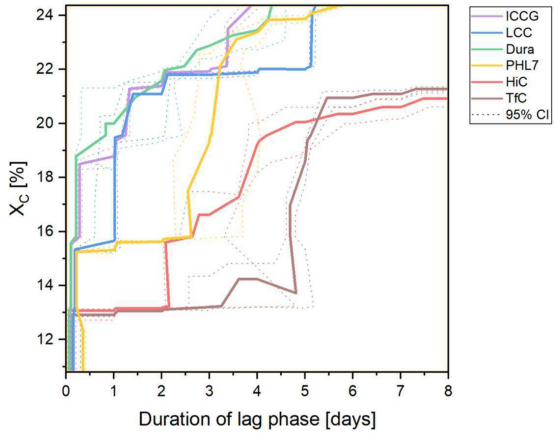

Figure 2. Contour plot representing the substrate X_C as a function of the duration of the lag phase. The graph is composed of the contour plots from Figure 1; lines are shown ± 95% confidence limits (95% CI). The right side of each border represents the threshold at which the product formation corresponded to less than 1% of the maximal value obtained during the eight days of enzymatic treatment. This threshold was defined as the duration of the lag phase. No product formation was observed at $X_C > 19.6\%$ for either *HiC* or *TfC*; the duration of the lag phase displayed above this value may therefore be misleading as it is based on extrapolation. Hence these curves are represented by dashed lines.

became 4- and 5-fold lower than those of LCC or DuraPETase at X_C 24.4%, and 12-fold lower than the product release rate achieved by LCC_{ICCG} at this X_C.

These data reveal that PHL7 is more negatively affected by increased substrate crystallinity than LCC, LCC_{ICCG} and DuraPETase (Table 1). This finding is in agreement with a recent study[44] where it was shown that PHL7 (denoted PES–H1[44]) had several-fold lower activity on highly crystalline PET particle samples ($X_C = 26\%$) than LCC_{ICCG}, despite performing nearly on par with LCC_{ICCG} on amorphous PET film.[44] As evident from Figure 1 and Figure 3, *HiC* and *TfC* generally had substantially lower rates than the other enzymes, corresponding to ~36 and 16-fold lower rates, respectively, than LCC_{ICCG} at 10.8% X_C, and *HiC* and *TfC* did not show any detectable product formation during the eight days of incubation at $X_C > 19.6\%$ (Figure 3E,F).

Tolerance of the enzymes to X_C

The linear regions observed in Figure 3A–F indicate that the concentration of productive enzyme-substrate complexes formed was constant during the duration of the enzymatic treatment. This could be because the number of attackable sites on the PET substrate surface exceeds the saturation level, or because the enzymatic action results in the excavation of new attackable sites as the hydrolysis progresses.[45]

To quantify the influence of substrate crystallinity on kinetic rates, we propose using the term *tolerance* as a comparable measure on how the different enzymes are affected by the increase in substrate crystallinity. Here, the tolerance towards X_C is defined as the relative decrease in product formation rate (in %) as a function of the X_C. These rates, displayed in Figure 3H, were calculated by normalizing the observed rates, shown in Figure 3G, with respect to the rate obtained on the most amorphous sample ($X_C = 10.8\%$). Here it was observed that the normalized rates at intermediate X_C values of 15.5% to 22.1% were highest on LCC followed by LCC_{ICCG}, while DuraPETase and PHL7 had similar activity up until X_C 19.6%. At this point the normalized rate of DuraPETase plateaued while it kept decreasing for PHL7. At the highest X_C (24.4%) the LCC_{ICCG}, LCC, and DuraPETase retained approximately the same relative product formation rates (30–40%) as they had on the most amorphous sample. The rate of PHL7 at 24.4% X_C, however, dropped to 6% (Figure 3H).

The X_C at which the product formation rate had decreased to half of that on the most amorphous sample was quantified by linear interpolation of the tolerance curves (Figure 3H). This parameter was denoted as $X_{C,50}$ and represents a quantitative measure of an enzyme's tolerance to increased X_C. The $X_{C,50}$ values (Figure 3I) corroborated that LCC and LCC_{ICCG} had highest tolerance towards X_C followed by DuraPETase and PHL7, whereas the tolerances of *TfC* and *HiC* were the lowest as their activity dropped to very low levels at X_C above 15% (Table 1).

Change in PET surface topology resulting from the enzymatic treatment

The molecular arrangement of the polymer chains within PET crystals consist of densely packed lamellae structures which are separated by rigid amorphous regions.[46] These crystalline

Table 1. Product formation rate for each of the six PET-hydrolases obtained at each of the six levels of X_C. The values were quantified based on the linear regression of Figure 3A–F.

Enzyme	Product formation rate [$mM_{BHETeq}\,day^{-1}$] at level Xc					
	10.8%	13.2%	15.8%	19.6%	22.1%	24.4%
LCC_{ICCG}	$14.4 \pm 0.54^{[a,b]}$	$15.62 \pm 0.73^{[a]}$	$12.33 \pm 0.43^{[b]}$	$7.9 \pm 0.21^{[c]}$	$6.48 \pm 0.34^{[c,d]}$	$5.35 \pm 0.35^{[d]}$
LCC	$8.35 \pm 0.18^{[a]}$	$7.36 \pm 0.43^{[a,b]}$	$7.88 \pm 0.16^{[a]}$	$6.28 \pm 0.06^{[b]}$	$5.5 \pm 0.51^{[b]}$	$2.69 \pm 0.16^{[c]}$
DuraPETase	$10.9 \pm 0.83^{[a]}$	$8.13 \pm 0.5^{[b]}$	$6.67 \pm 0.12^{[b]}$	$3.12 \pm 0.10^{[c]}$	$3.68 \pm 0.48^{[c]}$	$3.26 \pm 0.10^{[c]}$
PHL7	$10.8 \pm 0.18^{[a]}$	$12.3 \pm 0.5^{[a]}$	$6.97 \pm 0.68^{[b]}$	$3.25 \pm 0.35^{[c]}$	$2.43 \pm 0.27^{[c,d]}$	$0.65 \pm 0.07^{[d]}$
HiC	$0.60 \pm 0.0071^{[a]}$	$0.39 \pm 0.039^{[b]}$	$0.13 \pm 0.002^{[c]}$	$0.009 \pm 0.001^{[c]}$	–	–
TfC	$1.39 \pm 0.025^{[a]}$	$1.07 \pm 0.11^{[b]}$	$0.016 \pm 0.003^{[c]}$	$0.038 \pm 0.007^{[c]}$	–	–

[a]–[d] Indicate statistically significant differences between the data for the individual enzymes ($p < 0.05$), where [a] is significantly higher than [b], which is significantly higher than c etc.

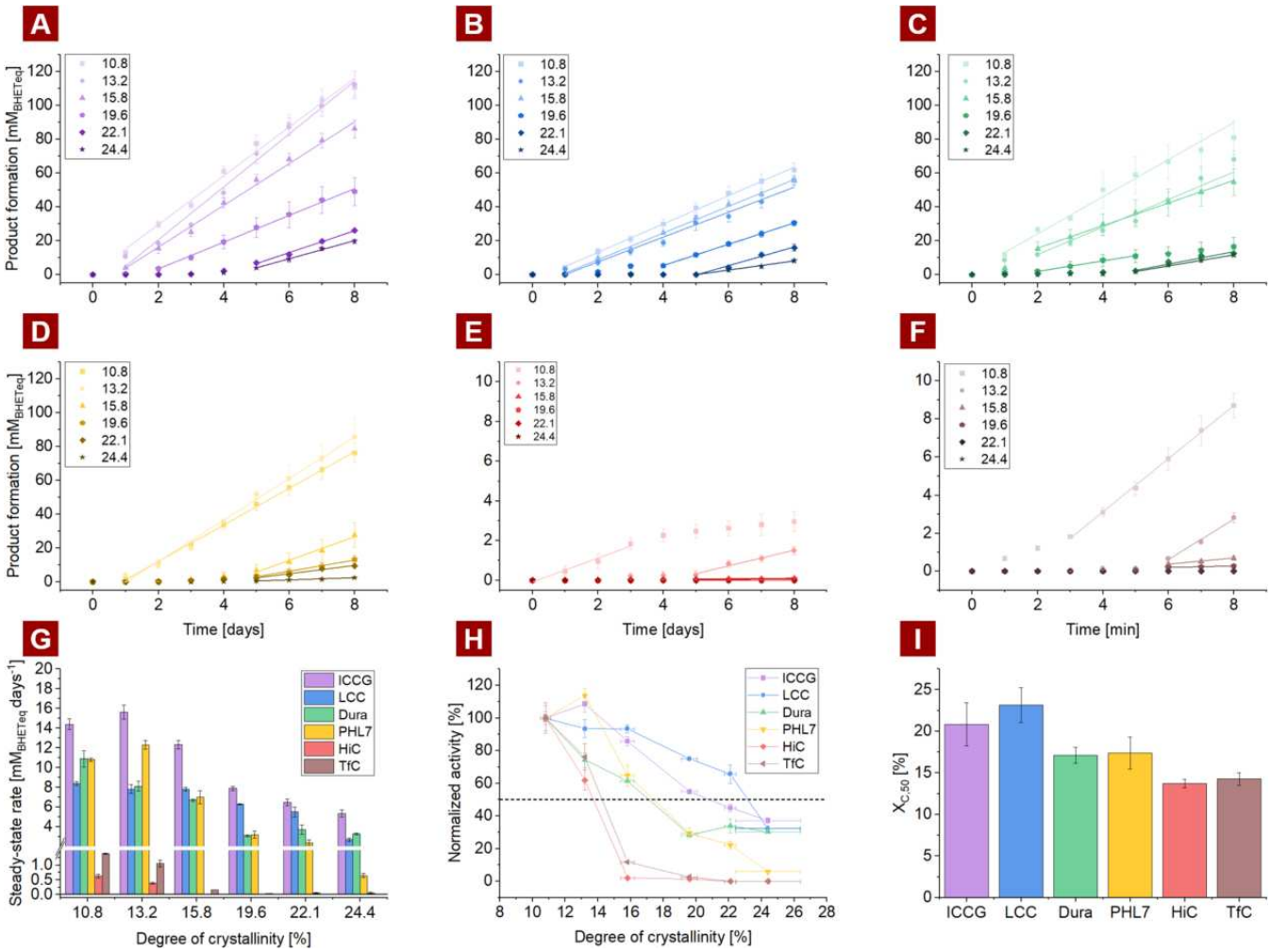

Figure 3. Linear regression of the progress curves (presented in Figure 1) during enzymatic degradation of PET at various degrees of X_C using A) LCC_{ICCG}, B) LCC, C) DuraPETase, D) PHL7, E) *Hi*C and F) *Tf*C. G) Product formation rate at the linear region of the progress curves (A–F) the error bars represent the standard error of the linear regression. H) Tolerance curves displaying the relative product formation rates (derived from the rates in G) as a function of the X_C. The rates at the various X_C samples are normalized with respect to rates measured on the most amorphous sample ($X_C = 10.8\,\%$). The error bars represent the standard error of both the relative rate and the X_C. I) X_C threshold at which normalized activity has been halved ($X_{C,50}$) – these values have been calculated from the tolerance curves in H. the error bars represent the standard error of the $X_{C,50}$.

lamellae are arranged in a higher-level structure, which is dependent on the crystallization process.[47] The backbone of the polymeric chains in both the crystalline lamellae and the rigid amorphous regions (RAF) are associated with *trans* conformations, while the mobile amorphous regions (MAF) surrounding the crystals are considered to adopt *gauche* conformations.[28,48] Hence, the change in surface topography, resulting from the enzymatic treatment, would reflect the selectivity towards these regions, as it is only the degradable fractions which are removed from the insoluble substrate during enzymatic treatment.

The assessment of the duration of the lag phases and the rate responses of the enzymes on the PET samples at various X_C levels clearly demonstrated that PHL7 responded differently than the other enzymes. We therefore decided to evaluate whether these differences manifested via the surface erosion (change in surface topology) caused by the enzymatic treatment.

The surface erosion resulting from the eight days of enzymatic treatment was evaluated using light microscopy (Figure 4) (Due to the very low product formation by *Hi*C and *Tf*C, these enzymes were not included in this assessment). The changes in topology resulting from the individual enzymatic treatments clearly demonstrated that the degradation pattern varied profoundly amongst the enzymes and with increasing X_C. The differences among the enzymes were particularly evident on the more crystalline samples ($X_C > 10.8\,\%$). The samples treated by PHL7 produced a more apparent and heterogeneous surface erosion resulting in formation of crater-like-structures (Figure 4).

The density of these structures furthermore decreased with increased X_C. The PET disk samples treated with DuraPETase, LCC, or LCC_{ICCG}, on the other hand, resulted in less obvious

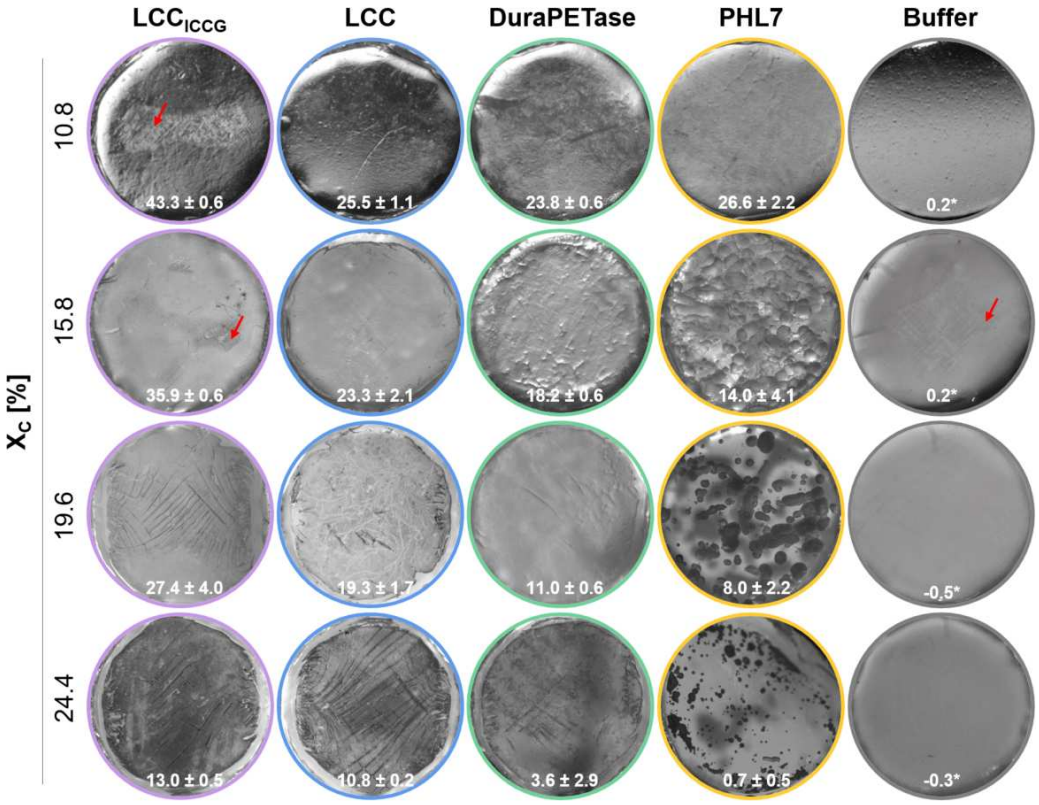

Figure 4. Light microscopy imaging of the PET disks (Ø = 6 mm) after eight days of enzymatic treatment treated with DuraPETase, LCC, LCC$_{ICCG}$, PHL7. Each image represents one whole side of PET disks at various X_C. The weight loss (in %) of the disks after the 8-days of incubation are shown in white font. The red arrows indicate grid-like structures observed both before (15.8% X_C) and after (10.8 and 15.8% X_C) enzyme treatment.

surface erosion, despite their significant PET degrading action. The PET disks at $X_C > 15.8\%$ treated with DuraPETase, LCC, or LCC$_{ICCG}$ however resulted in the exposure of what we assume are crystal structures (Figure 4).

SEM imaging of PET samples treated by LCC$_{ICCG}$ and PHL7

The structural features resulting from the enzymatic degradation were studied in more detail using SEM. As previously reported,[22] the surface of the low crystalline sample treated by LCC$_{ICCG}$ appeared smooth (Figure 5A), while the surfaces of the crystalline samples had more rough and porous structures (Figure 5B,C), similar to those previously observed.[22] However, as a result of the prolonged degradation, more well-defined microstructures appeared on the surfaces of these samples (Figure 5A–C). The appearance of these microstructures adds to our understanding of the porous structures we previously observed,[22] indicating that the solid section of the structures is made up of a mix of hydrolyzable and un-hydrolyzable regions. These findings suggest that the highly ordered structures that emerge after extended treatment are un-hydrolyzable PET crystals that become exposed as the amorphous regions are removed. This interpretation is consistent with mechanistic theories suggested by others.[49,50]

The grid-like structures that were observed resemble 90° branching angle dendritic crystal formations reported in crystalline poly(ethylene oxide) materials.[51]

The degradation of the samples with intermediate X_C (15.8–19.3%) by DuraPETase, LCC and LCC$_{ICCG}$ revealed seaweed shaped crystal structures (data shown for LCC$_{ICCG}$ in Figure 5B). These structures are associated with higher crystallization temperatures than the dendritic crystals with 90° branching angles[51] and are presumed to be associated with surface crystals.[52]

Sheet-like structures were exposed as a result of the enzymatic degradation of the highest X_C disks and are presumed to be due to the prolonged annealing at 115 °C.

Except from the grid-like structure, the surface topology resulting from the enzymatic degradation of the most amorphous samples using LCC$_{ICCG}$ or PHL7 appeared smooth at the resolution obtained by the SEM. A previous study has however shown that enzymatic treatment of amorphous PET film by LCC and PHL7 results in the formation of smaller and less distinct crater structures, covering the entirety of the PET substrate.[29,45,46] Such crater structures were also observed on the thermally annealed PET samples ($X_C > 10.8\%$) treated by PHL7 (Figure 4). However, the size of these craters was bigger than those previously reported on amorphous PET[53]. The magnification by SEM of the craters resulting from the enzymatic treatment with PHL7 revealed that the topology of

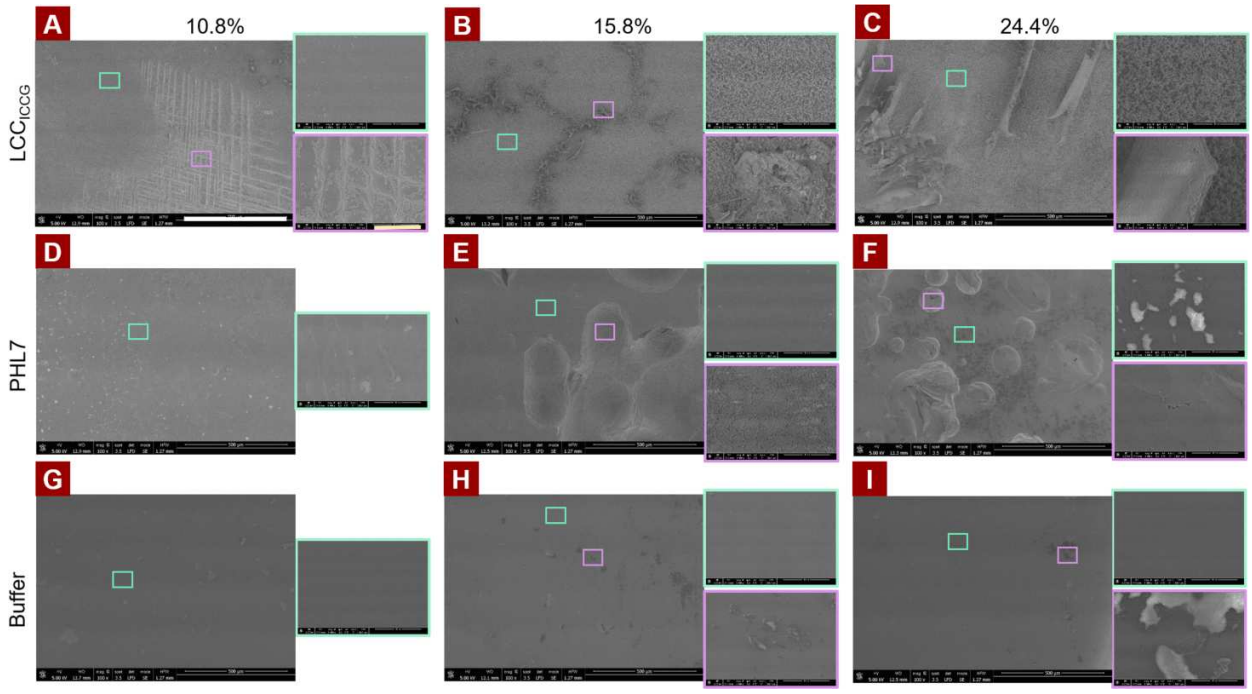

Figure 5. SEM imaging of PET disk at 10.8, 15.8 and 24.4% X_C after eight-days of treatment by either LCC$_{ICCG}$ (A–C), PHL7 (D–F), or in buffer without enzyme (G–I). The images are magnified at either 100× (large images) or 1500× (smaller images) magnification using SEM. The boxes which has been drawn on the 100× images are not the exact location of the 1500× magnification, but represent the features which has been enlarged. The two scale bars in A represents 500 μm (white) or 30 μm (yellow).

the craters varied with the X_C. At intermediate X_C (15.8%) the craters appeared porous, while the surrounding areas were smooth (Figure 5E). Such porous structures were also obtained on the samples having X_C of 15.8% and 24.4% for the DuraPETase, LCC and LCC$_{ICCG}$ (Figure 5B,C; data not shown for LCC and DuraPETase). The pore sizes resulting from the treatment of the PET disks with these enzymes were however larger than those observed for PHL7. The porous structures of the samples treated with the other enzymes were, unlike the ones observed for PHL7, distributed homogeneously throughout the surface, except for the exposed crystal structures mentioned in the previous section.

Structural comparison of the enzymes

To understand the differences between the actions of the different enzymes, it is relevant to compare structures and surface electrostatics of the enzymes. Overall, the structures of the four most active PET-hydrolases, LCC, LCC$_{ICCG}$, DuraPETase, and PHL7, turned out to be quite similar with a maximum RMSD (root mean square deviation) of 0.922 nm between DuraPETase and LCC$_{ICCG}$. (Full RMSD comparison is given in Table S1).

In particular, multiple sequence alignment shows that the active site residues are highly conserved (Figure S3). These similarities are also highly evident from a visual comparison of the active site region (Figure S4), as recently reported elsewhere, as well.[54] DuraPETase is by far the enzyme that differs most from the other enzymes (Table S1 and Figure S4), containing 2 areas of insertion (residues 109–111 and 217–219) and a region of deletion (between residues 35 and 36), all of which modify surface loops to some extent. LCC$_{ICCG}$ and LCC are naturally the most similar differing by only four point mutations.[18]

A notable difference between these four thermostable PET-hydrolases is their respective differences in surface charge (Figure 6). In general, the surfaces of DuraPETase, LCC$_{ICCG}$ and LCC have positive electrostatic potentials across the solvent-excluded surface. The exception being a negative pocket located somewhat adjacent to the active site (Figure 6). In contrast, PHL7 has large pockets of negative electrostatic potential located on the rear side almost directly opposite to the active site (Figure 6).

Proposed course of the enzymatic degradation of semi-crystalline PET material

The enzymatic degradation of PET is an interfacial process occurring at the surface of the PET material. As the surface T_g is presumably lower than the reaction temperature of 55 °C (could be as low as ~40 °C[30]), the PET chains are at their mobile state (MAF), thus allowing them to change between conformations (*gauche* or *trans*). In contrast, when the X_C increases the PET chain mobility is gradually hindered as the proportion of RAF increases.[55] We therefore posit that the higher tolerance to X_C of certain PET hydrolases (i.e., LCC and LCC$_{ICCG}$) are due to their

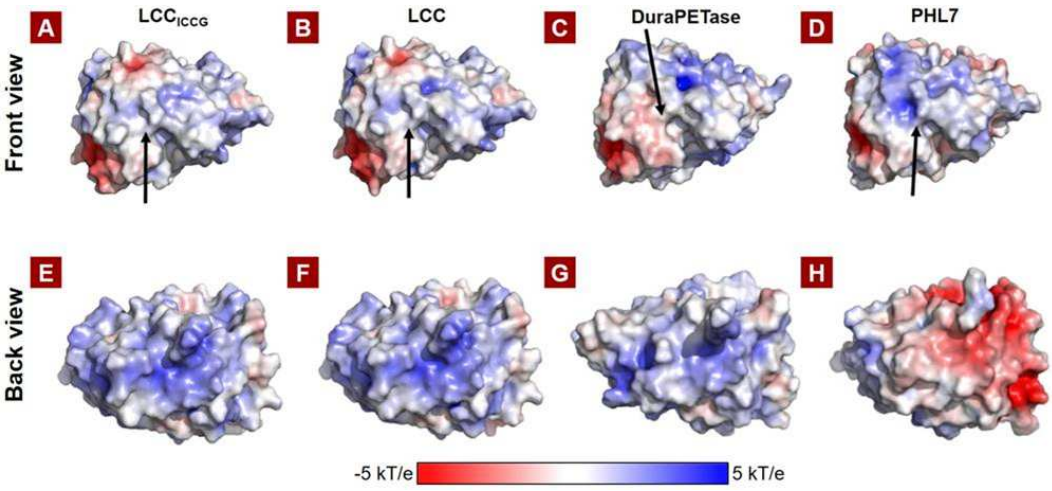

Figure 6. Electrostatic potential of solvent excluded area for four thermostable PET-hydrolases. A and E: DuraPETase; B and F: LCC$_{ICCG}$; C and G: LCC; and D and H: PHL7. Calculated using the APBS plugin in PyMOL. The active site is highlighted with an arrow. The front (A–D) and Back view (E–H) are defined according to the placement of the active site. The scale bar located at the bottom indicates the electrostatic potential of the surface.

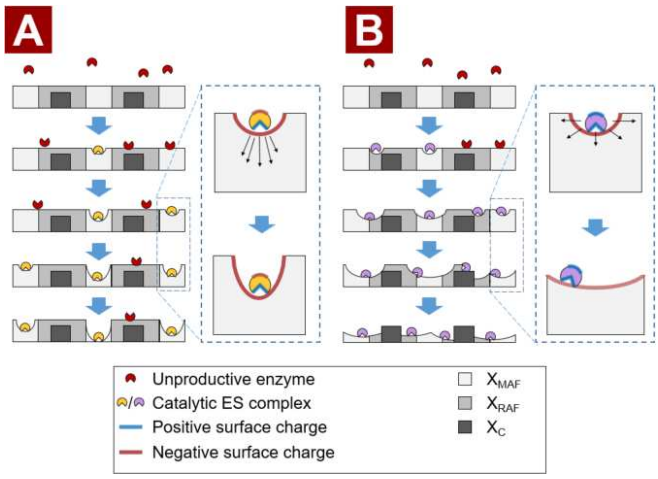

Figure 7. Schematic representation of the proposed degradation mechanism of PHL7 and LCC$_{ICCG}$. A) PHL7 may bind *un*productively (red enzymes) on the entirety of the surface of the substrate. If PHL7 is exposed to MAF regions (light gray) it may form a productive Enzyme-Substrate (ES) complex (yellow enzymes), resulting in degradation of the PET. Once PHL7 is bound in a productive ES complex it is more likely to form a new productive ES complex with an adjacent ester bond (pseudo processivity). PHL7 is only capable of degrading in one direction, as the enzyme is aligned by repulsion forces between the negative charge on the backside of PHL7 and the negative charges of the carboxylic end-groups of the hydrolyzed PET. B) LCC$_{ICCG}$ may bind unproductively (red enzymes) on the entirety of the surface of the substrate. If LCC$_{ICCG}$ is exposed to MAF or RAF regions (light- and dark gray) it may from a productive ES complex (purple enzymes), resulting in degradation of the PET. LCC$_{ICCG}$ is not repelled by the negative charges resulting from the hydrolysis, and is thereby capable of rotating, and thus degrading PET in all directions to result in a more uniform degradation pattern compared to PHL7.

broader conformational selectivity towards the *trans* conformation of the PET chains. This selectivity is governed by the flexibility of the active site, allowing it to facilitate binding to rigid PET chains existing in either a *gauche* or *trans* conformation. This interpretation agrees with the recent findings of Guo et al.[25] Combining the topology analysis results (Figure 4 and 5) with the data in Figure 2 (showing extended lag phases for PHL7), we propose that the duration of the lag phase is primarily determined by the enzyme's conformational selectivity, as a lower density of attackable sites reduces the likelihood of forming a productive enzyme-substrate complex.

Enzymatic degradation of PET using PET hydrolases follow a random/endo-type chain scissoring that does not immediately result in the release of soluble products[30,56] As the average chain length, at the surface, becomes shorter, due to endo-type degradation, the probability of a cleavage, resulting in the direct release of a soluble product, becomes larger. Hence, an increase in the product formation rate is expected during the initial stage of degradation (determined as the lag phase) until a steady-state rate is achieved. The steady state rate is achieved either under saturation of the enzyme (low X_C) or when the number of attackable sites has become saturated (high X_C).

Thus, at low X_C the rate is determined by the enzyme concentration, while at higher X_C the rate is determined by the density of attackable sites at the surface, thus explaining the longer lag phases at higher X_C. We also ascribe the longer lag phases on the more crystalline PET to non-specific adhesion of the enzyme to the PET substrate, which may be more profound on the crystalline regions, as demonstrated recently for a carbohydrate binding module on similar PET disks as those employed in this study.[57]

Hydrolysis of polyester material, including PET, results in a net increase in negative charges at the surface. This is due to the exposure of deprotonated carboxylic acid at the end of the polymeric chains upon bond cleavage.[56] It is therefore likely that the negative pocket located on the back of PHL7 (Figure 6H) could result in a repulsion force between the enzyme and substrate interface. This electrostatic repulsion would prevent PHL7 from swirling near the PET surface and instead retain the enzyme in position to act in an apparent pseudo processive way once an initial bond cleavage has taken place.

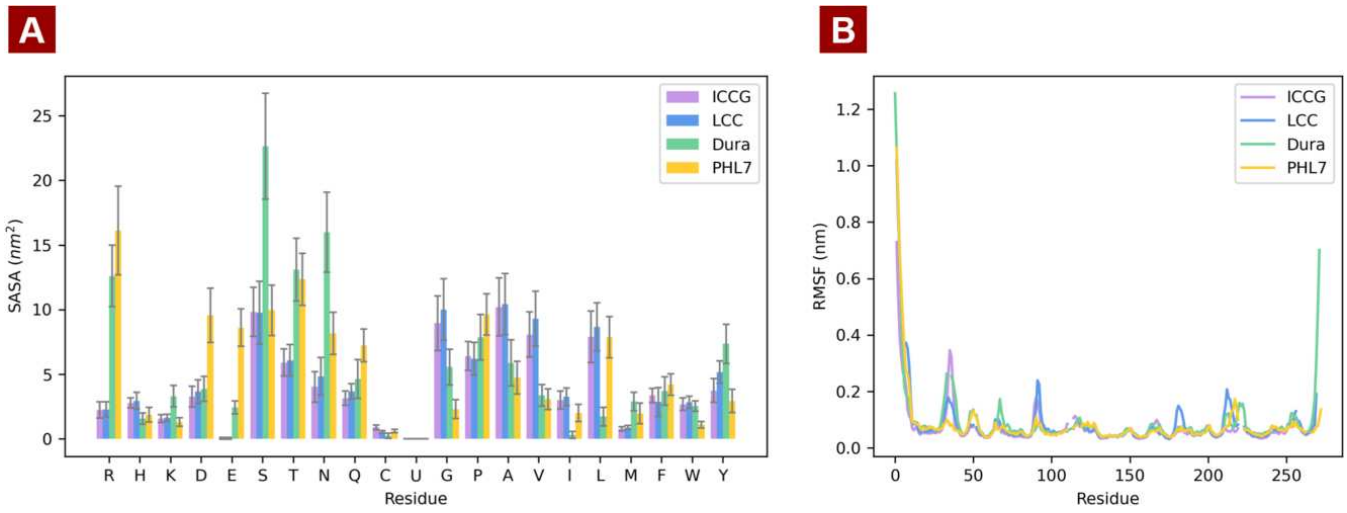

Figure 8. A) Aligned and gaped RMSF for each thermostable PETase during the 100 ns molecular dynamic simulation. B) Aligned and gaped RMSF for each thermostable PETase during the 100 ns molecular dynamic simulation. Note, residue numbering is done from the trimmed sequence (without gaps) as given in the multiple sequence alignment (MSA) (Figure S3). SASA is solvent accessible surface areas.

Hydrolysis of PET using PHL7 is therefore more likely to happen in the same direction, compared to enzymes without a negative pocket on the backside (LCC, $LCC_{ICCG,}$ and DuraPETase) (Figure 6E–G). This mechanism of PHL7 would result in distinct crater structures. A schematic representation of the proposed degradation mechanisms of PHL7 and LCC_{ICCG} is shown in Figure 7.

Degradation of highly crystalline PET particles

The hypothesis that PHL7 has a reduced preference for more *trans*, less mobile RAF conformations that increase with increasing X_C, was investigated further using prolonged enzymatic treatments on extremely crystalline PET particles (Ø < 300 µm, $X_C = 38\,\%$) using DuraPETase, LCC, LCC_{ICCG}, or PHL7 (Figure S5). Here it was observed that PHL7 produced a maximal degradation yield of 2.5 %, which corresponded to about half the yield achieved by DuraPETase and less than half of the yield of LCC and LCC_{ICCG}, respectively (Table 2 and Figure S5).

Table 2. Maximal conversion yields calculated from the concentration of solubilized products (in terms of BHETeq) after 6 days of incubation of highly crystalline PET particles, X_C of 38 %, at 55 °C pH 8.

Enzyme	Maximal yield [%][d]
LCC	6.93[a] ± 0.37
LCC_{ICCG}	5.47[b] ± 0.21
DuraPETase	4.72[b] ± 0.24
PHL7	2.53[c] ± 0.05

[a]–[c] Different superscript letters indicate statistically significant differences between the data for each enzyme ($p < 0.05$); [a] is significantly higher than [b], and [b] is significantly higher than [c]. [d] Maximal yield was calculated based on the product formation measured in terms of BHET equivalents (BHETeq).

The maximal yields obtained for LCC_{ICCG} were, however, significantly lower than what was previously reported (23.5 %[29]). A possible explanation for this discrepancy could be the much lower (16 fold) enzyme to substrate ratio used in the present study (0.2 µM enzyme per 32 g L^{-1} substrate against 1 µM per 10 g L^{-1}). Nevertheless, it was shown that the tolerance to X_C (Figure 3I) correlated to the maximal conversion yield achieved for the different enzymes. The inefficiency of PHL7 on crystalline PET samples exemplifies this correlation and the findings support the proposed hypothesis that PHL7 has less selectivity towards the more crystalline regions exposed on the surface of the annealed samples.

Total solvent accessible surface area and molecular dynamics comparison of the enzymes

To understand the difference in action between the enzymes and notably investigate the cause of the difference in electrostatic potential, the solvent accessible surface area (SASA) of each residue of each enzyme structure across the 100 ns stable molecular dynamic simulation was assessed. The average and std error of each residue for the 100 ns simulation was then binned and added dependent on residue type.

This analysis showed that PHL7 has a larger number than the other enzymes of charged (arginine R, aspartic acid D and glutamic acid E) residues which are solvent accessible (Figure 8A). DuraPETase also has a larger number of arginine R residues which are solvent accessible, as well as a significantly larger number of solvent-accesible serine S moieties than the other enzymes (Figure 8A).

As part of the comparison between these four enzymes, a molecular dynamic simulation was also conducted with the results shown in Figure S6. All four PET-hydrolases were generally stable throughout the simulation with an RMSD of

less than 0.5 nm. Manual inspection of any major changes in RMSD were found to be movement of the N or C termini and not significant movement in the overall structure.

During this 100 ns time period, the RMSF (root mean square fluctuation) of each residue was assessed in a way that the aligned residues between each structure could be compared. The results are shown in Figure 8B.

All four structures show increased flexibility in approximately the same locations (namely residues 30–40 and 89–92), though the effect is less for PHL7, possibly due to hydrogen bonding interactions between the bulkier glutamine at residue 33 (34) vs serine in LCC_{ICCG} and LCC (Figure S3).

Both the DuraPETase and PHL7 have increased flexibility at residue 50, which is a distance away from the active site,[44] due to the insertion of a glutamine for PHL7 and as a result of the double glycine for DuraPETase.

LCC_{ICCG} has decreased flexibility at both 179–184 and 210–225 when compared to LCC (Figure 8B), which is likely a direct consequence of the D/C and F/I mutations from LCC to LCC_{ICCG}. The structural comparison highlighting the added disulfide bond is shown in Figure S7.

LCC_{ICCG} is a quadruple variant of LCC engineered towards increased activity (F243I) and stability (D238C/S283C and Y127G). The selection criteria for increased activity was based on its specific activity on PET substrate at a crystallinity of 10.3 %.[18]

It is interesting to note that the present tolerance assessment (Figure 3I) disclosed that the four mutations differentiating LCC_{ICCG} from LCC did have a profound effect on the response of the LCC enzyme to increased crystallinity, despite its decreased flexibility, i.e., higher structural rigidity.

Conclusions

By evaluating the influence of X_C on the enzymatic degradation by six PET-hydrolases, it was shown that increasing levels of X_C resulted in increasing duration of the lag phase and decreasing steady-state product formation rates for all enzymes once the lag phase had been overcome. The impact of these effects was highly enzyme dependent. PHL7 was more negatively affected by increased X_C than DuraPETase, LCC and LCC_{ICCG}. It was also shown that PHL7 catalyzed degradation of thermally annealed PET disks produced crater like structures on the PET surface, while the other enzymes left behind a smooth PET surface. The longer lag phases and lower tolerance to X_C are suggested caused by a lower selectivity of PHL7 towards crystalline regions of PET but could not be fully explained by the higher negative surface charge or differences in enzyme flexibility by molecular dynamics analysis. However, it can be concluded, that in addition to the importance of the enzyme surface charge (Figure 7), the conformational selectivity of the enzymes with higher tolerance to X_C is due to additional enzyme properties, namely: (1) How well the enzyme can bind to the chains, (2) how fast the active site conformation dynamics allow such binding to form a productive enzyme-substrate complex, and (3) the degree of non-productive binding.

The interplay between the catalytic site topology, overall enzyme dynamics, and surface electrostatics for maximizing performance of PET degrading enzymes is currently under investigation. One of the goals is to understand how to design the optimal PET-hydrolase. The LCC_{ICCG} has been engineered to have improved catalytic activity and stability via only two mutations in the active site of the wild-type LCC enzyme (F243I and Y127G) maximizing enzyme-substrate contact. In addition, the thermostability was improved by replacing a divalent metal-binding site in the LCC with a disulfide bridge quite near the active site (D238C and S283C).[15] Although a fast and thermostable enzyme has been obtained, it is not yet completely clear how to design the perfect PET-hydrolase as several factors have significance. Indeed, it is not understood why the LCC and the LCC_{ICCG} have high tolerance to increased X_C, or why the LCC_{ICCG} exhibits high tolerance despite having lower overall flexibility compared to the wild type LCC (Figure 8).

It is tempting to speculate whether the products released may affect the reaction behavior of the different enzymes. Any negative effects of the solubilized products would be higher with higher release rates and therefore not explain the lower enzymatic rates with increased X_C, and the rate data obtained in the present study do not imply any positive, accelerating effects either. From the data obtained, the seemingly uniform attack on the PET disk surface by LCC_{ICCG}, which resulted in a smooth surface, appears to be a result of enzymatic action brought on by even movement of the enzymes across the surface of the PET disk. LCC, DuraPETase and PHL7 had almost similar activities on the amorphous PET, with LCC tending to be lowest, and had nearly identical soluble product profiles, yet differed in terms of tolerance to X_C. The surface electrostatics did not reveal any notable features for LCC_{ICCG} vs. LCC or DuraPETase. Considering the surface electrostatics (Figure 6), the catalytic action of LCC_{ICCG} likely involves fast, consistent movement, including swirling of the enzyme upon detachment from the substrate before the next attack. In contrast, based on the surface electrostatics analysis, we suggest that the peculiar formation of craters by the PHL7 action is directly related to the negative (backside) surface charge of PHL7 found by surface electrostatics and solvent accessible surface area analysis of charged residues, which may clinch the enzyme in position to act in a pseudo processive manner once the initial bond cleavage has taken place.

Classic post-consumer plastic (polyester) degradation and recycling methods include mechanical and chemical recycling.[58,59] For PET, mechanical recycling involves washing and shredding of the material, and then regranulation via extrusion.[59] The traditional mechanical recycling method of extrusion significantly reduces the tensile strength of PET. Thus, during the initial mechanical recycle, elongation at break is reduced by a factor of 4, and tensile strength and elongation at break are reduced further with each round of recycling.[59] Recent processes involve open-loop recycling via manufacture of textile fibers or blending of the material into mixed construction materials such as concrete.[58] For "virgin" PET fibers, of relevance for PET textiles recycling, a hybrid chemo-

enzymatic treatment involving pressurized, hot zinc acetate pre-treatment under high pressure (at 250 °C, 40 bar) followed by *Hi*C treatment the polymer was reported to yield 97% pure terephthalic acid (TPA).[60] However, the energy costs of the pretreatment were obviously significant, but not calculated. Even if the material has been properly sorted, for example, as is gradually becoming the case for used PET bottles with a recycling rate of nearly 60%,[58] the recycling rate of 60% means that the rest, i.e., approximately 40%, currently ends up in landfills or as waste spread elsewhere, emphasizing the need for better recycling approaches.

The industrial implementation of PET degrading enzymes is now a reality led by the French company Carbios. In addition to protein engineering of enzymes to improve the performance, as exemplified by the development of the LCC_{ICCG},[15] other innovative approaches to improve catalytic efficiency of PET degrading enzymes on PET of high crystallinity are gradually emerging. These include, for example, extrusion based pretreatment of PET to decrease X_C[48] and, for example, design of whole-cell surface display PET-hydrolase systems.[49] The low activity of PET-hydrolases towards crystalline PET regions nevertheless remains a bottleneck in terms of industrial application, and a better understanding of the structural and dynamic aspects in relation to the function, attack mode, lag phase, and kinetic rates of the enzymes on PET of high crystallinity is the key to develop better enzyme-assisted PET recycling processes.

Systematic examination of enzyme performance, including lag phase duration, in response to X_C, and the new quantitative tolerance assessment of enzymes to X_C are valuable characterization metrics to identify and engineer enzymes that are efficient on highly crystalline PET.

Experimental Section

Enzymes

The six PET-hydrolases studied in this work for the enzymatic degradation of PET were LCC_{ICCG} [Genbank: AEV21261.1] F243I/D238C/S283C/Y127G), PHL7 [Genbank: AEV21261.1], *Hi*C [Genbank: AAE13316.1], LCC [Genbank: AAE13316.1], DuraPETase [Genbank: GAP38373.1] and *Tf*C [Genbank: AAZ54921.1]. The LCC_{ICCG}, *Tf*C, and *Hi*C were expressed and purified as previously described.[22,61,62] The DuraPETase and PHL7 were both heterologously expressed in *Bacillus subtilis*, as described previously[63] with the following modifications: The native signal peptide was replaced by the signal peptide from *B. licheniformis* α-amylase AmyL (FJ556804.1), and a histidine tag with a short linker (LEHHHHHH) was added to the C-terminal. Enzyme concentrations were determined by absorbance at 280 nm using theoretical extinction coefficients.

PET substrates

Amorphous PET sheets with a thickness of 1 mm (Goodfellow Cambridge Ltd, Huntingdon, UK) (Cat. No. ES303010) were used as the starting material. PET disks were prepared by punching the PET sheet with a generic whole punch generating uniform PET disks with a dimension of; Ø = 6 mm, ~32 mg. The X_C of the PET disks were systematically modified in the range from 10.8–24.4% by annealing at 115 °C using a dry heat treatment method as described previously.[28] PET disks with the lowest X_C of 10.8% were briefly annealed at 85 °C for 5 min, to eliminate any enthalpy relaxation caused by physical ageing of the polymer.

Semi-crystalline PET with a X_C of 37.5%[28] and with a particle size < 300 μm (reported by the supplier) was purchased from Goodfellow Cambridge Ltd (Cat. No. ES306030). The PET-powder was suspended in the reaction buffer prior to assaying.

Differential scanning calorimetry

The X_C of the PET-disks were determined by differential scanning calorimetry (DSC) analysis. Measurements were performed using on a Pyris 1 Calorimeter (Perkin Elmer, Waltham, MA, USA). The procedure involved a constant heating rate of 10 °C min^{-1} using PET samples weighing 8.5 ± 0.5 mg. The initial temperature was set to 20 °C and was steadily increased to 270 °C. Measurements of X_C were determined as described previously.[28]

Standard conditions for enzymatic hydrolysis

200 nM enzyme was suspended in a 500 mM glycine NaOH buffer, for a total reaction volume of 1 mL in Protein LoBind tubes (Eppendorf). The reactions were initiated by addition of PET samples and kept at 55 °C and 950 rpm in an incubator shaker (KS 4000 ic control, IKA). Samples were withdrawn at selected times and the supernatant was immediately transferred to a UV-transparent microplate (Corning Inc., Corning, New York, USA) (Cat. No. 3635)) for spectrophotometric analysis using a plate-reader (Molecular Devices, SpectraMax Paradigm). All experimental runs were conducted in triplicates.

Reaction Progress for PET-film

All reactions were initiated by transferring a PET disk to the reaction mixture. Every 24 h, supernatant was withdrawn and diluted appropriately to a final volume of 200 μL for spectrophotometric analysis. Afterwards, the enzymatically treated PET disk was washed using a 1% SDS (sodium dodecyl sulfate)- and 70% ethanol solution. This sequence of events was repeated in iterations over eight days with the result that the PET disks were subjected to a fresh enzyme load and reaction mixture every 24 h.

After termination of the experiment the treated disks were collected and subjected to gravimetric determination of weight loss. Of notice, PET disks were handled cautiously to preserve the integrity of the surface structure of the substrate sample.

Reaction Progress for PET particles

Enzymatic hydrolysis of semi-crystalline powder PET was carried out at a PET concentration of 32 mg mL^{-1}. Every 24 h, the reaction mixture was centrifuged for 1 min at 1000 rpm, and 10 μL of the supernatant was then transferred to a total volume of 200 μL of the reaction buffer as preparation for spectrophotometric analysis. This procedure was repeated over 6 days.

Enzymatic product release

Absorbance of withdrawn supernatant samples from enzymatic reactions was measured at 240 nm. The release of hydrolytic products was quantified against standard curve of bis(hydroxyethyl terephthalate) (BHET), and the products were calculated as BHET equivalents (BHETeq) exploiting the fact that mono-aromatic products have been reported to exhibit practically comparable

extinction coefficients, as described previously.[41] The product profile resulting from the enzymatic treatment of the "amorphous" X_C disks ($X_C = 10.8\%$) was moreover characterized by analyzing the product profiles in supernatants at each time point by reverse phase High Performance Liquid Chromatography (HPLC) as follows: At each time point, the particular sample was quenched with HCl (1 M) and briefly vortexed to obtain a homogeneous suspension of the precipitate resulting from the lowering of the pH. Each sample (2 μL) was then immediately transferred to a HPLC vial, diluted 100-fold, and injected for analysis on a Vanquish Flex UHPLC system equipped with a (250 mm × 4.6 mm) C18 column and a UV/Vis variable wavelength detector (Thermo Scientific, Waltham, MA, USA). Samples (10 μL) were eluted at a flow rate of 1 mL min^{-1} at 40 °C from a ratio of 1:5 of Eluent A (acetonitrile) and Eluent B (7.5 mM formic acid in 5% *v/v* acetonitrile) for 7.5 min, then, the amount of Eluent B was gradually increased until a 1:1 ratio was reached after 12.5 min, and this ratio was then kept for 5 min. The flow rate and peak analyses were controlled using the Chromeleon Chromatography studio software (version 7.3.1) (Thermo Scientific, Waltham, MA, USA). The samples were quantified against authentic standards of terephthalic acid (TPA), mono(hydroxyethyl terephthalate) (MHET), BHET, and a di-aromatic compound consisting of two ethylene glycol (EG) and two TPA moieties (TETE). TPA and BHET were purchased from Sigma-Aldrich, while MHET and TETE were synthesized in house as described previously.[42]

Light microscopy

Analysis of the enzymatic footprint imprinted on the surface of PET disks were evaluated after eight days of enzymatic treatment as described above, by high-quality images enlarged 125× using a Leica M205 C microscope (Leica Microsystems, Germany).

Scanning electron microscopy

The surface features exposed by the enzyme treatment were investigated using Scanning electron microcopy using the procedure described previously.[28] The imaging was performed in low vacuum at an acceleration voltage of 5 kV using a large-field detector (LTD).

Structural comparison

The sequence of the four most active PET-hydrolases (LCC, LCC_{ICCG}, PHL7, DuraPETase) was trimmed to remove signal peptides (SignalP, 6.0)[64] and HIS tags. The structure of each sequence was then modeled using Alphafold (v2.1.0) with MSA generation against the reduced database.[65] The relaxed structure with the highest plDTT score was selected for further analysis (DuraPETase: 94.93, LCC_{ICCG}: 93.32, LCC: 93.21, PHL7: 96.62) and where applicable, checked against available structures from the PDB (*Is*PETase: 6ANE, LCC: 4EB0, PHL7: 7NEI). The four structures were assessed in PyMOL Molecular Graphics System, Version 2.0 Schrödinger, LLC (New York, NY, USA) with a MSA of all four (Clustal Omega 1.2.4)[66] used to highlight regions of difference between structures. Additionally, electrostatics potential molecular surface was calculated using the Adaptive Poisson-Boltzmann Solver (APBS) plugin of PyMOL.[67]

Molecular dynamics

The four PET-hydrolases were run in an MD simulation using GROMACS (v 2022.2)[68] using the Charmm36-jul2021 FF and TIP3P_CHARMM water.[69] The systems were neutralized with Na^+ or Cl^- where applicable and minimized with 50000 steps via steepest descent minimization. Afterward, a 100 ps NVT equilibration (300 K), followed by a 100 ps NPT equilibration (300 K, 1.0 bar) were performed. All systems were run in 100 ns blocks of production MD simulation until a 100 ns time course of relatively stable root-mean-square deviations (RMSD) was observed. This 100 ns stable region was used for analysis of root-mean-square fluctuations (RMSFs) and solvent accessible surface areas (SASA).

Acknowledgements

This work was supported by the Novo Nordisk Foundation Grant NNFSA170028392, the Innovation Fund Denmark (0224-00033), the Villum Foundation (Project no. 40815), and DTU Bioengineering, Technical University of Denmark, Denmark.

Conflict of Interests

The authors declare no conflict of interest.

Data Availability Statement

The data that support the findings of this study are available from the corresponding author upon reasonable request.

Keywords: PET crystallinity · PET-hydrolase · PET surface erosion · enzyme surface electrostatics · molecular dynamics

[1] Plastics Europe, *Plastics – the Facts 2022* **2022**, https://plasticseurope.org/knowledge-hub/plastics-the-facts-2022/.
[2] R. Geyer, J. R. Jambeck, K. L. Law, *Sci. Adv.* **2017**, *3*, e170078.
[3] World Economic Forum Ellen MacArthur Foundation McKinsey & Company, *The New Plastics Economy: Rethinking the Future of Plastics* **2016**.
[4] P. C. F. Buchholz, G. Feuerriegel, H. Zhang, P. Perez-Garcia, L.-L. Nover, J. Chow, W. R. Streit, J. Pleiss, *Proteins Struct. Funct. Bioinf.* **2022**, *90*, 1443–1456.
[5] S. Yoshida, K. Hiraga, T. Takehana, I. Taniguchi, H. Yamaji, Y. Maeda, K. Toyohara, K. Miyamoto, Y. Kimura, K. Oda, *Science* **2016**, *351*, 1196–1199.
[6] IUBMB **2023**, https://iubmb.qmul.ac.uk/.
[7] F. Kawai, T. Kawabata, M. Oda, *ACS Sustainable Chem. Eng.* **2020**, *8*, 8894–8908.
[8] R. Wei, G. Von Haugwitz, L. Pfaff, J. Mican, C. P. S. Badenhorst, W. Liu, G. Weber, H. P. Austin, D. Bednar, J. Damborsky, U. T. Bornscheuer, *ACS Catal.* **2022**, *12*, 3382–3396.
[9] F. Kawai, *Catalysts* **2021**, *11*, 1–10.
[10] R. Wei, W. Zimmermann, *Microb. Biotechnol.* **2017**, *10*, 1302–1307.
[11] C. C. Chen, X. Han, X. Li, P. Jiang, D. Niu, L. Ma, W. Liu, S. Li, Y. Qu, H. Hu, J. Min, Y. Yang, L. Zhang, W. Zeng, J. W. Huang, L. Dai, R. T. Guo, *Nat. Catal.* **2021**, *4*, 425–430.
[12] A. K. Urbanek, A. M. Mirończuk, A. García-Martín, A. Saborido, I. de la Mata, M. Arroyo, *Biochim. Biophys. Acta Proteins Proteomics* **2020**, *1868*, 140315.
[13] H. P. Austin, M. D. Allen, B. S. Donohoe, N. A. Rorrer, F. L. Kearns, R. L. Silveira, B. C. Pollard, G. Dominick, R. Duman, K. El Omari, V. Mykhaylyk, A. Wagner, W. E. Michener, A. Amore, M. S. Skaf, M. F. Crowley, A. W. Thorne, C. W. Johnson, H. Lee Woodcock, J. E. McGeehan, G. T. Beckham, *Proc. Natl. Acad. Sci. USA* **2018**, *115*, E4350–E4357.
[14] T. Fecker, P. Galaz-Davison, F. Engelberger, Y. Narui, M. Sotomayor, L. P. Parra, C. A. Ramírez-Sarmiento, *Biophys. J.* **2018**, *114*, 1302–1312.

[15] S. Joo, I. J. Cho, H. Seo, H. F. Son, H. Y. Sagong, T. J. Shin, S. Y. Choi, S. Y. Lee, K. J. Kim, *Nat. Commun.* **2018**, *9*, 382.
[16] S. Brott, L. Pfaff, J. Schuricht, J. N. Schwarz, D. Böttcher, C. P. S. Badenhorst, R. Wei, U. T. Bornscheuer, *Eng. Life Sci.* **2022**, *22*, 192–203.
[17] H. Lu, D. J. Diaz, N. J. Czarnecki, C. Zhu, W. Kim, R. Shroff, D. J. Acosta, B. R. Alexander, H. O. Cole, Y. Zhang, N. A. Lynd, A. D. Ellington, H. S. Alper, *Nature* **2022**, *604*, 662–667.
[18] V. Tournier, C. M. Topham, A. Gilles, B. David, C. Folgoas, E. Moya-Leclair, E. Kamionka, M. L. Desrousseaux, H. Texier, S. Gavalda, M. Cot, E. Guémard, M. Dalibey, J. Nomme, G. Cioci, S. Barbe, M. Chateau, I. André, S. Duquesne, A. Marty, *Nature* **2020**, *580*, 216–219.
[19] H. F. Son, I. J. Cho, S. Joo, H. Seo, H. Y. Sagong, S. Y. Choi, S. Y. Lee, K. J. Kim, *ACS Catal.* **2019**, *9*, 3519–3526.
[20] Y. Ma, M. Yao, B. Li, M. Ding, B. He, S. Chen, X. Zhou, Y. Yuan, *Engineering* **2018**, *4*, 888–893.
[21] A. Mrigwani, M. Pitaliya, H. Kaur, B. Kasilingam, B. Thakur, P. Guptasarma, *Biotechnol. Bioeng.* **2022**, *9*, 674–686.
[22] T. B. Thomsen, C. J. Hunt, A. S. Meyer, *New Biotechnol.* **2022**, *69*, 28–35.
[23] E. Erickson, T. J. Shakespeare, F. Bratti, B. L. Buss, R. Graham, M. A. Hawkins, G. König, W. E. Michener, J. Miscall, K. J. Ramirez, N. A. Rorrer, M. Zahn, A. R. Pickford, J. E. McGeehan, G. T. Beckham, *ChemSusChem* **2022**, *15*, e202101932.
[24] R. Wei, D. Breite, C. Song, D. Gräsing, T. Ploss, P. Hille, R. Schwerdtfeger, J. Matysik, A. Schulze, W. Zimmermann, *Adv. Sci.* **2019**, *6*, 1900491.
[25] B. Guo, S. R. Vanga, X. Lopez-Lorenzo, P. Saenz-Mendez, S. R. Ericsson, Y. Fang, X. Ye, K. Schriever, E. Bäckström, A. Biundo, R. A. Zubarev, I. Furó, M. Hakkarainen, P. O. Syrén, *ACS Catal.* **2022**, *12*, 3397–3409.
[26] I. Karacan, *Fibers Polym.* **2005**, *6*, 186–199.
[27] X. Guo, J. Wang, *Mar. Pollut. Bull.* **2019**, *142*, 1–14.
[28] T. B. Thomsen, C. J. Hunt, A. S. Meyer, *MethodsX* **2022**, *9*, 101815.
[29] R. K. Brizendine, E. Erickson, S. J. Haugen, K. J. Ramirez, J. Miscall, A. R. Pickford, M. J. Sobkowicz, J. E. Mcgeehan, G. T. Beckham, *ACS Sustainable Chem. Eng.* **2022**, *10*, 9131–9149.
[30] N. A. Tarazona, R. Wei, S. Brott, L. Pfaff, U. T. Bornscheuer, A. Lendlein, R. Machatschek, *Chem Catal.* **2022**, *2*, 3573–3589.
[31] S. Sulaiman, S. Yamato, E. Kanaya, J. J. Kim, Y. Koga, K. Takano, S. Kanaya, *Appl. Environ. Microbiol.* **2012**, *78*, 1556–1562.
[32] S. Chen, X. Tong, R. W. Woodard, G. Du, J. Wu, J. Chen, *J. Biol. Chem.* **2008**, *283*, 25854–25862.
[33] Å. M. Ronkvist, W. Xie, W. Lu, R. A. Gross, *Macromolecules* **2009**, *42*, 5128–5138.
[34] C. Sonnendecker, J. Oeser, P. K. Richter, P. Hille, Z. Zhao, C. Fischer, H. Lippold, P. Blázquez-Sánchez, F. Engelberger, C. A. Ramírez-Sarmiento, T. Oeser, Y. Lihanova, R. Frank, H. G. Jahnke, S. Billig, B. Abel, N. Sträter, J. Matysik, W. Zimmermann, *ChemSusChem* **2022**, *15*, e202101062.
[35] Y. Cui, Y. Chen, X. Liu, S. Dong, Y. Tian, Y. Qiao, R. Mitra, J. Han, C. Li, X. Han, W. Liu, Q. Chen, W. Wei, X. Wang, W. Du, S. Tang, H. Xiang, H. Liu, Y. Liang, K. N. Houk, B. Wu, *ACS Catal.* **2021**, *11*, 1340–1350.
[36] H. Levine, J. Grenet, L. Slade, *Eur. Polym. J.* **1993**, *30*, 339–345.
[37] M. Oda, Y. Yamagami, S. Inaba, T. Oida, M. Yamamoto, S. Kitajima, F. Kawai, *Appl. Microbiol. Biotechnol.* **2018**, *102*, 10067–10077.
[38] K. Shinotsuka, V. N. Bliznyuk, H. E. Assender, *Polymer* **2012**, *53*, 5554–5559.
[39] J. P. Jog, *J. Macromol. Sci. Part C* **1995**, *35*, 531–553.
[40] M. Barth, T. Oeser, R. Wei, J. Then, J. Schmidt, W. Zimmermann, *Biochem. Eng. J.* **2015**, *93*, 222–228.
[41] J. Arnling Bååth, K. Borch, P. Westh, *Anal. Biochem.* **2020**, *607*, 113873.
[42] S. W. Schubert, K. Schaller, J. A. Bååth, C. Hunt, K. Borch, K. Jensen, J. Brask, P. Westh, S. Schubert, *ChemBioChem* **2022**, *24*, e202200516.
[43] L. Avilan, B. R. Lichtenstein, G. König, M. Zahn, M. D. Allen, L. Oliveira, M. Clark, V. Bemmer, R. Graham, J. E. Mcgeehan, A. R. Pickford, *ChemSusChem* **2023**, *16*, e202202277.
[44] L. Pfaff, J. Gao, Z. Li, A. Jäckering, G. Weber, J. Mican, Y. Chen, W. Dong, X. Han, C. G. Feiler, Y. F. Ao, C. P. S. Badenhorst, D. Bednar, G. J. Palm, M. Lammers, J. Damborsky, B. Strodel, W. Liu, U. T. Bornscheuer, R. Wei, *ACS Catal.* **2022**, *12*, 9790–9800.
[45] M. Andersen, J. Kari, K. Borch, P. Westh, *Math. Biosci.* **2018**, *296*, 93–97.
[46] W. Hu, L. Zha, *Controlling the morphology of polymers: Multiple scales of structure and processing*, Springer International Publishing **2016**, pp. 101–143.
[47] Z. Bartczak, *Polimery* **2017**, *62*, 787–799.
[48] P. G. Karagiannidis, A. C. Stergiou, G. P. Karayannidis, *Eur. Polym. J.* **2008**, *44*, 1475–1486.
[49] C. M. Carr, D. J. Clarke, A. D. W. Dobson, *Front. Microbiol.* **2020**, *11*, 2825.
[50] F. Kawai, T. Kawabata, M. Oda, *Appl. Microbiol. Biotechnol.* **2019**, *103*, 4253–4268.
[51] G. Zhang, X. Zhai, Z. Ma, L. Jin, P. Zheng, W. Wang, S. Z. D. Cheng, B. Lotz, *ACS Macro Lett.* **2012**, *1*, 217–221.
[52] K. Shinotsuka, H. Assender, *J. Appl. Polym. Sci.* **2016**, *133*, 44269.
[53] R. Frank, D. Krinke, C. Sonnendecker, W. Zimmermann, H. G. Jahnke, *ACS Catal.* **2022**, *12*, 25–35.
[54] P. K. Richter, P. Blázquez-sánchez, Z. Zhao, F. Engelberger, C. Wiebeler, G. Künze, R. Frank, D. Krinke, E. Frezzotti, Y. Lihanova, P. Falkenstein, J. Matysik, W. Zimmermann, N. Sträter, C. Sonnendecker, *Nat. Commun.* **2023**, *14*, 1–11.
[55] H. Chen, Z. Liu, P. Cebe, *Polymer* **2009**, *50*, 872–880.
[56] A. Eberl, S. Heumann, T. Brückner, R. Araujo, A. Cavaco-Paulo, F. Kaufmann, W. Kroutil, G. M. Guebitz, *J. Biotechnol.* **2009**, *143*, 207–212.
[57] A. P. Rennison, P. Westh, M. S. Møller, *Sci. Total Environ.* **2023**, *870*, 3–9.
[58] K. Ragaert, L. Delva, K. Van Geem, *Waste Manage.* **2017**, *69*, 24–58.
[59] Z. O. G. Schyns, M. P. Shaver, *Macromol. Rapid Commun.* **2021**, *42*, 2000415.
[60] F. Quartinello, S. Vajnhandl, V. Valh, T. J. Farmer, A. Lobnik, E. Herrero, *Microb. Biotechnol.* **2017**, *10*, 1376–1383.
[61] C. Adams, B. Schmidt, *Detergent compositions containing Thermobifida fusca lipase and methods of use thereof* **2011**, WO2011/084412 A1.
[62] T. Sandal, S. Kauppinen, L. V. Kofod, *An enzyme with lipolytic activity WO1996013580 A1* **1995**, US005827719 A.
[63] K. Jensen, P. R. Østergaard, R. Wilting, S. F. Lassen, *BMC Biochem.* **2010**, *11*, 47.
[64] F. Teufel, J. J. Almagro Armenteros, A. R. Johansen, M. H. Gíslason, S. I. Pihl, K. D. Tsirigos, O. Winther, S. Brunak, G. von Heijne, H. Nielsen, *Nat. Biotechnol.* **2022**, *40*, 1023–1025.
[65] J. Jumper, R. Evans, A. Pritzel, T. Green, M. Figurnov, O. Ronneberger, K. Tunyasuvunakool, R. Bates, A. Žídek, A. Potapenko, A. Bridgland, C. Meyer, S. A. A. Kohl, A. J. Ballard, A. Cowie, B. Romera-Paredes, S. Nikolov, R. Jain, J. Adler, T. Back, S. Petersen, D. Reiman, E. Clancy, M. Zielinski, M. Steinegger, M. Pacholska, T. Berghammer, S. Bodenstein, D. Silver, O. Vinyals, A. W. Senior, K. Kavukcuoglu, P. Kohli, D. Hassabis, *Nature* **2021**, *596*, 583–589.
[66] F. Sievers, A. Wilm, D. Dineen, T. J. Gibson, K. Karplus, W. Li, R. Lopez, H. McWilliam, M. Remmert, J. Söding, J. D. Thompson, D. G. Higgins, *Mol. Syst. Biol.* **2011**, *7*, 539.
[67] E. Jurrus, D. Engel, K. Star, K. Monson, J. Brandi, L. E. Felberg, D. H. Brookes, L. Wilson, J. Chen, K. Liles, M. Chun, P. Li, D. W. Gohara, T. Dolinsky, R. Konecny, D. R. Koes, J. E. Nielsen, T. Head-Gordon, W. Geng, R. Krasny, G. W. Wei, M. J. Holst, J. A. McCammon, N. A. Baker, *Protein Sci.* **2018**, *27*, 112–128.
[68] M. J. Abraham, T. Murtola, R. Schulz, S. Páll, J. C. Smith, B. Hess, E. Lindah, *SoftwareX* **2015**, *1–2*, 19–25.
[69] J. Huang, S. Rauscher, G. Nawrocki, T. Ran, M. Feig, B. L. De Groot, H. Grubmüller, A. D. MacKerell, *Nat. Methods* **2016**, *14*, 71–73.

Manuscript received: February 25, 2023
Revised manuscript received: April 11, 2023
Accepted manuscript online: April 19, 2023
Version of record online: ■■, ■■

RESEARCH ARTICLE

Crystal clear: We evaluate the significance of poly(ethylene terephthalate) (PET) crystallinity on enzymatic degradation rates of six PET hydrolysing enzymes, present a new quantitative assessment of PET crystallinity tolerance of the enzymes, and provide structural comparisons and molecular dynamics simulations of the enzymes to explain their differences in attack mode, lag phase, and enzymatic rate responses to increased PET substrate crystallinity.

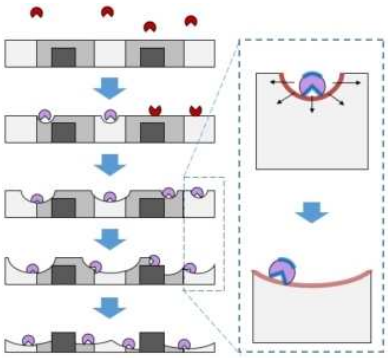

*T. B. Thomsen, S. Schubert, Dr. C. J. Hunt, Dr. K. Borch, Dr. K. Jensen, Dr. J. Brask, Prof. P. Westh, Prof. A. S. Meyer**

Paper IV

Relationships of crystallinity and reaction rates for enzymatic breakdown of poly (ethylene terephthalate), PET.

Sune W. Schubert*, Thore B. Thomsen*, Kristine S. Clausen, Cameron J. Hunt, Kim Borch, Kenneth Jensen, Jesper Brask, Anne S. Meyer, Peter Westh

In preparation

*Contributed equally

IV

Intentionally left blank

RESEARCH ARTICLE

Relationships of crystallinity and reaction rates for enzymatic degradation of poly (ethylene terephthalate), PET

Sune W. Schubert[a,d], Thore B. Thomsen[a,d], Kristine S. Clausen, Anders Malmendal[b], Cameron J. Hunt[a], Kim Borch[c], Kenneth Jensen[c], Jesper Brask[c], Anne S. Meyer[a], and Peter Westh*[a]

[a] S. W. Schubert, T. B. Thomsen, K. S. Clausen, C. J. Hunt, A. S. Meyer, P. Westh
Department of Biotechnology and Biomedicine
Technical University of Denmark
Søltofts Plads, DK-2800 Kgs. Lyngby, Denmark
E-mail: petwe@dtu.dk
[b] A. Malmendal
Institute of Natural Science and Environmental Chemistry.
Roskilde University
Universitetsvej 1, 28C.1, DK-4000 Roskilde, Denmark
[c] K. Borch, K. Jensen, J. Brask
Novozymes A/S
Biologiens Vej 2, DK-2800 Kgs. Lyngby, Denmark
[d] These authors contributed equally: S. W. Schubert, T. B. Thomsen,

Supporting information for this article is given via a link at the end of the document.

Abstract: Biocatalytic degradation of plastic waste is anticipated to become a crucial component in future recycling systems. However, enzymatic degradation of crystalline poly (ethylene terephthalate) (PET) remains consistently poor. Herein, we employed functional assays to elucidate the molecular underpinnings of this limitation. This included utilizing complementary activity assays to monitor the degradation of PET disks with varying substrate crystallinity (X_C), as well as kinetic parameters for soluble PET fragments. Our results indicate that a proficient PET-hydrolase, LCC_{ICCG}, operates through an endolytic mode of action, and that its activity is limited by conformational constraints in the PET polymer. Such constraints become more pronounced at high X_C values, which limit the density of productive sites on the PET surface. Our experimental findings demonstrated that endo-type chain-scissions occur during the initial lag phase. Moreover, these catalytic events partially alleviated conformational constraints in the polymeric PET, thereby facilitating the upwards concave progress curves for the formation of soluble products.

Introduction

Over the last decades, the scientific community has made substantial progress in identifying and engineering enzymes capable of degrading or modifying plastics, including the widely used polyester, poly(ethylene terephthalate) (PET).[1,2] Notable advancements include the discovery of a bacterium that utilizes PET waste as its sole carbon and energy source[3] and the identification and protein engineering of enzyme variants with sufficient activity for use in industrial PET-monomer recovery.[4–7] However, PET-hydrolases consistently showcase high sensitivity towards the degree of crystallinity (X_C) of the substrate.[8,9]

Crystalline PET comprises regions of highly ordered and densely packed PET chains, which stabilize the polymeric structure and renders it less susceptible to enzymatic degradation.[10] Many post-consumer products exhibit high X_C values as a result of manufacturing processes and usage conditions.[6,11,12] This poses a significant challenge for the efficient utilization of PET-hydrolases for industrial-scale recycling of PET. Currently, the most viable strategy to overcome the recalcitrance of crystalline PET involves implementing a pretreatment step that includes micronization and decrystallization of the PET feedstock. However, this approach involves high energy and water consumption.[13,14] This situation has spurred the search for enzymes capable of degrading more crystalline polyesters, potentially drawing inspiration from the well-established ability of hydrolases to degrade naturally occurring crystalline polymers, such as cellulose[15] and chitin.[16]

In this study, we investigated the characteristics of the PET-hydrolase, LCC_{ICCG}, which is generally considered a promising candidate for large-scale industrial applications.[1,4,17] To assess its catalytic activity, we employed two complementary assays described previously.[18] This involved continuous pH-stat measurements to detect the release of protons resulting from cleavage of ester bonds, while reversed-phase high-performance liquid chromatography (RP-HPLC) was utilized for the analysis of the product profile and quantification of soluble product formation. By analyzing the product profile in the early stage of a reaction and assays performed against PET disks with varying X_C, we gained a comprehensive understanding of how substrate crystallinity impacts the mode of action of the PET-hydrolase.

Results

Progress curves

The time course for the degradation of PET disks with different X_C was monitored by two complementary methods, HPLC and pH-stat measurements. Our HPLC protocol was capable of quantifying six different product types in the aqueous phase. These were the three mono-aromatic compounds terephthalic acid (T), mono(2-hydroxyethyl) terephthalic acid (ET), and bis(2-hydroxyethyl) terephthalate (ETE). In addition, we could resolve one peak for oligomers with respectively two, three or four aromatic rings. Each of these peaks encompassed three molecules with either zero, one or two ethylene glycol (EG) as end-groups. As an example, the fragments TET, ETET and ETETE, which all have two aromatic rings, co-eluted as a single

peak during RP-HPLC analysis. In the following, we will refer to soluble fragments with two or more aromatic rings as oligo ethylene glycol terephthalates (OETs). In contrast to the HPLC measurements, the pH-stat detected all hydrolytic reactions, irrespective of whether they produced a soluble product or not.

Results in Fig. 1 show the release of protons (pH stat measurements, blue trace, left ordinate) and soluble products (HPLC measurements, symbols, right ordinate) during the hydrolysis of PET disks with different degrees of crystallinity, X_C. Under the conditions used in this experiment, concentrations of tri- and tetra-aromatic OETs were either undetectable or near the detection limit (high nM range). Thus, Fig. 1 only includes the remaining four products (T, ET, ETE and di-aromats).

To facilitate further analyses of Fig. 1, we introduced a function, R, which specified the ratio of total hydrolytic activity to soluble products. Total hydrolytic activity was defined as the number of moles of hydroxide ions delivered by the pH stat system divided by the total reaction volume. These hydroxide ions neutralized protons produced by the enzyme reaction, and we call this concentration C_{H+}. The overall release of organic products, C_{org}, was defined as the sum of all compounds detected by HPLC in Fig. 1, C_{org}=[T]+[ET]+[ETE]+[di-aromats]. The ratio, R, may be written:

$$R = \frac{C_{H^+}}{C_{org}} \qquad (1)$$

To illustrate our interpretation of this function, we note that R>>2 corresponds to a mode of action where the enzymatic reaction is dominated by cleavages across PET chains distant from chain ends (endo-type activity). This type of reaction generates long insoluble OETs, and hence releases protons without concurrent soluble (organic) products. Conversely, cleavage near the terminal of insoluble polymers (exo-type activity), will release commensurate amounts of protons and soluble products and hence show R ~ 1. As a final example, complete hydrolyzation of a PET chain will yield R=2 since there are two ester bonds for each aromatic ring. (For further details, see Fig. S1). We note that a narrow distribution of activity across fewer PET-chains will yield a relatively lower R-value towards 2, since this mode of action requires fewer hydrolytic events to generate soluble products. We do not include EG in the definition of C_{org} (we cannot detect this product in the HPLC protocol). The R-value can therefore be regarded as a descriptor of abundance of endo-type cleavages, as the value is biased in regard to hydrolysis of certain soluble products (i.e., TE to T).

Figure 2 illustrates how R changes with time when LCC_{ICCG} degrades PET disks of different crystallinity. The figure also includes the functions, C_{H^+} and C_{org}, that define R (eq. 1). These results confirmed earlier reports on a lag phase for the release of soluble products, which became more prominent on substrates with high X_C.[8,19] For total hydrolysis, C_{H^+}, the lag phase was less pronounced and, in some cases was absent. As a result, the ratio, R, became larger in the initial stages of experiments for high-crystallinity substrates. Specifically, experiments with X_C=15.6% or 18.5% yielded R-values around 10 after 30-90 min. Quantification of R earlier in the reaction was not attainable because C_{org} was too low to measure, but we clearly detected proton release, and this implies an initial reaction with high R-value on crystalline substrates. As argued above, this implied that initial hydrolysis of crystalline substrate was slow and dominated by an endolytic mode of action (ten or more protons were released for every soluble product). However, irrespective of the initial X_C, R approached 2 after the lag phase. We emphasize that these changes in the mode of action all occur under conditions where the total degree of conversion is very low. Thus, the final degree of conversion for the measurements in Fig. 2 ranged from 0.1 to 1.7%.

Product profile

The results in Fig. 2 sparked interest in the initial product profile and to investigate this further, we designed a shorter experiment with a higher sampling rate. The aim of this experiment was to elucidate the profile of OETs released directly from the insoluble polymer. Thus, we used a lower enzyme concentration and higher substrate loads compared to the experiments shown in Figs. 1-2 (see Methods) to limit secondary hydrolysis of OETs in the aqueous phase. Unfortunately, the time resolution of the pH-stat system was inadequate for the desired sampling rate, and we therefore relied solely on HPLC detection in these experiments. Results in Fig. 3 show that we were able to monitor progress curves for all six product types that were detectable in HPLC (see section above). These six species were present in comparable amounts after 60 s contact time (Fig. 3A), while products with four aromatic rings dominated during earlier stages of the reaction (Fig. 3B). In accordance with Fig. 1, products with mono- and di-aromatic products became by far the most prevalent after several minutes of reaction, probably due to secondary hydrolysis of soluble OETs in the aqueous phase (see Tab 1).

While the relative abundance of tetrameric products decreased rapidly (see Fig. 3B), their absolute value remained practically constant (1-2 µM) throughout these experiments (see Fig. 3A). This steady concentration might be attributed to low solubility and/or the rate of secondary hydrolysis in the aqueous phase. To assess these factors, we estimated the solubility of the tetrameric PET fragment under the experimental conditions used and approximated it to be 6-8 µM (see supplementary information, Fig. S2). We also determined the kinetic parameters, in terms of Michaelis-Menten kinetics, for LCC_{ICCG} acting on soluble PET fragments (Tab. 1). These results showed that the specificity constant k_{cat}/K_M for the tetra-aromatic OET was comparable to TETE but an order of magnitude lower compared to TETET. Taken together, these observations suggest that the steady concentration of tetra-aromatic product in Fig. 3B could rely on both low solubility (the aqueous concentration approaches saturation) and slower secondary turnover compared to smaller OETs.

Reduction in the molar mass of PET chains

In an attempt to assess the frequency of respectively endo- and exo-lytic activity we analyzed the average chain-length of PET, degree of polymerization (DP), as a function of the degree of substrate conversion. We used a previously established approach,[9] based on partial hydrolysis of a PET sample, dissolution of remaining solids in an organic solvent and detecting the end-group concentration by nuclear magnetic resonance (NMR) (see methods and SI for details). Like most other methodologies in this area, this approach suffers from the

limitation that the bulk of the PET material (which is not modified by the enzyme) may dominate when all solid residue is dissolved. This has previously been discussed by Kawai et al.[20] To minimize this effect, we extended the enzymatic hydrolysis to high degrees of conversion (>70% weight loss). Nevertheless, results in Fig. 4 showed an essentially constant average chain length with a DP ranging from 225 to 250 throughout these experiments.

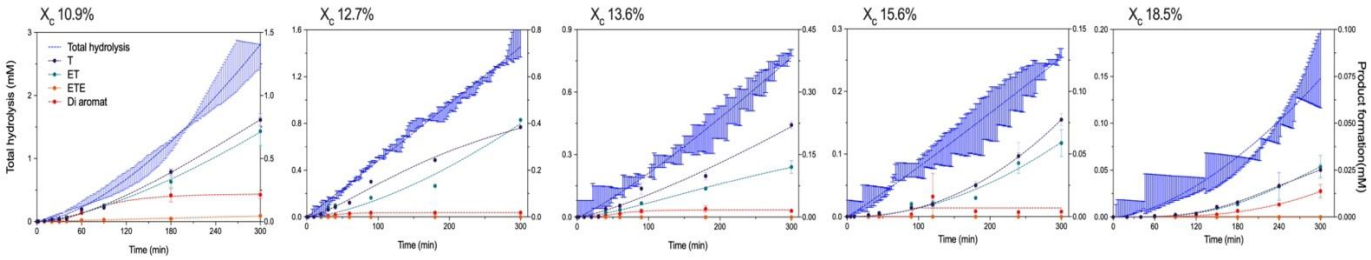

Figure 1. Progress curves for the activity against PET disks with varying degrees of crystallinity. Blue symbols represent the proton release from cleavage of ester bonds (left ordinate), providing a measure of total hydrolytic activity. Remaining curves depict the concentration of individual monomeric products and TETE, as indicated by the color code (right ordinate). Error bars were calculated as the standard deviation from two independent experiments.

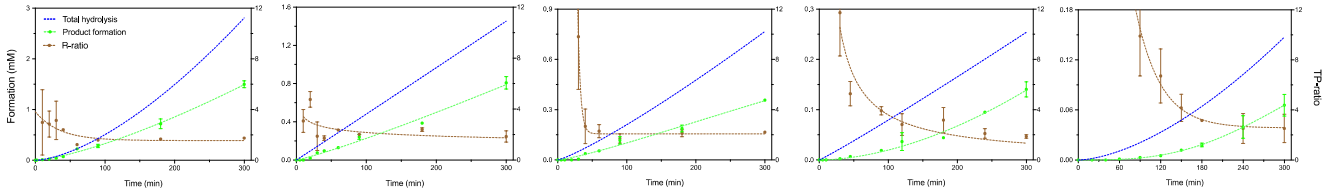

Figure 2. Progress curves showing the ratio between proton release and product formation in reactions performed against PET disks with varying X_C values. The left ordinate displays pooled product formation (green symbols), denoted as the sum of compounds listed in Fig. 1, while the R-ratio (brown symbols), defined in Eq. (1), is displayed on the right ordinate. The blue trace represents the hydrolytic curves shown in Fig. 1. Elevated *R*-values in the early stages of the reaction for PET disks with higher X_C indicate that the amount of protons released is approximately 10-fold higher than the accumulation of soluble products. Error bars represent the standard deviation from two independent experiments.

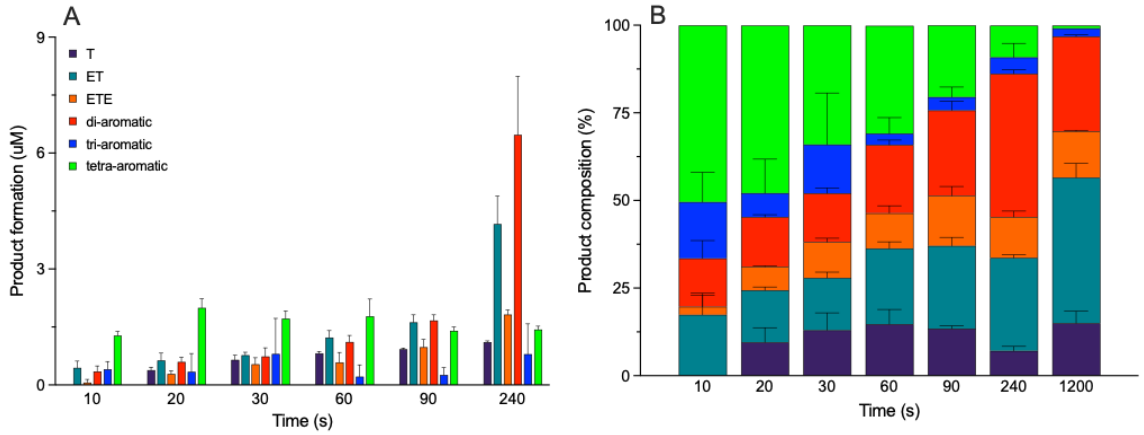

Figure 3. Investigation of the product profile during the early stage of an enzymatic PET hydrolysis course. Experiments were conducted at 65 °C using an enzyme load of 30 nM LCC_{ICCG} against 30 thin amorphous PET disks (X_C = 4.6%, 7 mg). These reaction conditions were deliberately chosen to minimize the rate of secondary hydrolysis of the released reaction products. Figure A) displays the concentrations of the six aromatic product species resolved using RP-HPLC at different time points, with the color code for each product specified in the panel. Figure B) illustrates the experimental results shown in Figure A, presented as the relative abundance of each product species. Error bars represent the standard deviation from two independent experiments.

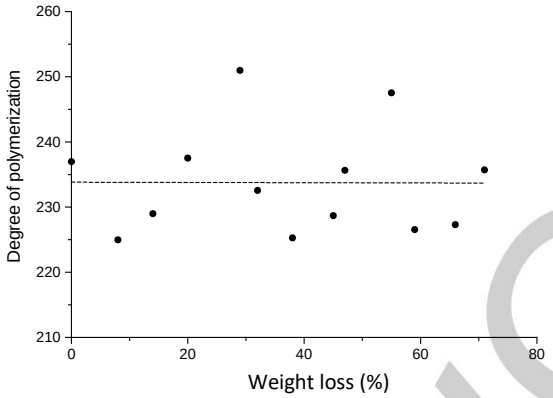

Figure 4. NMR analysis of treated PET disks used to investigate the mode of action of PET-hydrolase, LCC_{ICCG}. The relative weight loss of partially degraded PET disks are plotted as a function of the DP. Substrates were analyzed up to a weight loss of 75%, using thin PET disks to increase the surface-to-mass ratio (250 µm thickness, ~7 mg). This figure is adapted from study III.

LCC_{ICCG} kinetic data			
	K_M (mM)	k_{cat} (s^{-1})	n[M^{-1} s^{-1}]
ET	0,92 (± 0.22)	0,058 (± 0.0024)	62,37 (± 5,58)
ETE	0,75 (± 0.27)	8,2 (± 1.22)	1.11×10^4 ($\pm 1.19 \times 10^3$)
TETE	0,21 (± 0.091)	9,1 (± 2.71)	4.40×10^4 ($\pm 3.08 \times 10^3$)
TETET	0,67 (± 0.61)	331 (± 142)	5.62×10^5 ($\pm 1.5 \times 10^5$)
TETETET	ND	ND	5.08×10^4 ($\pm 7.5 \times 10^3$)
[a] ND = not detected			

Tabel 1. Kinetic parameters examined for LCC_{ICCG} acting on soluble PET fragments. The low solubility of the tetrameric compound precluded saturation for this substrate, and consequently, k_{cat} and K_M values could not be determined. Instead, we were able to evaluate their ratio, the specificity constant.

Discussion

Recent advancements in the discovery and engineering of PET-hydrolases have laid the groundwork for industrial-scale monomer recovery from polyester waste through bioprocessing[1,17,21,22]. Nevertheless, challenges remain for this technology to become an integral part of a circular economy. A primary concern is the limited ability of known PET-hydrolases to convert substrate with the degree crystallinity (X_C>20%)[8,9,19,23–26] that is typical for PET waste. While there is ample empirical evidence of the recalcitrance of crystalline PET, its molecular underpinnings are yet to be fully elucidated. Commonly proposed explanations include inaccessibility of scissile bonds, which is linked to low mobility of PET chains within or near crystalline regions.[10,27,28] This interpretation is consistent with a study on the material properties of PET, which revealed suppressed chain dynamics, when amorphous samples annealed above the glass transition temperature slowly crystallized.[29] Moreover, enzymatic activity has been associated with polymer chain conformation, underscoring the significance of mobility for the formation of productive enzyme-ligand complexes. [30,31]

The structural data discussed above have offered valuable insights into the causes of recalcitrance, and the current work aims to investigate this topic further from a functional perspective. Our starting point was numerous observations of an initial lag phase for PET-hydrolases,[8,18,24,32,33] which has been reported to be especially pronounced for crystalline substrates. This was also evident in the current study, as progress curves for soluble products formation ($C_{org,}$ Fig. 2) displayed initial lag phases, which became more pronounced as the X_C increased. Progress curves for total hydrolysis (C_{H^+} in Fig. 2) showcased the well-known decline in activity with increasing X_C (Fig. 2), but unlike C_{org}, this function displayed short-lived or no lag phase. This implied that initial hydrolysis of crystalline substrates by LCC_{ICCG} was

characterized by endolytic activity which rapidly released soluble products. In contrast, we found *R*-values above 10 for the most crystalline substrates. This indicated that ten or more protons were released initially for every soluble product.

This observation is in line with a recent study of the lag phase[19] for a number of PET-hydrolases, including efficient enzymes such as LCC_{ICCG},[4] PHL7,[5] and duraPETase.[7] The lag phases reported in this study extended up to several days for substrates with high crystallinity (>20 % X_C). Nevertheless, soluble products emerged after even longer contact times, and in some cases, the post-lag reaction rate reached a level that was comparable (within a factor of 2-3) to the initial rate measured on the amorphous substrates (X_C = 12.1%). These observations and the current results collectively support the interpretation that the initial enzyme reaction involves endo-type chain scissions, which are limited by the conformation of the PET polymer (i.e. *trans* or *gauche*). Hence, the reaction only occurs if the chain is able to attain a structure that is compatible with the active site of the enzyme. Loci on the PET surface that permits this mode of action serves as "attack sites" for the enzyme but are likely to be scarcely distributed on the surface of crystalline PET due to conformational constraints, such as the linear all-*trans* crystalline structures, or the highly trans RAF. This effect may be more profound due to the rigid nature of these microstructures, even at temperatures above T_g.[34]

This interpretation could explain both the low rate of proton release (as attack sites are scarce) and the absence of soluble, organic products (as randomly placed attack sites across PET-chains will produce mostly long and insoluble PET fragments) (Fig. 2). A comparable explanation has been proposed by Tarazona et al.[35]. Perhaps most importantly, this attack-site interpretation could also explain the basic origin of lag phase kinetics, because breakage of one ester bond would promote local chain mobility and hence create new attack sites for the enzyme. In other words, the initial enzymatic modification gradually renders crystalline PET more reactive, and this leads to upward curvature of the progress curve (see Fig. 5).

The initial reaction pathway was further illustrated by the short-term product-profiles shown in Fig. 3. We first note that these results contradict the often-stated conclusion that PET-hydrolases primarily release the mono-aromatic compounds ET and ETE via combined endo-type cuts that successively enable exolytic action on the polymer. [9,20,35–38] However, after 10 s, the summed concentrations of monomeric products accounted for less than 20% of soluble products. Later in the reaction, ET indeed became much more prevalent, but based on the amount of OETs released continuously (Fig. 3A), and their high turnover rates (Tab. 1), we propose that ET predominantly accumulates as the result of secondary hydrolysis of OETs in the aqueous phase.

This interpretation parallels conclusions based on kinetic modeling of the degradation of nanoPET.[18] Such a mode of action that predominantly proceeds via endo-type activity is also in line with the occurrence of longer soluble fragments (OETs), as observed in Fig. 3. In the simplest interpretation, where attack sites are completely randomly distributed, a random-endo pathway would generate equal amounts of all OETs and mono aromats. We did indeed observe quite comparable concentrations after e.g., 60 s, but there was a dominance of tetra-aromatic compounds in the earliest part of the experiment (~50%) (see Fig. 3B). Interestingly, Eberl et al.[39] similarly reported a high abundance of tetra-aromatic products in the insoluble fraction of enzyme treated PET samples. If indeed so, preference for the direct release of tetra-aromatic products could rely on either enzyme structure or chain conformation. We are not aware of structural features of LCC_{ICCG} that could promote binding of tetra-aromatic moieties in the product site, and hence favor the release of such products. Alternatively, the distribution in Fig. 3 could rely on local structure and mobility of the polymer. Specifically, if a bond located four segments away from a broken ester became prone to enzymatic attack, there would be a preference for primary release of such products. Further analyses of this problem would require more experimental work, including quantification of longer fragments in the insoluble fraction of the hydrolysate.

An endo-lytic mechanism as proposed above is expected to impart rapid chain shortening to the surface layer. Nevertheless, our NMR analysis of the average chain length failed to detect any evident reduction in DP even at 70% conversion of the substrate (Fig. 4). A similar result was recently reported in a study conducted by Kawai et al.[40] using another PET-hydrolase and experimental methodology. Both studies used all insoluble PET residue in the analysis, and this may hamper the interpretation as it is not straightforward to assess what fraction of the residue was exposed to the enzyme and what fraction made up the (unexposed) PET bulk. However, it is notable that no changes occurred in Fig. 4, even at high degrees of conversion, and we suggest that this could be caused by the aforementioned linkage between chain mobility and attack sites. Thus, if bond breakage promotes local chain mobility, it would generate a preference for repeated attacks on the same (more flexible) strand, and it follows that this chain would be preferentially solubilized. Our experimental data, which show *R*-values approaching 2 over the course of hydrolysis (see Fig. 2), further support this interpretation by demonstrating a constrained distribution of enzymatic activity on PET chains. A further assessment of this interpretation would require data on the average chain length in the surface layer, and we are currently pursuing options for this type of assay.

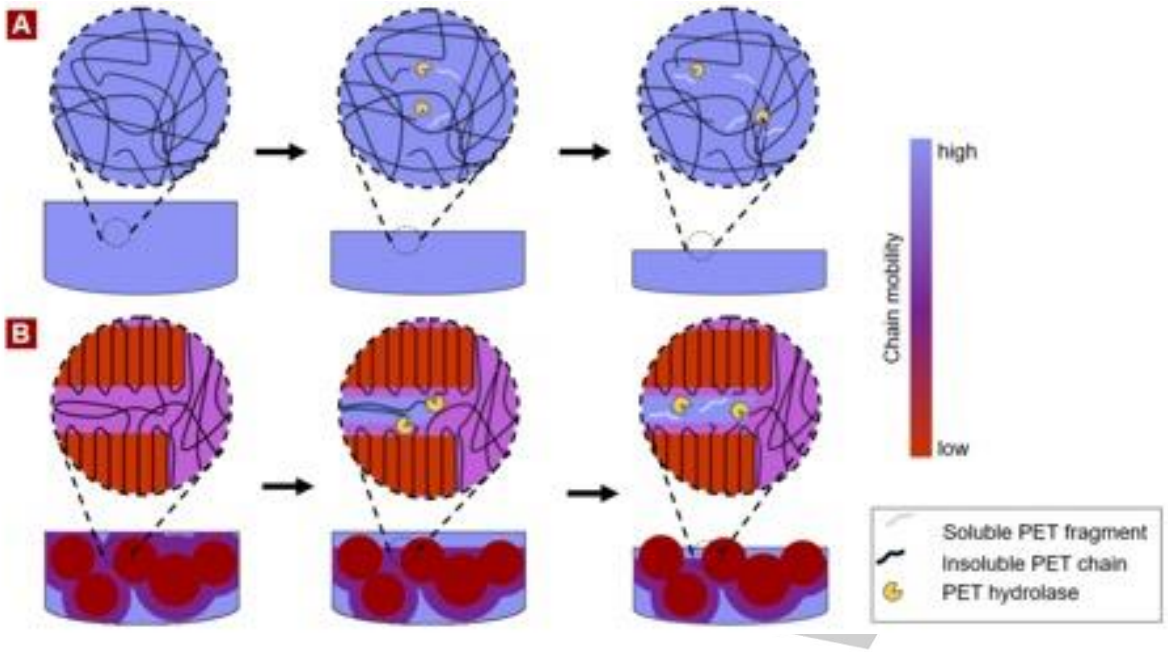

Figue 5. A schematic illustration of the hypothesized mode of action, by which LCC_{ICCG} hydrolyses regions of PET that comprise PET chains with varying degrees of conformational constraints in their mobility (red represents low chain mobility, while blue signifies high). Scheme A) presents a PET sample characterized by high mobility of PET chains, which are more readily susceptible to enzymatic hydrolysis. We suggest that degradation of these regions does not substantially increase the inherently high chain mobility and susceptibility of scissile bonds during the reaction. In contrast, Scheme B) illustrates a PET sample with low chain mobility. In accordance with the presented results in this study, multiple studies have reported that the degradation of crystalline PET samples involves an initial lag phase during which no soluble products are released. However, in Fig. 2, we observed initially high R-ratio that gradually declined over the course of the lag phase and transitioned towards 2 once a consistent reaction rate in product formation had been established. This observation suggests the occurrence of endo-type activity promote local chain mobility and hence expose new attack sites for the enzyme. This may account for the initial lag phase and the gradual transition towards product formation, while the R-ratio decreased.

Conclusion

We have studied the activity of the enzyme LCC_{ICCG} on PET substrates with different crystallinity, and used the results to assess the origins of the recalcitrance of crystalline PET. A combined interpretation of current results and previous structural data suggested that conformational constraints of the PET chain, which become severe with increasing crystallinity, limit the initial enzyme reaction. This suggests that the structure of a constrained polymer rarely fits the architecture of the enzyme's active site, and as a result, the density of productive sites (attack sites) is low on the surface of crystalline PET. This scarcity of attack sites results in a low reaction rate as seen broadly for crystalline substrates. It also explains initial dominance of endolytic reactions and insoluble products reported here (R≥10, Fig. 2) because activity is limited to scattered attack sites. However, slow, endolytic activity was found to change the mode of reaction even at very low degrees of conversion, and soluble products quickly became more prevalent (R=2, Fig. 2). We propose that this reflects a gradual and local alleviation conformational constraints. Thus, breakage of an ester bond may promote mobility of adjacent chain segments and hence the ability of these segments to combine productively with the enzyme. This produces more attack sites and leads and a type of synergy that generates an upward curvature of the progress curve. We suggest that this underpins the distinctive lag phase kinetics for crystalline substrates reported here and earlier. An interpretation based on local flexibility is also in line with the rapid decline of the R value (Fig. 2) for crystalline substrates because clustering of cuts would release more soluble products than random cuts, and hence drive down R as it is indeed observed. Finally, local alleviation of constraints could lead to a preference for repeated cuts in the same strand in accord with the observations in Fig. 4.

Experimental Section

Enzymes

The PET-hydrolase LCC_{ICCG} was expressed in a heterologous system using *Escherichia coli* cells and purified according to the method described by Thomsen et al.[41] The enzyme concentration was determined by measuring the absorbance at 280 nm and utilizing the calculated molar extinction coefficients.[42]

PET substrates

PET disks with a diameter of 6 mm and weighing approximately 32 mg were produced using a generic hole punch and 1 mm thick PET sheets (Goodfellow Cambridge Ltd, Huntingdon, UK, Cat. No. ES303010). To increase the surface-to-mass ratio for PET disks subjected to NMR analysis, we incorporated thinner PET disks with a thickness of 250 µm and a weight of approximately 7 mg (Goodfellow Cambridge Ltd, Huntingdon, UK, Cat. No. ES301445).

T and ETE, which were utilized as standard samples, were purchased from Sigma. However, ET was not commercially

available and was therefore produced in-house via enzymatic hydrolysis of 10 mM ETE over a period of 5 h. The purity of the ET product was determined to be > 90%, as assessed by RP-HPLC analysis.[42]

Synthesis of TETETET

A series of synthesis steps were conducted to obtain the PET fragment TETETET. This included Mono-*t*Bu terephthalate (tBu-T) which was purchased from Enamine Ltd (NJ, USA), while all other chemicals were purchased from Merck and used without further purification. Thin-layer chromatography (TLC) was performed on pre-coated silica gel on aluminum foil with a fluorescent indicator, and spots were visualized under 254 nm UV light. Flash chromatography was carried out using an automated Biotage Selekt system with pre-packed Biotage Sfär silica gel cartridges. NMR spectra were recorded at 25 °C on a Bruker Avance IIIHD 400 MHz instrument equipped with a 5 mm room temperature BBFO probe (see Fig S3 for NMR spectra).

Initially, Mono-tBu terephthalate was dissolved in DCM-$SOCl_2$ (9:1, 100 mL), and a catalytic amount of DMF was added. The reaction was refluxed (approximately 45 °C) under N_2 overnight, resulting in a color change from milky white to clear light yellow. The solution was then evaporated using a rotary evaporator to yield a white solid product, which was used without further purification. Next, ethylene glycol (1 mL, 18 mmol) was dissolved in DCM-pyridine (4:1, 50 mL). Molecular sieves (4 Å) were added, and the mixture was stirred under N2 for 1 h. Subsequently, *t*Bu-T-Cl was added, and the solution was refluxed (45-50 °C) under N2 overnight. TLC analysis (EtOAc-hexane 1:4) showed the formation of *t*Bu-TET-*t*Bu (Rf 0.6) and tBu-TE (Rf 0.3). The reaction mixture was evaporated, redissolved in DCM, and extracted with water to remove excess ethylene glycol. The solution was then evaporated onto silica and dry-loaded onto a flash column. Purification was carried out with a gradient from 0 to 50% EtOAc in hexane. Following this, *t*Bu-TET-*t*Bu was dissolved in TFA-DCM (1:1, 5 mL) and stirred for 1 h at room temperature. The solution was then evaporated to dryness, yielding a white solid powder product of TET, which was used without further purification. TET was dissolved in DCM-SOCl2 (9:1, 20 mL), and a catalytic amount of DMF was added. The reaction was refluxed (approximately 45 °C) under N_2 overnight, before being evaporated using a rotary evaporator to yield a white solid product, which was used without further purification. This product, tBu-TE, was dissolved in pyridine-CHCl3 (1:1, 50 mL) and 4 Å molecular sieves were added. The mixture was stirred at room temperature under N_2 for 2 h before Cl-TET-Cl was added. The reaction proceeded over the weekend (72 h) at room temperature. TLC analysis in both EtOAc-pentane 1:1 (Rf product 0.9) and acetone-DCM 1:20 (Rf product 0.9) was conducted. The reaction mixture was filtered, evaporated, redissolved in $CHCl_3$, and evaporated on silica. Purification by flash chromatography was performed using a gradient from 0-5% acetone in DCM. NMR analysis showed the target compound, albeit with a minor *t*Bu-TE impurity. Lastly, *t*Bu-TETETET-*t*Bu was deprotected in TFA-DCM (1:1, 10 mL) for 2 h at room temperature. The mixture was then carefully evaporated under 100 mbar vacuum to approximately 1 mL, followed by the addition of DCM. The solution was left at 4 °C overnight to precipitate. After decanting the supernatant, the white crystals were dried under vacuum and collected from the round-bottom flask. NMR analysis revealed the desired TETETET with trace amounts of TE (see Fig. S3 in supplementary section).

Isothermal crystallization

PET disks with varying X_C were prepared through thermal annealing, and X_C was determined using differential scanning calorimetry (DSC) measurements in triplicates on a Pyris 1 Calorimeter (Perkin Elmer, Waltham, Massachusetts, USA). These procedures have been described in detail in a previous study.[41] It should be noted that the untreated amorphous PET disk was annealed at 85 °C for 5 min to mitigate any enthalpy relaxation caused by ageing of the polymer.

Methods for monitoring enzymatic activity

Proton release detected by pH-stat analysis

The release of protons associated to enzymatic PET hydrolysis was monitored using the pH-stat system TitroLine® 7000 automated titrator (SI Analytics GmbH, Mainz, Germany). The reaction vessel consisted of a 10 mL vessel, equipped with a magnetic stirrer and a thermostat jacket connected to an external temperature-regulated water bath.

Activity measurements commenced with the addition of 9.5 mL of Milli-Q water to the vessel. Following this, the enzyme was added to achieve a final concentration of 150 nM, and the system was allowed to thermally equilibrate at 65 °C. The pH was then adjusted to 9.000, and the enzyme reaction was initiated by adding 9 PET disks (1 mm thickness). Subsequently, we continuously monitored the consumption of 20 mM NaOH required to maintain the pH at 9.000 over a 3-hour period. Initiation of the reaction with the substrate (rather than the enzyme) was preferred, as the enzyme stock solution influences the buffer capacity and pH of the solution. To minimize the uptake of atmospheric CO_2 and reduce evaporation of liquid from the system, the reaction vessel was tightly sealed with a lid. To evaluate this effect and any potential leakage from the base delivery system, parallel control experiments without the substrate were conducted. Individual experiments were conducted in duplicates.

Product formation detected by RP-HPLC analysis

Concurrently, while performing the procedure described above for the pH-stat analysis, we retrieved subsets of the reaction mixtures for HPLC analysis. Specifically, 10 subsets of 20 µL of the reaction mixture above the PET disks were regularly withdrawn throughout the 3-hour time course. All aliquots were diluted in 175 µL of Milli-Q water, and the reaction was quenched by the addition of 5 µL of 5 M HCl, as previously validated by Bååth et al.[42]

Furthermore, we investigated the product profile during the early stage of an enzymatic PET hydrolysis course. To achieve this, we deliberately exploited reaction conditions intended to suppress the catalytic rate of secondary hydrolysis of soluble products in the aqueous phase. This included using a low enzyme dosage of 30 nM against a high substrate load consisting of 30 thin amorphous PET disks (X_C = 4.6%, 7 mg). Experiments were conducted at a temperature of 65 °C in a reaction volume of 2.5

mL. Over a short period and up to 10 min following the initiation of the reaction, 8 subsets of 50 µL samples were regularly withdrawn and analyzed using RP-HPLC. Individual experiments were conducted in duplicates.

Quantification and product composition of soluble reaction products were analyzed by RP-HPLC using a Thermo Scientific Vanquisher system equipped with a Capital HPLC 250 mm x 4.6 mm C18 column. Samples were injected in volumes of 20 µL, employing a mobile phase consisting of 7.5 mM formic acid and 5% v/v acetonitrile at a 1:5 ratio for 7.5 min, followed by elution using acetonitrile for 12.5 min. The flow rate and column temperature were maintained at 1 mL/min and 40 °C, respectively. Analytes were detected using UV measurements at 240 nm, and peak analysis was performed using the Chromeleon Chromatography Data System software (version 7.3.1).

Mono-aromatic products (T, ET, and ETE) could be readily resolved and quantified against standard curves. Products with 2, 3, or 4 aromatic rings were also detected by HPLC; however, the different species within each of these groups (e.g., the di-aromatic products TET, TETE, and ETETE) exhibited similar retention times and eluted as one peak using the current experimental procedure. The peaks for di-, tri-, and tetra-aromatic compounds were identified and quantified using in-house synthesized standards TETE, TETET, and TETETET.[18] Reactions were conducted in duplicates and included control experiments without enzyme.

Determination of kinetic constants

The specificity constants for LCC_{ICCG} against PET fragments ET, ETE, TETE, TETET, and TETETET was determined. Reactions were conducted in low-binding microplates (Greiner Bio-One™ 655900) in volumes of 250 uL and with substrate concentrations ranging from 0 to 2 mM. The plates were incubated in an Eppendorf thermomixer at 50°C and 1100 rpm for contact times of 10 minutes (ETE, TETE, TETET, and ETETETE) or 2 hours (ET). To prevent secondary hydrolysis, enzyme concentrations were kept low, ranging from 0.01 to 0.5 µM depending on the substrate. This approach ensured that the detected initial steady-state rate represented the hydrolysis of the respective soluble PET fragment. To determine the specificity constant for TETETET, was derived using initial reaction rates due to its poor solubility. Also, to increase the solubility of the compound, we added 10% v/v DMSO to the reaction mixture, which consisted of 80 µM TETETET, 50 mM sodium phosphate buffer at pH 8, and was conducted at 50 °C and 1100 rpm. The reaction was initiated by adding LCC_{ICCG} at a final concentration of 50 nM. Quenching of the reaction was performed at specific time intervals (0, 10, 20, 30, 40, and 120 minutes) by adding 5 µL of 6 M HCl to 100 µL aliquots.
Duplicates and substrate blanks (for quantification of autohydrolysis) were included, and all reactions were quenched and analyzed by RP-HPLC as described above.

Assessing the solubility of PET fragments

A study was conducted to compare the solubility of various PET fragments released during enzymatic PET hydrolysis. To achieve this, concentration gradient from either 0-80 µM or 0-1 mM comprising T, ET, ETE, TET, TETE, TETET, ETETETE or TETETET PET fragments was prepared. Samples were adjusted to contain similar volumes of DMSO at either 0.7% v/v or 1.5% v/v. We note that presence of DMSO in the analyzed samples was unavoidable, as this solvent was already present in the stock solutions containing the PET fragments. These prepared PET fragment samples were introduced to a 96-well plate containing the reaction buffer used for experiments in Figs. 1 and 2. The plates were subsequently incubated at 65 °C for 1 h. After the incubation period, absorbance was measured for turbidity at 600 nm using spectrophotometric measurements in a plate reader (Molecular Devices SpectraMax Paradigm, San Jose, USA).

NMR analysis of partially degraded PET disks

NMR analysis was conducted on partially degraded PET disks (250 µm thickness) to study the DP as a function of the mass conversion of the PET disk. For this purpose, individual reactions were conducted using PET disks with an enzyme load of 150 nM at 65 °C in a reaction volume of 1 mL. Over a 72-hour duration, the PET disks were regularly withdrawn, dried, and subjected to gravimetric analysis to determine weight loss. Subsequently, the enzyme-treated PET disks, along with an untreated control sample, were dissolved in hexafluoroisopropanol (HFIP, ≥ 99%, Merck KGaA, Darmstadt, Germany) and stored at room temperature for 48 h to ensure complete dissolution. Aliquots of 8 µL of the dissolved PET solutions, with a final concentration of 15.0 g/L, were transferred into a 3 mm NMR tube and mixed with 142 µL of chloroform-d ($CDCl_3$, 99.5%).

All 1H solution NMR measurements were carried out at 25 °C using a Bruker Avance 800 MHz spectrometer (Bruker Biospin, Germany) operating at a 1H frequency of 800.09 MHz and equipped with a 5 mm TCI cryoprobe. The 1H NMR spectra were acquired using the zg experiment with a 1H 90° pulse length of 6.8 µs and a recycle delay of 15 s. A total of 64k data points spanning a spectral width of 20 ppm were collected in 256 transients. The spectra were processed using Topspin (Bruker). An exponential line broadening of 0.3 Hz was applied to the free induction decay prior to Fourier transformation, and the baseline was corrected. Individual baseline correction was applied for the signals at 4.49, 4.00, and 3.89 ppm using Matlab (The MathWorks Inc., Natick, USA). The intensities of all signals were measured in Matlab.
Estimation of the DP was performed as previously described by Wei et al.[9], which involved analyzing the peaks in the spectral regions of 7.8–8.2 ppm and 3.8–4.8 ppm. Integration ratios are provided under each signal, calculated relative to the CH2 signal at 4.0 ppm. To improve visibility, the intensities of 1H signals in yellow and purple are increased by factors of 16 and 32, respectively. The 13C satellites of the parent HFIP signal (δH, 4.41 ppm) are denoted by.

Acknowledgements

Funding

This work was supported by the Novo Nordisk foundation Grant NNFSA170028392 (to P. W.). In addition, this work was supported by a grant (Project no. 40815) from Villum Fonden, The Villum Experiment Programme

Conflict of Interest:

K.B., K.J., and J.B. work for Novozymes A/S, a major manufacturer of industrial enzymes.

References

[1] V. Tournier, S. Duquesne, F. Guillamot, H. Cramail, D. Taton, A. Marty, I. André, *Chem Rev* **2023**. *123* (9), 5612-5701.
[2] F. Kawai, *Catalysts* **2021**, *11*, 1–10.
[3] S. Yoshida, K. Hiraga, T. Takehana, I. Taniguchi, H. Yamaji, Y. Maeda, K. Toyohara, K. Miyamoto, Y. Kimura, K. Oda, *Science (1979)* **2016**, *351*, 1196–1199.
[4] V. Tournier, C. M. Topham, A. Gilles, B. David, C. Folgoas, E. Moya-Leclair, E. Kamionka, M. L. Desrousseaux, H. Texier, S. Gavalda, M. Cot, E. Guémard, M. Dalibey, J. Nomme, G. Cioci, S. Barbe, M. Chateau, I. André, S. Duquesne, A. Marty, *Nature* **2020**, *580*, 216–219.
[5] C. Sonnendecker, J. Oeser, P. K. Richter, P. Hille, Z. Zhao, C. Fischer, H. Lippold, P. Blázquez-Sánchez, F. Engelberger, C. A. Ramírez-Sarmiento, T. Oeser, Y. Lihanova, R. Frank, H. G. Jahnke, S. Billig, B. Abel, N. Sträter, J. Matysik, W. Zimmermann, *ChemSusChem* **2022**, *15*
[6] E. L. Bell, R. Smithson, S. Kilbride, J. Foster, F. J. Hardy, S. Ramachandran, A. A. Tedstone, S. J. Haigh, A. A. Garforth, P. J. R. Day, C. Levy, M. P. Shaver, A. P. Green, *Nature Catalysis 2022 5:8* **2022**, *5*, 673–681.
[7] Y. Cui, Y. Chen, X. Liu, S. Dong, Y. Tian, Y. Qiao, R. Mitra, J. Han, C. Li, X. Han, W. Liu, Q. Chen, W. Wei, X. Wang, W. Du, S. Tang, H. Xiang, H. Liu, Y. Liang, B. Wu, *ACS Catal.* **2021**, *11*, 1340–1350.
[8] T. B. Thomsen, C. J. Hunt, A. S. Meyer, *N Biotechnol* **2022**, *69*, 28–35.
[9] R. Wei, D. Breite, C. Song, D. Gräsing, T. Ploss, P. Hille, R. Schwerdtfeger, J. Matysik, A. Schulze, W. Zimmermann, *Adv. Sci.* **2019**, *6*, 1900491.
[10] R. Wei, C. Song, D. Gräsing, T. Schneider, P. Bielytskyi, D. Böttcher, J. Matysik, U. T. Bornscheuer, W. Zimmermann, *Nat. Commun.* **2019**, *10*, 5581.
[11] Z. Zhang, S. Huang, D. Cai, C. Shao, C. Zhang, J. Zhou, Z. Cui, T. He, C. Chen, B. Chen, T. Tan, *Green Chemistry* **2022**, *24*, 5998–6007.
[12] A. M. de Castro, A. Carniel, D. Stahelin, L. S. Chinelatto Junior, H. de A. Honorato, S. M. C. de Menezes, *Process Biochemistry* **2019**, *81*, 85–91.
[13] M. E. Grigore, *Recycling* **2017**, *2*.
[14] Z. O. G. Schyns, M. P. Shaver, *Macromol Rapid Commun* **2021**, *42*.
[15] H. Østby, L. D. Hansen, S. J. Horn, V. G. H. Eijsink, A. Várnai, *Journal of Industrial Microbiology & Biotechnology 2020 47:9* **2020**, *47*, 623–657.
[16] G. Vaaje-Kolstad, S. J. Horn, M. Sørlie, V. G. H. Eijsink, *FEBS J* **2013**, *280*, 3028–3049.
[17] A. Singh, N. A. Rorrer, S. R. Nicholson, E. Erickson, J. S. DesVeaux, A. F. T. Avelino, P. Lamers, A. Bhatt, Y. Zhang, G. Avery, L. Tao, A. R. Pickford, A. C. Carpenter, J. E. McGeehan, G. T. Beckham, *Joule* **2021**, *5*, 2479–2503.
[18] S. Schubert, ; Warming, K. ; Schaller, J. Bååth, ; Arnling, C. ; Hunt, K. ; Borch, K. ; Jensen, J. ; Brask, P. Westh, S. W. Schubert, K. Schaller, J. A. Hunt, C. Borch, K. Jensen, J. Westh, K. Schaller, J. A. Bååth, C. Hunt, K. Borch, K. Jensen, J. Brask, *ChemBioChem* **2023**, *24*, e202200516.
[19] T. B. Thomsen, S. Schubert, C. J. Hunt, K. Borch, K. Jensen, J. Brask, P. Westh, A. S. Meyer, *ChemSusChem* **2023**, e202300291.
[20] F. Kawai, Y. Furushima, N. Mochizuki, N. Muraki, M. Yamashita, A. Iida, R. Mamoto, T. Tosha, R. Iizuka, S. Kitajima, *AMB Express* **2022**, *12*.
[21] I. Taniguchi, S. Yoshida, K. Hiraga, K. Miyamoto, Y. Kimura, K. Oda, *ACS Catal* **2019**, *9*, 4089–4105.
[22] A. Kushwaha, L. Goswami, M. Singhvi, B. S. Kim, *Chemical Engineering Journal* **2023**, *457*.
[23] L. Pfaff, J. Gao, Z. Li, A. Jäckering, G. Weber, J. Mican, Y. Chen, W. Dong, X. Han, C. G. Feiler, Y. F. Ao, C. P. S. Badenhorst, D. Bednar, G. J. Palm, M. Lammers, J. Damborsky, B. Strodel, W. Liu, U. T. Bornscheuer, R. Wei, *ACS Catal* **2022**, *12*, 9790–9800.
[24] T. B. Thomsen, S. W. Schubert, C. J. Hunt, P. Westh, A. S. Meyer, *Enzyme Microb Technol* **2023**, *162*, 110142.
[25] E. Erickson, T. J. Shakespeare, F. Bratti, B. L. Buss, R. Graham, M. A. Hawkins, G. König, W. E. Michener, J. Miscall, K. J. Ramirez, N. A. Rorrer, M. Zahn, A. R. Pickford, J. E. McGeehan, G. T. Beckham, *ChemSusChem* **2022**, *15*.
[26] H. Lu, D. J. Diaz, N. J. Czarnecki, C. Zhu, W. Kim, R. Shroff, D. J. Acosta, B. R. Alexander, H. O. Cole, Y. Zhang, N. A. Lynd, A. D. Ellington, H. S. Alper, *Nature* **2022**, *604*, 662–667.
[27] C. M. Carr, D. J. Clarke, A. D. W. Dobson, *Front. Microbiol.* **2020**, *11*, 571265.
[28] F. Kawai, T. Kawabata, M. Oda, *ACS Sustain Chem Eng* **2020**, *8*, 8894–8908.
[29] R. P. Choudhury, J. S. Lee, R. M. Kriegel, W. J. Koros, H. W. Beckham, *Macromolecules* **2012**, *45*, 879–887.
[30] B. Guo, X. Lopez-Lorenzo, Y. Fang, E. Bäckström,] Antonio, J. Capezza, S. Reddy Vanga, I. Furó, M. Hakkarainen, O. Syrén, *ChemSusChem* **2023**, e202300742.
[31] B. Guo, S. R. Vanga, X. Lopez-Lorenzo, P. Saenz-Mendez, S. R. Ericsson, Y. Fang, X. Ye, K. Schriever, E. Bäckström, A. Biundo, R. A. Zubarev, I. Furó, M. Hakkarainen, P. O. Syrén, *ACS Catal* **2022**, *12*, 3397–3409.
[32] T. B. Thomsen, C. J. Hunt, A. S. Meyer, *MethodsX* **2022**, *9*, 101815.
[33] R. K. Brizendine, E. Erickson, S. J. Haugen, K. J. Ramirez, J. Miscall, D. Salvachúa, A. R. Pickford, M. J. Sobkowicz, J. E. Mcgeehan, G. T. Beckham, *ACS Sustain Chem Eng* **2022**, *10*, 9131–9140.
[34] H. Chen, Z. Liu, P. Cebe, *Polymer (Guildf)* **2009**, *50*, 872–880.
[35] N. A. Tarazona, R. Wei, S. Brott, L. Pfaff, U. T. Bornscheuer, A. Lendlein, R. Machatschek, **2022**, DOI 10.1016/j.checat.2022.11.004.
[36] Å. M. Ronkvist, W. Xie, W. Lu, R. A. Gross, *Macromolecules* **2009**, *42*, 5128–5138.

[37] M. Barth, T. Oeser, R. Wei, J. Then, J. Schmidt, W. Zimmermann, *Biochem Eng J* **2015**, *93*, 222–228.
[38] P. Falkenstein, Z. Zhao, A. Di Pede-Mattatelli, G. Künze, M. Sommer, C. Sonnendecker, W. Zimmermann, F. Colizzi, J. Matysik, C. Song, *ACS Catal* **2023**, *13*, 6919–6933.
[39] A. Eberl, S. Heumann, T. Brückner, R. Araujo, A. Cavaco-Paulo, F. Kaufmann, W. Kroutil, G. M. Guebitz, *J Biotechnol* **2009**, *143*, 207–212.
[40] T. Kawabata, M. Oda, F. Kawai, *J Biosci Bioeng* **2017**, *124*, 28–35.
[41] T. B. Thomsen, C. J. Hunt, A. S. Meyer, *MethodsX* **2022**, *9*, 101815.
[42] J. Arnling Bååth, K. Borch, P. Westh, *Anal Biochem* **2020**,

Supplementary information

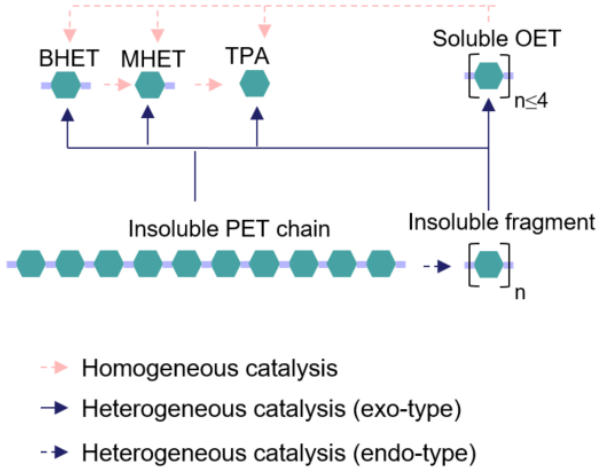

Fig S1. Overview of the various catalytic events mediated by PET-hydrolases during the enzymatic degradation of PET. Heterogeneous catalysis on insoluble PET chains can manifest as either endo- or exo-type activity (indicated by the blue arrow). The heterogeneous endo-type activity is characterized by the cleavage of a PET chain distant from its terminal ends, which results in the release of a proton without formation of soluble products. In contrast, a heterogeneous exo-type cut, occurring near a PET chain terminal, releases equivalent amounts of protons and soluble products. Throughout the hydrolysis process, soluble products are liberated from the bulk PET and undergo homogeneous catalysis in the aqueous phase (indicated by the pink arrow). Here, secondary hydrolysis of soluble OETs containing up to four aromatic rings proceeds towards terminal T.

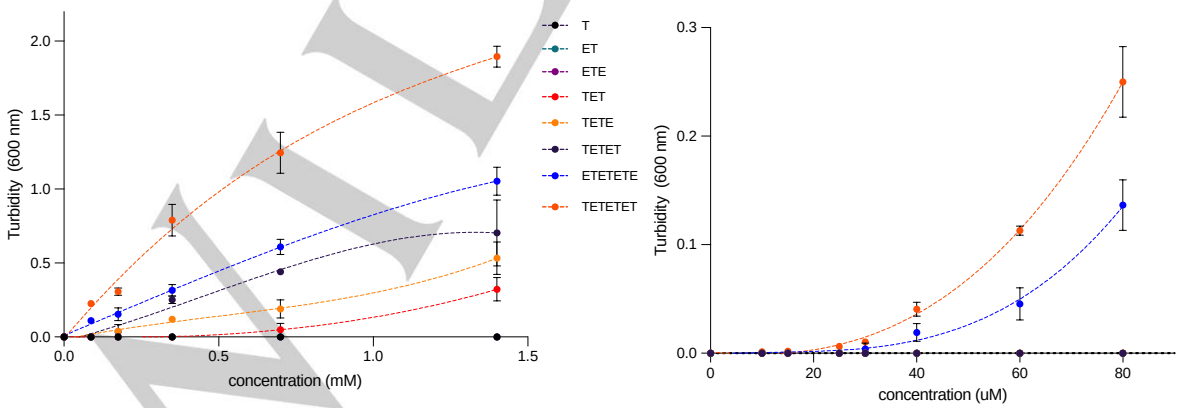

Fig S2. Comparison of the solubility of various PET fragments released during enzymatic PET hydrolysis. A concentration gradient comprising different species of mono-, di-, tri-, and tetrameric PET fragments was introduced to a 96-well plate containing the reaction buffer utilized in Figs. 1 and 2. The plates were incubated at 65 °C for 1 h, after which absorbance was measured at 600 nm. This turbidity signal served to assess the degree of solubility of the PET fragments. As several PET fragments were stored in DMSO stock solutions, we adjusted the concentration of all samples to contain similar volumes of DMSO. Figure A included 0.7% v/v DMSO, while this value was 1.5% for figure B. We recognize that the presence of DMSO likely enhanced the solubility of the analyzed PET fragments. In scheme A showing concentrations of the PET fragments in the 0-80 nM range, signals were only detected for ETETETE and TETETET, from which their solubility levels were determined to be roughly 6-8 µM and 20-25 µM, respectively.

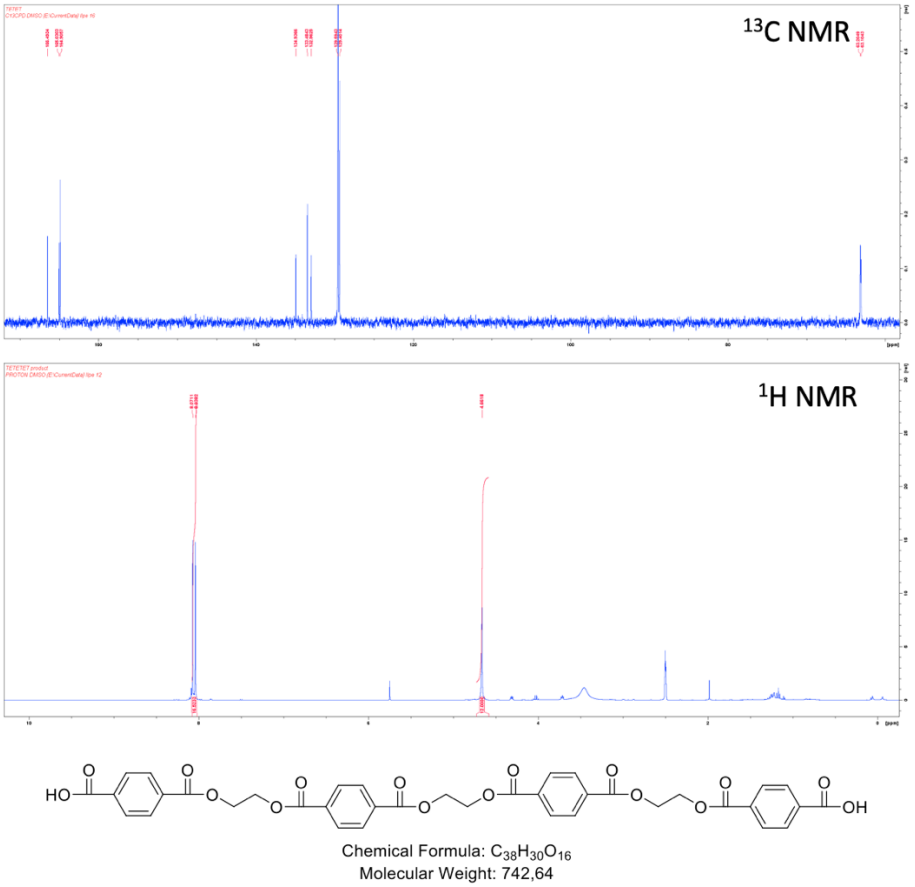

Figure S3. Characterization of TETETET. Upper panel show the ^{13}C NMR spectra for the in-house synthesized PET fragment while the lower panel show the ^{1}H NMR spektra.

Intentionally left blank

Paper V

A new continuous assay for quantitative assessment of enzymatic degradation of poly(ethylene terephthalate) (PET)

Thore B. Thomsen*, Sune W. Schubert*, Cameron J. Hunt, Peter Westh, Anne S. Meyer

Enzyme and Microbial Technology **2023** (167) 1101442

*Contributed equally

V

Intentionally left blank

Enzyme and Microbial Technology 162 (2023) 110142

Contents lists available at ScienceDirect

Enzyme and Microbial Technology

journal homepage: www.elsevier.com/locate/enzmictec

A new continuous assay for quantitative assessment of enzymatic degradation of poly(ethylene terephthalate) (PET)

Thore Bach Thomsen [1], Sune W. Schubert [1], Cameron J. Hunt, Peter Westh, Anne S. Meyer [*]

Department of Biotechnology and Biomedicine, Technical University of Denmark, Søltofts Plads, DK-2800 Kgs. Lyngby, Denmark

ARTICLE INFO

Keywords:
Enzymatic PET degradation
Assay development
PET hydrolase
Biotechnology
Interfacial enzymology
Heterogeneous catalysis

ABSTRACT

Enzymatic degradation of poly(ethylene terephthalate) (PET) has emerged as a promising route for ecofriendly biodegradation of plastic waste. Several discontinuous activity assays have been developed for assessing PET hydrolyzing enzymes, usually involving manual sampling at different time points during the course of the enzymatic reaction. In this work, we present a novel, compartmentalized UV absorbance assay for continuous detection of soluble hydrolysis products released during enzymatic degradation of PET. The methodology is based on removal of the walls separating two diagonally adjacent wells in UV-transparent microplates, to ensure passage of soluble enzymatic hydrolysis products between the two adjacent wells: One well holds an insoluble PET disk of defined dimensions and the other is used for continuous reading of the enzymatic product formation (at 240 nm). The assay was validated by quantifying the rate of mixing of the soluble PET degradation product BHET (bis(2-hydroxyethyl) terephthalate) between the two adjacent wells. The assay validation also involved a simple adjustment for water evaporation during prolonged assays. With this new assay, we determined the kinetic parameters for two PET hydrolases, DuraPETase and LCC_{ICCG}, and verified the underlying assumption of steady-state reaction rates. This new continuous assay enables fast exploration and robust kinetic characterization of PET degrading enzymes.

1. Introduction

Over the last century, synthetic polymers have become an integral part of modern life due to their versatile and durable properties [1,2]. Accordingly, the production of plastics has increased rapidly, reaching an annual production of 367 Mt in 2020 [3]. This high production has led to an increasing amount of plastic waste, which due to poor collecting rates, poses an ecological challenge due to its accumulation in landfills and marine environments [4].

Although the most widely used plastics are synthetic polymers, new discoveries have shown that microbial enzymes are capable of degrading certain types, notably poly(ethylene terephthalate) (PET) [5–7]. These discoveries have provided a new starting point for enzyme-driven PET recycling [8,9]. The enzymes that are active on PET include certain esterases (EC 3.1.1.1 and EC 3.1.1.2), lipases (EC. 3.1.1.3), cutinases (EC 3.1.1.74), and notably the new class of enzymes categorized as PET hydrolases (PETases) (EC 3.1.1.101) [6,7]. Currently, several efforts focus on discovery, characterization, and protein engineering of PET degrading enzymes [10–12].

Proper performance assessment and comparison of PET degrading enzymes relies on robust and accurate assays. Several different analytical methods have been established for investigating the enzymatic degradation of PET [13]. A few of these assays permit continuous analysis, e.g. involving pH-stat [14], turbidimetry [15], calorimetry [16], or impedance spectroscopy measurement [17]. However, none of these continuous assays fulfill the requirement for assessing the enzymatic degradation of PET in a simple setup that permits small reaction volumes (to test limited amounts of enzymes) and allows for multiple reactions to be run in parallel.

Suspension-based assays that apply UV-absorption spectroscopy to detect the hydrolysis products are among the most commonly used for PET hydrolases [18–20]. The analytical principle of these UV-absorption assays is based on the high absorbance of the phenyl-groups present in the soluble enzymatic degradation products of PET, i.e. terephthalic acid

Abbreviations: PET, poly(ethylene terephthalate); BHET, bis(2-hydroxyethyl) terephthalate; MHET, mono(2-hydroxyethyl)terephthalic acid; TPA, terephthalic acid.

* Corresponding author.
E-mail address: asme@dtu.dk (A.S. Meyer).

[1] These authors contributed equally to this study.

https://doi.org/10.1016/j.enzmictec.2022.110142
Received 14 August 2022; Received in revised form 1 October 2022; Accepted 12 October 2022
Available online 14 October 2022

(TPA), mono(2-hydroxyethyl)terephthalic acid (MHET), and bis (2-hydroxyethyl)terephthalic acid (BHET) [21,22]. A limitation of the UV absorbance assay is that PET itself absorbs at 240 nm and thus that larger insoluble substrate particles result in light scattering. It is therefore not possible to run the reaction continuously in a plate reader using a standard microplate, as the presence of the PET substrate interferes with the measurement, and the assays must therefore be run discontinuously. Such discontinuous assays usually require a significant amount of diligent manual sampling to attain accurate and comparable results, and since the enzymatic degradation of PET is a slow process that furthermore only slowly achieves a steady-state, especially at increased substrate crystallinity [18,23–25], the sampling usually has to take place over extended time periods.

Here, we demonstrate and validate a compartmentalized UV absorbance assay for continuous detection of soluble hydrolysis products during enzymatic degradation PET, i.e., a continuous assay that can be run in UV-transparent microplates. The applicability of the continuous assay is evaluated through inverse Michaelis-Menten (^{inv}MM) kinetics [26] on two thermostable PET degrading enzymes: LCC_{ICCG}, a variant of the leaf-branch compost cutinase (LCC) [12], and DuraPETase, a variant of the *Ideonella sakaiensis* PETase [27], and by analyzing the simulated rates of mixing of the hydrolysis products versus the enzyme catalyzed product formation rates.

2. Materials and methods

2.1. Enzymes

LCC_{ICCG} was heterologously expressed in *E. coli* SHuffle T7 competent cells (New England Biolabs, Ipswich, Massachusetts, USA), while DuraPETase was heterologously expressed in the *E. coli* BL21 (DE3) competent cells (New England Biolabs, Ipswich, MA, USA) as described previously [18].

2.2. Substrate

The PET material used as substrate was 1 mm thick amorphous PET sheets (Goodfellow Cambridge Ltd, Huntingdon, UK) (Cat. No. ES303010), punched into uniform disks (Ø=6 mm) using a generic hole punch. In order to remove the enthalpy relaxation caused by ageing of the polymer, the PET disks were annealed at 85 °C for 5 min, and subsequently quenched in ice water for 30 s as described in [25]. The starting crystallinity of this PET material was 9.1 ± 1.3%, as measured by differential scanning calorimetry (DSC) as described earlier [25].

2.3. Modification of microplates

To allow for continuous spectrophotometric measurements of product formation resulting from PET hydrolase action, a UV-transparent flat-bottom well microplate (made up of polystyrene with UV-transmissible well bottoms) (Corning Inc., Corning, New York, USA) (Cat. No. 3635) was modified to ensure unrestricted passage of soluble enzymatic hydrolysis products between two diagonally adjacent wells (Fig. 1). The modification involved cautious removal of the interjoining walls of two diagonally adjacent wells using a DREMEL® Rotary Tool (with a 4.8 mm routing bit) (DREMEL, Racine, Wisconsin, USA). During experimental runs, one well contained the PET disk (denoted as the reaction well), while the other well (denoted as the analytical well) was used for continuous UV detection of the soluble PET degradation products formed during reaction. The modified plates were subjected to quality control to ensure that the interconnected wells were not leaking into the neighboring wells of each set of diagonally adjacent set of wells (Supplementary information, Fig. S1).

2.4. Continuous activity assays

The continuous assay was used to measure the product formation as a function of time during the action of DuraPETase and LCC_{ICCG}, respectively. Each enzyme was added to the connected wells in dosages ranging from 20 nM to 800 nM in 650 μL of 50 mM Glycine-NaOH buffer at pH 9, and preheated at 50 °C for 10 min in an Epoch 2 microplate spectrophotometer (BioTek, Winooski, Vermont, USA). Subsequently, a PET disk was placed into the reaction well and UV absorbance was detected at 240 nm in the analytical well for up to 90 min at intervals of 45 s. A shaking step lasting 3 s was included between each measurement. The UV absorbance of the enzymatic product formation at 240 nm was converted into molar amounts using commercially available BHET as standard. BHET was chosen as the standard since the molar absorption of BHET has been reported to reflect the sum of the pooled absorbance from all soluble PET degradation products [22]. To verify that this also applied under the experimental conditions in this study, we prepared standard curves for both BHET and MHET (Supplementary information, Fig. S2). On this premise, the molar amounts are given in terms of nmol BHET equivalents (BHETeq). Following enzymatic treatment of a PET disk, the reaction mixture was furthermore analyzed using direct light scatter to ensure that no particles were present that could interfere with the light pathway used to detect product formation (data not shown).

For the ^{inv}MM kinetics analysis, the initial rates, v_i, of the PET hydrolase action were determined from the slopes of the progress curves of the enzyme catalyzed reactions achieved at different enzyme dosage levels, E_0. The kinetic parameters for interfacially acting enzymes are thus described as the inverse maximal reaction rate, $^{inv}V_{max}$, and the inverse Michaelis-constant, $^{inv}K_M$, respectively, derived as previously described [26], i.e. according to Eq. (1):

$$v_i = \frac{^{inv}V_{max} \cdot E_0}{^{inv}K_M + E_0} \quad (1)$$

2.5. Evaporation

Any possible evaporation occurring during the prolonged incubation required for the assay measurements was assessed at 50 °C. This was accomplished by quantifying the residual volume of 650 μL water samples in the microplates after incubation for 0 min, 30 min, 60 min and 120 min. The residual volume was quantified by weighing the

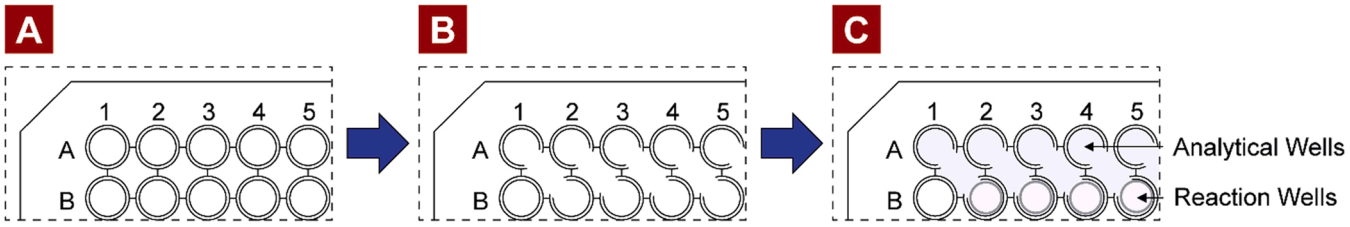

Fig. 1. Schematic representation of the modified microplates. A) Standard UV 96-well micrplate. B) Modified microplate used in the continous asssay. The two digonally adjacent wells were conntected by removing the well walls using a DREMEL® Rotary Tool. C) Experimental set-up of the contious assay. Each connected well is filled with an enzyme solution (light blue color). An insoluble PET substrate is added to the reaction well, while the A_{240} is meassured in the analytical well.

remaining water in a connected set of two diagonal wells by pipetting. In addition, the effect of prolonged incubation on the absorbance of a 100 μM BHET solution (650 μL) was evaluated over a 2 h incubation period at 50 °C.

2.6. Mixing of BHET between the wells

A study was conducted to quantify the rate of mixing of the soluble hydrolysis products (solutes) in the reaction well and the analytic well. To investigate any potential influence of the presence of the PET disk on the mass transfer of soluble products, the experiment was conducted with and without the presence of a PET disk in the reaction well (Supplementary information, Fig. S3). It was assumed that the mixing of the contents in the reaction- and analytical well can be described as a well-mixed two tank system with a constant molar flow in both directions, i.e. according to the following kinetic scheme (2):

$$n_{rw} \underset{k_r}{\overset{k_f}{\rightleftharpoons}} n_{aw} \tag{2}$$

Here n_{rw} and n_{aw} are the molar amount of solutes in the reaction- and analytical well, while k_f and k_r are the rate constants for the forward and reverse mass flow, respectively. At equilibrium, the concentration of solutes is the same in both wells, thus corresponding to an equilibrium constant equal to 1. Since both wells have the same volume, it follows that the rate constants, k_f and k_r, must be the same. Hence, $k_f = k_r = k$. A differential equation of the change in n_{rw} with time, t, can be derived from the kinetic scheme in (3):

$$\frac{\Delta n_{aw}}{\Delta t} = k \cdot n_{rw}(t) - k \cdot n_{aw}(t) \tag{3}$$

The $n_{rw}(t)$ at a given time can furthermore be expressed as function of $n_{aw}(t)$:

$$n_{rw}(t) = 2 \cdot n_{eq} - n_{aw}(t) \tag{4}$$

Here n_{eq} is the molar amount in both wells at equilibrium. By adding (4) to (3) and integrating the equation an expression of $n_{aw}(t)$ emerges (Eq. (5)):

$$n_{aw}(t) = n_{eq} + \exp(-2 \cdot k \cdot t) \cdot c \tag{5}$$

Here c is the constant of integration. The rate constant k of the system was quantified by fitting experimental data to (5). A global fit, at which k was fixed, was performed using OriginPro software (OriginLab Corporation, Northampton, Massachusetts, USA). An additional experiment was conducted to verify that the mixing constant of MHET was similar to that of BHET (Supplementary information, Fig. S3).

2.7. Simulation of mixing of solutes during enzymatic reactions

The response of the system, was evaluated by simulating the amount of solutes in both wells, coupling (3) with an expression of the change of solutes in the reaction well, which can be described as in Eq. (6):

$$\frac{\Delta n_{rw}}{\Delta t} = V \cdot v + k \cdot n_{aw}(t) - k \cdot n_{rw}(t) \tag{6}$$

Here V denotes the total volume of the connected wells, while v is the product formation rate of the enzymatic reaction occurring in the reaction well. It was assumed that the concentration of substrate was in such excess that $v \approx v_i$ during the course of the reactions included in the simulation.

The product formation rate of the experimental data was then simulated by solving the differential Eqs. (3) - (6) numerically using MATLAB software (MathWorks, Natick, Massachusetts, USA). The observed product formation rates at the linear regions of the progress curves along with the estimated rate constant of the mixing were used as input values in the simulation.

3. Results and discussion

3.1. Continuous detection soluble products by UV spectrophotometry

The release of soluble products from the hydrolysis of PET using two PET hydrolases, DuraPETase and LCC_{ICCG}, was monitored continuously via detection by UV absorption. By connecting two adjacent wells in a microplate by removing the wall structure between two diagonally positioned wells, it was possible to run the enzymatic reaction in the reaction well while detecting the UV absorbance of the supernatant in the analytical well. During enzymatic hydrolysis, the insoluble PET disk was physically retained in the reaction well by the compartmentalized design of the interconnected wells. This compartmentalization prevented any interference to the optical light path used for absorbance measurements in the analytical well. Although one side of the PET disk faced downwards towards the bottom of the microplate, the accessibility of the enzymes to both sides of the substrate PET disk was not restricted (Supplementary information, Fig. S4).

A schematic representation of the plate design is displayed in Fig. 1.

3.2. Inverse Michaelis-Menten kinetics of two thermostable PET hydrolases

The performance of the continuous assay was evaluated by quantifying the kinetic parameters ${}^{inv}V_{max}$ and ${}^{inv}K_M$, for both LCC_{ICCG} and DuraPETase. The enzymatic reaction rates at various enzyme concentrations were obtained for each enzyme by monitoring the product formation in the analytical well during enzymatic treatment. Reactions were performed at 50 °C, corresponding to the maximal incubation temperature of the plate reader, and at pH 9, the pH optimum of both LCC_{ICCG} and DuraPETase [18].

The absorbance of a solute measured in the plate reader is only proportional to its concentration within a certain range (i.e. Lambert-Beer's law). The upper detection limit of the product formation, measured by the continuous assay, is therefore limited to the range of this proportionality which corresponded to an upper limit of ~80 nmol BHETeq (Supplementary information, Fig. S2).

The progress curves at various enzyme concentrations of LCC_{ICCG} and DuraPETase are displayed in Fig. 2. A distinct lag phase in the progression of the product formation was observed during the initial treatment (~30–80 min depending on the conditions). After this point, the rate stabilized at a constant, which we define as the initial steady state rate. The rates were converted into μM min^{-1} by dividing the initial rates, determined from Fig. 2A and B, with the starting volume (650 μL).

The estimated rates were plotted against the enzyme concentration (Fig. 3A and B) and fitted to the ^{inv}MM equation, displayed in Eq. 1, to obtain the kinetic parameters, ${}^{inv}V_{max}$ and ${}^{inv}K_M$, listed in Table 1.

No significant difference were observed between the ${}^{inv}K_M$ of LCC_{ICCG} and DuraPETase. These values were in the same range as previously reported ${}^{inv}K_M$ values of other PET degrading enzymes [19,28].

The ${}^{inv}V_{max}$, on the other hand, was more than 6-fold higher for LCC_{ICCG} compared to DuraPETase; the ${}^{inv}V_{max}$ is interpreted as the maximum rate the enzyme can achieve on an insoluble substrate, and implies that all accessible attack sites on the surface of the substrate are constantly occupied by the enzyme. The data verify the applicability of the assay for evaluating kinetics of PET hydrolases. The experimental data show that LCC_{ICCG} outperforms DuraPETase at these reaction conditions even if the optimal reaction temperature for LCC_{ICCG} is in fact 20 °C higher.

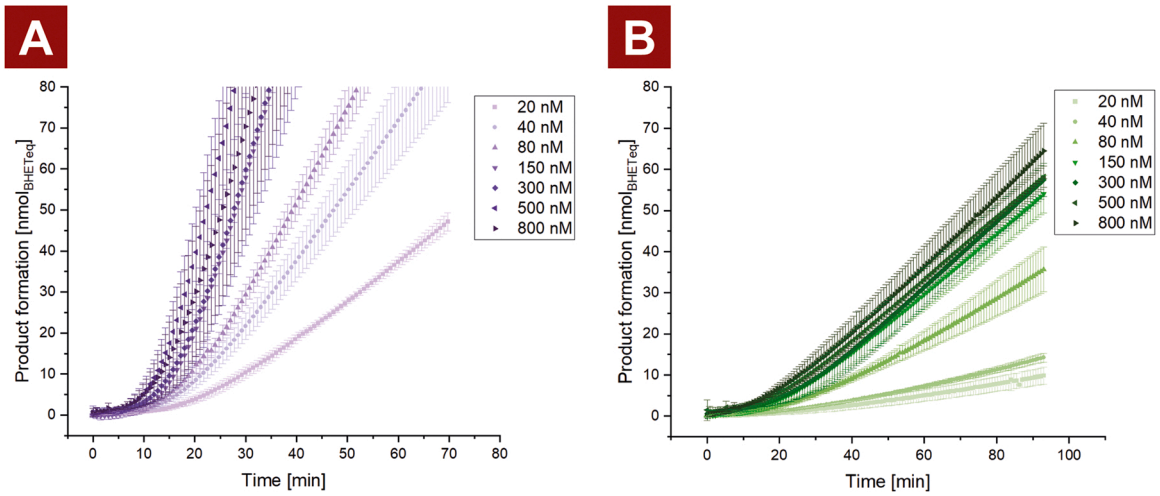

Fig. 2. Progress curves at various initial enzyme concentrations (20–800 nM) for A) LCC_{ICCG} and B) DuraPETase. The reactions were performed at 50 °C in 50 mM Glycine-buffer pH 9 for a maximum of 100 min. The data points and error bars represent the average value and standard deviations (n = 3).

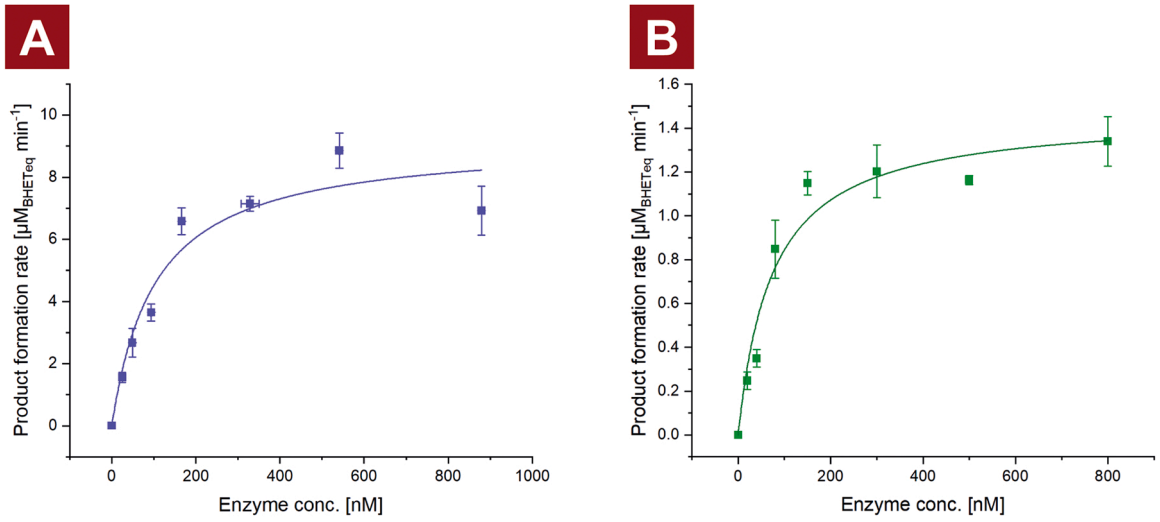

Fig. 3. Inverse Michaelis-Menten (^{inv}MM) curves of A) LCC_{ICCG} and B) DuraPETase displaying the product formation rates as a function of the enzyme load. The symbols and error bars represent the average and standard deviation (n = 3) of the linear region of the experimental data. The solid lines are non-linear regression fit of the experimental data to the ^{inv}MM equation (Eq. (1)). The reactions were performed at 50 °C in 50 mM Glycine-buffer pH 9 for a maximum of 100 min. Enzyme dosages and product levels were adjusted to account for water evaporation during the course of reaction.

Table 1
Kinetic constants derived from the ^{inv}MM fits of LCC_{ICCG} and DuraPETase shown in Fig. 3. The values are the fit parameters ± the standard deviation of these based on three replicate measurements for each enzyme. Different superscript letters a and b indicate statistically significant differences between the data for each enzyme ($p < 0.05$), where a is significantly higher than b.

	$^{inv}K_M$ [nM]	$^{inv}V_{max}$ [μM$_{BHETeq}$ min^{-1}]
LCC_{ICCG}	$104^a \pm 35$	$9.2^a \pm 0.9$
DuraPETase	$101^a \pm 28$	$1.5^b \pm 0.1$

3.3. Validation of the continuous assay

3.3.1. Evaporation

As the continuous assay is an open system, water may evaporate from the wells during incubation in the plate reader. A reduction in the reaction volume is therefore expected to occur during the enzymatic reactions. The evaporation from the interconnected wells was monitored at standard reaction conditions (50 °C over a 2 h incubation period) (Fig. 4A). This corresponded to a linear evaporation rate of 2.15 ± 0.13 μL min^{-1}. It can therefore be expected that ~40% of the total reaction volume had evaporated after two hours of incubation. The enzyme concentrations from Fig. 3 A and B were therefore adjusted according to the expected residual volume, at the time at which the rates were calculated. This was done to account for the increasing enzyme concentration caused by evaporation.

The effect of prolonged incubation on the absorbance of reaction products, was evaluated by incubating 72 nmol of BHET at standard conditions (Fig. 4B). A constant signal was observed during the two hours of incubation, despite a ~40% reduction in the sample volume caused by the evaporation. This phenomenon can be explained by the Lambert-Beer's law ($A = C \cdot l \cdot \varepsilon$), as the increase in concentration, (C), caused by the reduction in sample volume, is inversely proportional with the length of the optical light path (l), at which the absorbance measure is taken.

Threfore, we consider it a fair assumption that the absorbance monitored by the continuous assay is representative with the actual

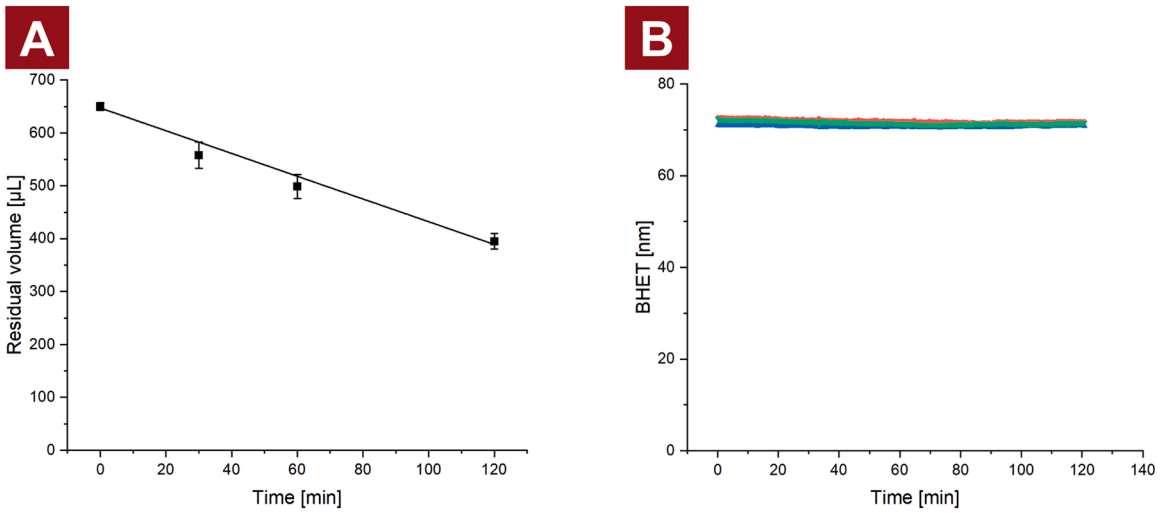

Fig. 4. A) Correlation between residual volume of 650 µL water samples and incubation time at 50 °C, the correlation follows a linear trend (y = -(2.15 ± 0.13) x + 647 ± 7, R^2 0.99). The average volume and standard deviation (n = 3) are represented by data points and error bars. B) Change in signal, in nmol BHETeq of three individual samples (represented by red, black, or blue data points) of 72 nmol BHET during 120 min incubation at 50 °C.

molar amount of BHETeq released during the enzyme reaction.

3.3.2. *Mixing of solutes between the wells*

A key prerequisite for the continuous assay is that sufficient mixing of contents in the interconnected wells is achieved. We note that the reaction mixture is subjected to physical shaking which dictates that the mass transfer of soluble products between the wells cannot be regarded as diffusion alone, but instead as a combined effect of diffusion and mixing. This will allow the system to obtain a steady-state, at which the product formation rate measured in the analytical well is equal to the rate of the enzymatic reaction in the reaction well.

The rate constant of the mixing was quantified by monitoring the absorbance in the analytical well, after a small amount of a concentrated BHET suspension had been added into the reaction well of individual samples (Fig. 5). The mixing constant of the system was estimated to be 0.247 ± 0.002 min^{-1} using global fitting of the experimental data (Fig. 5) to Eq. (5).

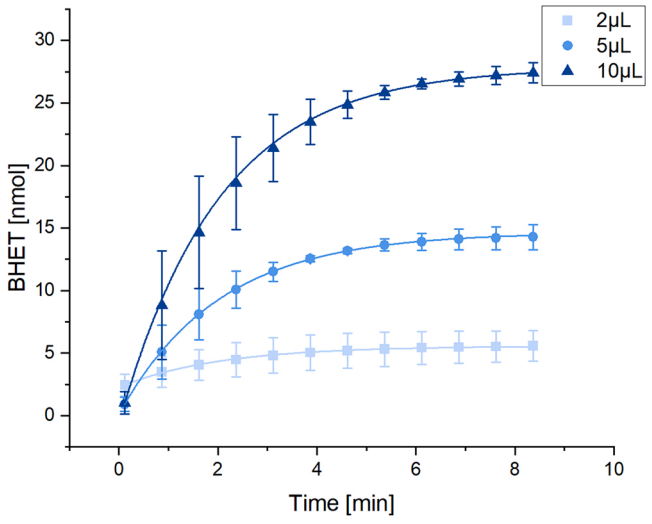

Fig. 5. A) Change in BHETeq in the analytical well after adding of three different volumes of a concentrated BHET suspension (2.5 mM) into the reaction well. The average and standard deviation (n = 3) of the experimental data is represented by data points and error bars. The solid lines represent the non-linear global fit of Eq. (5) to the experimental data.

As a consequence of the separation of the reaction well and the analytical well, a delay in the observed product formation rate is expected during the initial incubation. This delay, determined by the mixing rate constant, is equivalent to the time it takes for the detected rate in the analytical well to be equivalent to the product formation rate in the reaction well. The expected product formation measured in the analytical well was simulated using the differential Eqs. (3) and (6) using the estimated rate constant from Fig. 5 and the rate of the linear regions from Fig. 2A and B as input values. This was done to compare the acceleration of the rate observed experimentally with the acceleration associated with the time delay caused by the mixing.

A comparison between the observed and simulated product formation in the analytical well is displayed in Fig. 6A, while the on-set time, defined as the time it takes to reach 95% of the product formation rate at steady state, is displayed in Table 2.

From Fig. 6A it is evident that the reaction rate of the simulated product formation reaches a steady-state after 8 min which, depending on the conditions, was 3.5–10 times faster than the corresponding actual rates. The mixing constant was neither affected by the presence of a PET disk in the reaction well or the type of hydrolysis products (i.e., BHET or MHET) (Supplementary information, Table S1). However, the mixing constant was apparently affected by other parameters, including the specific dimensions of the passage between the interconnected wells in the prepared microplates. As outlined in 2.3 we therefore recommend complete removal of the interjoining walls of two diagonally adjacent wells for successful assay results. The mixing constant used in this study for simulating product formation was conservatively selected to represent the lowest experimental mixing constant obtained throughout our study. The data emphasize the importance of continuous monitoring of the product formation when quantifying the reaction rates, as single end-point measures may result in an underestimation of the rates.

4. Conclusion

In order to thoroughly study the characteristics of PET hydrolases, it is important to assess the progression of the rate by which soluble hydrolysis products are released from a PET sample during enzymatic treatment. In this study, we demonstrated the applicability of our continuous activity assay for the quantification of released soluble hydrolysis products from PET disks treated with two PET hydrolases, DuraPETase or LCC_{ICCG}.

Both enzymes showed a clear trend where the initial rate increased gradually until a constant rate had been reached. In turn, these constant

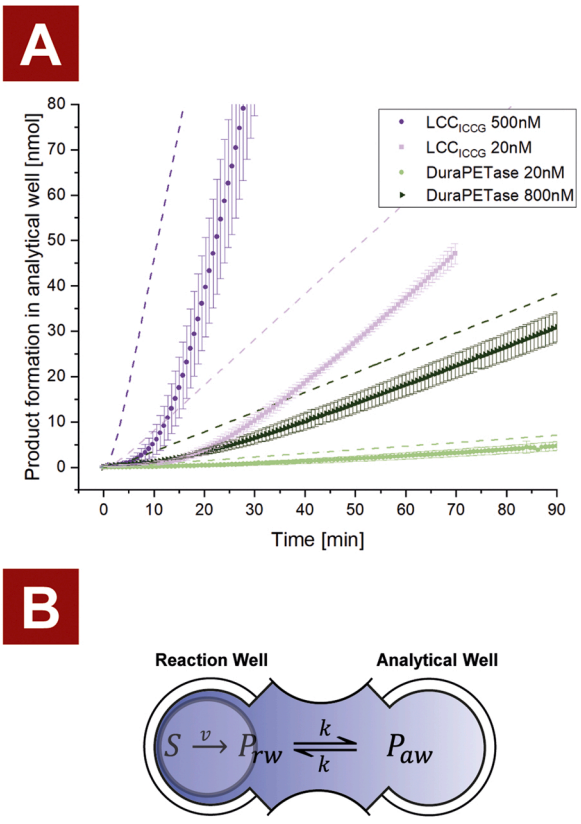

Fig. 6. A) Comparison of a simulated product formation (dashed lines) in the analytical well with the experimentally obtained product formation data (progress curves from Fig. 2 (points)). These progress curves include the enzyme loads that correspond to the lowest and highest product formation rates obtained for LCC$_{ICCG}$ (purple) and DuraPETase (green). The simulated progress curves were calculated as the amount of hydrolysis products constrained to the analytical well (V=325 μL). Thus, for comparison, the product formation of the simulated data were multiplied by 2 to adjust for the difference in reaction volume between one and two wells. B) Kinetic reaction scheme used for the simulation model.

Table 2
Product formation rates and on-set times for enzymatic reactions achieved at low and high dosage levels of each enzyme, LCC$_{ICCG}$ and DuraPETase. On-set time is defined as the time it takes to reach 95% of the product formation rate for the experimental observation and the simulation of the progress curves (Fig. 6A).

	Product formation rate [nmol min^{-1}]	**On-set time Simulated data** [min]	**On-set time Experimental data** [min]
500 nM LCC$_{ICCG}$	5.75	8	28
20 nM LCC$_{ICCG}$	1.01	8	56
800 nM DuraPETase	0.87	8	58
20 nM DuraPETase	0.16	8	83

rates were used to derive kinetic parameters under the assumption of steady-state kinetics. The results obtained were in line with values reported in the literature. In summary, this continuous activity assay offers a novel tool for further characterization of PET degrading enzymes. The continuous monitoring assay is fast and simple, and has potential as a high-throughput method for kinetic assessment of new putative PET degrading enzymes or engineered PET hydrolases in expression libraries.

As a final remark it is important to state that this assay is not limited to the characterization of PET degrading enzymes, as it can be used to characterize other enzyme working on insoluble substrates. This does only require that the products from enzymatic reactions can be measured by absorbance or other types of optical spectroscopy.

CRediT authorship contribution statement

Thore Bach Thomsen: Conceptualization, Investigation, Methodology, Visualization, Formal analysis, Writing. **Sune W. Schubert:** Conceptualization, Investigation, Methodology, Formal analysis, Writing. **Cameron J. Hunt:** Conceptualization, Methodology, Formal analysis, Funding acquisition, Resources, Writing. **Peter Westh:** Supervision, Funding acquisition. **Anne S. Meyer:** Conceptualization, Project administration, Supervision, Funding acquisition, Resources, Writing.

Declaration of Competing Interest

There are no competing interest to declare. All authors declare no conflict of interests.

Data availability

Data will be made available on request.

Acknowledgments

Funding from The H.C. Ørsted Cofund Postdoc Program, Technical University of Denmark. We also wish to thank Camilo Andres Amaya Chica for excellent technical support during the assay development.

Appendix A. Supporting information

Supplementary data associated with this article can be found in the online version at doi:10.1016/j.enzmictec.2022.110142

References

[1] J.H. Lee, K.S. Lim, W.G. Hahm, S.H. Kim, Properties of recycled and virgin poly (ethylene terephthalate) blend fibers, J. Appl. Polym. Sci. 128 (2013) 1250–1256, https://doi.org/10.1002/app.38502.
[2] T. Thiounn, R.C. Smith, Advances and approaches for chemical recycling of plastic waste, J. Polym. Sci. 58 (2020) 1347–1364, https://doi.org/10.1002/pol.20190261.
[3] Plastics Europe Market Research Group (PEMRG), Conversio Market & Strategy GmbH. Plastics Europe Association of Plastics Manufacturers Plastics—The Facts 2021 An analysis of European Plastics Production, Demand Waste Data (2021).
[4] R. Geyer, J.R. Jambeck, K.L. Law, Production, use, and fate of all plastics ever made, Sci. Adv. (2017) 3, https://doi.org/10.1126/sciadv.1700782.
[5] M.A.M.E. Vertommen, V.A. Nierstrasz, M.Van Der Veer, M.M.C.G. Warmoeskerken, Enzymatic surface modification of poly(ethylene terephthalate), J. Biotechnol. 120 (2005) 376–386, https://doi.org/10.1016/j.jbiotec.2005.06.015.
[6] Y. Shosuke, H. Kasumi, T. Toshihiko, T. Ikuo, Y. Hironao, M. Yasuhito, et al., A bacterium that degrades and assimilates poly(ethyleneterephthalate), Science (80-) 351 (2016) 1196–1199.
[7] P.C.F. Buchholz, Golo Feuerriegel, H. Zhang, P. Perez-Garcia, L.-L. Nover, Jennifer Chow, et al., Plastics degradation by hydrolytic enzymes: The plastics-active enzymes database—PAZy, Proteins Struct. Funct. Bioinforma. (2022), https://doi.org/10.1002/PROT.26325.
[8] R. Wei, W. Zimmermann, Microbial enzymes for the recycling of recalcitrant petroleum-based plastics: how far are we? Micro Biotechnol. 10 (2017) 1308–1322, https://doi.org/10.1111/1751-7915.12710.
[9] A. Carniel, V. Waldow, A. de, A.M. de Castro, A comprehensive and critical review on key elements to implement enzymatic PET depolymerization for recycling purposes, Biotechnol. Adv. (2021) 52, https://doi.org/10.1016/j.biotechadv.2021.107811.
[10] H.P. Austin, M.D. Allen, B.S. Donohoe, N.A. Rorrer, F.L. Kearns, R.L. Silveira, et al., Characterization and engineering of a plastic-degrading aromatic polyesterase, Proc. Natl. Acad. Sci. USA 115 (2018) E4350–E4357, https://doi.org/10.1073/pnas.1718804115.
[11] H. Lu, D.J. Diaz, N.J. Czarnecki, C. Zhu, W. Kim, R. Shroff, et al., Machine learning-aided engineering of hydrolases for PET depolymerization, Nat 2022 6047907 604 (2022) 662–667, https://doi.org/10.1038/s41586-022-04599-z.

[12] V. Tournier, C.M. Topham, A. Gilles, B. David, C. Folgoas, E. Moya-Leclair, et al., An engineered PET depolymerase to break down and recycle plastic bottles, Nature 580 (2020) 216–219, https://doi.org/10.1038/s41586-020-2149-4.
[13] V. Pirillo, L. Pollegioni, G. Molla, Analytical methods for the investigation of enzyme-catalyzed degradation of polyethylene terephthalate, FEBS J. 288 (2021) 4730–4745, https://doi.org/10.1111/febs.15850.
[14] Å.M. Ronkvist, W. Xie, W. Lu, R.A. Gross, Cutinase-Catalyzed hydrolysis of poly (ethylene terephthalate, Macromolecules 42 (2009) 5128–5138, https://doi.org/10.1021/ma9005318.
[15] M.R. Belisário-Ferrari, R. Wei, T. Schneider, A. Honak, W. Zimmermann, Fast Turbidimetric Assay for Analyzing the Enzymatic Hydrolysis of Polyethylene Terephthalate Model Substrates, Biotechnol. J. 14 (2019) 10–14, https://doi.org/10.1002/biot.201800272.
[16] K. Vogel, R. Wei, L. Pfaff, D. Breite, H. Al-Fathi, C. Ortmann, et al., Enzymatic degradation of polyethylene terephthalate nanoplastics analyzed in real time by isothermal titration calorimetry, Sci. Total Environ. 773 (2021), 145111, https://doi.org/10.1016/j.scitotenv.2021.145111.
[17] R. Frank, D. Krinke, C. Sonnendecker, W. Zimmermann, H.G. Jahnke, Real-Time Noninvasive Analysis of Biocatalytic PET Degradation, ACS Catal. 12 (2022) 25–35, https://doi.org/10.1021/ACSCATAL.1C03963/ASSET/IMAGES/LARGE/CS1C03963_0004.JPEG.
[18] T.B. Thomsen, C.J. Hunt, A.S. Meyer, Influence of substrate crystallinity and glass transition temperature on enzymatic degradation of polyethylene terephthalate (PET), N. Biotechnol. 69 (2022) 28–35, https://doi.org/10.1016/j.nbt.2022.02.006.
[19] J. Arnling Bååth, K. Borch, K. Jensen, J. Brask, P. Westh, Comparative Biochemistry of Four Polyester (PET) Hydrolases, ChemBioChem 22 (2021) 1627–1637, https://doi.org/10.1002/cbic.202000793.
[20] Y. Ma, M. Yao, B. Li, M. Ding, B. He, S. Chen, et al., Enhanced poly(ethylene terephthalate) hydrolase activity by protein engineering, Engineering 4 (2018) 888–893, https://doi.org/10.1016/j.eng.2018.09.007.
[21] E.Z.L. Zhong-Johnson, C.A. Voigt, A.J. Sinskey, An absorbance method for analysis of enzymatic degradation kinetics of poly(ethylene terephthalate) films, Sci. Rep. 2021 111 11 (2021) 1–9, https://doi.org/10.1038/s41598-020-79031-5.
[22] J. Arnling Bååth, K. Borch, P. Westh, A suspension-based assay and comparative detection methods for characterization of polyethylene terephthalate hydrolases, Anal. Biochem (2020) 607, https://doi.org/10.1016/j.ab.2020.113873.
[23] A.C. Chang, A. Patel, S. Perry, Y.V. Soong, C. Ayafor, H.W. Wong, et al., Understanding Consequences and Tradeoffs of Melt Processing as a Pretreatment for Enzymatic Depolymerization of Poly(ethylene terephthalate, Macromol. Rapid Commun. (2022) 2100929, https://doi.org/10.1002/marc.202100929.
[24] R.K. Brizendine, E. Erickson, S.J. Haugen, K.J. Ramirez, J. Miscall, A.R. Pickford, et al., Particle size reduction of poly(ethylene terephthalate) increases the rate of enzymatic depolymerization but does not increase the overall conversion extent, ACS Sustain Chem. Eng. 10 (2022) 9131–9149, https://doi.org/10.1021/acssuschemeng.2c01961.
[25] T.B. Thomsen, C.J. Hunt, A.S. Meyer, Standardized method for controlled modification of poly (ethylene terephthalate) (PET) crystallinity for assaying PET degrading enzymes, MethodsX 9 (2022), 101815, https://doi.org/10.1016/J.MEX.2022.101815.
[26] J. Kari, M. Andersen, K. Borch, P. Westh, An inverse michaelis-menten approach for interfacial enzyme kinetics, ACS Catal. 7 (2017) 4904–4914, https://doi.org/10.1021/acscatal.7b00838.
[27] Y. Cui, Y. Chen, X. Liu, S. Dong, Y. Tian, Y. Qiao, et al., Computational Redesign of a PETase for Plastic Biodegradation under Ambient Condition by the GRAPE Strategy, ACS Catal. 11 (2021) 1340–1350, https://doi.org/10.1021/acscatal.0c05126.
[28] J. Arnling Bååth, K. Jensen, K. Borch, P. Westh, J. Kari, Sabatier principle for rationalizing enzymatic hydrolysis of a synthetic polyester, JACS Au 2 (2022) 1223–1231, https://doi.org/10.1021/jacsau.2c00204.

Intentionally left blank

Paper VI

Current knowledge on the effect of substrate crystallinity of Poly(ethylene terephthalate) (PET) on its enzymatic degradation.

Thore B. Thomsen, Kristoffer Almdal, Anne S. Meyer

Submitted

VI

Intentionally left blank

Significance of poly(ethylene terephthalate) (PET) substrate crystallinity on enzymatic degradation

Thore Bach Thomsen[a], Kristoffer Almdal[b], Anne S Meyer[a*]

[a]Department of Biotechnology and Biomedicine, DTU Bioengineering, Protein Chemistry and Enzyme Technology Section, Building 221, Technical University of Denmark, 2800 Kgs. Lyngby, Denmark

[b]DTU Chemistry, Building 206, Technical University of Denmark, 2800 Kgs. Lyngby, Denmark

[*] Corresponding author: asme@dtu.dk, address as above

Abstract

Poly(ethylene terephthalate) (PET) is a semi-crystalline plastic polyester material with a global production volume of 83 Mt/year. PET is mainly used in textiles, but also widely used for packaging materials, notably plastic bottles, and a major contributor to environmental plastic waste accumulation. Currently, less than 10% of PET is recycled; however, now that enzymes have been demonstrated to catalyze PET degradation, new options for sustainable bio-recycling of PET materials via enzymatic catalysis have emerged. The enzymatic degradation rate is strongly influenced by the properties of PET, notably the degree of crystallinity, X_C: The higher the X_C of the PET material, the slower the enzymatic rate. Crystallization of PET, resulting in increased X_C, is induced thermally (via heating) and/or mechanically (via stretching), and the X_C of most PET plastic bottles and microplastics exceeds what currently known enzymes can readily degrade. The enzymatic action occurs at the surface of the insoluble PET material and improves when the polyester chain mobility increases. The chain mobility increases drastically when the temperature exceeds the glass transition temperature, T_g, which is ~40°C at the surface layer of PET. Since PET crystallization starts at 70°C, the ideal temperature for enzymatic degradation is just below 70°C to balance high chain mobility and enzymatic reaction activation without inducing crystal formation. This paper reviews the current knowledge on the properties of PET as an enzyme substrate and summarizes the most recent knowledge of how the crystalline and amorphous regions of PET form, and how the X_C and the T_g impact the efficiency of enzymatic PET degradation.

Keywords: Polyester; Plastic bottles; Substrate crystallinity; PET hydrolases; PET recycling.

Abbreviations: BHET, Bis(2-Hydroxyethyl) terephthalate; EG, ethylene glycol; MAF, mobile amorphous fraction; MHET, mono(2-hydroxyethyl)terephthalic acid; RAF, rigid amorphous fraction; T_g, glass transition temperature; TPA, terephthalic acid; X_C, degree of crystallinity.

1. Introduction

Plastic pollution has become a global environmental concern due to the ubiquitous presence of plastics within aquatic and terrestrial environments [1,2]. Still, the annual demand for plastics keeps increasing 3-4% per year, and the global annual production of plastics reached ~390 Mt in 2021 (excluding plastics used in textile fibers), with 90% produced from fossil-based feedstock [3]. By including the production of synthetic textile fibers, which amounts to 68.2 Mt/year [4], the total global plastic production is nearly ~460 Mt/year.

Poly(ethylene terephthalate) (PET) is a type of polyester plastic, which is mainly used for textile fibers, but also renowned as the most widely used type of plastic used for plastic bottles, notably single-use bottles for soft drinks and water [3,5]. Such single-use plastic bottles are categorized as post-consumer packaging materials. Because of their short lifespan and low collection rate, post-consumer packaging materials are major contributors to plastic pollution. The total annual production of post-consumer packaging materials is currently 72 Mt, of which 32% is leaked outside the collection system [6], and ultimately ending up as plastic pollution in both marine and terrestrial environments [7].

Various regional, national, and global policies have been implemented to mitigate plastic pollution and promote a circular economy of plastics [8,9]. To highlight the urgency, it is noted, that the European Union Directive (EU) 2019/904 has set a collection target of 90% of single-use plastics by 2029, as well as a requirement that by 2025, at least 25% of plastic bottles within the EU contain recycled plastics (30% by 2030) [10].

PET is a semi-crystalline thermoplastic type of polyester and is manufactured at a global production volume of ~83 Mt/year, thus constituting 52% of the total global fiber production [4] and 6.2% of the global plastic production (textiles excluded) [3]. The newest PET production data from Europe include about 10% recycled PET, indicating a profound increase in recycling. Yet, most of the globally produced PET is synthesized from scratch from fossil oil via oxidation of the aromatic hydrocarbon compound *p*-xylene, derived directly from petroleum, to terephthalic acid (TPA) [11]. The PET polyester resin is then obtained by esterification or transesterification between TPA or dimethyl terephthalate and ethylene glycol (EG), followed by polymerization [12]. For use as packaging material or bottles, the PET resin is manufactured to the desired shape via injection molding (blow-molding) or extrusion. A recent life-cycle-assessment of PET bottles showed that 84% of the environmental burden quantified in terms of resource consumption, climate change, ecosystem quality, and human health is caused by the production of PET resin [5].

To address the negative environmental impact of plastics - including PET - there is obviously an urgent need to drastically intensify sustainable recycling efforts. The conventional methods for recycling of PET principally involve mechanical and thermal treatment, *i.e.*, washing and shredding of the material, and then regranulation via extrusion [13]. In the case of PET, this type of mechanical recycling typically results in a lower quality of the recycled product compared to the original (virgin) material. Specifically, the treatment causes changes in appearance, meaning color and brittleness, and in material properties at the molecular level such as lower molecular weight (M_w), polymer chain length (M_n), polydispersity index (M_w/M_n), resulting in decreased

tensile strength. The crystallization rates of recycled PET also increase leading to a higher X_C of the re-processed products [14–16]. In addition, the existing commercially viable recycling processes are constrained to certain PET products, as not all PET products can be effectively recycled by classic means. This includes textile blends of different fiber types such as polyester, cotton, etc., which are common in clothing and other textile fabrics [17].

Development and implementation of new technologies are therefore clearly required in order to facilitate higher recycling rates and improve the quality of the recycled products [18]. Plastics, including PET, are considered resistant to biodegradation. However, the realization that certain enzymes can catalyze degradation of PET [19,20], notably the discovery in 2016 of the bacterium *Ideonella sakaiensis*, that can use PET as its major carbon and energy source for growth [21], has significantly boosted the efforts for sustainable PET recycling, notably recycling of PET plastic bottles, yielding high quality recycled products. PET degrading enzymes may also be used to recycle textile blends by specifically degrading the PET polyester fibers alone or in combination with other enzymes that target other fibers in the material, such as cellulases that target cotton, or in combination with a chemical pretreatment [17,22].

Although the continued discovery and protein engineering of efficient PET degrading enzymes have created novel opportunities for industrial biotechnology-based PET recycling, less attention has been paid to the fact that the activity of the PET degrading enzymes is strongly influenced by the physical properties of PET, notably the degree of crystallinity (X_C). The X_C is defined as the fraction of the total PET polymer chains that are in the crystalline structure state [23–25]. In addition, the surface glass transition temperature, T_g, of PET and the local mobility of the amorphous PET chains affect the amenability of PET to enzymatic attack and degradation. This paper reviews the enzymatic conversion of PET with particular emphasis on the distinct complexity of PET as a semi-crystalline substrate for enzymatic depolymerization.

1.1. Enzymatic recycling of PET

The use of plastic degrading enzymes in biocatalysis-based recycling of PET has recently been introduced as a new promising technology enabling the production of recycled products of the same quality as the virgin plastic [26], and enzyme-based technology has already shown great potential for industrial-scale PET recycling, thus allowing for closed-loop circular economy processes [24,27]. In addition, unlike thermo-mechanically recycled PET, the enzyme-based approach permits the degradation products to be used as feedstock for the manufacture of other products, including other types of polyester materials such as polyhydroxy alkanoates (PHAs) [28].

Although plastics are man-made polymers, several enzymes are capable of degrading synthetic polyesters, even if they are not their natural substrate [29–31]. The PET hydrolase class, EC 3.1.1.101, was created in 2016 based on the discovery of the PET degrading enzyme enabling *I. sakaiensis* 201-F6 to utilize PET as its sole carbon source. *I. sakaiensis* 201-F6 also secretes a MHETase (EC 3.1.1.102), which catalyzes the further conversion of mono(2-hydroxyethyl)terephthalic acid (MHET), a product of the PET hydrolase reaction, into TPA and EG)[21,32]. The vast majority of PET degrading enzymes are however classified as cutinases (EC 3.1.1.47) [33–35] or carboxyl esterases (EC 3.1.1.1) [36], and certain arylesterases [37] (EC 3.1.1.2) and lipases [23] (EC 3.1.1.3) are also known to be active on PET.

An overview of all characterized PET hydrolases is listed in the plastic active enzymes database, the PaZy database, and it is seen that most of these enzymes originate from either the *Actinobacteriota* or the *Pseudomonadota* phyla [36]. A phylogenetic tree covering all entries from the PaZy database and linking these to their microbial origin (phylum level) and EC numbers are displayed in Figure 1. This phylogenetic tree also displays the dominance of hitherto known PET degrading enzymes originating from Actinobacteria (grey nodes) and Pseudomonadota (turquoise blue nodes), but also reveals that enzymes that have some activity on PET are found in a range of different microbial organisms, including archae (Genbank Accession no. RLI42440, a feruloyl esterase type of enzyme) and fungi (Genbank Accession no. AAA33335.1, a cutinase originating from a *Fusarium* spp.). This variety signifies the diversity of PET hydrolyzing enzymes and underscores the likely possibility that several more may be discovered in the future.

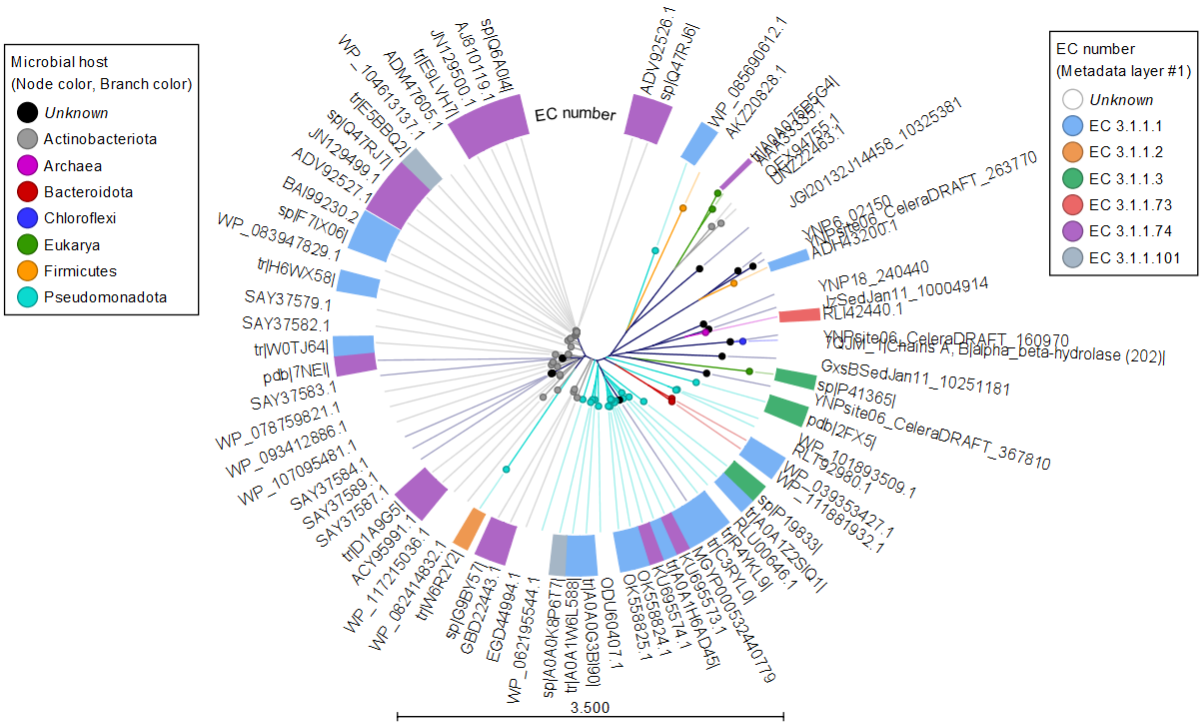

Figure 1. Phylogenic tree of all currently characterized PET hydrolases. The phyla of the microbial host are indicated by node color, while the EC number is highlighted by the surrounding colors of the tree.

2. Features of PET as a semi-crystalline material

PET consists of repeating units of TPA and EG, covalently bound via ester bonds, and it is the ester bonds that are catalytically hydrolyzed by PET degrading enzymes. In the melt state above the melting temperature, T_m, (260°C) PET is a disordered random coil polymer melt. If the melt is cooled sufficiently quickly - quenched – to temperatures below the T_g of PET (75°C for amorphous PET) [25], then the amorphous random coil structure is preserved. However, solid PET is usually in a semi-crystalline state which contains both highly ordered domains (crystals) as well as glassy

amorphous domains. It is the amount of crystals, i.e. the level of highly ordered crystalline domains, which define the X_C of PET polyester materials [38]. Although high cooling rates are readily achievable in standard processing, the material properties such as gas permeability of amorphous PET are not always desirable for the material use [39]. Hence, PET products, including plastic bottles and textile fibers tend to have a high X_C [40,41].

2.1. Crystallization of PET

The crystalline regions - or crystals - in PET material form when the polymeric chains in the amorphous state align, which in turn happens when the chain mobility/energy of the material is sufficiently high. A high chain mobility/energy can be achieved by either thermal or mechanical means, which is why heating and mechanical molding lead to the formation of crystals, and thus an increase in the X_C of the PET material [42]. Thermally induced crystallization takes place at temperatures above the T_g (75°C) [43], and notably occurs when the PET material is slowly cooled from melt or kept at temperatures above the T_g. The crystallization process is quenched by cooling the material to a temperature below the T_g of PET. The rate at which the crystallization occurs increases with temperature, until it reaches its maximum at 174°C [44]. Beyond this temperature, the crystallization rate starts to decrease due to excessive chain mobility. On the other hand, at temperatures below T_g, the mobility of the chains is restricted, leading to limited crystallization [43]. Other factors such as moisture content [45] and molecular weight of the polymers in the PET material [46] also influence the crystallization of PET.

The mechanically induced crystallization of PET may typically be induced via stretching the material. This process is referred to as stress or strain induced crystallization, and requires stretching of the PET material at temperatures above T_g [42]. The X_C caused by strain induced crystallization increases with both temperature and strain rate [47]. The increased crystallinity can lead to improvements in the mechanical properties of PET material such as higher modulus, toughness, stiffness, tensile strength, and hardness [48]. The ability of changing the X_C, and hence the mechanical properties of PET by strain induced crystallization is utilized in many applications of PET processing, most notably in the manufacturing of blow-molded PET bottles, textile fibers, and oriented films [49]. The X_C of a PET material is therefore heavily dependent on its processing history and due to the changes taking place at the molecular chain level, the X_C may not be uniform throughout a PET material. An example of this is illustrated by the X_C of a PET bottle [41], presented in Figure 2. Here it is evident that the finish/neck and base center have a lower X_C (1.2% and 11.7%, respectively) than the rest of the bottle, that has X_C >25% [41]. Furthermore, plastic waste in the environment, including microplastics, may undergo weathering/aging because of solar exposure and thermal aging, which increases the X_C [50].

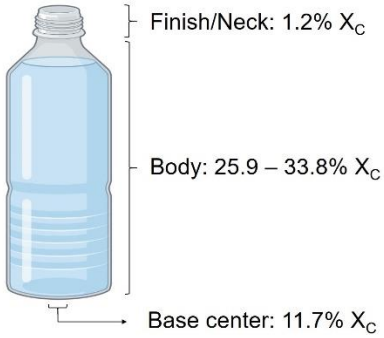

Figure 2. The degree of crystallinity varies in different regions of a PET bottle. The figure is a schematic representation adapted from Lu et. al. [41].

2.2. Details of the structure and morphology of PET crystals

During crystallization, the PET chains undergo a conformational change from a predominantly *trans-gauche-trans* to a linear all-*trans* conformation; a schematic representation of the all-*trans* conformation of a PET chain is shown in Figure 3A. Although the linear all-*trans* conformation of the free PET chain is energetically less favorable than a *trans-gauche-trans* conformation, the all-*trans* confirmation of a crystal structure is stabilized by intermolecular π/π stacking of the aromatic rings of the TPA moieties, which is why the all-*trans* is the prevalent chain conformation in PET crystals [51]. In other words, this means that there is a decrease in *gauche* conformations with increasing X_C [52,53]. The unit cell structure of PET crystals has been extensively studied, and has been shown to form triclinic crystals [54]. However, the unit cell parameters of PET crystals are not universal, as they are highly dependent on the crystallization and manufacturing process parameters. These parameters include the crystallization temperature, draw ratio, and subsequent annealing temperature and time [54].

Within a PET crystal the polymer chains are arranged in densely packed lamellae structures. These crystalline lamellae are separated by amorphous regions, and interconnected by PET chains, known as tie molecules, which are crossing the crystal-amorphous interface [55]. As illustrated in Figure 3B, the morphological parameters of a PET crystal may be quantified in terms of the average crystalline lamellae thickness (l_c), the average interlamellar amorphous layer thickness (l_a), and the long period (L), which is the sum of l_c and l_a [56] (Figure 3B). Due to the effect of temperature and mechanical stress on the crystallization, the morphology of the PET crystal, and hence the values of l_c, l_a, and L are obviously highly dependent on the crystallization process and the processing conditions [56,57].

The crystallization of PET can be divided into nucleation and crystal growth. During nucleation, amorphous PET chains align in the lamellar structure, thus forming the nucleus of a new crystal. The formation of nuclei is followed by the development of the crystals, the crystal/lamellae growth phase. The growth phase can be further divided into two stages, primary and secondary crystallization. Primary crystallization designates the initial stage of crystal growth, which is associated with growth of the heterogeneous crystal structures (as outlined below, this entails that the lamellae and the rigid amorphous fraction structures expand the boundaries of the PET crystal). The secondary crystallization takes place within the boundaries of a crystal structure, and is associated with either thickening (increase in l_c and reduction in l_a) of the lamellae structures

and/or formation of new lamellae within a crystal (formation of spherulites) [44,58]. The crystalline lamellae are furthermore arranged in a higher-level structure. The anatomy of the higher-level structure is also dependent on the crystallization process [59–61]. A simplified representation of the lamellar crystal structures and distribution of the crystal structures is illustrated in Figure 3C.

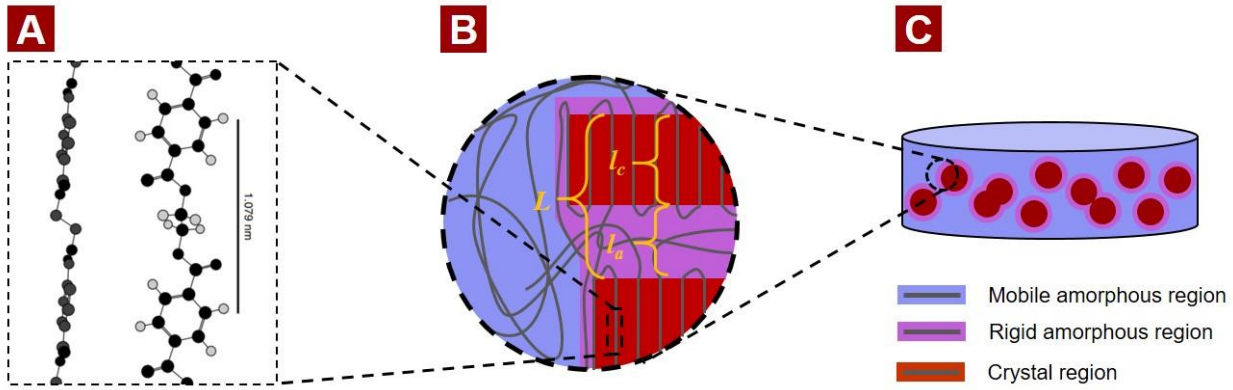

Figure 3. Schematic representation of the structural details of the crystal structure of a PET crystal within semi-crystalline PET: A) side and front view of the all-*trans* molecular confirmation of a structural moiety (two TPA and one EG moiety) of the polymeric chain of a PET crystal; B) Molecular arrangement and lamellar structure of the polymeric chains in semi-crystal PET (l_a, l_c, and L, are explained in the text); C) Schematic representation of the spherical crystalline regions in a semi-crystalline PET material.

Thermally induced crystals manifest as highly branched spherulites (bulk crystals) or as micelles (surface crystals) [38,59,62]. The size of these crystals is influenced by the annealing temperature, as larger crystals are formed at higher temperatures [43,59]. The visual appearance of thermally annealed PET samples becomes progressively more opaque with increasing X_C, resulting from the increased light scattering caused by the crystals [63]. Studies by *in situ* Atomic Force Microscopy of the annealing of spin coated PET film (thickness up to 680 nm), have revealed that surface crystals begin to form at 70°C, whereas crystal formation in the bulk material starts at 85°C [61]. However, no bulk crystals were observed on films thinner than 10 nm within a temperature range of 50 to 190°C [61]. In contrast to thermally induced crystals, the crystal structures resulting from strain induced crystallization are generally elongated in rod-like or fibrillary structures [60]. Here, the lamella are oriented in the direction of the strain, while the lamellar structures following thermally induced crystals are oriented randomly [57]. The crystal size of PET samples which have undergone strain induced crystallization are moreover smaller than thermally induced crystals. PET material with stress/strain induced crystals may therefore appear transparent due to the small crystal size [42].

2.3. Amorphous fractions

In its melt form the PET chains adopt a disordered random coil-state, as mentioned above. These chains are highly flexible, leading to highly entangled structures. The entanglement molecular weight (MW_e) of PET, which is a measure of the molecular weight between two chain entanglements, is typically between 1450 to 2120 g/mol [64] corresponding to an entanglement between every 7.5 to 11 repeating units (*i.e.*, the mono(2-hydroxyethyl) terephthalate MHET units)

in a PET chain. This amorphous state of the polymeric chains is maintained in the solid state if the polymer melt is cooled rapidly to temperatures below the T_g, *i.e.*, below 75°C [25].

The amorphous fraction of PET can be further divided into two different fractions, namely a mobile amorphous fraction (MAF) and a rigid amorphous fraction (RAF). The MAF consists of the amorphous regions between the crystal structures, while the RAF is associated with the interface between the crystal and the amorphous regions (Figure 3B). This interface also includes the interlamellar spacing within PET crystals (quantified as l_a, Figure 3B). Therefore, the RAF content of a PET sample increases with the X_C, while the MAF content decreases [42,65,66]. The RAF and MAF content of a PET sample is also affected by the crystal morphology [67]. A recent study has shown that the RAF content in a biaxially oriented PET film was higher than in thermally annealed samples (at 120 and 190°C), even though the X_C was highest in biaxially oriented PET film [57]. Compared to the chains in the MAF, the mobility of the chains within the RAF is more physically restrained by the crystal lamellae as shown in Figure 3B. As a consequence, the RAF remains in its glass-state, while only the MAF transitions into the mobile rubber-state once heated above the T_g value [65]. The overall T_g of PET may be lowered by the presence of additives [68] or by absorption of water molecules, conferring a plasticizing effect on PET [69,70], that impact the enzymatic attack and hence the enzymatic depolymerization of PET, to be discussed further below.

2.4. The enzymatic degradation mechanism on semi-crystalline PET

Given the complexity of the enzymatic degradation of PET the exact details of the molecular enzymatic attack mechanisms, and the interactions between insoluble PET and PET hydrolases during reaction are still unclear [71]. Nevertheless, already in 2009, by studying PET chain length distribution using MALDI-TOF and the changes in surface chemistry by X-ray photoelectron spectroscopy (XPS) of enzyme treated PET with a lipase and a cutinase, respectively, Eberl et. al. proposed that the enzymatic degradation of PET was facilitated by random (endo-type) chain scissoring [72].

This interpretation was based on the observations that the enzymatic treatment of PET increased the surface polarity, and increased the level of smaller insoluble fragments (fewer than 11 TPA moieties) in the insoluble substrate [72]. They furthermore demonstrated that the degradation pattern differed between two PET degrading enzymes, as one (the *Thermobifida fusca* cutinase) appeared have a higher preference for chain scissoring at the terminal, exo-type, releasing more soluble products than the other enzyme (the *Thermomyces lanuginosus* lipase), which instead accumulated more smaller insoluble fragments, indicating a higher preference for endo-type chain scissoring [72]. The insoluble polymeric chains are then hydrolyzed into smaller soluble products. These degradation products are primarily EG, TPA, MHET, and Bis(2-Hydroxyethyl) terephthalate (BHET) [26,73], but larger PET oligomers containing two or more aromatic rings have also been observed [23,74,75].

Several PET degrading enzymes are moreover capable of degrading the soluble products, such as BHET and MHET [75–77]. Consequently, the enzymatic depolymerization of the insoluble PET may be competitively inhibited by its degradation products, e.g., as shown for BHET and MHET on the TfCut2 enzyme [76]. A degradation mechanism taking the crystalline and amorphous regions of PET into consideration was recently updated by Wei and coworkers [78]. They

suggested that the MAF regions could be degraded by both endo and exo-type chain scission, while the RAF and PET crystals can only be degraded via endo-type scission. This hypothesis was deducted by an assessment of the molecular weight distribution of enzymatically treated PET samples [78]. A schematic representation of this mechanism is presented in Figure 4.

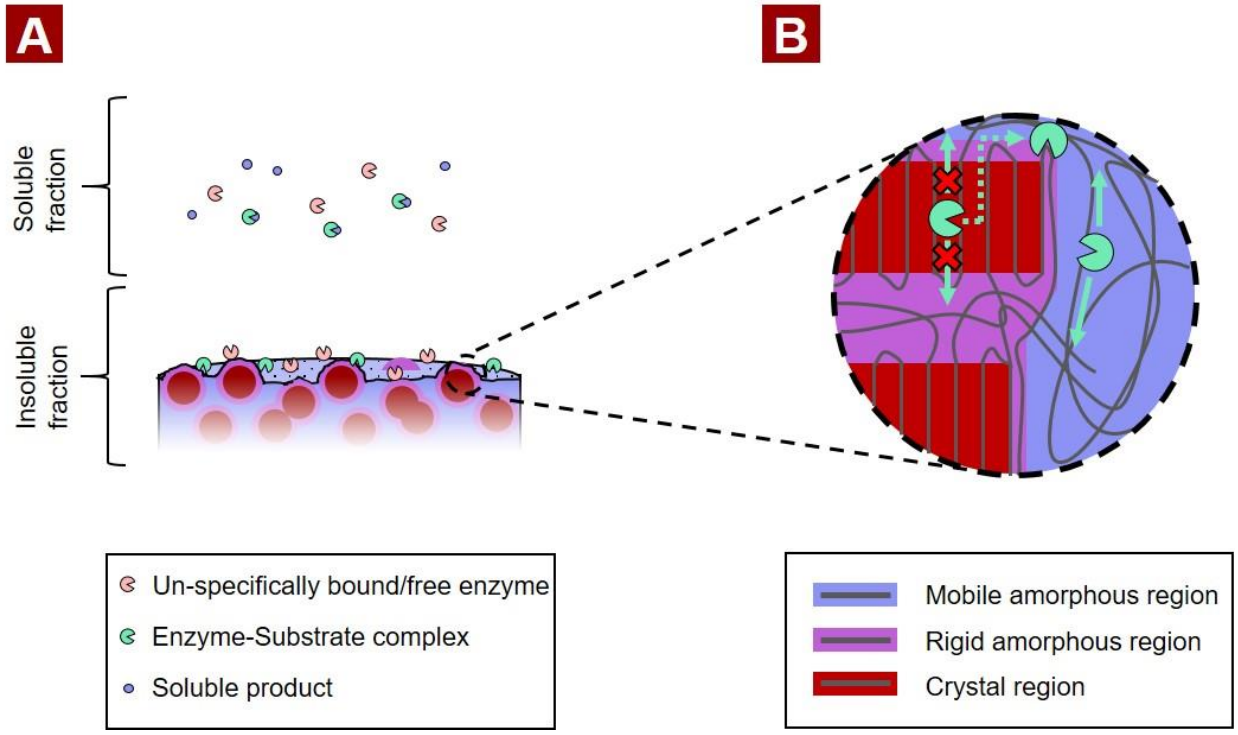

Figure 4. Schematic representation of the hypothesized enzymatic degradation mechanism of semi-crystalline PET. A) Proposed distribution of enzymes during enzymatic degradation of PET. The enzymes in the soluble fraction may either be unbound free enzyme or bound in an enzyme-substrate complex to soluble hydrolysis products resulting from the enzymatic degradation of PET. The interfacial enzymes bound to the insoluble substrates may either be productive (resulting in hydrolysis) or unproductive. B) Schematic representation of the currently presumed enzymatic attack restrictions in response to the crystallinity features of semi-crystalline PET, adapted from Wei et. al [78].

The course of the different degradation routes of PET degrading enzymes was recently studied in more detail by Schubert et. al who, using stochastic modeling of the evolution in the product profile during enzymatic treatment, quantified the preference for endo- or exolytic chain scissoring of four different PET hydrolases. The work showed that efficient PET hydrolases (notably the LCC enzyme) were characterized by a preference for endo-type chain scissoring [75].

It has also recently been shown that no soluble products are released during the initial incubation period of several types of PET material. This includes PET from commercial packaging material [41], extruded PET made from recycled PET flakes [79], and amorphous PET samples which have been thermally annealed [25]. This phenomenon has been previously been described as a lag phase [25]. The duration of these lag phases was shown to depend on the specific surface area of the substrate [79] and the X_C [25], and notably with the enzyme catalyzing the reaction

[80]. Notably, higher X_C resulted in extended lag phases. During enzymatic treatment of different low crystalline PET samples (X_C < 4%) from packaging material, a lag phase was observed only on three of these samples (#29, 38, and 43) [41]. This observation could therefore indicate that the duration of the lag phases may be affected by other uncharacterized properties of the PET material than the X_C. A deeper insight into the causes of the lag phase would enlighten the exact degradation mechanism of PET degrading enzymes. This could furthermore unravel potential synergies between PET degrading enzymes, as both the duration of the lag phase and the steady state reaction rate vary from enzyme to enzyme [80].

2.5. Surface modification caused by enzymatic treatment of PET

Evidently, the main enzymatic degradation reaction of PET takes place at the interface of the insoluble substrate and the reaction medium, and the enzymatic action is therefore associated with a change in surface topology of the PET substrate. This change, both the extent and the resulting surface topology, is heavily dependent on the X_C of the PET substrate [25].

The changes in surface topology of an amorphous PET sample resulting from the enzymatic degradation by different enzymes have recently been studied using two of the most promising wild type PET hydrolases, PHL7 and LCC [81–83]. These studies showed that the enzymatic degradation of PET resulted in the formation of small shallow pits at the surface of PET samples, and the pits increased in diameter with increasing exposure time [83]. Subsequently new pits were originating within the existing pits, and ultimately replenishing these [81]. This degradation pattern would eventually reach a “steady-state”, at which the decrease in the PET film thickness would appear as a uniform degradation [82]. A similar observation was shown on amorphous PET film treated by LCC_{ICCG} [25] – the LCC_{ICCG} being the protein engineered, Ca^{2+} independent thermostable gold standard enzyme for PET degradation. The surface erosion on more crystalline PET samples (X_C 15-27%), induced via thermal annealing, were also studied by scanning electron microscopy of the surface erosion induced by enzymatic action revealed that certain areas seemed left “untouched” during the enzymatic degradation. Under the microscope these regions appeared as smooth, flat surface regions within the porous pattern that developed progressively to produce a gradually finer erosion pattern as the enzymatic treatment progressed (Figure 5). As the X_C increased the size of the porous structures seemed to increase as well [25]. The “untouched” structures were presumably associated with crystal structures resulting from the thermal annealing, as they were not observed on the samples with a lower X_C (<15%) [25]. Prolonged annealing of these samples did, furthermore, result in the exposure of larger crystal structures [80] as shown in Figure 6B. Interestingly, it was observed that the surface erosion of PHL7 resulted in large crater formations, rather than the porous structures obtained by LCC_{ICCG}, these differences were attributed to the selectivity of the enzymes towards RAF [80].

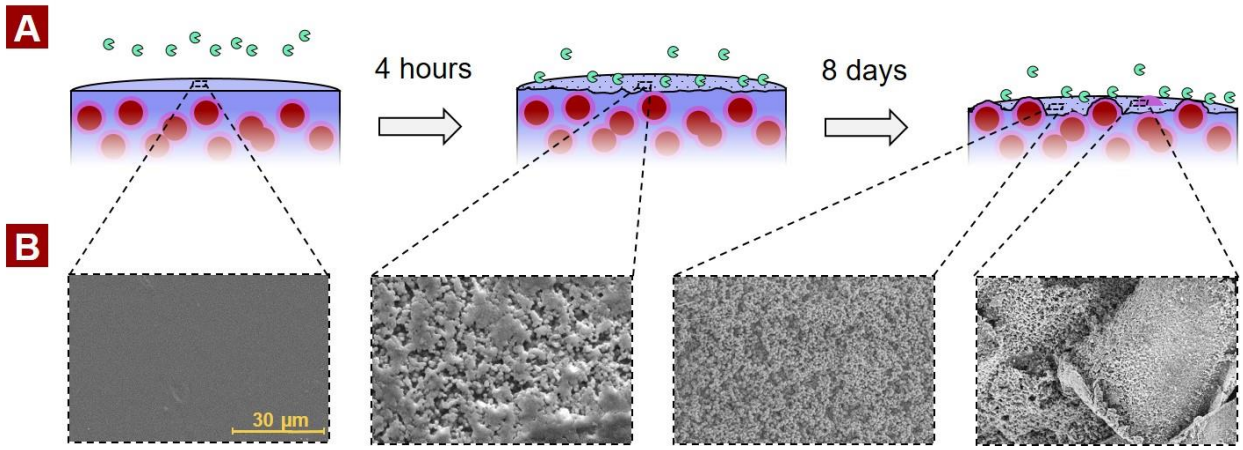

Figure 5. Change in surface topology during enzymatic degradation of semi-crystalline PET. A) Schematic representation of the surface erosion of a PET film caused by enzymatic treatment. B) SEM images of the surface erosion caused by enzymatic treatment of annealed PET disk (XC = 23.3%) using LCC_{ICCG} adapted from [25]Thomsen et al.,[80]

2.6. Effect of X_C on enzymatic degradation of PET

The activity of PET degrading enzymes is, as previously mentioned, highly affected by the X_C of the PET substrate. Several studies have shown how the enzymatic hydrolysis of PET samples with a high X_C is very limited compared to amorphous or low X_C samples [23,24,78,84]. The same trend was observed on commercial PET bottles, as the activity on the more crystalline regions (e.g. body) was significantly lower than the less crystal regions (e.g. the finish/neck) [41,85]. Thermally induced crystallization has been used to quantify the effect of the X_C on the activity of PET hydrolases. This includes both iso-thermal [25] and non-isothermal crystallization [86]. Here both studies showed that the activity is affected in a non-linear matter, and that activity is almost depleted at X_C > 17-20%. A recent comparative assessment of six thermostable PET hydrolases performed by the authors of this paper reviled that this threshold varied between the enzymes [80]. For a quantitative assessment of this phenomenon we defined the term tolerance, which corresponded the X_C at which the residual activity corresponded to 50% of what was obtained on a PET sample of low X_C. The tolerance to X_C of these enzymes is summarized in the upper part of Table 1.

Despite this, it has been shown that PET particles at higher X_C values (>30%) was amendable to enzymatic hydrolysis [52,87–89]. The overall extent of reaction was, however, lower compared to substrate at lower X_C [52,88], and may be explained by the disproportionally large surface area of the small substrate particles.

Brizendine et. al recently studied the effect of particle size on the degradation of highly crystalline PET (32.5–35.7% X_C) and Cryo-grinded PET particles (7 to 15% X_C). This study revealed that the reaction rate increased with the specific surface area (SSA), while the overall extent of reaction was unaffected by the particle size [88]. Kaabel et. al showed that the extent of reaction could be improved via a mechano-enzymatic hydrolysis (ball milling followed by an enzymatic treatment at 55°C) of a PET powder slurry [89]. Here, nearly 50% yield of TPA was reached after 21 cycles in their process. Another attempt to increase the efficiency of PET degrading enzymes towards the

crystalline regions was made by improving the selectivity towards the *trans* confirmation [90]. This improvement was achieved by engineering an *Is*PETase via rational design assisted by MD simulation and molecular docking [90]. The S238A variant showed a 2.8-fold higher activity on *trans*-enriched PET substrate compared to the WT [90]. The selectivity towards the crystalline regions has also been assessed through a comparative evaluation of 51 putative PET hydrolases from 7 district phylogenetic groups [91]. Here three enzymes displayed a higher activity on crystalline PET powder compared to amorphous PET powder. These tree enzymes 503, 602, and 711 are highlighted in Table 1.

Table 1. List of enzymes that have been characterized in terms of their tolerance to PET crystallinity. A. Direct tolerance to X_C as threshold when activity was halved[a]; B. Relative ratio, termed selectivity ratio, between the activity on amorphous (X_C 6.2%) and highly crystalline PET (X_C 39.3%).

A. Assessment of tolerance, adapted from [80]

Enzyme	Origin (Phylum)	EC number	Tolerance (% X_C)[a]
LCC (sp|G9BY57|)	Actinobacteriota	3.1.1.74	23.2 ± 2.6
LCC_{ICCG} (sp|G9BY57|)	Actinobacteriota	3.1.1.74	20.9 ± 2.1
DuraPETase (sp|A0A0K8P6T7|)	Pseudomonadota	3.1.1.101	17.1 ± 0.9
PHL7 (pdb|7NEI|)	-	3.1.1.74	17.4 ± 1.9
TfC (AJ810119.1)	Actinobacteriota	3.1.1.74	14.3 ± 0.8
HiC (tr|A0A075B5G4|)	Eukarya	3.1.1.74	13.7 ± 0.5

B. Relative product formation on crystalline PET powder vs on amorphous film [91]

Enzyme	Origin (Phylum)	EC number	Selectivity ratio[b]
LCC_{ICCG} (sp|G9BY57|)	Actinobacteriota	3.1.1.74	0.19
503 (EGD44994.1)	Actinobacteriota	-	1.30
602/Tcur0390 (ACY95991.1)	Actinobacteriota	3.1.1.74	2.79
711/est119 (sp|F7IX06|)	Actinobacteriota	3.1.1.1	2.13

[a] Calculated at the X_C (%) at which the reaction rate was half the of the rate obtained on amorphous PET (10.8% X_C) [80]; [b] Calculated as the ratio between the activity of the enzyme on crystalline PET powder (X_C=39.3%) divided by the activity on amorphous powder (X_C=6.2%) [91]

As pointed out in this review, currently a main limitation of biocatalytic recycling of plastics is the limited activity of the currently characterized PET degrading enzymes on PET of relevant crystallinity, *i.e.*, X_C>~20% (Table 1) [24,25,41,78]. A pre-treatment step involving extrusion and micronization is therefore currently required for efficient degradation of PET using enzymes [24]. An impact analysis of the enzymatic recycling of PET has pointed out that the elimination of the pretreatment step would decrease the minimal selling price of the degradation products by 12% and reduce its greenhouse gas emission by 38% [27]. This is under the assumption that the catalytic efficiency of the enzymes remains unchanged.

3. Effect of T_g on enzymatic degradation of PET

Water may act as a plasticizer PET, and a decrease in T_g of PET material is therefore expected during enzymatic treatment, as these reactions are performed in aqueous solutions. We recently investigated the effect of decreased T_g values of PET on enzymatic degradation efficiency [52]: By soaking a PET sample in water for 24 hours at 65°C, the T_g was lowered from 75°C to 61°C, without affecting the X_C. The activity of the thermostable LCC variant, LCC_{ICCG}, was measured on both the untreated (T_g = 75°C) and the soaked (T_g = 61°C) PET samples (sheets), at a reaction temperature between the T_g value of the two samples (68°C). It would be expected that the mobility of the PET chains in the soaked sample would be greater when the reaction temperature was above the T_g (Figure 6A). However, the activity of the LCC_{ICCG} enzyme was, not affected by the decreased T_g [52] (Figure 6B. Table 2). These results indicate that the increase in activity at temperatures near T_g is mainly driven by the thermal activation of enzyme activity (k_{cat}), provided the enzyme is sufficiently thermostable, rather than by the increased chain mobility of the substrate.

In fact, as previously indicated, it has been shown the T_g at the surface of PET is substantially lower than the T_g of bulk PET [92–94]. Consequently, the local T_g of a thicker PET sample would gradually increase from the surface into the bulk of the samples, as illustrated in Figure 6. This observation also explains the on-set temperatures of surface and bulk crystals, as crystallization may only occur at the surface when the temperature is below the bulk T_g and above the surface T_g. The decreasing T_g at the surface is however suppressed by the RAF associated with the increase in X_C resulting from the formation of surface crystals s [94]. It is therefore not suitable to run reaction at 70°C or above, as the crystallization, and thus increase in X_C, occurring at these high temperatures lowers the reaction rate of the enzyme [24]. The optimal reaction temperature on PET of PET degrading enzymes may therefore be governed by the crystallization of the substrate rather than by thermal inactivation of the enzyme [25].

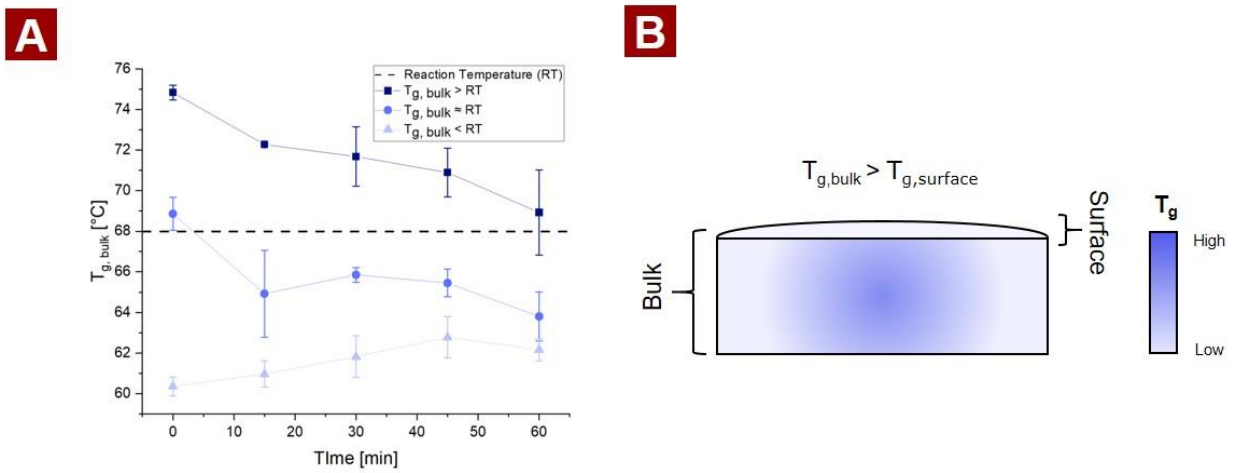

Figure 6. A) Change in T_g during 1 hour of incubation with LCC_{ICCG} at 68°C [25]. B) Schematic representation of the T_g gradient trend in a PET sample.

Table 2. Change in T_g and X_C during the enzymatic treatment of PET disks using LCC_{ICCG} at pH 9 and a temperature of reaction (TR) of 68°C. Disks were subjected to different soaking conditions to achieve distinct starting T_g values. The reaction rate was assessed for each substrate with $T_{g,\,bulk}$ > TR, $T_{g,\,bulk}$ ≈ TR, and $T_{g,\,bulk}$ < TR. The data presented in the table are adapted from [25].

	Soaking condition	$T_{g,bulk\ start}$ [°C]	$T_{g,bulk\ final}$ [°C]	$X_{C\ start}$ [%]	$X_{C\ final}$ [%]	Rate [mM/h]
$T_{g,\,bulk}$ > TR	n/a	74.8 ± 0.36[a]	68.8 ± 2.10[a]	11.2 ± 0.97[a]	10.9 ± 1.47[a]	4.81 ± 0.83[a]
$T_{g,\,bulk}$ ≈ TR	24h, 45°C	68.9 ± 0.81[b]	63.8 ± 1.20[b]	11.5 ± 1.08[a]	10.7 ± 0.89[a]	4.56 ± 0.64[a]
$T_{g,\,bulk}$ < TR	24h, 65°C	60.35 ± 0.46[c]	62.2 ± 0.54[b]	11.7 ± 0.22[a]	11.2 ± 0.58[a]	4.38 ± 0.86[a]

The complexity of the T_g effect versus the direct enhanced enzymatic reaction rate effect, *i.e.*, the Arrhenius effect, is corroborated by the findings that the activity of PET hydrolases increases drastically in the temperature range from 50 to 70°C on a low X_C PET film, compared to on a highly crystalline PET powder [95]. The same is found on poly(vinyl acetate), which has a lower T_g of 32°C [34,96]. It is tempting to infer that these findings are a result of the MAF of amorphous PET film undergoing transition to its more mobile state during this temperature interval. Such transition has been shown to occur at temperatures as low as 40°C [97]. However, this explanation does not hold for a crystalline sample, as it presumably has a limited content of MAF. Similarly, no transition occurs for poly(vinyl acetate), as it devitrifies at lower temperatures than PET [96].

Due to the complexity of the PET substrate as highlighted in this review it is evident that other, yet uncharacterized factors may also affect the enzymatic degradation PET. This includes the change in surface electrostatics at the surface of PET caused by the exposure of two acid groups, when a PET chain is hydrolyzed in an endo-type manner [72,80]. Moreover, the extent of entanglement, which can be quantified in terms of MW_e, could potentially affect the enzymatic degradation of PET. To the best of our knowledge, this aspect has not yet been studied in relation to the enzymatic hydrolysis of PET. Nevertheless, we speculate that the greater presence of entanglements could hinder sterically the accessibility of the most hydrolysable regions of the PET substrate via the entanglements blocking the formation of an enzyme-substrate complex.

4. Conclusions and future trends

The fractional composition of PET as a substrate for biorecycling, especially the relative level of crystalline regions, *i.e.*, the degree of crystallinity, X_C, strongly affects the activity of PET degrading enzymes. When the X_C exceeds ~20% [25,86], the activity of the currently known PET degrading enzymes such as LCC_{ICCG}, DuraPETase, and PHL7, is limited - if not completely abolished - which is a major challenge for enzymatic recycling of PET, as most waste PET, notably the PET constituting the major part of plastic bottles, is highly crystalline (X_C>25%) [41]. Such

high crystallinity is a result of the thermo-mechanical molding process of the PET polymer resin to the desired shape at high temperature (> 260°C) because crystals form during the slow cooling from temperatures above the T_g of 75°C, and because of stretching of the hot material at temperatures above the T_g - the latter phenomenon being referred to as strain induced crystallization.

In the budding industrial enzyme based recycling of PET bottles, a pretreatment step is therefore used to make the substrate more amorphous and thus amendable to enzymatic degradation [27,98]. This pretreatment is, however, undesirable as it is highly energy demanding. To achieve as enzymatic high turnover rates (k_{cat}) as possible, industrial enzymatic reactions are to be run at as high temperatures as possible, to enable a thermal rate activation of the enzyme and to facilitate the transition of the mobile amorphous PET chains into their more mobile state. This transition occurs at the T_g of the material. However, it has been observed that this transition occurs at temperatures considerably lower than the T_g of the bulk material, particularly at the surface in an aqueous environment (40°C) [97]. Although highly thermostable PET degrading enzymes have now been developed by protein engineering, the nature of the thermal crystallization of PET dictates that the maximal reaction temperature of the enzymatic processing step is max. 65-68°C, as reaction above ~70°C, which is significantly below the T_m of current PET degrading enzymes [24], reduces reaction rate and hydrolysis yield of the enzymes [24,25].

Recently EU has passed legislation requiring that a tax of EUR 0.80 per kilo be imposed on newly produced plastics - *i.e.* plastics which are not made from recycled plastics [99]. This is equivalent to approx. 100 to 160 per cent of the costs of the precursors used for the molding of new PET products [27] and is expected to have a positive impact on the recycling of plastics, and further fuel the enzymatic recycling of plastics as a sustainable technology option. For this to be successful, a better understanding of the degradation mechanism of PET degrading enzymes on semi-crystalline PET of $X_C > 20\%$ is therefore required to determine how the activity against the crystalline regions PET can be improved. This can only be achieved by directing the research within the field of plastic degrading enzymes into the characterization of substrate and enzyme interactions. The currently characterized enzymes has therefore been assayed using different types of substrate [35]. It is difficult the compare results between studies as the enzymes have been characterized under different conditions and on substrates of varying (or undefined) crystallinity. Hence, better, standardized assay analysis methods are required using standardized PET substrates of known (high) X_C, to quantitatively characterize the action kinetics of PET degrading enzymes [52,71]. We anticipate that the next important step forward in advancing the field of enzymatic PET degradation and recycling is to develop a deeper understanding of the significance of the PET as a semi-crystalline enzyme substrate. This would ideally reveal the sequential features required for efficient degradation of the crystalline regions and allow for rational approach for selection or development of efficient PET degrading enzymes with high activity towards the crystalline regions.

Acknowledgements

Financial support from The Villum Experiment Programme, Grant no. 40815, is highly acknowledged.

Credit author statement

TBT and ASM: Conceptualization. TBT: Original draft preparation and Visualization. TBT, KA and ASM: Writing, Reviewing, Editing.

References

[1] Geyer R, Jambeck JR, Law KL. Production, use, and fate of all plastics ever made. Sci Adv 2017;3:e1700782. https://doi.org/10.1126/sciadv.1700782.

[2] European Commission. A circular economy for plastics – Insights from research and innovation to inform policy and funding decisions. 2019. https://doi.org/10.2777/269031.

[3] Plastics Europe. Plastics – the Facts 2022. Available at: Https://Plasticseurope.Org/Knowledge-Hub/Plastics-the-Facts-2022/: 2022.

[4] Textile Exchange. Preferred Fiber & Materials Market Report 2021. Available at: Https://Textileexchange.Org/Knowledge-Center/Reports/Preferred-Fiber-Materials-Market-Report-2021//: 2021.

[5] Ingrao C, Wojnarowska M. Findings from a streamlined life cycle assessment of PET-bottles for beverage-packaging applications, in the context of circular economy. Sci Total Environ 2023;892:164805. https://doi.org/10.1016/j.scitotenv.2023.164805.

[6] World Economic Forum Ellen MacArthur Foundation McKinsey & Company. The New Plastics Economy: Rethinking the future of plastics. Available at: Https://Ellenmacarthurfoundation.Org/the-New-Plastics-Economy-Rethinking-the-Future-of-Plastics: 2016.

[7] Barnes DKA, Galgani F, Thompson RC, Barlaz M. Accumulation and fragmentation of plastic debris in global environments. Philos Trans R Soc B Biol Sci 2009;364:1985–98. https://doi.org/10.1098/rstb.2008.0205.

[8] Knoblauch D, Mederake L. Government policies combatting plastic pollution. Curr Opin Toxicol 2021;28:87–96. https://doi.org/10.1016/j.cotox.2021.10.003.

[9] Nielsen TD, Hasselbalch J, Holmberg K, Stripple J. Politics and the plastic crisis: A review throughout the plastic life cycle. Wiley Interdiscip Rev Energy Environ 2020;9:e360. https://doi.org/10.1002/wene.360.

[10] European Council. Directive (Eu) 2019/904 of the European Parliament and of the Council of 5 June 2019 on the reduction of the impact of certain plastic products on the environment. Available at: Https://Eur-Lex.Europa.Eu/Legal-Content/EN/ALL/?Uri=LEGISSUM%3A4393034: 2019.

[11] Luo ZW, Lee SY. Biotransformation of p-xylene into terephthalic acid by engineered Escherichia coli. Nat Commun 2017;8:1–8. https://doi.org/10.1038/ncomms15689.

[12] Aharoni SM. Industrial-Scale Production of Polyesters, Especially Poly(Ethylene Terephthalate). In: Fakirov S, editor. Handb. Thermoplast. Polyesters, Wiley-VCH; 2002, p. 59–103. https://doi.org/10.1002/3527601961.ch2.

[13] Schyns ZOG, Shaver MP. Mechanical Recycling of Packaging Plastics: A Review. Macromol Rapid Commun 2021;42:1–27. https://doi.org/10.1002/marc.202000415.

[14] Badia JD, Strömberg E, Karlsson S, Ribes-Greus A. The role of crystalline, mobile amorphous and rigid amorphous fractions in the performance of recycled poly (ethylene terephthalate) (PET). Polym Degrad Stab 2012;97:98–107.

https://doi.org/10.1016/J.POLYMDEGRADSTAB.2011.10.008.
[15] Ragaert K, Delva L, Van Geem K. Mechanical and chemical recycling of solid plastic waste. Waste Manag 2017;69:24–58. https://doi.org/10.1016/j.wasman.2017.07.044.
[16] Torres N, Robin JJ, Boutevin B. Study of thermal and mechanical properties of virgin and recycled poly(ethylene terephthalate) before and after injection molding. Eur Polym J 2000;36:2075–80. https://doi.org/10.1016/S0014-3057(99)00301-8.
[17] Jönsson C, Wei R, Biundo A, Landberg J, Schwarz Bour L, Pezzotti F, et al. Biocatalysis in the Recycling Landscape for Synthetic Polymers and Plastics towards Circular Textiles. ChemSusChem 2021;14:4028–40. https://doi.org/10.1002/cssc.202002666.
[18] Geyer R, Kuczenski B, Zink T, Henderson A. Common Misconceptions about Recycling. J Ind Ecol 2016;20:1010–7. https://doi.org/10.1111/jiec.12355.
[19] Marten E, Müller RJ, Deckwer WD. Studies on the enzymatic hydrolysis of polyesters. II. Aliphatic-aromatic copolyesters. Polym Degrad Stab 2005;88:371–81. https://doi.org/10.1016/j.polymdegradstab.2004.12.001.
[20] Müller RJ, Schrader H, Profe J, Dresler K, Deckwer WD. Enzymatic degradation of poly(ethylene terephthalate): Rapid hydrolyse using a hydrolase from T. fusca. Macromol Rapid Commun 2005;26:1400–5. https://doi.org/10.1002/marc.200500410.
[21] Yoshida S, Hiraga K, Takehana T, Taniguchi I, Yamaji H, Maeda Y, et al. A bacterium that degrades and assimilates poly(ethylene terephthalate). Science (80-) 2016;351:1196–9. https://doi.org/10.1126/science.aad6359.
[22] Quartinello F, Vajnhandl S, Volmajer Valh J, Farmer TJ, Vončina B, Lobnik A, et al. Synergistic chemo-enzymatic hydrolysis of poly(ethylene terephthalate) from textile waste. Microb Biotechnol 2017;10:1376–83. https://doi.org/10.1111/1751-7915.12734.
[23] Vertommen MAME, Nierstrasz VA, Veer M Van Der, Warmoeskerken MMCG. Enzymatic surface modification of poly(ethylene terephthalate). J Biotechnol 2005;120:376–86. https://doi.org/10.1016/j.jbiotec.2005.06.015.
[24] Tournier V, Topham CM, Gilles A, David B, Folgoas C, Moya-Leclair E, et al. An engineered PET depolymerase to break down and recycle plastic bottles. Nature 2020;580:216–9. https://doi.org/10.1038/s41586-020-2149-4.
[25] Thomsen TB, Hunt CJ, Meyer AS. Influence of substrate crystallinity and glass transition temperature on enzymatic degradation of polyethylene terephthalate (PET). N Biotechnol 2022;69:28–35. https://doi.org/10.1016/j.nbt.2022.02.006.
[26] Zimmermann W. Biocatalytic recycling of polyethylene terephthalate plastic. Philos Trans R Soc A 2020;378. https://doi.org/10.1098/RSTA.2019.0273.
[27] Singh A, Rorrer NA, Nicholson SR, Erickson E, DesVeaux JS, Avelino AFT, et al. Techno-economic, life-cycle, and socioeconomic impact analysis of enzymatic recycling of poly(ethylene terephthalate). Joule 2021. https://doi.org/10.1016/j.joule.2021.06.015.
[28] Tiso T, Narancic T, Wei R, Pollet E, Beagan N, Schröder K, et al. Towards bio-upcycling of polyethylene terephthalate. Metab Eng 2021;66:167–78. https://doi.org/10.1016/j.ymben.2021.03.011.
[29] Zumstein MT, Rechsteiner D, Roduner N, Perz V, Ribitsch D, Guebitz GM, et al. Enzymatic Hydrolysis of Polyester Thin Films at the Nanoscale: Effects of Polyester Structure and Enzyme Active-Site Accessibility. Environ Sci Technol 2017;51:7476–85. https://doi.org/10.1021/ACS.EST.7B01330.

[30] Tokiwa Y, Suzuki T. Hydrolysis of polyesters by lipases. Nature 1977;270:76–8. https://doi.org/10.1038/270076a0.
[31] Wei R, Zimmermann W. Microbial enzymes for the recycling of recalcitrant petroleum-based plastics: how far are we? Microb Biotechnol 2017;10:1308–22. https://doi.org/10.1111/1751-7915.12710.
[32] IUBMB. IUBMB Nomenclature Home Page 2016. https://iubmb.qmul.ac.uk/enzyme/EC3/0101b.html#101 (accessed August 10, 2023).
[33] Sulaiman S, You DJ, Kanaya E, Koga Y, Kanaya S. Crystal structure and thermodynamic and kinetic stability of metagenome-derived LC-cutinase. Biochemistry 2014;53:1858–69. https://doi.org/10.1021/bi401561p.
[34] Ronkvist ÅM, Xie W, Lu W, Gross RA. Cutinase-Catalyzed hydrolysis of poly(ethylene terephthalate). Macromolecules 2009;42:5128–38. https://doi.org/10.1021/ma9005318.
[35] Kawai F. The current state of research on PET hydrolyzing enzymes available for biorecycling. Catalysts 2021;11:1–10. https://doi.org/10.3390/catal11020206.
[36] Buchholz PCF, Feuerriegel G, Zhang H, Perez-Garcia P, Nover L-L, Chow J, et al. Plastics degradation by hydrolytic enzymes: The plastics-active enzymes database—PAZy. Proteins 2022;90:1443–56. https://doi.org/10.1002/PROT.26325.
[37] Haernvall K, Zitzenbacher S, Yamamoto M, Schick MB, Ribitsch D, Guebitz GM. A new arylesterase from Pseudomonas pseudoalcaligenes can hydrolyze ionic phthalic polyesters. J Biotechnol 2017;257:70–7. https://doi.org/10.1016/j.jbiotec.2017.01.012.
[38] Bartczak Z. Deformation of semicrystalline polymers – the contribution of crystalline and amorphous phases. Polimery 2017;62:787–99. https://doi.org/10.14314/POLIMERY.2017.787.
[39] Webb HK, Arnott J, Crawford RJ, Ivanova EP. Plastic degradation and its environmental implications with special reference to poly(ethylene terephthalate). Polymers (Basel) 2013;5:1–18. https://doi.org/10.3390/polym5010001.
[40] Karacan I. An in Depth Study of Crystallinity, Crystallite Size and Orientation Measurements of a Selection of Poly(Ethylene Terephthalate) Fibers. Fibers Polym 2005;6:186–99.
[41] Lu H, Diaz DJ, Czarnecki NJ, Zhu C, Kim W, Shroff R, et al. Machine learning-aided engineering of hydrolases for PET depolymerization. Nat 2022 6047907 2022;604:662–7. https://doi.org/10.1038/s41586-022-04599-z.
[42] Zekriardehani S, Jabarin SA, Gidley DR, Coleman MR. Effect of Chain Dynamics, Crystallinity, and Free Volume on the Barrier Properties of Poly(ethylene terephthalate) Biaxially Oriented Films. Macromolecules 2017;50:2845–55. https://doi.org/10.1021/acs.macromol.7b00198.
[43] Mandal S, Dey A. PET Chemistry. Recycl Polyethyl Terephthalate Bottles 2019:1–22. https://doi.org/10.1016/b978-0-12-811361-5.00001-8.
[44] Jog JP. Crystallization of Polyethyleneterephthalate. J Macromol Sci Part C 1995;35:531–53. https://doi.org/10.1080/15321799508014598.
[45] Jabarin SA. Crystallization kinetics of poly(ethylene terephthalate). III. Effect of moisture on the crystallization behavior of PET from the glassy state. J Appl Polym Sci 1987;34:103–8. https://doi.org/10.1002/APP.1987.070340109.
[46] Baldenegro-Perez LA, Navarro-Rodriguez D, Medellin-Rodriguez FJ, Hsiao B, Avila-Orta

CA, Sics I. Molecular weight and crystallization temperature effects on poly(ethylene terephthalate) (PET) homopolymers, an isothermal crystallization analysis. Polymers (Basel) 2014;6:583–600. https://doi.org/10.3390/polym6020583.

[47] Llana PG, Boyce MC. Finite strain behavior of poly(ethylene terephthalate) above the glass transition temperature. Polymer (Guildf) 1999;40:6729–51. https://doi.org/10.1016/S0032-3861(98)00867-2.

[48] Demirel B, Yaraş A, Elçiçek H. Crystallization Behavior of PET Materials. BAÜ Fen Bil Enst Derg Cilt 2011;13:26–35.

[49] Gorlier E, Haudin JM, Billon N. Strain-induced crystallisation in bulk amorphous PET under uni-axial loading. Polymer (Guildf) 2001;42:9541–9. https://doi.org/10.1016/S0032-3861(01)00497-9.

[50] Guo X, Wang J. The chemical behaviors of microplastics in marine environment: A review. Mar Pollut Bull 2019;142:1–14. https://doi.org/10.1016/j.marpolbul.2019.03.019.

[51] Kurita T, Fukuda Y, Takahashi M, Sasanuma Y. Crystalline Moduli of Polymers, Evaluated from Density Functional Theory Calculations under Periodic Boundary Conditions. ACS Omega 2018;3:4824–35. https://doi.org/10.1021/acsomega.8b00506.

[52] Thomsen TB, Hunt CJ, Meyer AS. Standardized method for controlled modification of poly (ethylene terephthalate) (PET) crystallinity for assaying PET degrading enzymes. MethodsX 2022;9:101815. https://doi.org/10.1016/J.MEX.2022.101815.

[53] Karagiannidis PG, Stergiou AC, Karayannidis GP. Study of crystallinity and thermomechanical analysis of annealed poly(ethylene terephthalate) films. Eur Polym J 2008;44:1475–86. https://doi.org/10.1016/j.eurpolymj.2008.02.024.

[54] Liu J, Geil PH. Crystal structure and morphology of poly(ethylene terephthalate) single crystals prepared by melt polymerization. J Macromol Sci - Phys 1997;36:61–85. https://doi.org/10.1080/00222349708220415.

[55] Hu W, Zha L. Theoretical aspects of polymer crystallization. Control. Morphol. Polym. Mult. Scales Struct. Process., Springer International Publishing; 2016, p. 101–43. https://doi.org/10.1007/978-3-319-39322-3_4.

[56] Baldenegro-Perez LA, Navarro-Rodriguez D, Medellin-Rodriguez FJ, Hsiao B, Avila-Orta CA, Sics I. Molecular Weight and Crystallization Temperature Effects on Poly(ethylene terephthalate) (PET) Homopolymers, an Isothermal Crystallization Analysis. Polym 2014, Vol 6, Pages 583-600 2014;6:583–600. https://doi.org/10.3390/POLYM6020583.

[57] Li Y, Makita Y, Zhang G, Rui G, Li ZM, Zhong GJ, et al. Effects of Rigid Amorphous Fraction and Lamellar Crystal Orientation on Electrical Insulation of Poly(ethylene terephthalate) Films. Macromolecules 2020;53:3967–77. https://doi.org/10.1021/acs.macromol.0c00646.

[58] Lu XF, Hay JN. Isothermal crystallization kinetics and melting behaviour of poly(ethylene terephthalate). Polymer (Guildf) 2001;42:9423–31. https://doi.org/10.1016/S0032-3861(01)00502-X.

[59] Al Raheil IAM. Morphology and crystallization of poly(ethylene terephthalate). Polym Int 1994;35:189–95. https://doi.org/10.1002/pi.1994.210350209.

[60] Jabarin SA. Strain-induced crystallization of poly(ethylene terephthalate). Polym Eng Sci 1992;32:1341–9. https://doi.org/10.1002/pen.760321802.

[61] Shinotsuka K, Assender H. In situ AFM study of near-surface crystallization in PET and PEN. J Appl Polym Sci 2016;133. https://doi.org/10.1002/app.44269.

[62] Mitchell GR, Tojeira A. Controlling the morphology of polymers: Multiple scales of structure and processing. 2016. https://doi.org/10.1007/978-3-319-39322-3.
[63] Tsai RS, Lee DK, Fang HY, Tsai HB. Crystalline study of amorphous poly(ethylene terephthalate) sheets through annealing. Asia-Pacific J Chem Eng 2009;4:140–6. https://doi.org/10.1002/apj.189.
[64] Cusano I, Campagnolo L, Aurilia M, Costanzo S, Grizzuti N. Rheology of Recycled PET. Materials (Basel) 2023;16:1–23. https://doi.org/10.3390/ma16093358.
[65] Androsch R, Wunderlich B. The link between rigid amorphous fraction and crystal perfection in cold-crystallized poly(ethylene terephthalate). Polymer (Guildf) 2005;46:12556–66. https://doi.org/10.1016/J.POLYMER.2005.10.099.
[66] Di Lorenzo ML, Righetti MC, Cocca M, Wunderlich B. Coupling between Crystal Melting and Rigid Amorphous Fraction Mobilization in Poly(ethylene terephthalate). Macromolecules 2010;43:7689–94. https://doi.org/10.1021/MA101035H.
[67] Slobodian P. Rigid amorphous fraction in poly(ethylene terephthalate) determined by dilatometry. J Therm Anal Calorim 2008;94:545–51. https://doi.org/10.1007/s10973-007-8566-x.
[68] Choi J, Cakmak M. Morphological evolution during thermal and strain induced crystallization in poly(ethylene terephthalate)/poly(ether imide) blend films. Polymer (Guildf) 2016;84:10–20. https://doi.org/10.1016/J.POLYMER.2015.12.038.
[69] Levine H, Grenet J, Slade L. Water as a plasticizer: physico-chemical aspects of low-moisture polymeric systems. Eur Polym J 1993;30:339–45. https://doi.org/10.1017/cbo9780511552083.002.
[70] Chen Y, Lin Z, Yang S. Plasticization and crystallization of poly(ethylene terephthalate) induced by water. J Therm Anal Calorim 1998;52:565–8. https://doi.org/10.1023/A:1010123723719.
[71] Ellis LD, Rorrer NA, Sullivan KP, Otto M, McGeehan JE, Román-Leshkov Y, et al. Chemical and biological catalysis for plastics recycling and upcycling. Nat Catal 2021;4:539–56. https://doi.org/10.1038/s41929-021-00648-4.
[72] Eberl A, Heumann S, Brückner T, Araujo R, Cavaco-Paulo A, Kaufmann F, et al. Enzymatic surface hydrolysis of poly(ethylene terephthalate) and bis(benzoyloxyethyl) terephthalate by lipase and cutinase in the presence of surface active molecules. J Biotechnol 2009;143:207–12. https://doi.org/10.1016/J.JBIOTEC.2009.07.008.
[73] Austin HP, Allen MD, Donohoe BS, Rorrer NA, Kearns FL, Silveira RL, et al. Characterization and engineering of a plastic-degrading aromatic polyesterase. Proc Natl Acad Sci U S A 2018;115:E4350–7. https://doi.org/10.1073/pnas.1718804115.
[74] Arnling Bååth J, Novy V, Carneiro L V., Guebitz GM, Olsson L, Westh P, et al. Structure-function analysis of two closely related cutinases from Thermobifida cellulosilytica. Biotechnol Bioeng 2022;119:470–81. https://doi.org/10.1002/BIT.27984.
[75] Schubert SW, Schaller K, Bååth JA, Hunt C, Borch K, Jensen K, et al. Reaction pathways for the enzymatic degradation of poly(ethylene terephthalate): What characterizes an efficient PET-hydrolase? ChemBioChem 2022;24:e202200516. https://doi.org/10.1002/CBIC.202200516.
[76] Barth M, Oeser T, Wei R, Then J, Schmidt J, Zimmermann W. Effect of hydrolysis products on the enzymatic degradation of polyethylene terephthalate nanoparticles by a polyester

hydrolase from Thermobifida fusca. Biochem Eng J 2015;93:222–8. https://doi.org/10.1016/J.BEJ.2014.10.012.

[77] Arnling Bååth J, Borch K, Jensen K, Brask J, Westh P. Comparative Biochemistry of Four Polyester (PET) Hydrolases. ChemBioChem 2021;22:1627–37. https://doi.org/10.1002/cbic.202000793.

[78] Wei R, Breite D, Song C, Gräsing D, Ploss T, Hille P, et al. Biocatalytic Degradation Efficiency of Postconsumer Polyethylene Terephthalate Packaging Determined by Their Polymer Microstructures. Adv Sci 2019;6. https://doi.org/10.1002/advs.201900491.

[79] Chang AC, Patel A, Perry S, Soong Y V., Ayafor C, Wong HW, et al. Understanding Consequences and Tradeoffs of Melt Processing as a Pretreatment for Enzymatic Depolymerization of Poly(ethylene terephthalate). Macromol Rapid Commun 2022:2100929. https://doi.org/10.1002/marc.202100929.

[80] Thomsen TB, Schubert S, Hunt CJ, Borch K, Jensen K, Brask J, et al. Rate Response of Poly(Ethylene Terephthalate)-Hydrolases to Substrate Crystallinity: Basis for Understanding the Lag Phase. ChemSusChem 2023;202300291:1–14. https://doi.org/10.1002/cssc.202300291.

[81] Frank R, Krinke D, Sonnendecker C, Zimmermann W, Jahnke HG. Real-Time Noninvasive Analysis of Biocatalytic PET Degradation. ACS Catal 2022;12:25–35. https://doi.org/10.1021/acscatal.1c03963.

[82] Lippold H, Kahle L, Sonnendecker C, Matysik J, Fischer C. Temporal and spatial evolution of enzymatic degradation of amorphous PET plastics. Npj Mater Degrad 2022;6:1–6. https://doi.org/10.1038/s41529-022-00305-6.

[83] Sonnendecker C, Oeser J, Richter PK, Hille P, Zhao Z, Fischer C, et al. Low Carbon Footprint Recycling of Post-Consumer PET Plastic with a Metagenomic Polyester Hydrolase. ChemSusChem 2022;15. https://doi.org/10.1002/cssc.202101062.

[84] Weinberger S, Haernvall K, Scaini D, Ghazaryan G, Zumstein MT, Sander M, et al. Enzymatic surface hydrolysis of poly(ethylene furanoate) thin films of various crystallinities. Green Chem 2017;19:5381–4. https://doi.org/10.1039/c7gc02905e.

[85] Wallace NE, Adams MC, Chafin AC, Jones DD, Tsui CL, Gruber TD. The highly crystalline PET found in plastic water bottles does not support the growth of the PETase-producing bacterium Ideonella sakaiensis. Environ Microbiol Rep 2020;12:578–82. https://doi.org/10.1111/1758-2229.12878.

[86] Erickson E, Shakespeare TJ, Bratti F, Buss BL, Graham R, Hawkins MA, et al. Comparative Performance of PETase as a Function of Reaction Conditions, Substrate Properties, and Product Accumulation. ChemSusChem 2022;15. https://doi.org/10.1002/CSSC.202101932.

[87] Arnling Bååth J, Borch K, Westh P. A suspension-based assay and comparative detection methods for characterization of polyethylene terephthalate hydrolases. Anal Biochem 2020;607. https://doi.org/10.1016/j.ab.2020.113873.

[88] Brizendine RK, Erickson E, Haugen SJ, Ramirez KJ, Miscall J, Pickford AR, et al. Particle Size Reduction of Poly(ethylene terephthalate) Increases the Rate of Enzymatic Depolymerization But Does Not Increase the Overall Conversion Extent. ACS Sustain Chem Eng 2022;10:9131–49. https://doi.org/10.1021/acssuschemeng.2c01961.

[89] Kaabel S, Daniel Therien JP, Deschênes CE, Duncan D, Friščic T, Auclair K. Enzymatic

depolymerization of highly crystalline polyethylene terephthalate enabled in moist-solid reaction mixtures. Proc Natl Acad Sci U S A 2021;118. https://doi.org/10.1073/pnas.2026452118.

[90] Guo B, Vanga SR, Lopez-Lorenzo X, Saenz-Mendez P, Ericsson SR, Fang Y, et al. Conformational Selection in Biocatalytic Plastic Degradation by PETase. ACS Catal 2022;12:3397–409. https://doi.org/10.1021/acscatal.1c05548.

[91] Erickson E, Gado JE, Avilán L, Bratti F, Brizendine RK, Cox PA, et al. Sourcing thermotolerant poly(ethylene terephthalate) hydrolase scaffolds from natural diversity. Nat Commun 2022;13. https://doi.org/10.1038/s41467-022-35237-x.

[92] Zhang Y, Zhang J, Lu Y, Duan Y, Yan S, Shen D. Glass Transition Temperature Determination of Poly(ethylene terephthalate) Thin Films Using Reflection−Absorption FTIR. Macromolecules 2004;37:2532–7. https://doi.org/10.1021/MA035709F.

[93] Shinotsuka K, Bliznyuk VN, Assender HE. Near-surface crystallization of PET. Polymer (Guildf) 2012;53:5554–9. https://doi.org/10.1016/J.POLYMER.2012.09.048.

[94] Zuo B, Liu Y, Liang Y, Kawaguchi D, Tanaka K, Wang X. Glass Transition Behavior in Thin Polymer Films Covered with a Surface Crystalline Layer. Macromolecules 2017;50:2061–8. https://doi.org/10.1021/acs.macromol.6b02740.

[95] Ding Z, Xu G, Miao R, Wu N, Zhang W, Yao B, et al. Rational redesign of thermophilic PET hydrolase LCCICCG to enhance hydrolysis of high crystallinity polyethylene terephthalates. J Hazard Mater 2023;453:131386. https://doi.org/10.1016/j.jhazmat.2023.131386.

[96] Ronkvist ÅM, Lu W, Feder D, Gross RA. Cutinase-catalyzed deacetylation of poly(vinyl acetate). Macromolecules 2009;42:6086–97. https://doi.org/10.1021/ma900530j.

[97] Tarazona NA, Wei R, Brott S, Pfaff L, Bornscheuer UT, Lendlein A, et al. Rapid depolymerization of poly(ethylene terephthalate) thin films by a dual-enzyme system and its impact on material properties. Chem Catal 2022;2:3573–89. https://doi.org/10.1016/j.checat.2022.11.004.

[98] Tournier V, Duquesne S, Guillamot F, Cramail H, Taton D, Marty A, et al. Enzymes' Power for Plastics Degradation. Chem Rev 2023;123:5612–701. https://doi.org/10.1021/acs.chemrev.2c00644.

[99] WTS Global. Plastic Taxation in Europe: Update 2023. Available at: Https://Wts.Com/Global/Publishing-Article/20230522-Plastic-Taxation-Europe-Update-2023~publishing-Article: 2023.

Paper VII

Kinetic assessment of the enzymatic degradation of Poly(ethylene terephthalate) (PET) at various degree of crystallinity

Thore B. Thomsen, Tobias Radmer, Anne S. Meyer

Early draft manuscript

VII

Intentionally left blank

Kinetic assessment of the enzymatic degradation of Poly(ethylene terephthalate) (PET) at various degree of crystallinity

Thore Bach Thomsen, Tobias Radmer, Anne S. Meyer*

Department of Biotechnology and Biomedicine, Protein Chemistry and Enzyme Technology Section, DTU Bioengineering, Technical University of Denmark, Kgs., Lyngby 2800, Denmark

*Corresponding author. E-mail Asme@dtu.dk

Abstract

Plastic pollution poses a significant environmental challenge, with Poly(ethylene terephthalate) (PET) being a major contributor due to its extensive use in packaging and other applications. Enzymatic degradation of PET offers a promising solution, but its kinetics and dependence on substrate composition remain poorly understood. In this study, we investigated the enzymatic degradation of PET using the benchmark PET hydrolase LCC_{ICCG}. PET substrates with varying compositions of mobile amorphous fraction (X_{MAF}), rigid amorphous fraction (X_{RAF}), and crystallinity (X_C) were employed to study the kinetics of the enzymatic reation. We observed a substantial reduction in the maximum reaction rate ($^{inv}V_{max}$) with increasing X_C, corresponding to a 3 fold reduction from 8.6% to 12.2% X_C.

Although substrate specificity towards the amorpous fractions (in terms of X_{MAF} and X_{RAF}) was initially considered, the intricate nature of PET substrate complexity became evident, suggesting the involvement of additional factors. Interestingly, X_{MAF} emerged as a better descriptor for the density of attack sites (Γ_{max}) compared the entire amorphous region. Furthermore, we established a correlation between the duration of the lag phase (t_{lag}) and the steady-state rate v_{ss}, indicating an initial random/endo-type degradation pattern. The extended t_{lag} associated with increased X_C was proposed to result from higher substrate entanglement density and unproductive enzyme binding to crystalline regions. These findings enhance our understanding of PET enzymatic degradation kinetics and its dependence on substrate composition.

1 Introduction

Plastic pollution has emerged as a pressing global environmental concern, threatening both aquatic and terrestrial ecosystems [1,2]. The demand for plastics continues to rise, resulting in a substantial production of 390 Mt in 2021 (excluding plastic used in textile fibers) [3]. Among these plastics, Poly(ethylene terephthalate) (PET), accounting for 10% of the annual plastic production [1], holds a significant role in contributing to environmental plastic pollution. This stems from the widespread usage of PET in packaging material and plastic bottles [2,3], which are associated with short lifespan and poor collection rates [4].

PET is a semi-crystalline polymer characterized by both highly-ordered crystalline regions and amorphous regions [5,6]. The polymer chains within the PET crystals form densely packed lamellae structures, separated by an amorphous layer [5]. The amorphous regions of PET can

be subdivided into two distinct fractions: the mobile amorphous fraction (MAF) and the rigid amorphous fraction (RAF). MAF resides within the amorphous regions between distinct crystal structures, whereas RAF surrounds the crystalline lamella, including the interlamellar spacing within PET crystals. Consequently, the RAF content in a PET sample generally increases with the X_C, while the MAF content decreases [7–9]. Due to a molecular connection between the RAF and the rigid crystal lamellae, the mobility of the RAF is more constrained compared to the mobility of MAF. As a result, only MAF transitions into a mobile "rubbery"-state upon heating above its glass transition temperature (T_g), a process known as devitrification, while RAF remains in the rigid "glassy"-state [8]. Complete devitrification of RAF has been proposed to occur at 200°C [10]. MAF and RAF does also differ by their molecular orientation, as MAF is pronominally at a gauche conformation, RAF is composed of mainly trans, while the Crystalline fraction is all-trans [11,12].

In recent years, certain enzymes, such as cutinases (EC 3.1.1.74), have demonstrated activity against PET alongside their natural substrates [13–16]. This discovery has paved the way for enzymatic recycling of plastics. In this process, enzymes break down PET into its constituent monomeric building blocks, which then serve as the feedstock for synthesis of new PET with properties equivalent to virgin PET [17–19]. This enzymatic recycling process offers the potential for establising a closed-loop circular economy, as the quality of the recycled PET, unlike conventional recycling methods, is preserved. Furthermore, the degradation products obtained from enzymatic degradation can be utilized in other applications [20].

The aim of this study was to investigate the substrate preference of the benchmark PET hydrolase LCC_{ICCG} [17]. This was done by using the inverse Michealis-Menten (^{inv}MM) approach [21] to quantify the kinetic constants at increasing levels of X_C. By employing a continuous assay, for monitoring of the product formation over time, we were further capable of correlating the lag phase, which constitute the initial degradation of the PET[22,23], with the steady-state rate and X_C.

2 Experimental Section

Enzyme

LCC_{ICCG} was expressed in BL21 (DE3) competent cells (New England Biolabs, Ipswich, MA, USA) as previously described in [23]

Substrate preparation

1 mm thick "Amorphous" PET Sheet cat. No. ES30301(Goodfellow, Cambridge Ltd, Huntingdon, UK) was used starting material. The PET sheet was cut into uniform disk of Ø=6mm using a generic hole punch. The crystallinity of the PET substrate induced via thermal annealing as described in [12]. The fractional composition of the substrate (X_C, X_{MAF}, and X_{RAF}) were quantified DSC as described in [12]. All DSC measurements were made in triplets

Enzyme activity assay

The enzyme activity assay was performed directly in an Epoch 2 microplate spectrophotometer (BioTek, Winooski, Vermont, USA), using the compartmentalized set-up described in [24]. The reactions were operated at the maximal incubation temperature of 50ºC in 650 µL (total volume) of 50 mM glycine-NaOH buffer at pH 9 for up to 120 min. The substrate concentration was fixed to one disk. The initial enzyme concentration was 20 to 800 nM. Each reaction was performed in

triplets. The v_{ss} was quantified by linear regressing at the constant region of the progress curves, while the t_{lag} was quantified as the intercept between the linear regression of vss and the baseline, as shown in Fig 1. Linear regression was performed using Origin 2021 (OriginLab Corporation, Northampton, MA, USA).

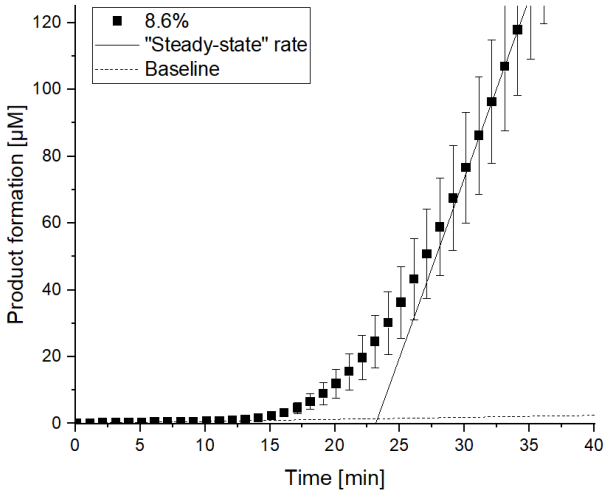

Fig 1: Example of the quantification of v_{ss} and t_{lag} from a progress curve

Invers Michealis-Menten kinetics

The kinetic constants $^{inv}V_{max}$ and $^{inv}K_M$ were quantified to fitting the v_{ss} at different enzyme concentration to the invers Michaelis-Menten equation, as described in [21] using Origin 2021 (OriginLab Corporation, Northampton, MA, USA). The enzyme concentration was adjusted was adjusted for the evaporation occurring during the reaction as described in [24].

Prediction model for describing the t_{lag} as a function of v_{ss} and X_C

Multiple linear regression of the t_{lag} as a function v_{ss} and XC of was performed using SAS jmp 15 (SAS institute, Cary, NC, USA). The following terms were included for the multiple regression of t_{lag}: intercept, v_{ss}, v_{ss}^2, X_C, X_C^2, and the interaction term v_{ss}:X_C. The prediction model of t_{lag} was subsequently generated using backwards selection: the term with the highest p-value was stepwise removed until the p-value of each remaining term was > 0.05.

3 Results and discussion

It has previously been shown that the initial stage of the enzymatic degradation, referred to as the lag phase, is characterized by the absence of product release. This phenomenon has been observed to be influenced by several factors, including the enzyme catalyzing the reaction [25], the specific surface area of the substrate [22], and the X_C of the substrate [12,23]. Consequently, determining the kinetics of PET substrate with increasing X_C is challenging due to the need for extensive sampling.

To circumvent this challenge, we employed a compartmentalized spectrophotometric assay, enabling continuous monitoring of product formation during the enzymatic degradation of PET [24]. Fig 2A displays representative progress curves of the of the product formation, in BHETeq [26], during enzymatic hydrolysis of PET at increasing X_C. These curves clearly illustrate how the

lag phase increased with X_C. Due to evaporation of the reaction media, the reaction time was limited to 120 min, as previously discussed in [24]. The X_C used for the ^{inv}MM kinetics were therefore limited to ~12% as the t_{lag} would extend beyond the maximal incubation time at higher X_C.

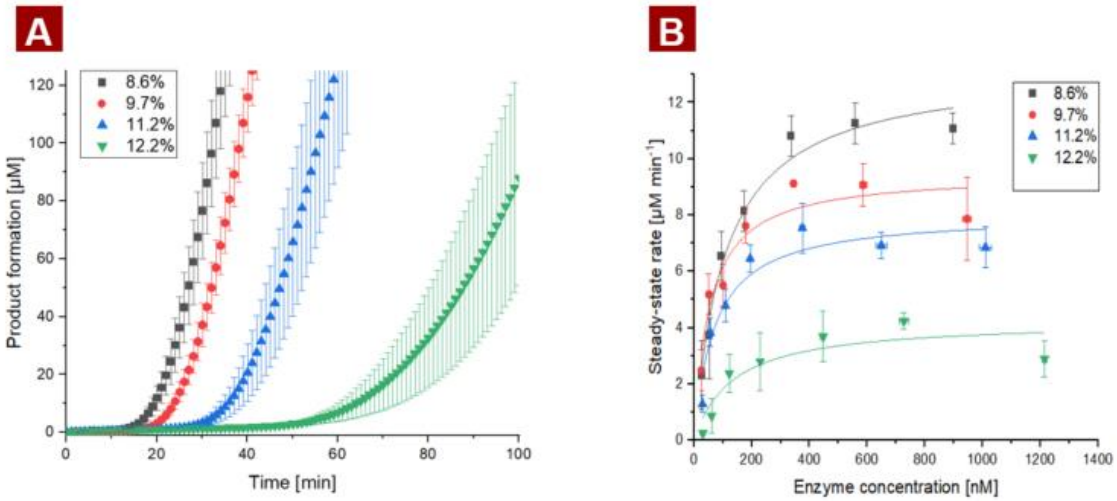

Fig 2: A) Progress curves displaying the soluble product formation during enzymatic degradation of PET disks at various X_C (8.6 to 12.2%) using 300nM LCC_{ICCG} at 50°C pH 9. B) ^{Inv}MM curves of LCC_{ICCG} substrate at various X_C (ranging from 8.6% to 12.2%). The steady-state rate was estimated from the linear region of the progress curves as indicated in Fig 1.

Table 1: Composition of the substrate (X_C, X_{MAF}, and X_{RAF}) used for the ^{inv}MM (Fig 2B) and kinetic constants ($^{inv}V_{max}$, $^{inv}K_m$) Different subscript letters (a, b, or c) indicate a statistically difference.

Annealing condition	X_C [%]	X_{MAF} [%]	X_{RAF} [%]	$^{inv}V_{max}$ [µM s^{-1}]	$^{inv}K_m$ [µM]	$^{inv}V_{max}/^{inv}K_m$ [min^{-1}]
5 min at 85°C	8.6 ± 0.78^{a}	77.4 ± 1.9^{a}	13.8 ±1.2^{a}	0.22 ± 0.011^{a}	0.11 ± 0.018^{a}	2.0 ± 0.44^{a}
3 min at 115°C	9.7 ± 0.45^{ab}	70.9 ± 5.9^{ab}	19.4 ± 6.4^{a}	0.16 ± 0.011^{b}	0.054 ± 0.016^{a}	2.9 ± 1.1^{a}
4 min at 115°C	11.2 ± 0.31^{ab}	64.4 ± 2.6^{ab}	24.5 ± 2.8^{a}	0.13 ± 0.010^{b}	0.072 ± 0.0220^{a}	1.9 ± 1.8^{a}
5 min at 115°C	12.2 ± 0.89^{b}	62.3 ± 1.9^{ab}	25.8 ± 0.78^{a}	0.07 ± 0.011^{c}	0.13 ± 0.074^{a}	0.5 ± 0.865^{a}

3.1 Steady-state Kinetics

Despite the relatively limited range of X_C of the substrate considered in the ^{Inv}MM analysis, it was observed that the increase in X_C from 8.6% to 12.2% let to a significant 3-fold reduction in the $^{inv}V_{max}$ from 0.22 to 0.07 µMs^{-1}, as outlined in Table 1.

As elucidated by Kari et. al [21] the $^{inv}V_{max}$ may be defied as the product of the catalytic constant (k_{cat}), initial substrate loading in g/L ($S_{0,mass}$) and density of attack sites (Γ_{max}) :

$$^{inv}V_{max} = S_{0,mass} * \Gamma_{max} * k_{cat} \quad \text{(Eq. 1)}$$

Given that $S_{0,mass}$ remains unaffected by the thermal annealing, and may therefore be considered as the same across all reactions, the observed reduction in $^{inv}V_{max}$ can be ascribed to either a reduction in Γ_{max}, a decrease in the apparent k_{cat} or a combination of both factors. It is well-

established that PET degrading enzymes are incapable of degrading the crystalline regions of PET[23,27–30]. Consequently, it becomes evident that increase in X_C would lead to a decrease in Γ_{max}.

To Investigate whether Γ_{max} could solely be correlated to the fractional composition of the PET in terms of the rigid all-*trans* X_C, the rigid *trans*-rich X_{RAF}, or the mobile *gauche*-rich X_{MAF}, two scenarios were proposed as to describe the substrate specificity of LCC_{ICCG}:

- **Scenario 1:** The entire amorphous fraction of PET (MAF and RAF) is degraded equally by LCC_{ICCG}, while the crystalline regions resist enzymatic hydrolysis. Hence, $\Gamma_{max} = X_{MAF} + X_{RAF} = 100 - X_C$
- **Scenario 2:** Only MAF is degraded by LCC_{ICCG}, hence both RAF and crystalline regions resist enzymatic hydrolysis. Hence, $\Gamma_{max} = X_{MAF}$

In both scenarios, it was assumed that the enzyme acts solely on the specified amorphous regions, and it was further assumed that k_{cat} remains unaffected by substrate type (i.e., MAF or RAF) or changes in fractional composition. To assess whether either of the substrate preferences outlined in the scenarios could be directly correlated with Γ_{max}, the normalized $^{inv}V_{max}$ was plotted against the normalized substrate composition, following the specifications of scenario 1 or 2. The slope of these plots would then indicate the relative change in $^{inv}V_{max}$ as a function of the relative change in substrate composition. However, the slopes for both scenarios were >1, with a value of 3.0 ± 0.7 for scenario 1 and 15 ± 2.8 for scenario 2, as illustrated in Fig 2B.

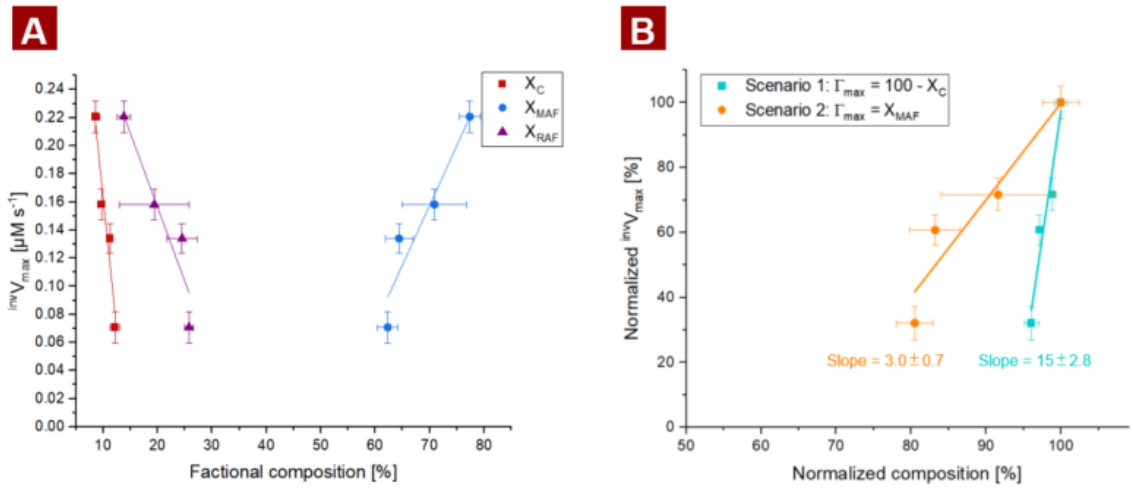

Fig 3: A) Correlation $^{Inv}V_{max}$ between the fractional composition of the PET substrate in terms of X_C, X_{RAF} or X_{MAF}. B) Normalized $^{Inv}V_{max}$, estimated from the ^{Inv}MM curves plotted against the normalized amorphous fraction (100% - X_C) (Scenario 1) or the normalized X_{MAF} (scenario 2). The bold lines represent the linear regression of the fit.

The analysis revealed that neither X_C nor X_{MAF} in isolation could fully account for the reduction in $^{inv}V_{max}$. However, X_{MAF} emerged as a better descriptor of Γ_{max}, as the slope of scenario 2 (Γ_{max} = X_{MAF}) was five times lower than scenario 1 (Γ_{max} = 100% - X_C). It is noteworthy that the relative decrease in $^{inv}V_{max}$ caused by LCC_{ICCG} due to increasing X_C was more significant than the influence of X_C on the v_{ss} of LCC_{ICCG}, as reported in previous studies [23,25]. These discrepancies likely arose from variations in experimental conditions. As mentioned earlier, the continuous assay

was conducted for a limited duration of two hours at 50°C. Consequently, factors such as increased chain mobility induced by temperature or enhanced surface erosion leading to a higher specific surface area due to prolonged degradation may have impacted tolerance towards X_C.

3.2 Duration of the lag phase

Continuous monitoring of product formation provided an in-depth analysis of the lag phase. In addition to the v_{ss} used in the ^{inv}MM curves, presented in Fig 2B, the t_{lag} was quantified from all enzymatic reactions. While v_{ss} was defined as the linear region of the progress curves, t_{lag} was empirically defined as the intersection between the regression line of v_{ss} and the baseline, as illustrated in Fig 1.

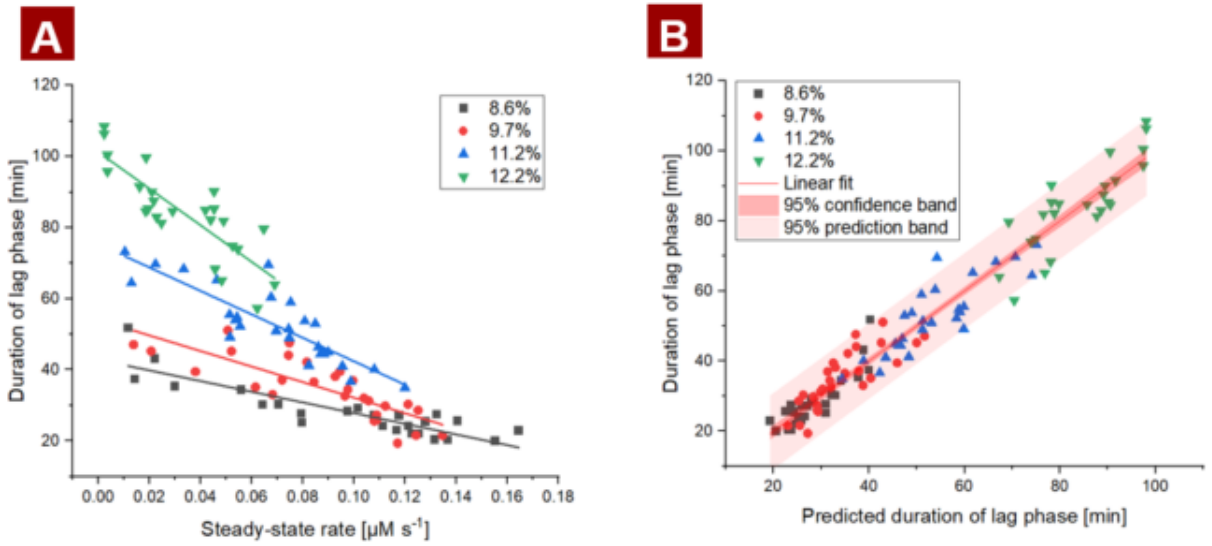

Fig 3: *A) correlation between the steady-state rate and the duration of the lag phase for each data point (n=3) included in the invers MM plot in figure 2. B) Multiple linear regression of the all individual data points from the figure 2. The model includes the following parameters: intercept, X_C, rate, and the interaction term between X_C and rate..*

A notable correlation was observed between t_{lag} and v_{ss}, as evidenced by the linear regressions depicted in Fig. 3A. This inverse proportionality between t_{lag} and v_{ss} was further amplified at increasing in X_C. In fact, the t_{lag} at a given experimental condition could be predicted based on the v_{ss} and X_C alone as evident from the multiple regression (R^2=0.95) displayed in Figure 3B.

These observations consolidated previous explanations that the lag phase was a result of a random/endo-type degradation pattern of insoluble PET chains [25,31]. Consequently, the average degree of polymerization (DP) of the PET chains exposed at the surface would decrease during the initial stage. This would increase the likelihood of chain scissoring at the terminals, leading to the formation of a soluble product. The rate of product formation would thus be inversely proportional to the average DP of the exposed PET chains at the surface. Therefore, t_{lag} could be attributed to the time required to hydrolyze the necessary number of ester bonds to reach a steady-state where the average DP of the exposed polymer chains remained constant. The increase in t_{lag} due to an increase in X_C would consequently imply that the required number of ester bonds to reach a steady-state also increases with X_C. This phenomenon could potentially be attributed to the density of entanglements in the amorphous regions. It has been established

that crystal formation during annealing at temperatures below 120°C (which applies to this study) does not result in unravel the entanglements in the amorphous regions [32]. Consequently, the relative density of entanglements in the amorphous regions would increase as X_C increases. We speculate if these entanglements could potentially shield the free ends of the polymeric chains, which are necessary to yield a soluble product. Which would explain the longer t_{lag} at increasing X_C. Another explanation could result from unproductive binding of the enzymes to the crystalline regions, which has previously been shown to be the major interaction between PET and PET degrading enzymes [33].

4 Conclusion

In this study, we conducted a kinetic evaluation of the enzymatic degradation of PET by the benchmark PET hydrolase LCC_{ICCG} using PET substrate with different compositions of X_{MAF}, X_{RAF} and X_C. We observed that as the crystalline content of PET, represented by X_C, increased, there was a significant reduction in the $^{inv}V_{max}$. We hypothesized that this reduction was directly liked to substrate specificity in terms of X_{MAF} and X_{RAF}. Interestingly, the substrate composition alone could not explain the profound reduction in $^{inv}V_{max}$. Thus emphasizing the complex nature the PET substrate. However, we found that X_{MAF} is a better descriptor for the Γmax, than the entire amorphous region. Furthermore, our study revealed that the t_{lag} could be predicted by the v_{ss} and X_C alone. This observation suggest that the t_{lag} is resulting from an initial random/endo-type degradation leading to a reduction in the average chain length at the surface without releasing any soluble products. We further proposed that the longer resulting from increased X_C was attributed to a more dense engagements and unproductive binding of the enzyme to the crystalline regions. In conclusion, our study advances our understanding of PET enzymatic degradation, specifically in relation to substrate composition, particularly X_C, X_{RAF} and X_{MAF}. Future investigations may delve deeper into the structural and mechanistic aspects of PET degradation enzymes concerning substrate structural features to optimize their performance and broaden their applications in plastic waste management. These insights offer promising prospects for more efficient and sustainable plastic recycling solutions.

References

[1] Geyer R, Jambeck JR, Law KL. Production, use, and fate of all plastics ever made. Sci Adv 2017;3:e1700782. https://doi.org/10.1126/sciadv.1700782.

[2] European Commission. A circular economy for plastics – Insights from research and innovation to inform policy and funding decisions. 2019. https://doi.org/10.2777/269031.

[3] Plastics Europe. Plastics – the Facts 2022. Available at: Https://Plasticseurope.Org/Knowledge-Hub/Plastics-the-Facts-2022/: 2022.

[4] World Economic Forum Ellen MacArthur Foundation McKinsey & Company. The New Plastics Economy: Rethinking the future of plastics. Available at: Https://Ellenmacarthurfoundation.Org/the-New-Plastics-Economy-Rethinking-the-Future-of-Plastics: 2016.

[5] Hu W, Zha L. Theoretical aspects of polymer crystallization. Control. Morphol. Polym.

Mult. Scales Struct. Process., Springer International Publishing; 2016, p. 101–43. https://doi.org/10.1007/978-3-319-39322-3_4.

[6] Bartczak Z. Deformation of semicrystalline polymers – the contribution of crystalline and amorphous phases. Polimery 2017;62:787–99. https://doi.org/10.14314/POLIMERY.2017.787.

[7] Zekriardehani S, Jabarin SA, Gidley DR, Coleman MR. Effect of Chain Dynamics, Crystallinity, and Free Volume on the Barrier Properties of Poly(ethylene terephthalate) Biaxially Oriented Films. Macromolecules 2017;50:2845–55. https://doi.org/10.1021/acs.macromol.7b00198.

[8] Androsch R, Wunderlich B. The link between rigid amorphous fraction and crystal perfection in cold-crystallized poly(ethylene terephthalate). Polymer (Guildf) 2005;46:12556–66. https://doi.org/10.1016/J.POLYMER.2005.10.099.

[9] Di Lorenzo ML, Righetti MC, Cocca M, Wunderlich B. Coupling between Crystal Melting and Rigid Amorphous Fraction Mobilization in Poly(ethylene terephthalate). Macromolecules 2010;43:7689–94. https://doi.org/10.1021/MA101035H.

[10] Chen H, Cebe P. Vitrification and devitrification of rigid amorphous fraction of PET during quasi-isothermal cooling and heating. Macromolecules 2009;42:288–92. https://doi.org/10.1021/ma802104a.

[11] Chen H, Liu Z, Cebe P. Chain confinement in electrospun nanofibers of PET with carbon nanotubes. Polymer (Guildf) 2009;50:872–80. https://doi.org/10.1016/j.polymer.2008.12.030.

[12] Thomsen TB, Hunt CJ, Meyer AS. Standardized method for controlled modification of poly (ethylene terephthalate) (PET) crystallinity for assaying PET degrading enzymes. MethodsX 2022;9:101815. https://doi.org/10.1016/J.MEX.2022.101815.

[13] Zumstein MT, Rechsteiner D, Roduner N, Perz V, Ribitsch D, Guebitz GM, et al. Enzymatic Hydrolysis of Polyester Thin Films at the Nanoscale: Effects of Polyester Structure and Enzyme Active-Site Accessibility. Environ Sci Technol 2017;51:7476–85. https://doi.org/10.1021/ACS.EST.7B01330.

[14] Tokiwa Y, Suzuki T. Hydrolysis of polyesters by lipases. Nature 1977;270:76–8. https://doi.org/10.1038/270076a0.

[15] Wei R, Zimmermann W. Microbial enzymes for the recycling of recalcitrant petroleum-based plastics: how far are we? Microb Biotechnol 2017;10:1308–22. https://doi.org/10.1111/1751-7915.12710.

[16] Sulaiman S, Yamato S, Kanaya E, Kim JJ, Koga Y, Takano K, et al. Isolation of a novel cutinase homolog with polyethylene terephthalate-degrading activity from leaf-branch compost by using a metagenomic approach. Appl Environ Microbiol 2012;78:1556–62. https://doi.org/10.1128/AEM.06725-11.

[17] Tournier V, Topham CM, Gilles A, David B, Folgoas C, Moya-Leclair E, et al. An

engineered PET depolymerase to break down and recycle plastic bottles. Nature 2020;580:216–9. https://doi.org/10.1038/s41586-020-2149-4.

[18] Zimmermann W. Biocatalytic recycling of polyethylene terephthalate plastic. Philos Trans R Soc A 2020;378. https://doi.org/10.1098/RSTA.2019.0273.

[19] Müller RJ, Schrader H, Profe J, Dresler K, Deckwer WD. Enzymatic degradation of poly(ethylene terephthalate): Rapid hydrolyse using a hydrolase from T. fusca. Macromol Rapid Commun 2005;26:1400–5. https://doi.org/10.1002/marc.200500410.

[20] Tiso T, Narancic T, Wei R, Pollet E, Beagan N, Schröder K, et al. Bio-upcycling of polyethylene terephthalate. BioRxiv 2020:2020.03.16.993592. https://doi.org/10.1101/2020.03.16.993592.

[21] Kari J, Andersen M, Borch K, Westh P. An Inverse Michaelis-Menten Approach for Interfacial Enzyme Kinetics. ACS Catal 2017;7:4904–14. https://doi.org/10.1021/acscatal.7b00838.

[22] Chang AC, Patel A, Perry S, Soong Y V., Ayafor C, Wong HW, et al. Understanding Consequences and Tradeoffs of Melt Processing as a Pretreatment for Enzymatic Depolymerization of Poly(ethylene terephthalate). Macromol Rapid Commun 2022:2100929. https://doi.org/10.1002/marc.202100929.

[23] Thomsen TB, Hunt CJ, Meyer AS. Influence of substrate crystallinity and glass transition temperature on enzymatic degradation of polyethylene terephthalate (PET). N Biotechnol 2022;69:28–35. https://doi.org/10.1016/j.nbt.2022.02.006.

[24] Thomsen TB, Schubert SW, Hunt CJ, Westh P, Meyer AS. A new continuous assay for quantitative assessment of enzymatic degradation of poly(ethylene terephthalate) (PET). Enzyme Microb Technol 2023;162:110142. https://doi.org/10.1016/j.enzmictec.2022.110142.

[25] Thomsen TB, Schubert S, Hunt CJ, Borch K, Jensen K, Brask J, et al. Rate Response of Poly(Ethylene Terephthalate)-Hydrolases to Substrate Crystallinity: Basis for Understanding the Lag Phase. ChemSusChem 2023;202300291:1–14. https://doi.org/10.1002/cssc.202300291.

[26] Arnling Bååth J, Borch K, Westh P. A suspension-based assay and comparative detection methods for characterization of polyethylene terephthalate hydrolases. Anal Biochem 2020;607. https://doi.org/10.1016/j.ab.2020.113873.

[27] Erickson E, Shakespeare TJ, Bratti F, Buss BL, Graham R, Hawkins MA, et al. Comparative Performance of PETase as a Function of Reaction Conditions, Substrate Properties, and Product Accumulation. ChemSusChem 2022;15. https://doi.org/10.1002/CSSC.202101932.

[28] Wei R, Breite D, Song C, Gräsing D, Ploss T, Hille P, et al. Biocatalytic Degradation Efficiency of Postconsumer Polyethylene Terephthalate Packaging Determined by Their Polymer Microstructures. Adv Sci 2019;6. https://doi.org/10.1002/advs.201900491.

[29] Vertommen MAME, Nierstrasz VA, Veer M Van Der, Warmoeskerken MMCG. Enzymatic surface modification of poly(ethylene terephthalate). J Biotechnol 2005;120:376–86. https://doi.org/10.1016/j.jbiotec.2005.06.015.

[30] Weinberger S, Haernvall K, Scaini D, Ghazaryan G, Zumstein MT, Sander M, et al. Enzymatic surface hydrolysis of poly(ethylene furanoate) thin films of various crystallinities. Green Chem 2017;19:5381–4. https://doi.org/10.1039/c7gc02905e.

[31] Tarazona NA, Wei R, Brott S, Pfaff L, Bornscheuer UT, Lendlein A, et al. Rapid depolymerization of poly(ethylene terephthalate) thin films by a dual-enzyme system and its impact on material properties. Chem Catal 2022;2:3573–89. https://doi.org/10.1016/j.checat.2022.11.004.

[32] Rastogi R, Vellinca WP, Rastogi S, Schick C, Meijer HEH. The three-phase structure and mechanical properties of poly(ethylene terephthalate). J Polym Sci Part B Polym Phys 2004;42:2092–106. https://doi.org/10.1002/POLB.20096.

[33] Badino SF, Bååth JA, Borch K, Jensen K, Westh P. Adsorption of enzymes with hydrolytic activity on polyethylene terephthalate. Enzyme Microb Technol 2021;152:109937. https://doi.org/10.1016/J.ENZMICTEC.2021.109937.